

See discussions, stats, and author profiles for this publication at: <https://www.researchgate.net/publication/263414067>

An Optimum Approach to Monte Carlo Burn-Up

Thesis · April 2007

CITATIONS

8

READS

2,138

1 author:



Wim Haeck

Los Alamos National Laboratory

96 PUBLICATIONS 1,322 CITATIONS

[SEE PROFILE](#)

Een optimale benadering van Monte Carlo met depletie

An Optimum Approach to Monte Carlo Burn-Up

Wim Haeck

Promotor: prof. dr. C. Wagemans
Proefschrift ingediend tot het behalen van de graad van
Doctor in de Ingenieurswetenschappen: Toegepaste Natuurkunde

Vakgroep Subatomaire en Stralingsfysica
Voorzitter: prof. dr. D. Ryckbosch
Faculteit Ingenieurswetenschappen
Academiejaar 2006 - 2007



ISBN 978-90-8578-141-7
NUR 925, 961
Wettelijk depot: D/2007/10.500/15

Contents

Preface	v
Samenvatting	vii
Summary	ix
Abbreviations	xi
Symbols	xiii
List of publications	xix
1 Introduction and background	1
1.1 Monte Carlo and advanced nuclear systems	1
1.2 Monte Carlo and burn-up applications	3
1.3 Nuclear data and burn-up applications	4
1.4 Main objectives	5
2 The ORIGEN depletion code	7
2.1 Basic concepts and tasks of a burn-up code	7
2.2 The origin of ORIGEN	11
2.3 The matrix exponential method	12
2.4 Cross section, decay and photon libraries	14
2.5 Hard-coded data and approximations	16
2.5.1 The total recoverable energy per fission	16
2.5.2 Burn-up dependent cross sections	18
2.5.3 The neutron yield per fission	18
2.5.4 Neutron yields from (α,n) reactions	19
3 The mechanics of Monte Carlo	21
3.1 The Monte Carlo concept	21
3.2 The particle transport simulation process	23
3.2.1 Working of a general Monte Carlo code	23
3.2.2 The particular case of MCNP(X)	25
3.3 Tally estimators	28
3.4 Criticality and fixed source calculations	30
4 Analysis of Monte Carlo with burn-up	33
4.1 Nuclear data tables and code performance	33
4.2 Monte Carlo simulation time	36
4.3 Criticality calculation correction	39
4.4 Reaction rate calculation time	40
4.5 CPU time increase	41

4.5.1	Time increase in MCNP and MCNPX	41
4.5.2	Example: a cell of ^{238}U	42
4.5.3	An infinite lattice of fuel pins	46
4.6	Accumulation of fission products	47
4.7	The optimum for Monte Carlo burn-up	49
5	Accelerating Monte Carlo with burn-up	51
5.1	An alternate approach to calculating reaction rates	51
5.2	An efficient and optimal approach	54
5.3	Accuracy	56
5.3.1	The concept of accuracy	56
5.3.2	Optimising the energy structure	56
5.3.3	Global agreement	60
5.4	Convergence and stability	62
6	Nuclear data for burn-up applications	65
6.1	Nuclear data requirements	65
6.2	ENDF - Evaluated Nuclear Data File	66
6.2.1	The ENDF format and nuclear data libraries	66
6.2.2	ENDF file and library structure	67
6.3	Neutron cross section data	69
6.4	Isomeric branching ratio	72
6.5	Direct fission product yields	75
6.6	Neutron yield per fission	77
6.7	The total recoverable energy per fission	80
6.7.1	Components of fission energy release	80
6.7.2	Energy and system dependence	82
6.7.3	Using the correct value	86
6.8	Decay data	87
7	ALEPH-DLG: nuclear data preparation and validation	91
7.1	Validated application libraries	91
7.2	Preparation of a nuclear data library	92
7.2.1	What was done in the past	92
7.2.2	NJOY processing in ALEPH-DLG	96
7.3	ALEPH-DLG and NJOY post-processing	97
7.3.1	Library QA	97
7.3.2	Common NJOY warnings	98
7.3.3	Resonance reconstruction	99
7.3.4	Unresolved Probability Tables	100
7.3.5	Cross section plots and MCNP(X) testing	101
7.4	Nuclear data validation	103
7.4.1	General remarks on library validation	103
7.4.2	Criticality benchmarks	103

7.4.3 LLNL Pulsed Spheres	104
8 ALEPH: a Monte Carlo burn-up code	111
8.1 Efficient, flexible and easy to use	111
8.2 Calculation flow and features	112
8.3 Irradiation capabilities	115
8.3.1 The specific normalisation power	115
8.3.2 Constant power	116
8.3.3 Constant flux	117
8.3.4 Calculating burn-up	118
8.4 Updating material compositions	118
9 High burn-up fuel	121
9.1 Self-shielding and the high burn-up structure	121
9.2 TRANSURANUS and TUBRNP	122
9.3 Modelling high burn-up fuel pins with ALEPH	123
9.4 Experimental measurements	125
9.5 Evolution of the neutron spectra	126
9.6 Absolute plutonium and neodymium content	126
9.7 Radial plutonium and burn-up profiles	131
10 The MALIBU experimental data	137
10.1 The MALIBU program	137
10.2 Calculating the GGU2 fuel sample	138
10.2.1 Modelling a PWR fuel assembly	138
10.2.2 Burn-up indicators	140
10.2.3 Actinides	143
10.2.4 Fission products	145
10.3 Sensitivity to nuclear data	147
10.3.1 The ^{236}U fission cross section	147
10.3.2 The ^{241}Am (n,γ) branching ratio to ^{242g}Am	148
10.4 Sensitivity to modelling effects	150
11 Control plate movement in the High Flux Isotope Reactor	153
11.1 Description of the HFIR	153
11.2 Modelling burn-up in the HFIR	155
11.3 Control plate movement	156
11.4 Neutron spectra and flux values	159
11.5 Evolution of individual nuclides	159
11.5.1 Fuel depletion	159
11.5.2 Depletion of burnable poison	164
11.5.3 Fission product accumulation	165
11.6 Fractional absorption criterion	167
11.7 Burn-up oscillations	169

12 Fuel management in hybrid systems	171
12.1 The physics of sub-critical multiplying systems	171
12.2 The MYRRHA Accelerator Driven System	174
12.3 Modelling burn-up in an ADS	177
12.4 Fuel management calculations	178
12.4.1 Requirements for fuel management	178
12.4.2 Integral system parameters	178
12.4.3 Flux, power and burn-up distributions	182
12.4.4 Mass balance and transmutation performance	186
13 Final conclusions and future developments	193
13.1 An optimal approach to Monte Carlo burn-up	193
13.2 Nuclear data and ALEPH-DLG	195
13.3 ALEPH	197
13.4 Future developments	199

Preface

Lying in front of you is the result of an adventure that started about 5 years ago when I arrived 20 minutes early for a class on radiation and radio-protection given by professor Hubert Thierens at Ghent University. Since we had some time to kill, we talked about what I hoped to do with my life. It was then that I heard for the first time of SCK•CEN's Doctoral Programme. A few months later (on October 1, 2002), I started my first day at the now defunct Reactor Physics and MYRRHA Department of SCK•CEN.

It is often said that a few key moments determine our lives completely. For me, that was definitely one of them although I probably didn't realise it at the time. I dare not think what would have happened if I had arrived on time for that class. However, now is not the time to dwell on what ifs but more on what *is*.

Before we continue, there are a number of people that I would like to thank for their help and support. First and foremost there are professor Cyriel Wagemans and Bernard Verboomen, respectively my university supervisor and SCK•CEN mentor. They encouraged me to see beyond what everybody else thinks is normal and ultimately to question everything.

I would like to acknowledge the financial support of SCK•CEN's Doctoral Programme, the MYRRHA project and Hamid Aït Abderrahim in particular for making this a reality.

I would like to thank my friends and colleagues from SCK•CEN for their trust in my work. In particular, Edouard Malambu, Thierry Aoust, Nadia Messaoudi and Vitaly Sobolev for teaching me the tricks of the trade in my early years and for the confidence in my work later on. Furthermore, Luc Borms for encouraging me to try C++ and for his technical help, Gert Van den Eynde for his help concerning numerical techniques, Herman Vermeulen, Kris Pennemans and everybody else at Infoplan and the Knowledge Center because they don't realize how valuable they are to our line of work, Ben Vanhaeren for making the Fermi cluster what it is today and Kristien Smans and Michèle Coeck just for listening. And of course Milena Matijasevic, Hanane Derradji, Wouter Van Renthergem, Paul Borgermans, Flyura Djurabekova, Dirk Maes, Marco Van Uffelen, Frederik Slachmuylers and everybody else with whom I have spent many evenings to help make Mol my home.

During the last four years I have also had the opportunity to meet experts of various fields of research that have helped me shape this work. First of all John Hendrickx (LANL, USA) for some fruitful discussions both by e-mail and in person on the internal workings of MCNPX and for his friendship, guidance and encouragement from the other side of the ocean. I am also grateful to Arjan Koning (NRG, The Netherlands), Jean-Christophe Sublet (CEA, France), Robert Mills (Nexia Solutions, UK), Christopher Dean (Serco Assurance, UK), Robin Forrest (UKAEA, UK), Yolanda Rugama and Hans Henriksson (NEA-OECD, France) and the JEFF Group for accepting the new guy on the nuclear

data block so quickly and because nuclear data would simply not be the same without them. I would also like to thank Joachim Miss (IRSN, France) and Emanuele Martinolli (AREVA NP, France) for their interest in this work.

Some of the applications in this work would have been impossible without the trust and support of people like Ned Xoubi and Trent Primm (ORNL, USA) for the HFIR calculations and comparisons with MONTEBURNS and Arndt Schubert and Paul Van Uffelen (ITU, Germany) for the high burn-up PWR calculations. I am also grateful towards all partners in the MALIBU program for allowing me to use the MALIBU data to validate my work. In particular I would like to thank Mireille Gysemans, Andrew Dobney and Leo Sannen (SCK•CEN) and Danièle Boulanger (Belgonucléaire, Belgium) for giving me this chance.

And last but not least, I would also like to thank my family and friends who remained in “de Vlaanders” when I went to Mol for not forgetting about me. In particular, I would like to thank my parents and my brother. Without them, I would not be as I am today.

I dedicate this work to prof. Fernand Vanmassenhove who could not witness its completion. He would have been proud.

Wim Haeck
January 2007

Samenvatting

Een belangrijke drijfveer achter het gebruik van Monte Carlo depletiecodes kan gevonden worden in de mogelijkheden van dergelijke codes om de meest nauwkeurige lokale neutronen spectra en flux waarden in om het even welke realistische 3D geometrie te berekenen. Deze mogelijkheden samen met het feit dat deze codes nucleaire data kunnen gebruiken in hun basisvorm maar ook in hun meest complexe vorm (continue energie werkzame doorsneden, gedetailleerde energie-hoek correlaties, fysica van verscheidene types deeltjes, etc.) kunnen van Monte Carlo depletiecodes potentieel krachtige rekencodes maken, en dan zeker voor hybride en geavanceerde nucleaire systemen.

Aan de andere kant hebben deze codes een beperkt succes door de vrij lange rekentijd die nodig is om een gedetailleerde en nauwkeurige berekening uit te voeren, zelfs met de moderne computertechnologie die ons nu ter beschikking staat. Om dit probleem te omzeilen, moeten gebruikers vaak het aantal nuclides in de activatieketens beperken of overwegen om langere stappen in de bestralingshistoriek en/of grotere depletiezones te gebruiken. In alle gevallen zal dit zijn weerslag hebben op de nauwkeurigheid.

Er moet altijd een balans zijn tussen nauwkeurigheid en wat bereikt kan worden (onder aanvaardbare omstandigheden). Dus als de tijd die nodig is voor de Monte Carlo simulatie zo laag mogelijk is en als het berekenen van de data voor de depletiecode verwaarloosbaar is, dan kunnen we zo nauwkeurig zijn als we maar willen. En dat is de optimale situatie voor Monte Carlo met depletie.

Het gebruik van CPU tijd is voornamelijk te vinden in de berekening van de werkzame doorsnede (en het opzoeken van het energie interval) die nodig zijn voor de simulatie en zeker voor de berekening van de data voor de depletiecode. De ideale oplossing zou het invoeren zijn van een datatabel van werkzame doorsneden die allemaal dezelfde energiepunten gebruiken. Het berekenen van de data voor de depletiecode wordt dan verwaarloosbaar in vergelijking met de simulatie zelf. Daar komt dan nog bij dat de rekentijd voor de simulatie zelf geminimaliseerd wordt. Spijtig genoeg bestaan geen Monte Carlo codes die een dergelijk formaat hanteren (behalve natuurlijk de veelgroeps Monte Carlo codes).

Een andere oplossing is het verminderen van het aantal keer dat de code het energie interval moet opzoeken voor het berekenen van de data voor de depletiecode zodat het verwaarloosbaar wordt. Dit kan onder andere door het gebruik van een veelgroepsbenadering waarbij de Monte Carlo code een heel fijn veelgroepsspectrum berekent om de data voor de depletiecode te berekenen na de simulatie. Dit is geen benadering of hybride techniek omdat het niets aan de simulatie verandert. Het is gewoon een andere manier om de integraal te berekenen. Met de juiste optimalisatie van de veelgroepsstructuur is deze alternatieve methode in perfecte overeenstemming met traditionele Monte Carlo (het verschil is altijd kleiner dan de standaardafwijking).

Met deze benadering valt de afhankelijkheid van de rekentijd van het aantal nuclides en types van reacties in de activatieketens weg. Dit laat ons toe om een maximale nauwkeurigheid te bereiken voor een minimum aan rekentijd omdat we alle nuclides en alle reacties kunnen gebruiken van in het begin.

De veelgroepsbenadering is geïmplementeerd in ALEPH, een Monte Carlo depletiecode die zich rond ORIGEN 2.2 en elke versie van MCNP of MCNPX plaatst. Het basisidee achter ALEPH was het maken van een efficiënte, flexibele en gebruiksvriendelijke code. Door het voorzien van een eenvoudig te begrijpen interface nemen we de druk weg van de gebruiker. Voor een gebruiker is het alsof hij een eenvoudig MCNP(X) probleem draait met enkele extra "opties". De code heeft vele mogelijkheden, onder andere het simuleren van bewegende controlestaven of het modelleren van de variatie van de boor concentratie in koelwater tijdens de bestralingshistoriek.

Met ALEPH-DLG kunnen we garanderen dat de werkzame doorsneden die gebruikt worden in MCNP(X) hetzelfde zijn als deze die gebruikt wordt voor de veelgroepsbenadering. De code automatiseert het volledige proces van het maken van bibliotheekbestanden met NJOY voor MCNP(X) en voor gebruik met de veelgroepsbenadering. De code maakt NJOY invoerbestanden die op maat gemaakt zijn voor elke nuclide en verwerkt de uitvoer van NJOY om te zien of alles perfect verwerkt werd. Wanneer ALEPH-DLG iets vindt dat niet normaal is, dan zal de code en waarschuwing geven of een correctieve actie ondernemen.

Dankzij ALEPH-DLG kan ALEPH de werkzame doorsneden voor elke nuclide en reactie in de activatieketens lezen uit ENDF bestanden die verwerkt zijn door NJOY tot MCNP(X). Uitgaand van deze continue energie werkzame doorsneden data bibliotheken berekent ALEPH dan een veelgroeps werkzame doorsnede. Door een convolutie met het berekende veelgroepsspectrum worden deze dan omgezet in de één groeps werkzame doorsneden voor gebruik in ORIGEN 2.2.

ALEPH is een code met verscheidene toepassingsgebieden, zoals aangegeven wordt met de verschillende toepassingen in dit werk. Er zijn validatieberekeningen met experimentele data, namelijk een enkele PWR splijtstofstift met een hoge versplijting waarbij rekening gehouden werd met de ruimtelijke zelfafscherming en een PWR splijtstofelement (in het kader van het MALIBU programma). De laatste twee toepassingen demonstreren het gebruik van ALEPH in 3D reactorberekeningen, meer bepaald met de HFIR reactor (waarbij gebruik gemaakt werd van de simulatie van bewegende controle elementen) en de MYRRHA ADS (waarbij een vaste externe protonenbron gebruikt wordt) die het gebruik van ALEPH voor splijtstofbeheer illustreert. Andere mogelijke toepassingsgebieden zijn studies van de splijtstofcyclus, afval karakterisatie, schattingen voor radio-isotopen productie, etc.

Summary

The incentive of creating Monte Carlo burn-up codes arises from its ability to provide the most accurate locally dependent spectra and flux values in realistic 3D geometries of any type. These capabilities linked with the ability to handle nuclear data not only in its most basic but also most complex form (namely continuous energy cross sections, detailed energy-angle correlations, multi-particle physics, etc.) could make Monte Carlo burn-up codes very powerful, especially for hybrid and advanced nuclear systems.

Still, such Monte Carlo burn-up codes have had limited success mainly due to the rather long CPU time required to carry out very detailed and accurate calculation, even with modern computer technology. To work around this issue, users often have to reduce the number of nuclides in the evolution chains or to consider either longer irradiation time steps and/or larger spatial burn-up cells, jeopardizing the accuracy of the calculation in all cases.

There should always be a balance between accuracy and what is (reasonably) achievable. So when the Monte Carlo simulation time is as low as possible and if calculating the cross sections and flux values required for the depletion calculation takes little or no extra time compared to this simulation time, then we can actually be as accurate as we want. That is the optimum situation for Monte Carlo burn-up calculations.

The CPU time consumption of Monte Carlo burn-up codes is mainly due to the calculation of all the cross section values (and in particular the energy grid search) during the Monte Carlo simulation and especially during the reaction rate calculation. The ideal solution would be to adopt some form of universal unionised cross section tables (where every cross section is linearised on the same energy grid). With this format, calculating reaction rates will become negligible compared to the simulation time and it will also minimise the basic Monte Carlo simulation. Unfortunately, no Monte Carlo code exists that uses universal unionised cross section tables (except for the obvious multi-group Monte Carlo codes).

Another solution is to reduce the number of grid searches for the reaction rate calculation so that it becomes negligible versus the simulation time for existing Monte Carlo codes like MCNP(X). This can be done by adopting the multi-group binning approach where the Monte Carlo code provides a very fine multi-group spectrum to calculate the reaction rates outside the Monte Carlo simulation. This alternate approach is neither an approximation nor is it a true hybrid method as it does not interfere in any way with the Monte Carlo simulation itself. At its core, it is just another way to calculate an integral. With proper optimisation of the group structure used for the integration, this alternate method and traditional Monte Carlo are in excellent agreement (all values are within one standard deviation).

With this approach, the dependence upon the number of reaction rates in the calculation time disappears. This allows us to achieve maximum accuracy

for a minimum of CPU time since we can actually calculate as much reaction rates as we want by default.

The multi-group binning approach has been implemented into ALEPH, a Monte Carlo burn-up code that wraps itself around ORIGEN 2.2 and any version of MCNP or MCNPX. The main idea behind ALEPH was to provide the Monte Carlo community with a general purpose Monte Carlo burn-up code that is efficient, flexible and user friendly. By providing an easy to understand user interface, we also take away the burden from the user. For the user, it is as if he is running a simple MCNP(X) problem but with some “extra” options. The code has many features and capabilities, such as the possibility to simulate moving control elements and modelling the variation of boron concentration in the coolant during the irradiation.

With the ALEPH-DLG auxiliary code, we can insure that MCNP(X) and the multi-group binning approach use exactly the same data. ALEPH-DLG automates the entire process of generating library files with NJOY. It produces tailor made NJOY input files for every nuclide and processes the NJOY output to check proper processing. Should ALEPH-DLG find anything out of the ordinary, it will either warn the user or perform corrective actions.

Thanks to ALEPH-DLG, ALEPH can simply read the microscopic cross sections of every reaction and nuclide considered in the transmutation chains from the ENDF files processed by NJOY for the preparation of the MCNP(X) data libraries. ALEPH then transforms the continuous energy cross section into a multi-group cross section which is convoluted with the spectrum calculated by the Monte Carlo code into the single group spectral averaged cross sections needed by ORIGEN 2.2.

ALEPH is a multi-purpose code, as evidenced by the applications used in this work. There are benchmark and validation calculations for a single PWR fuel pin up to high burn-up taking into account spatial self-shielding and a PWR fuel assembly calculation (in the framework of the MALIBU program). The last two applications demonstrate the use of ALEPH for full 3D reactor calculations using the HFIR (with variable geometry to simulate control plate movement) and the MYRRHA ADS (with a fixed external proton source) to illustrate how the code can be used for fuel management.

Abbreviations

ACE	A Compact ENDF
ADS	Accelerator Driven System
ASCII	American Standard Code for Information Interchange
ABWR	Advanced Boiling Water Reactor
BUU	Burn-Up Credit
BWR	Boiling Water Reactor
CANDU	CANada Deuterium Uranium
CEA	Commissariat à l'Énergie Atomique
CERN	Conseil Européen pour la Recherche Nucléaire
CPU	Central Processing Unit
CSEWG	Cross Section Evaluation Working Group
EFIT	European Facility for Industrial Transmutation
EFPD	Effective Full Power Day
ENDF	Evaluated Nuclear Data File
ENSDF	Evaluated Nuclear Structure Data File
EPMA	Electron Probe MicroAnalysis
EPR	European Pressurised Reactor
ESBWR	Economic Simplified Boiling Water Reactor
EU	European Union
GFR	Gas cooled Fast Reactor
GIF	Generation IV International Forum
HBS	High Burn-up Structure
HFIR	High Flux Isotope Reactor
IAEA	International Atomic Energy Agency
IAEA-NDS	IAEA Nuclear Data Section
ICP-MS	Inductively Coupled Plasma Mass Spectrometry
ICT	Insulated Core Transformer
IRMM	Institute for Reference Materials and Measurements
ITU	Institute for Transuranium Elements
JEF	Joint European File
JEFF	Joint European Fission and Fusion
JENDL	Japanese Evaluated Nuclear Data Library
JRC	Joint Research Centre
LANL	Los Alamos National laboratory
LFR	Lead cooled Fast Reactor
LLNL	Lawrence Livermore National Laboratory
LMFBR	Liquid Metal Fast Breeder Reactor
MALIBU	Mox And UOX LWR fuels Irradiated to high Burn-Up
MC	Monte Carlo
MCNP	Monte Carlo Neutron Photon
MCNPX	MCNP eXtended
MCNP(X)	MCNP or MCNPX

MIT	Massachusetts Institute of Technology
MOX	Mixed OXide
MYRRHA	Multi-purpose hYbrid Research Reactor for Hightech Applications
NEA	Nuclear Energy Agency
NNDC	National Nuclear Data Centre
NRG	Nuclear Research & consultancy Group
nTOF	neutron Time Of Flight
OECD	Organisation for Economic Cooperation and Development
ORIGEN	Oak Ridge Isotope GENerator
ORIGEN-S	ORIGEN for Scale
ORNL	Oak Ridge National Laboratory
PBMR	Pebble Bed Modular Reactor
PDF	Probability Density Function
PWR	Pressurised Water Reactor
PSI	Paul Scherrer Institute
QA	Quality Assurance
SCK•CEN	Studiecentrum voor Kernenergie - Centre d'étude de l'Energie Nucléaire
SCWR	Super Critical Water-cooled Reactor
SFR	Sodium cooled Fast Reactor
US	United States
VHTR	Very High Temperature Reactor
XT-ADS	eXperimental facility demonstrating the technical feasibility of Transmutation in an Accelerator Driven System

Symbols

α		the slope of the time increase due to the calculation of reaction rates
β_{eff}	pcm	the effective delayed neutron fraction
δ_{MC}		the Monte Carlo standard deviation on a single group cross section
δ_{MG}		the relative deviation of a single group cross section calculated with the multi-group binning approach compared to the Monte Carlo value
ϵ		the accuracy of the multi-group binning approach
λ_i	s^{-1}	the total decay constant of nuclide i
λ_s		the branching ratio to the state s of the daughter nuclide
$\lambda_{s,g}$		the branching ratio of group g to the state s of the daughter nuclide
ν_α	$s^{-1} g^{-1}$	the neutron yield from (α, n) reactions
$\bar{\nu}_d$		the average number of delayed neutrons released after fission
$\bar{\nu}_p$		the average number of prompt neutrons released after fission
$\bar{\nu}_t$		the total average number of neutrons released after fission
$\bar{\nu}_{t,g}$		the total average number of neutrons released after fission in group g
$\bar{\nu}_{i,t}$		the total average number of neutrons released after fission of a nuclide i
ξ		a random number between 0 and 1
ρ	$g \text{ cm}^{-3}$	the density
ρ_i	$g \text{ cm}^{-3}$	the density of nuclide i
$\rho_{a,j}$	$g \text{ cm}^{-3}$	the density of the actinides that were initially present in material i
σ	barn	the microscopic cross section
$\sigma_{f,g}$	barn	the microscopic fission cross section of group g
σ_g	barn	the microscopic cross section of group g
σ_i	barn	the microscopic cross section of interval i between energies E_i and E_{i+1}
$\sigma_{i,a}$	barn	the microscopic absorption cross section of nuclide i
$\sigma_{i,e}$	barn	the microscopic elastic scattering cross section of nuclide i
$\sigma_{i,f}$	barn	the microscopic fission cross section of nuclide i

$\sigma_{i,r}$	barn	the microscopic cross section of nuclide i for a reaction r
$\sigma_{i,t}$	barn	the total microscopic cross section of nuclide i for a reaction r
$\sigma_{j,i}^k$	barn	the microscopic cross section of an inelastic reaction of type k of nuclide j
σ_s	barn	the microscopic cross section to the isomeric state s
$\sigma_{s,g}$	barn	the microscopic cross section of group g to the isomeric state s
σ^*	cm^{-1}	the macroscopic cross section
σ_a^*	cm^{-1}	the macroscopic absorption cross section
σ_c^*	cm^{-1}	the macroscopic capture cross section
σ_f^*	cm^{-1}	the macroscopic fission cross section
σ_s^*	cm^{-1}	the macroscopic scattering cross section
σ_t^*	cm^{-1}	the total macroscopic cross section
ϕ	$\text{cm}^{-2} \text{s}^{-1}$	the scalar flux
ϕ^*		the source efficiency
$\phi_{0,i}$	$\text{cm}^{-2} \text{s}^{-1}$	the scalar flux per source particle as calculated by MCNP(X)
$\phi_{0,i,g}$	$\text{cm}^{-2} \text{s}^{-1}$	the scalar flux of group g per source particle as calculated by MCNP(X)
ϕ_g	$\text{cm}^{-2} \text{s}^{-1}$	the scalar flux of group g
ϕ_{MC}	$\text{cm}^{-2} \text{s}^{-1}$	the normalized scalar flux
φ		the angular flux
φ_0		the fundamental mode of a multiplying system
φ_0^+		the adjoint flux of a multiplying system
φ_s		the flux distribution in a subcritical system
φ^*		the source efficiency of an ADS
χ_f		the energy spectrum of the fission neutrons
ψ_a		the absorption density
ψ_c		the collision density
Ω		the direction variable in the phase space
Ω'		the direction of a particle prior to a scattering reaction
Ω_a		the particle's direction before an absorption event
Ω_c		the particle's direction before a collision event
Ω_t		the direction of a particle track
a		a coefficient in the correlation formula for fission product kinetic energy
a_i		the constant coefficient of the linear interpolation formula of a cross section

A		the atomic mass number
A_i		the atomic mass number of a nuclide i
b		a coefficient in the correlation formula for fission product kinetic energy
b_i		the slope used of the linear interpolation formula of a cross section
B		the transition matrix of the system of Bateman equations
B_{ij}	s^{-1}	the element with indices i and j of the transition matrix
BU_j	MWd/kgHM	the burn-up of material j
C		the constant used to renormalise the scalar flux ϕ_{MC} to the absolute scalar flux ϕ
C_i^m		the column vector in the m^{th} recursion used to solve the Bateman equations
C_n		the polynomial constant of power $n - 1$
e	C	the elementary charge of an electron
E	eV	the energy of a particle
E'	eV	the energy of a particle prior to a scattering reaction
E_α	eV	the energy of an α particle
E_a	eV	the particle's energy prior to an absorption event
E_c	eV	the particle's energy prior to a collision event
E_g	eV	the begin energy of group g
E_i	eV	the begin energy of an interval in the cross section energy grid
E_t	eV	the energy of a particle track
f_e		the fraction of all interactions that is an elastic scattering event
f_a		the fraction of all interactions that is an absorption
f_k		the fraction of all interactions where a track is killed
f_t		the fraction of the cross section retrieval time needed for the flux accumulation
f_x		the fraction of the cross section retrieval time needed for the linear interpolation
F		the fission operator in the Boltzmann equation
g		a response function in the collision of absorption estimator
h		a response function in a Monte Carlo estimator
H		the total number of histories
I_p		the proton beam current
k		the Boltzmann constant
k_{eff}		the effective multiplication factor

k_{eff}^a		the absorption estimator for k_{eff}
k_{eff}^c		the collision estimator for k_{eff}
k_{eff}^t		the track length estimator for k_{eff}
k_s		the source multiplication factor
l	cm	the distance to the next interaction
l_t	cm	the length of a particle track
L		the neutron loss operator in the Boltzmann equation
L_{ij}		the decay branching ratio of nuclide j to nuclide i
L_j		the decay branching ratio for mode j
$L_{j,O}$		the decay branching ratio for mode j used by ORI-GEN 2.2
M		the average number of possible reactions per nuclide
M_i		the average number of possible inelastic reactions per nuclide
M_1		a coefficient in the criticality calculation correction
M_2		a coefficient in the criticality calculation correction
M_i		the average number of different inelastic reactions
n		the number of points in a cross section energy grid
n_i	barn $^{-1}$ cm $^{-1}$	the atomic density of nuclide i
N		the number of nuclides in a cell
N_A		the number of Avogadro
N_b		the number of burnable materials
N_c		the number of collisions in a cell
N_e		the number of tracks entering a cell
N_i		the number of interactions in a cell
N_k		the number of tracks killed a cell
N_r		the number of nuclides for which reaction rates are calculated
N_s		the number of source point in a criticality cycle
N_{tr}		the total number of tracks
$N_{tr,l}$		the total number of tracks in a cell l
p_i		the probability to interact with nuclide i
$p_{i,a}$		the probability of neutron absorption when interacting with nuclide i
$p_{i,r}$		the probability of reaction r when a neutron interacts with nuclide i
$P_{0,j}$	MW	the specific normalisation power in a material j
$P_{c,t}$	MW	the power produced in a set of materials
P_j	MW	the power produced in a material j

P_t	MW	the total power of a system
P_{MC}	MW	the power corresponding to the normalised flux ϕ_{MC}
Q_i	MeV	the energy release from fission for component i
Q_c	MeV	the average energy release by neutron capture per fission
$Q_{c,\gamma}$	MeV	the average energy release per neutron capture event
Q_f	MeV	the total recoverable energy release per fission
Q_k	MeV	the kinetic energy of the fission fragments
$Q_{\gamma,d}$	MeV	the energy of the delayed γ radiation released after fission
$Q_{\gamma,p}$	MeV	the energy of the prompt γ radiation released after fission
Q_β	MeV	the energy of the β radiation released after fission
Q_ν	MeV	the energy carried away by neutrino emission after fission
$Q_{d,f}$	MeV	the recoverable energy directly released by fission
$Q_{f,g}$	MeV	the recoverable energy directly released by fission in group g
$Q_{i,f}$	MeV	the total recoverable energy per fission of nuclide i
$Q_{n,d}$	MeV	the kinetic energy of the delayed neutrons released after fission
$Q_{n,p}$	MeV	the kinetic energy of the prompt neutrons released after fission
$Q_{s,f}$	MeV	the total energy release per fission averaged for the entire system
$Q_{t,f}$	MeV	the total energy release per fission
\mathbf{r}		the position vector
\mathbf{r}_a		the position of an absorption event
\mathbf{r}_c		the position of a collision event
\mathbf{r}_t		the position of an interaction event
R		the total number of reaction rates
R_i		the number of reaction rates needed for nuclide i
s_e		the external neutron source operator
S		the absolute number of source particles
t	s	time
t_0	s	reference time
t_s	s	the Monte Carlo simulation time
$t_{s,i}$	s	the Monte Carlo simulation time in cell i
t_s^{MC}	s	the Monte Carlo simulation time for a code using unionised cross section tables

t_s^{MG}	s	the Monte Carlo simulation time for a code using universal unionised or multi-group cross section tables
t_k	s	the criticality calculation correction to the Monte Carlo simulation time
$t_{k,i}$	s	the criticality calculation correction to the Monte Carlo simulation time in cell i
t_m	s	the time required to calculate a multi-group spectrum
t_r	s	the reaction rate calculation time
$t_{r,i}$	s	the reaction rate calculation time in cell i
t_{MC}	s	the total CPU time required for a single step in a Monte Carlo burn-up calculation
t_{MGB}	s	the total CPU time required for a single step in a Monte Carlo burn-up calculation when using the multi-group binning approach
T	K	the temperature
$T_{1/2}$	s	the decay half-life
$T_{1/2,O}$	s	the decay half-life used by ORIGEN 2.2
v	cm s^{-1}	the neutron speed
V	cm^3	the volume of a cell or set of cells
V_l	cm^3	the volume of cell l
w		the weight of a particle
w'		the weight of a particle after an absorption
w_c		the weight of a particle prior to a collision
w'_a		the reduced particle weight after an absorption event
w_t		the weight of a particle track
W		the total initial weight of all simulated histories
W_s		the source weight in a criticality calculation
X		the column vector of atomic densities
Y		the fission yield
Y_g		the fission yield in group g
$Y_{ij,r}$		the yield of nuclide i for a reaction r on nuclide j
Y_s		the neutron source yield per proton
Z		the proton number
Z_i		the proton number of a nuclide i

List of publications

W. HAECK, B. VERBOOMEN, A. SCHUBERT, P. VAN UFFELEN, "Application of EPMA Data for the Development of the Code Systems TRANSURANUS and ALEPH", accepted for publication in Microscopy and Microanalysis (2007)

W. HAECK, B. VERBOOMEN, "An Optimum Approach to Monte Carlo Burn-Up", accepted for publication in Nuclear Science and Engineering (June 2007)

B. VERBOOMEN, W. HAECK, P. BAETEN, "Monte Carlo Calculation of the Effective Neutron Generation Time", *Ann. Nucl. Energy*, **33**, pp. 911-916 (2006)

W. HAECK, E. MALAMBU, V. P. SOBOLEV, H. AIT ABDERRAHIM, "Assessment of americium and curium transmutation in magnesia based targets in different spectral zones of an experimental accelerator driven system", *J. Nucl. Mat.*, **352**, pp. 285-290 (2006)

H. AIT ABDERRAHIM, Th. AOUST, E. MALAMBU, V. SOBOLEV, K. VAN TICHELEN, D. DE BRUYN, D. MAES, W. HAECK, G. VAN DEN EYNDE, "MYRRHA, A Pb-Bi experimental ADS: specific approach to radiation protection aspects", *Radiat. Prot. Dosimetry*, **116**, pp. 433-441 (2005)

W. HAECK, B. VERBOOMEN, "Validation of Nuclear Data using Lawrence Livermore Pulsed Sphere Experiments", *The American nuclear Society's 14th Biennial Topical Meeting of the Radiation Protection and Shielding Division (RPSD 2006)*, Carlsbad, USA, April 3-6, 2006

W. HAECK, B. VERBOOMEN, "ALEPH - A Monte Carlo Burn-up Code", *International Conference on Emerging Nuclear Energy Systems (ICENES 2005)*, Brussels, Belgium, August 21 - 26, 2005

Th. AOUST, J. CUGNON, W. HAECK, "Actinide transmutation by spallation", *International Conference on Emerging Nuclear Energy Systems (ICENES 2005)*, Brussels, Belgium, August 21 - 26, 2005

W. HAECK, B. VERBOOMEN, H. AIT ABDERRAHIM, C. WAGEMANS, "An Efficient Approach to Monte Carlo Burn Up", *Monte Carlo 2005 Topical Meeting (MC2005)*, Chattanooga, USA, April 17-21, 2005

E. MALAMBU, V. P. SOBOLEV, W. HAECK, H. AIT ABDERRAHIM, "Modelling Incineration of Minor Actinides", *Advanced Reactors With Innovative Fuels (ARWIF 2005)*, Oak Ridge, USA, February 16-18, 2005

V. P. SOBOLEV, S. LEMEHOV, W. HAECK, H. AIT ABDERRAHIM, "Modelling Long Term Performances of Minor Actinide Fuel Targets in Experimental ADS MYRRHA", *Advanced Reactors With Innovative Fuels (ARWIF 2005)*, Oak Ridge, USA, February 16-18, 2005

S. PILATE, B. LANCE, H. GABAIEFF, A. SANTAMARINA, R. JACQMIN, D. BERNARD, B. VERBOOMEN, W. HAECK, J. C. KUIJPER, D. da CRUZ, "VALMOX: Validation of Nuclear Data for High Burn Up MOX Fuels - Final Re-

port”, Contract nr FIKS-CT-00191 (2005)

E. MALAMBU, W. HAECK, V. P. SOBOLEV, H. AIT ABDERRAHIM, “MA and LLFP Transmutation Performance Assessment in the MYRRHA Small-scale ADS”, *P&T: 8th Information Exchange Meeting*, Las Vegas, USA, November 9-11, 2004

W. HAECK, H. AIT ABDERRAHIM, C. WAGEMANS, “ K_{eff} and K_s Burn-Up Swing Compensation in MYRRHA”, *OECD/NEA - Fourth International Workshop on Utilization and Reliability of High Proton Power Accelerators (HPPA4)*, Korea, May 2004

H. AIT ABDERRAHIM, P. KUPSCHEUS, Ph. BENOIT, E. MALAMBU, V. P. SOBOLEV, Th. AOUST, K. VAN TICHELEN, B. ARIEN, F. VERMEERSCH, D. DE BRUYN, D. MAES, W. HAECK, “MYRRHA, A Multipurpose Accelerator Driven System for R&D. State-of-the-art at mid-2003”, *International Workshop on P&T and ADS Development 2003*, Mol, Belgium, October 6-8, 2003

Those who cannot remember the past are condemned to repeat it.

George Santayana (1863 - 1952)

Study the past if you would define the future.

Confucius (551 BC - 479 BC)



Introduction and background

1.1 Monte Carlo and advanced nuclear systems

Nuclear energy has become a mature technology which has benefited from decades of development and industrial experience. It has the great potential for contributing to future sustainable supply of energy, taking advantage of past experience and ongoing R&D programs on advanced nuclear systems.

Nuclear reactors are often catalogued using their “generation”. The PWR, BWR, CANDU, etc. reactors that are currently in service are generally referred to as generation II reactors. They were constructed and commissioned between 1965 and 1995. A generation III reactor is a development from these generation II nuclear reactor designs. The first generation III reactors (the Advanced Boiling Water Reactor or ABWR) were commissioned in Japan in 1996. Another generation III design that is currently being constructed is the European Pressurised Reactor (EPR). These generation III reactors incorporate evolutionary improvements in design which have been developed during the lifetime of the generation II reactor, such as improved fuel technology, passive safety systems and standardised design.

Generation IV reactors are a set of conceptual nuclear reactor designs that are currently being researched. These designs are generally not expected to be available for commercial construction before 2030. Research into these reactor types was officially started by the Generation IV International Forum (GIF) based on several technology goals. The primary goals being to improve nuclear safety, improve proliferation resistance, minimise waste and natural resource utilisation and to decrease the cost to build and run such plants. These designs include the Super Critical Water-cooled Reactor (SCWR, a water cooled thermal reactor), the Very High Temperature Reactor (VHTR, a thermal gas cooled reactor), the Molten Salt Reactor (MSR) and Lead, Sodium or Gas cooled Fast Reactors (respectively LFR, SFR and GFR).

More advanced generation III designs that are part revolutionary but fall short of generation IV by being at least part evolutionary are often termed generation III+ reactors. Examples of such generation III+ systems include

the Economic Simplified Boiling Water Reactor (ESBWR, based on the ABWR design), the AP1000 (based on the PWR) and the Pebble Bed Modular Reactor (PBMR, a high temperature helium cooled reactor with a direct cycle helium turbine).

Because they differ significantly from their mainstream generation II counterparts in both concept and design, these generation III, generation III+ and generation IV nuclear systems are often referred to as advanced nuclear systems.

Another area of intense research in the field of nuclear energy concerns the existing nuclear waste and on how to dispose of it. The accelerator driven system (ADS) is recognised as a promising system for the purpose of nuclear waste transmutation and minimisation of spent fuel radio-toxicity. The concept of an ADS consists of coupling a high energy proton accelerator to a spallation target (for instance a liquid metal target) surrounded by a sub-critical fast core. The primary neutron source created in the spallation target is multiplied in the sub-critical core and drives the reactor. The sub-critical operating state of an ADS introduces beneficial safety-related features allowing for the use of cores employing fuel systems containing pure transuramics with a large fraction of minor actinides, thereby offering increased incineration rates of minor actinide waste and minimal deployment of advanced (and expensive) partitioning and transmutation technologies. An example of such an ADS is the MYRRHA system which is currently being studied at SCK•CEN [1].

For these advanced nuclear systems and especially for the hybrid systems like ADS with its sub-criticality and external neutron source that make it radically different for any other system, the Monte Carlo method has become the preferred calculation tool. The MCNP line of Monte Carlo codes (MCNP4, MCNPX and MCNP5) [2, 3, 4] are the most common used Monte Carlo codes.

Monte Carlo has the ability to handle nuclear data not only in its most basic but also most complex form (namely continuous energy cross sections, complex interaction laws, detailed energy-angle correlations, multi-particle physics, $S(\alpha,\beta)$ tables for thermal neutron scattering by molecules and crystalline solids, unresolved resonance probability tables, etc.). These codes can also handle geometries from simple 1D to extremely complex 3D. Normal critical systems, sub-critical systems with an external source, etc. can all be calculated with a single code, practically without making any approximation.

In the past, Monte Carlo could only be applied to relatively simple problems to give reliable results in a reasonable amount of time. The development of computer technology and improvements in the basic Monte Carlo algorithms have also helped Monte Carlo techniques to become more and more mainstream. Today, a commercial PC based cluster environment offers the same computational power as a supercomputer for a fraction of the price. This fact combined with the possibility of parallel calculation inherent to Monte Carlo has made cluster computing and therefore Monte Carlo extremely popular.

1.2 Monte Carlo and burn-up applications

Proper fuel management is important for the operation of any nuclear reactor. It ensures that a core load meets its operational requirements (being energy output, neutron flux levels, etc.) within adequate safety margins. Fuel management calculations analyse depletion characteristics from the beginning to the end of the operational cycle and design and/or optimise reload configurations. These configurations have to maximise the operating flexibility, insure that the safety requirements are met and that the fuel costs are minimised. They also help define requirements such as initial fuel compositions, cycle length, changes in power densities during operation and help define the reactivity control during the cycle.

In fuel management calculations, three principle characteristics of the reactor core are determined:

- the evolution of the core reactivity;
- the power distributions to provide data for the safety design;
- the isotopic inventory at the end of the cycle to permit economic analysis.

but also other reactor physics parameters such as the control rod worth, the effective delayed neutron fraction β_{eff} and the effective neutron lifetime Λ_{eff} for the purpose of safety analysis over the course of the operational cycles.

The basis of fuel management is a depletion or burn-up calculation which provides accurate fuel compositions as a function of time. The depletion code is combined with other codes (transport codes, safety analysis codes, etc.) in a unique sequence to analyse the core and deplete it for many operational conditions.

Various depletion codes based on both deterministic and stochastic methods are available worldwide. APOLLO2 [5], WIMS [6], etc. are well known examples based on deterministic neutron transport methods. Most of these codes are what is referred to as “production codes”, in that they are used on a daily basis. They are used extensively for specific applications where their performance is enhanced through adjustments to integral experiments. In most cases, these codes are limited to simple geometries and/or specific systems making them unsuitable for the more exotic applications.

Since the late nineties, burn-up codes coupling Monte Carlo to depletion modules have got more and more attention, examples being MONTEBURNS [7] and MOCUP [8] (both based on MCNP [2]). Other examples of such burn-up codes are MC-REBUS [9], MCB [10], MCWO [11] and MCODE [12] which are all based on versions of MCNP. Since 2006 a depletion capability has been implemented as a standard feature in MCNPX 2.6.a and above by coupling of MCNPX with CINDER90 [13, 14, 15, 16, 17].

The incentive of creating such Monte Carlo burn-up codes arises from its ability to provide the most accurate locally dependent spectra and flux values in realistic 3D geometries of any type. And they can also provide answers in application areas where the traditional deterministic codes are lacking. These capabilities linked with the ability to handle nuclear data not only in its most basic but also most complex form (namely continuous energy cross sections, complex interaction laws, detailed energy-angle correlations, multi-particle physics, etc.) could make Monte Carlo burn-up codes very powerful, especially for the earlier mentioned hybrid and advanced nuclear systems.

Still, such Monte Carlo burn-up codes have had limited success mainly due to the rather long CPU time required to carry out any very detailed and accurate calculation, even with modern computer technology. To work around this issue, users often have to reduce the number of nuclides in the evolution chains or to consider either longer irradiation time steps (thereby reducing the number of burn-up steps) and/or larger spatial cells to burn, jeopardizing the accuracy of the calculation in all cases.

An example of this unfortunate practice is MCODE, an interface code between MCNP and ORIGEN2 developed at Massachusetts Institute of Technology (MIT) in 2003 [12, 18] where it is up to the user to select the actinides and fission products used in the calculation. Furthermore, MCODE only calculates the single group cross sections for the (n,γ) reaction for all defined fission products, neglecting reactions like $(n,2n)$, (n,α) and (n,p) . As a result, depletion of a neutron poison like ^{10}B will therefore be suspect as the (n,α) reaction is extremely important for this nuclide.

Another weak point (either true or conceived) of Monte Carlo burn-up codes is their complexity. These codes often use a script or link approach so that the user would have to understand and manage a large number of input and output files while the conversion of data from one form into another would introduce approximate results due to successive round off [14]. This can be solved by providing an easy to use interface that actually “hides” the burn-up code (which is something the new transmutation option in MCNPX has achieved [16]).

1.3 Nuclear data and burn-up applications

Both the Monte Carlo code and the depletion code share a basic need for microscopic cross section data, although in a different form. The depletion code only requires one group cross section for a limited number of reactions like the (n,γ) , $(n,2n)$, $(n,3n)$, (n,α) , (n,p) and the fission reactions. The Monte Carlo code on the other hand needs energy dependent cross sections for all possible reactions including elastic scattering, etc.

The other nuclear data requirements for both the transport and depletion module are however quite different. The Monte Carlo code needs for instance

energy spectra and angular distributions of secondary particles, etc. The depletion code on the other hand needs fission yield data, branching ratios to take into account isomer production, decay data, etc.

All of this data can be found in one form or another in the different sub-library files of any of the existing evaluated nuclear data libraries like JEF 2.2 [19], JEFF 3.1 [20], JENDL 3.3 [21], ENDF/B-VI.8 and the latest ENDF/B-VII.0 [22] which all use the ENDF format [23]. In the case of the fission Q_f -value there is a minor limitation because the γ radiation resulting from structural material activation is system dependent and can therefore not be included in an evaluation.

The importance of nuclear data is often overlooked or even ignored by many while it can make or break any calculation. You can have the best codes in the world but if the nuclear data that you are feeding into those codes is lacking, the results themselves will be questionable. By using data from the ENDF files, we would have no need of other third party data or models. The use of these ENDF files will therefore provide us with a consistent set of data, for both the depletion and transport module. This approach will also allow us to quickly change our data when newer (and better) evaluations become available, making the burn-up code very flexible in its use of nuclear data.

1.4 Main objectives

Summarized, the main objectives of this work are:

- To identify, develop and implement methods for Monte Carlo with burn-up to attain the highest accuracy for the smallest computing effort possible.
- To provide consistent sets of nuclear data that encompasses all aspects of the burn-up calculation (cross sections, number of neutrons per fission, fission Q -values, branching ratios to isomer states, fission yields, etc.)

The ultimate goal is to provide the Monte Carlo community with an efficient, flexible and easy to use alternative for Monte Carlo burn-up and activation calculations.

Prediction is very difficult, especially about the future.

Niels Bohr (1885 - 1962)

2

The ORIGEN depletion code

2.1 Basic concepts and tasks of a burn-up code

Every PhD in the field of reactor physics and neutron transport will ultimately fall back upon the Boltzmann transport equation, and this one is no exception. The Boltzmann equation describes the detailed neutron balance, i.e. the production and loss at every point in the phase space (energy E , position \mathbf{r} , direction Ω and time t). In its integro-differential form, it looks like this [24]:

$$\begin{aligned} \frac{1}{v} \frac{\partial}{\partial t} \varphi(\mathbf{r}, E, \Omega, t) = & -\Omega \cdot \nabla \varphi(\mathbf{r}, E, \Omega, t) - \sigma_t^*(\mathbf{r}, E, t) \varphi(\mathbf{r}, E, \Omega, t) \\ & + \int_0^\infty \int_{4\pi} \sigma_s^*(\mathbf{r}, E' \rightarrow E, \Omega' \rightarrow \Omega, t) \varphi(\mathbf{r}, E', \Omega', t) d\Omega' dE' \\ & + \frac{\chi_f(E)}{4\pi} \int_0^\infty \bar{v}_t(E') \sigma_f^*(\mathbf{r}, E', t) \int_{4\pi} \varphi(\mathbf{r}, E', \Omega', t) d\Omega' dE' \\ & + s_e(\mathbf{r}, E, \Omega, t) \end{aligned} \quad (2.1)$$

in which:

- v is the neutron speed;
- φ is the angular flux, which integrated over all directions gives the scalar flux ϕ :

$$\phi(\mathbf{r}, E, t) = \int_{4\pi} \varphi(\mathbf{r}, E, \Omega, t) d\Omega \quad (2.2)$$

- σ_t^* is the total macroscopic cross section given by:

$$\sigma_t^*(\mathbf{r}, E, t) = \sigma_s^*(\mathbf{r}, E, t) + \sigma_c^*(\mathbf{r}, E, t) + \sigma_f^*(\mathbf{r}, E, t) \quad (2.3)$$

where σ_s^* , σ_c^* and σ_f^* are respectively the macroscopic scattering, capture and fission cross section;

- χ_f is the energy spectrum of the fission neutrons;
- \bar{v}_t is the total average number of neutrons released after fission (both prompt \bar{v}_p and delayed \bar{v}_d);
- $\sigma_s^*(\mathbf{r}, E' \rightarrow E, \Omega' \rightarrow \Omega, t)$ is the macroscopic double differential scattering cross section, which gives us the macroscopic scattering cross section $\sigma_s^*(\mathbf{r}, E, t)$ by integrating $\sigma_s^*(\mathbf{r}, E' \rightarrow E, \Omega' \rightarrow \Omega, t)$ over all directions Ω' and energies E' of the outgoing neutrons:

$$\sigma_s^*(\mathbf{r}, E, t) = \int_0^\infty \int_{4\pi} \sigma_s^*(\mathbf{r}, E \rightarrow E', \Omega \rightarrow \Omega', t) d\Omega' dE' \quad (2.4)$$

- s_e is the external neutron source, which is independent of the angular flux φ .

The macroscopic cross sections σ^* that can be found in the Boltzmann equation are a function of the atomic densities n_i and microscopic cross sections σ of every nuclide involved in the neutron transport problem:

$$\sigma^*(\mathbf{r}, E, t) = \sum_i n_i(\mathbf{r}, t) \sigma_i(E) \quad (2.5)$$

The time dependence in the Boltzmann equation limits itself to the angular flux φ (and the associated scalar flux ϕ) and the compositions of the different materials in the transport problem through the atomic densities n_i . The time dependence of the angular and scalar flux is however a direct result from variations in the atomic densities.

The time dependence of those atomic densities (when the material is subjected to radiation or when it decays) is described by the Bateman equations, another set of coupled linear differential equations. For a particular nuclide i , these equations can be written in their most general form as:

$$\begin{aligned} \frac{d}{dt} n_i(\mathbf{r}, t) &= \sum_{j \neq i} L_{ij} \lambda_j n_j(\mathbf{r}, t) - \lambda_i n_i(\mathbf{r}, t) \\ &+ \sum_{j \neq i} \sum_r \int n_j(\mathbf{r}, t) Y_{ij,r}(E) \sigma_{j,r}(E) \phi(\mathbf{r}, E, t) dE \\ &- \sum_r \int n_i(\mathbf{r}, t) \sigma_{i,r}(E) \phi(\mathbf{r}, E, t) dE \end{aligned} \quad (2.6)$$

in which:

- n_i is the atomic density of nuclide i ;
- λ_i is the total decay constant of nuclide i ;

- L_{ij} is the decay branching ratio of nuclide j to nuclide i (the fraction of all disintegrations of nuclide j that results in the creation of nuclide i);
- $Y_{ij,r}$ is the yield of nuclide i for reaction r on nuclide j (the amount of nuclide i created in a reaction r on nuclide j);
- $\sigma_{i,r}$ is the microscopic cross section of nuclide i for a reaction r ;
- ϕ is the scalar particle flux.

This equation can be cast in a more compact form:

$$\frac{d}{dt} n_i(\mathbf{r}, t) = \sum_j B_{ij}(\mathbf{r}, t) n_j(\mathbf{r}, t) \quad (2.7)$$

where B_{ij} is an element of the transition matrix of the Bateman equations:

$$B_{ij}(\mathbf{r}, t) = \begin{cases} L_{ij}\lambda_j + \sum_r Y_{ij,r}(\mathbf{r}, t) \sigma_{j,r}(\mathbf{r}, t) \phi(\mathbf{r}, t) & \text{for } i \neq j \\ -\lambda_i - \sum_r \sigma_{i,r}(\mathbf{r}, t) \phi(\mathbf{r}, t) & \text{for } i = j \end{cases} \quad (2.8)$$

and where the following spectral averaged one group flux ϕ , yields $Y_{ij,r}$ and one group cross sections $\sigma_{i,r}$ are defined as:

$$\phi(\mathbf{r}, t) = \int \phi(\mathbf{r}, E, t) dE \quad (2.9)$$

$$Y_{ij,r}(\mathbf{r}, t) = \frac{\int Y_{ij,r}(E) \sigma_{j,r}(E) \phi(\mathbf{r}, E, t) dE}{\int \sigma_{j,r}(E) \phi(\mathbf{r}, E, t) dE} \quad (2.10)$$

$$\sigma_{i,r}(\mathbf{r}, t) = \frac{\int \sigma_{i,r}(E) \phi(\mathbf{r}, E, t) dE}{\int \phi(\mathbf{r}, E, t) dE} \quad (2.11)$$

Together with the Boltzmann equation, the Bateman equations form a complete and closed system of equations for the description of time dependent particle transport.

There exists also a time dependence in both the atomic densities and even the microscopic cross sections themselves due to temperature effects like thermal expansion of the materials in the system, the Doppler effect on the cross section resonances, etc. To take such effects into account would require the use of the heat transfer equations, the Navier-Stokes equation, etc. in addition to the Boltzmann equation and Bateman equations, which will unnecessarily overcomplicate the problem.

The existence of delayed neutrons also introduces a time dependent effect. The time scale in which these delayed neutrons are released after fission (which is of the order of seconds to minutes) is however so small compared to the time period in burn-up applications that it can be ignored for our type

of applications. For transient calculations however these delayed neutrons cannot be ignored.

Solving these equations in this form is practically impossible. In order to simplify the time dependence, an activation code (also known as a depletion, evolution or burn-up code) will iterate between a steady state transport calculation (which uses either deterministic or stochastic methods) and a zone by zone material evolution through the Bateman equations. In this case, the material compositions in every one of those zones are considered spatially constant when determining the particle flux in the steady state transport calculation and the particle flux (and the associated spectrum) is assumed to be constant in space and time during a time step in the evolution calculation. As such, the spectral averaged quantities given above are spatially averaged in each burn-up zone:

$$\phi(t) = \frac{\int \int \phi(\mathbf{r}, E, t) dEdV}{\int dV} \quad (2.12)$$

$$Y_{ij,r}(t) = \frac{\int \int Y_{ij,r}(E) \sigma_{j,r}(E) \phi(\mathbf{r}, E, t) dEdV}{\int \int \sigma_{j,r}(E) \phi(\mathbf{r}, E, t) dEdV} \quad (2.13)$$

$$\sigma_{i,r}(t) = \frac{\int \int \sigma_{i,r}(E) \phi(\mathbf{r}, E, t) dEdV}{\int \int \phi(\mathbf{r}, E, t) dEdV} \quad (2.14)$$

Ideally, these burn-up zones should properly account for the spatial dependence of the neutron flux in a reactor. This is also the case for the time steps to take into account the changes in the neutron spectrum during irradiation. Fissions products like ^{135}Xe and ^{149}Sm will act as a neutron poison which will have its impact on the neutron spectrum. Due to the large cross sections of ^{135}Xe , it is sometimes necessary to use a small time step (of the order of a few days) to properly take into account the build-up of this nuclide, especially for low burn-up fuel. On the other hand, neutron capture on fertile material like ^{238}U will ultimately result in the creation of fissile nuclides like ^{239}Pu and ^{241}Pu . During burn-up the importance of those created fissile nuclides will increase as the original fissile material is depleted, resulting in significant spectral changes because the cross sections of those nuclides are distinctly different.

The previously described method of solving the system of equations is of course not required if one adopts a stochastic treatment for the evolution of the material composition as well as for the transport calculation. Such a treatment has however not been attempted at present, as far as we know.

The basic tasks of a true depletion code can thus be summarized as follows for every step in the evolution calculation:

- perform a steady state transport calculation and update the spectral and spatial averaged one group yields $Y_{ij,r}$, cross sections $\sigma_{i,r}$ (for every possible nuclide and reaction in the transmutation chains), flux values ϕ and other relevant data for use by the depletion module;

- solve the Bateman equations for every burn-up zone in the problem using the data derived by the transport calculation;
- pass on the new material composition for the next step.

2.2 The origin of ORIGEN

The original Oak Ridge Isotope GENerator or ORIGEN code was developed in the late 1960s and early 1970s at Oak Ridge National Laboratory (ORNL) Chemical Technology Division as a tool for calculating nuclide build-up and decay. At the time, coupled neutron transport and depletion calculations as described in the previous section were very impractical and time consuming. ORIGEN was therefore developed as a standalone depletion module that made use of independently generated data libraries.

This first version of ORIGEN was primarily used for generating spent fuel and waste characteristics which served as a basis for the study and design of waste processing plants, etc. Because of the generic applications, ORIGEN only needed to be representative for those limited applications. This was entirely reflected in the data used by ORIGEN which consisted of tabulated thermal cross sections, resonance integrals and chain fission product yields. In addition, the resonance integrals of the primary fissile nuclides were adjusted to obtain a better agreement with experiments.

When ORIGEN was made available outside ORNL, it quickly became a popular tool due to its simplicity and its relative detailed output. When people started using ORIGEN for applications that required a lot more precision than the previous generic fuel cycle studies (like environmental studies which needed precise values for nuclides like ^3H , ^{14}C , etc.), it became clear that an update to the ORIGEN code was required.

At first, this was achieved by updating the data libraries but it eventually lead to the creation of ORIGEN2 in 1980 [25, 26, 27] which was updated to ORIGEN 2.1 in 1991 and finally to ORIGEN 2.2 in 2002. By the time ORIGEN 2.2 was released, the code had already been integrated into the SCALE code system [28] under the name ORIGEN-S.

We will use ORIGEN 2.2 for this work because it treats the most general case of the evolution chains with all of its cyclic chains and branches and because it was developed as a flexible standalone product that can be integrated easily in a true burn-up code (as described in the previous section). ORIGEN-S on the other hand was designed to be used along with other modules of the SCALE code system which generate cross section libraries in three groups corresponding to thermal, epi-thermal and fast neutrons. Those three group cross section libraries were introduced to improve the accuracy of the depletion calculation but such a treatment is useless for our purpose as we will use a Monte Carlo code to calculate the proper single group cross section values anyway.

2.3 The matrix exponential method

As mentioned in section 2.1, the cross sections and neutron flux are considered constant during a time step in the depletion calculation. As a result, the system of Bateman equations is a homogeneous set of first order ordinary differential equations with constant coefficients. From its inception, ORIGEN and its successors have used the matrix exponential method to solve this system of equations.

The solution of a homogeneous set of first order ordinary differential equations with constant coefficients can be written as:

$$X(t) = X(t_0) \exp(Bt) \quad (2.15)$$

where X is a column vector with the atomic densities n_i and B is the transition matrix (given by equation 2.8). The function $\exp(Bt)$ itself is the matrix exponential function. It behaves itself like a normal exponential function, with the exception that we calculate the exponential of a matrix instead of a real number:

$$\exp(Bt) = \sum_{m=0}^{\infty} \frac{(Bt)^m}{m!} \quad (2.16)$$

This method has essentially two distinct problems. The first being the memory requirements to store the entire matrix (which is a sparse matrix with both very large and very small numbers). The second being computational problems and stability of the method for a system with widely separated eigenvalues, which is certainly the case for the Bateman equations since the coefficients in the transition matrix range from half lives of seconds to billions of years.

The first problem is solved by applying a recursion algorithm for the computation of the matrix exponential function. The atomic density n_i of a nuclide can be computed with

$$n_i(t) = \sum_{m=0}^{\infty} C_i^m \quad (2.17)$$

where C_i^m is determined by recursion:

$$C_i^0 = n_i(t_0) \quad (2.18)$$

$$C_i^m = \frac{t}{m} \sum_j B_{ij} C_i^{m-1} \quad (2.19)$$

By working in this way, only one vector C_i^m along with the current solution must be stored by ORIGEN 2.2 instead of the entire transition matrix.

This is however impractical for a large number of nuclides. Furthermore, quite a lot of these nuclides will have short half lives which correspond to large norms of the matrix. For those nuclides, it is however possible to use

the secular or transient equilibrium and therefore determine the compositions for these nuclides analytically. ORIGEN 2.2 therefore only uses the matrix exponential method for those nuclides whose diagonal element is less than a pre-set value.

It is important to insure that the precision of the answer will not be lost due to the addition and subtraction of nearly identical numbers in equation 2.17. It has been shown [25] that the accuracy of the computed matrix exponential function can be maintained at any desired value by controlling the time step so that the norm of the matrix Bt is less than a predetermined value which is determined by the word length of the computer used for the calculations. The series expansion of the matrix exponential function itself (given by equation 2.16) is cut off using a rule of thumb derived for ORIGEN 2.2 that is a function of the norm of the transition matrix. This rule of thumb on the cut off of the series expansion limits the error to less than 0.1 % [25, 29].

For ORIGEN 2.2 the maximum value of the norm of the transition matrix B is set to 13.8155 which corresponds to a maximum number of 53 terms for the series expansion of the matrix exponential function. In general the norm is usually less than this maximum value and 30 terms or less are sufficient to properly evaluate the series.

For the calculation of the short lived nuclides, ORIGEN 2.2 makes a distinction between short lived nuclides that do not have long lived precursors and those that do. The solution for the first category is determined before the application of the matrix exponential method. These short lived nuclides will reach an equilibrium within the time step when their removal time is less than 14.4 % of the current time step. As a result, the simple asymptotic solutions that give this equilibrium value can be used to determine the composition at the end of the time step.

The second category of short lived nuclides is treated after the application of the matrix exponential method. In this case, the short lived nuclide is assumed to be in secular equilibrium with its parent at the end of any time interval. The concentration of the parent was determined earlier prior to this step. The concentration of the daughter is calculated through the application of equilibrium to the Bateman equations:

$$\frac{d}{dt}n_i = \sum_j B_{ij}n_j = 0 \quad (2.20)$$

This is a set of linear algebraic equations for the concentrations of the short lived nuclides. It is solved through the application of the Gauss-Seidel iterative technique. This iterative procedure converges very rapidly because cyclic chains are not usually encountered and the procedure is reduced to a direct solution.

At this point the concentration of all nuclides at the end of a time step has been calculated and stored. The results can then be output or used as the initial concentrations for the next time step.

2.4 Cross section, decay and photon libraries

As was explained previously, the single group cross sections used in the Bateman equations have to be weighted on the proper spectrum which in turn depends on the application. Designed as a stand-alone product, ORIGEN 2.2 therefore has a number of single group cross section libraries corresponding to specific reactor types, for instance a PWR with UO₂ or MOX based fuel, etc. Even though ORIGEN 2.2 comes with over 30 different libraries, its application field is limited to those specific reactor types. For newer reactor types like generation IV systems or even ADS new libraries would need to be constructed which requires a neutron transport calculation as was explained earlier. Furthermore, these ORIGEN 2.2 libraries are based on core averaged neutron spectra so they do not take into account spectral variations due to the heterogeneity of a reactor. Simulating a single fuel pin in a fuel assembly taking into account the influence of the neighbouring fuel pins is therefore impossible.

Due to the development history of both ORIGEN and ORIGEN2 there are some limitations in the possible reactions used by ORIGEN 2.2. They are even different for the various types of materials considered by ORIGEN. By default, ORIGEN 2.2 distinguishes between three types of materials: activation products, fission products and actinides (along with their daughters).

For activation products and fission products, ORIGEN 2.2 needs single group data for the (n,γ), (n,2n), (n,α) and (n,p) reactions. Actinides on the other hand also need data on the (n,γ) and (n,2n) reactions but instead of the (n,α) and (n,p) reaction they need the (n,3n) and fission reactions. In other words: (n,3n) is not considered for activation and fission products while (n,α) and (n,p) is not taken into account for actinides. ORIGEN 2.2 does however have the capability of adding more reactions (using so-called non standard flux dependent reactions [26]) but it is not used very often.

In addition to the reaction data described above, direct fission yield data is required to correctly account for the fission products. In ORIGEN 2.2, these fission yields are limited to the direct fission yields of only 8 primary actinides (²³²Th, ²³³U, ²³⁵U, ²³⁸U, ²³⁹Pu, ²⁴¹Pu, ²⁴⁵Cm and ²⁵²Cf) which is a legacy of the original ORIGEN code. The U and Pu isotopes are well represented in this list (ORIGEN and ORIGEN 2.2 were written for U and Pu based fuels). There also appears to be a rather large mass gap in the list of 8 actinides between ²⁴¹Pu and ²⁴⁵Cm.

ORIGEN assumed that fissioning actinides that were not in this list did not produce fission products. This assumption was necessitated by the fact that (at the time) no accurate fission yield data was available for most actinides and that using more actinides would significantly increase the memory requirements of the code.

It is an acceptable assumption for thermal reactors (differences are within a few tenths of a percent) but not in other types of reactors where the other

actinides are more important. This problem was “solved” in ORIGEN2 and its successors, but instead of increasing the number of actinides with direct fission yields (which would have been the obvious solution) ORIGEN2 used an approach that does not involve changing this list of 8 actinides.

First of all, ORIGEN 2.2 determines the most important actinide without direct fission yields and identifies the closest actinide from the list (this is often referred to as the closest connected actinide). Fission of actinides without direct fission yields will then use the yields of this closest connected actinide.

This might prove to be a problem for applications where there are already significant amounts of minor actinides present that are not included in this list of 8 actinides, like in systems using uranium-free fuel for the transmutation of minor actinides. On the other hand, these issues are of little importance for the more traditional applications for which ORIGEN and ORIGEN2 were designed in the first place. In a PWR reactor with UO₂ or MOX fuel, all important fissile and fertile actinides have direct fission yields (²³⁵U, ²³⁸U, ²³⁹Pu and ²⁴¹Pu). During the operation of such a reactor, small amounts of Am, Cm and other minor actinides will be produced. Their contribution to the total fission rate and therefore to the fission product inventory will be so small that using the fission yields of the closest connected actinide will barely be noticed.

Apart from the cross section libraries, ORIGEN 2.2 also needs a radioactive decay data library and a photon data library. The decay library contains all the radioactive decay data needed by ORIGEN 2.2 (being the different decay modes, decay branching ratios and half-lives) in addition to recoverable heat energy per disintegration, natural abundances and chemical toxicities.

The decay modes considered by ORIGEN 2.2 are β^- -decay (both to the ground state and first isomeric state), β^+ -decay or electron capture (both to the ground state and first isomeric state), α -decay, isomeric transitions (from an excited isomeric state to the ground state), spontaneous fission and β -decay followed immediately by neutron emission (as would be the case in the decay of ⁸⁹Br to ⁸⁸Kr).

The nuclide identifiers supplied by the decay libraries also defines the total list of all nuclides considered in the ORIGEN 2.2 calculations. If a cross section library contains data for a reaction that will lead to the production of a nuclide that is not included in the decay library, then the composition of this nuclide will not be reported by ORIGEN 2.2.

The photon library is used to determine the number of photons and the photon energy emission rate in 18 energy groups as a function of irradiation time or decay time. The photons included in this file are γ -rays, X-rays, conversion photons, secondary γ -rays from (α, n) interactions and fission product γ -rays from spontaneous fission and bremsstrahlung. Prompt γ -rays from fission and neutron capture are however not included [27].

With the making of ORIGEN2 in the beginning of the 1980s, these decay and photons libraries were updated using data from the Evaluated Nuclear Structure Data Files (or ENSDF file) and ENDF/B-IV nuclear data files (if the

data could not be found in these ENSDF files). Unfortunately no updates were made to these files since then.

Apart from these data files that can be changed and/or updated easily, ORIGEN 2.2 also uses other data that is hard-coded into the code. In ORIGEN terminology, these are often referred to as "miscellaneous initialisation data" although this does not even begin to cover the importance of some of them.

2.5 Hard-coded data and approximations

2.5.1 The total recoverable energy per fission

The value of the total recoverable energy per fission Q_f intervenes in the calculation of burn-up and neutron flux levels. ORIGEN 2.2 has three different irradiation modes: normal decay, constant flux and constant power. Because the Bateman equations use the absolute neutron flux, it is necessary to calculate the equivalent flux level in a constant power step. The power P produced in a reactor at every point in time is always proportional to the total neutron flux ϕ :

$$P = e \sum_i Q_{i,f} n_i \sigma_{i,f} \phi \quad (2.21)$$

where n_i , $\sigma_{i,f}$ and $Q_{i,f}$ are respectively the atomic density (in units of atoms barn $^{-1}$ cm $^{-1}$), the fission cross section (barn) and the total recoverable energy from fission (MeV) for actinide i .

The total recoverable energy from fission has basically three distinct components: the prompt energy release (the kinetic energy of the fission fragments, prompt β and γ radiation, etc.), the delayed energy release (delayed β and γ radiation, etc.) and the γ radiation resulting from structural material activation. This last component is often overlooked because it would require a coupled neutron and γ calculation.

The original ORIGEN code used a constant value of 200 MeV per fission (which is appropriate for ^{235}U) for the total recoverable energy per fission for every actinide. Even now, some depletion codes continue to use a fixed value like for instance 200 MeV for the total recoverable energy per fission.

This assumption worked quite well since the fission cross sections used by ORIGEN were adjusted to take into account the difference with the real value. However, for ORIGEN2 the decision was made to use the actual fission cross section as calculated by more sophisticated reactor physics codes. In order to calculate the proper neutron flux from a given power value, realistic values for the total recoverable energy per fission would have to be used.

A semi-empirical formula was created for ORIGEN2 to calculate the recoverable energy per fission simply because little to no recoverable fission energy data were available at the time:

$$Q_{i,f} = 1.29927 \cdot 10^{-3} (Z_i^2 \sqrt{A_i}) + 33.12 \quad (2.22)$$

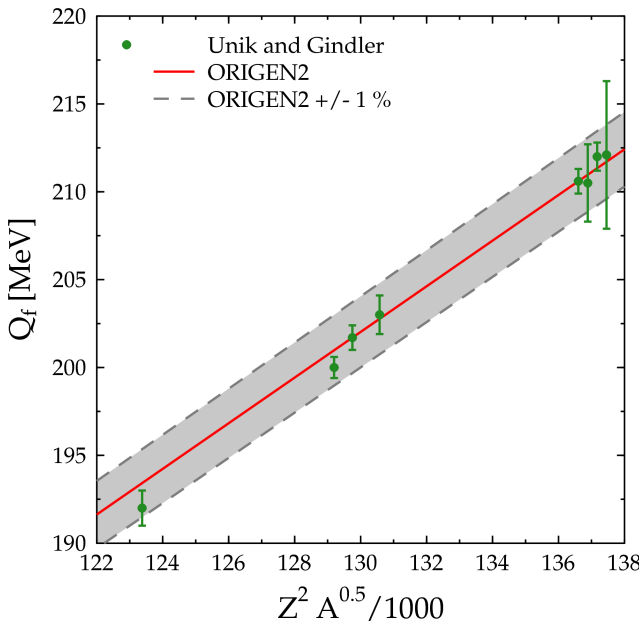


Figure 2.1: Total average recoverable energy from fission Q_f : ORIGEN2 semi-empirical formula versus Unik and Gindler data.

In this equation Z_i and A_i are respectively the proton and atomic mass number of the nuclide i . Equations of this form ($aZ^2\sqrt{A} + b$) are often used for the correlation of fission product kinetic energy, although most will use $-1/3$ (which is a result from the liquid drop model) as the exponent for the atomic mass number A instead of $1/2$ as it is used in this equation. This last value was chosen because it gave better results compared to the values determined by Unik and Gindler [25, 30]. The values of the coefficients a and b were determined by using the total recoverable energy per fission values for ^{235}U and ^{239}Pu as given by Unik and Gindler.

Unik and Gindler also included an estimate for the average energy release Q_c due to neutron capture in their values. When we define $Q_{c,\gamma}$ as the average energy released by an (n,γ) reaction in the fuel and structural materials of the system, they assumed that the average energy Q_c would be given by:

$$Q_c = (\bar{v}_t - 1) Q_{c,\gamma} \quad (2.23)$$

where \bar{v}_t is the total average number of neutrons released per fission so that $\bar{v}_t - 1$ is the average number of neutrons per fission that is absorbed in the different materials of a critical reactor system.

The value of $Q_{c,\gamma}$ itself will depend on the materials in the system so this value will differ from reactor to reactor. Unik and Gindler set this average energy to 6.53 ± 0.2 MeV/capture, based on calculations for a single reactor (the EBR-II reactor).

When compared to the other values available in the Unik and Gindler data, this formula predicts total recoverable energy per fission values within 1 % for nuclides between ^{232}Th and ^{242}Pu , as can be seen in figure 2.1. This formula appears to perform rather well but there is also a possibility to improve it. First of all, there exists a lot more evaluated data on the different components in fission energy release compared to 20-30 years ago. Furthermore, the following approximations were made when the original semi-empirical formula was derived:

- the total recoverable energy per fission was assumed to be independent of the energy of the neutron that induces the fission event;
- the estimate for the average energy Q_c released by all (n,γ) reactions per fission assumes a critical reactor;
- the estimate of the average energy $Q_{c,\gamma}$ released by an (n,γ) reaction was set to 6.53 ± 0.2 MeV, based on calculations for a single reactor type (an EBR-II type reactor) so that the application of this formula to another reactor with radically different structural materials or fuel can be rather dubious.

A detailed discussion of these approximations and their influence can be found in section 6.7. Either way, the fact that ORIGEN2 already incorporates an estimate for the neutron capture component is a solid advantage compared to other codes.

2.5.2 Burn-up dependent cross sections

The ORIGEN 2.2 cross section libraries are used to take into account the spectral differences between different reactor types. But apart from the dependence upon the reactor type, there is also the time dependence of the spectrum within a given reactor type due to burn-up.

To deal with this issue, ORIGEN 2.2 has foreseen burn-up dependent cross sections which are also hard coded, making it impossible to easily change them. Furthermore, those burn-up dependent cross sections are only provided for a few specific nuclides (mostly important actinides like ^{235}U , ^{236}U , ^{238}U , ^{237}Np , ^{238}Pu , etc.) and again only for a limited number of reactor types.

2.5.3 The neutron yield per fission

The total average number of neutrons per fission (or total average neutron yield per fission) does not intervene directly in the Bateman equations but it

is still an important parameter for constant power calculations. ORIGEN 2.2 uses these values to calculate the infinite multiplication factor of the materials that it depleted. ORIGEN 2.2 also distinguishes between neutron induced fission and spontaneous fission.

ORIGEN2 foresees two sets of neutron yields for neutron induced fission, one for thermal spectrum reactors (based on a PWR with UO₂ fuel) and one for fast reactors (based on an advanced oxide plutonium recycle LMFBR). They were calculated by weighing energy-dependent ENDF/B-IV and V data with multi-group neutron spectra which were also used to update the cross section libraries. At the time, it was shown that the thermal and fast values of the neutron yield per fission for the various actinides used by ORIGEN2 did not vary that much from each other [25]. As we will show later on (see section 6.6) this is still the case when we use current nuclear data files to compute these values.

For the neutron yield for spontaneous fission, ORIGEN 2.2 uses a combination of measured and calculated values. For this data, the developers relied on third party data that does not appear to come from a nuclear data evaluation.

2.5.4 Neutron yields from (α, n) reactions

Apart from the obvious depletion calculation, ORIGEN 2.2 is also used to determine other parameters like the delayed neutron source coming from (α, n) interactions. The neutrons resulting from the interaction of energetic α particles with a wide variety of light nuclides (like for instance Li and Be) are a second important source of decay induced neutrons. In the commercial nuclear fuel cycle, those target materials are rarely encountered and the primary source of α induced neutrons will usually be ¹⁸O. Because it was impossible to provide a single set of α induced neutron yields that is valid for any medium, a set of neutron yields appropriate for a heavy metal oxide matrix was included into ORIGEN 2.2.

The yields for seven principal contributors to the number of α induced neutrons (being ²³⁸Pu, ²³⁹Pu, ²⁴⁰Pu, ²⁴²Pu, ²⁴¹Am, ²⁴²Cm and ²⁴⁴Cm) are hard-coded into ORIGEN 2.2. For the α induced neutron yield of any other nuclide, ORIGEN 2.2 will use the following semi-empirical formula:

$$\nu_{\alpha} = 2.152 \cdot 10^{-12} E_{\alpha}^{14.01} \quad (2.24)$$

where E_{α} is the energy of the α particle (in eV).

The coefficients of this equation were based on measured α induced neutron yields for ²³⁹Pu and ²⁴²Cm. The results predicted by this equation agree well with experimental values for α particles in the 5 to 6.2 MeV range.

Shall we play a game?

Joshua, in "Wargames"

At any rate, I am convinced that He [God] does not play dice.

Albert Einstein (1879 - 1955)

3

The mechanics of Monte Carlo

3.1 The Monte Carlo concept

The process of Monte Carlo particle transport can be described as a numerical simulation of reality in which numerous histories are simulated to derive the statistical (i.e. average) behaviour of the whole through the use of the central limit theorem. This is exactly what the Boltzmann equation (see equation 2.1) describes: the *average* behaviour of the neutron population in a system.

While classic deterministic codes solve the integro-differential form of the Boltzmann equation or a simplified equation mathematically, Monte Carlo does not. Due to the successive approximations and simplifications used by deterministic methods, the true physics of the problem is often lost and replaced by the "physics" of the mathematics used to solve the Boltzmann equation. A good example of this is the ray effect in deterministic codes based on the discrete ordinates or S_N method [31].

The discrete ordinates method consists of a discretisation of the angular variable Ω in the Boltzmann equation so that neutrons will only travel in a few specific directions. Such an approximation actually changes the entire physical model behind neutron transport. The ray effect itself is a particularly annoying and persistent spatial distortion of the scalar and angular flux which occurs mostly in 2D and 3D geometries with isolated sources.

The analytical solution for the discrete ordinates approximation in a pure absorbing medium in the xy -plane for an isotropic line source along the z -axis consists of a sum of Dirac delta functions corresponding to the discrete directions used in the discrete ordinates approximation. In reality the flux will be non-zero everywhere and the isoflux lines in the xy -plane will be circles centred around the source. When the medium in this example is a slightly scattering medium, the calculated flux will be anomalously low in regions remote from the discrete directions. Fortunately, this effect does not appear that often in practical reactor applications but when it does occur it will be extremely difficult to distinguish spatial distortions caused by the ray effect from true flux variations.

The Monte Carlo method on the other hand is capable of simulating the true physics of the problem without any approximation. It is often said that Monte Carlo actually “solves” the integral form of the Boltzmann equation, which is true in a certain sense. The notion of the integral form of the Boltzmann equation or even the Boltzmann equation itself is not required to understand Monte Carlo because with Monte Carlo you directly describe the physics of the system through basic probability.

A cross section is just that: the probability for a neutron to interact with a given nuclide. And the same goes for the angular distributions and energy spectra of secondary particles, they all give a probability for certain angles and energies (they are defined as such in the basic nuclear data evaluations). The equation that describes the probability density of particles in the phase space governed by those probabilities will however be the same as the integral form of the Boltzmann equation [4, 32].

The most straightforward Monte Carlo simulation will be a numerical simulation of the real physical events using their inherent probabilities (defined by the cross sections and angular distributions). Such a direct simulation is often referred to as *analog* Monte Carlo, as in analogous with the true physics that governs the simulated problem.

On the other hand, there also exist methods which modify the analog simulation process in such a way that they give the same average values as analog Monte Carlo, while giving a variance (i.e. a statistical uncertainty) that is smaller than or at least equal to the analog case. As a result, such modified simulation processes can significantly speed-up a Monte Carlo simulation. We call these *non-analog* Monte Carlo simulation or variance reduction techniques.

The basic idea of variance reduction is to dedicate the maximum amount of CPU time to those particles that are most likely to make a meaningful contribution to the desired results and to avoid using CPU time for particles that are unlikely to do so. Such variance reduction techniques are for instance often used in shielding calculations where the convergence of analog Monte Carlo can be quite slow.

Most of these variance reduction techniques involve the assignment of a certain importance or weight w to every source particle and its corresponding tracks. The weight of a particle track represents the relative contribution of that track to the final result. The magnitude of this weight is determined in such a way that when the simulation deviates from the analog case, the expected physical result is preserved in the sense of statical averages.

During the simulation of the particle, its weight can be changed to for instance simulate particle absorption without actually terminating the particle. The simulation of the particle will then continue with a reduced weight until its weight is so low that it is no longer considered to be important enough. Particle tracks created during an absorption event (like for example fission) will have the same reduced weight as the original track. This technique is called implicit capture, survival biasing or absorption by weight reduction.

Another application of a particle's weight is geometry splitting and Russian roulette. Whenever a track enters a region with higher importance than the previous one, the particle track will be split in multiple tracks but each with a reduced weight. As a result, important particles are followed more often but the solution remains unchanged because of the conservation of particle weight. The reverse is also possible: when entering a region with lower importance, the track has a chance of being terminated which is determined through a game of Russian roulette based on the survival probability. If the particle survives it will do so with a higher weight in such a way to preserve the average particle weight in the entire simulation.

In this chapter, we will limit ourselves to describing the peculiarities of Monte Carlo codes as they relate to our problem of Monte Carlo burn-up calculations without going into detail about the mathematics behind the Monte Carlo method itself. People interested in a detailed mathematical treatment of all aspects of Monte Carlo particle transport are referred to the excellent book of Lux and Koblinger [32].

3.2 The particle transport simulation process

3.2.1 Working of a general Monte Carlo code

An overview of the basic Monte Carlo simulation process is sketched in figure 3.1. The numbers in this figure indicate blocks in which nuclear data is needed to proceed. This flowchart is typical of most Monte Carlo codes.

The Monte Carlo simulation always starts with an initial track that either comes from a neighbouring cell or that is created in a cell as a source particle or by an interaction such as fission, $(n,2n)$, etc. In this approach, a scattering interaction does not "create" a new particle track because the incident track simply changes direction and energy. Whenever the entering track is a source particle, the Monte Carlo code will have to sample the initial position, energy and direction of the source particle before beginning the simulation.

For every particle track, the Monte Carlo code must then determine the distance l to the next particle interaction (block 1 in figure 3.1). If there are N nuclides in this particular cell with atomic densities n_i and associated total microscopic cross section values $\sigma_{i,t}$ (at the energy E of the incoming track) and if ξ is a random number between 0 and 1, then the distance l to the next interaction will be given by [2, 4, 32]:

$$l = -\frac{\ln(\xi)}{\sigma_t^*(E)} = -\frac{\ln(\xi)}{\sum_{i=1}^N n_i \sigma_{i,t}(E)} \quad (3.1)$$

If the particle doesn't interact in this cell, it is transported to the cell boundary and enters the neighbouring cell. The simulation process will then con-

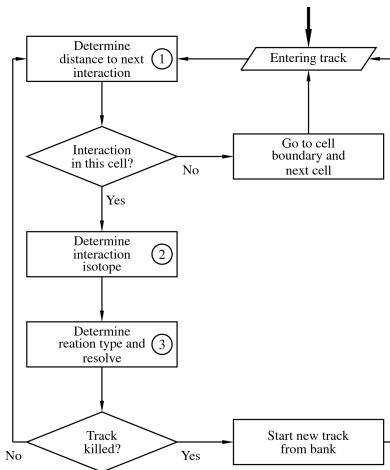


Figure 3.1: Overview of the Monte Carlo particle transport simulation flow applied to a general Monte Carlo code.

tinue in this new cell.

When an interaction does occur within the cell, the Monte Carlo code has to select the nuclide with which the particle will interact (block 2). For this purpose, the Monte Carlo code needs to calculate the nuclide interaction probability p_j associated with every nuclide j in the cell at the energy E of the interacting track. These probabilities are defined as the ratio of the atomic density n_j and the value of the total microscopic cross section $\sigma_{j,t}$ to the total macroscopic cross section σ_t^* in the cell, at the energy E of the interacting track:

$$p_j(E) = \frac{n_j \sigma_{j,t}(E)}{\sigma_t^*(E)} = \frac{n_j \sigma_{j,t}(E)}{\sum_{i=1}^N n_i \sigma_{i,t}(E)} \quad (3.2)$$

If ξ is again a random number between 0 and 1, then nuclide k is selected as the interacting nuclide if the following criterion is met:

$$\sum_{j=1}^{k-1} p_j(E) < \xi \sum_{j=1}^N p_j(E) \leq \sum_{j=1}^k p_j(E) \quad (3.3)$$

When the particle interacts with the particular isotope k , the Monte Carlo code will still need to determine the interaction type and resolve the interaction accordingly (block 3). For this purpose the code needs to calculate the values of all individual reaction cross sections $\sigma_{k,r}$ for every interaction in the

cell to determine the individual interaction probabilities $p_{k,r}$:

$$p_{k,r}(E) = \frac{\sigma_{k,r}(E)}{\sigma_{k,t}(E)} \quad (3.4)$$

The interaction type is then selected using the same method for the selection of the interacting isotope. The reaction r is thus chosen if:

$$\sum_{j=1}^{r-1} p_{k,j}(E) < \xi \leq \sum_{j=1}^r p_{k,j}(E) \quad (3.5)$$

where ξ is yet again a random number between 0 and 1.

After this step, the interaction is resolved by sampling the secondary particle's energy and angular distribution (if any outgoing tracks were created during the interaction). Depending upon the interaction, these are sampled independently of each other or the outgoing energy is determined through a function of the sampled outgoing angle or vice versa. There is unfortunately no general recipe for sampling energy and angular distributions because they depend on the reaction type and their representation in the nuclear data tables.

When the interaction has been resolved and when the created tracks have been banked, the simulation will then continue either with one of the resulting tracks or with a new track when the former track has been killed due to absorption, weight cut-off when using implicit capture, etc.

3.2.2 The particular case of MCNP(X)

The particle simulation in MCNP(X) is a bit different from what we described above because block 3 in the particle transport has already been optimized to some extent [2, 4] as is shown in the flowchart on the right of figure 3.2.

The calculation of the distance to the next interaction and the selection of the target nuclide is the same as described above (block 1 and 2). For every nuclide and particle track in the cell, a value for the total cross section must be evaluated. When the neutron is within the energy range below 4 to 5 eV, this total cross section is defined as the sum of the capture cross section from the normal cross section table with the elastic and inelastic scattering cross section from the $S(\alpha, \beta)$ table for thermal neutron scattering on molecules and crystalline solids (if such an $S(\alpha, \beta)$ table is present). When no $S(\alpha, \beta)$ table is available, the total cross section will be the regular one which can then be adjusted for thermal motion effects using the thermal free gas treatment. In this last case, no adjustment to cross sections is made if the elastic cross section in the cross section table was processed for the particular temperature of the cell.

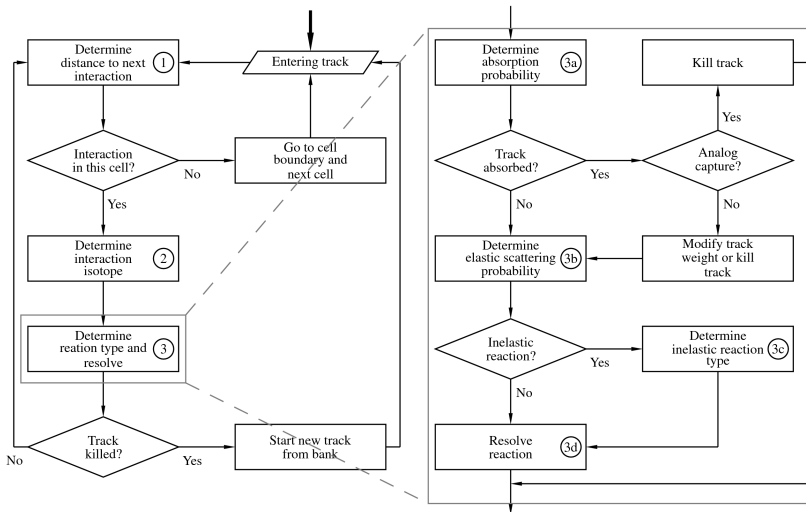


Figure 3.2: Overview of the Monte Carlo particle transport simulation flow with the optimisations used by MCNP and MCNPX in block 3.

Within MCNP(X) this is followed by a optional step of photon production for coupled neutron-photon problems when the target nuclide has a non-zero photon production cross section.

At this point MCNP(X) has selected the isotope k with which to interact. Now it will determine the absorption probability $p_{k,a}$ on this isotope instead of directly selecting a particular interaction (block 3a).

In MCNP(X) capture and absorption are used interchangeably. Both terms point to any reaction with no outgoing neutrons such as (n,γ) , (n,α) , (n,d) , etc. It doesn't matter if analog or implicit capture is used, MCNP(X) does this for every interaction in the cell (step 3a). This absorption probability $p_{k,a}$ is defined just like an individual interaction probability but only with absorption as a whole instead of a particular interaction type:

$$p_{k,a}(E) = \frac{\sigma_{k,a}(E)}{\sigma_{k,t}(E)} \quad (3.6)$$

where $\sigma_{k,a}$ is the total absorption cross section and $\sigma_{k,t}$ is the total cross section.

If the interaction is determined to be an absorption and if analog capture is used, the track is simply killed. When implicit capture is used, the weight w of the track is lowered to a new value w' by a fraction equal to the absorption probability $p_{k,a}$, in essence the portion of the particle's weight that was

absorbed:

$$w' = \left(1 - \frac{\sigma_{k,a}(E)}{\sigma_{k,t}(E)}\right) w = (1 - p_{k,a}(E)) w \quad (3.7)$$

A fraction $p_{k,a}$ of both the track's energy and weight is also deposited into the cell, contributing to any tallies in the cell. If the new particle weight falls below a threshold value, the track is either killed or the weight is increased to above the threshold value. This is determined by a game of Russian roulette.

When the track hasn't been killed during the absorption phase of the simulation, MCNP(X) will determine if the interaction is either elastic scattering or an inelastic reaction (block 3b). As was the case with absorption and capture, the meaning of inelastic reaction in MCNP(X) is rather broad: these are all reactions except elastic scattering with an outgoing neutron such as inelastic scattering, fission, etc. MCNP(X) chooses this reaction type by determining the probability of having an elastic reaction (given as the ratio between the elastic cross section $\sigma_{k,e}$ to the difference of the total and absorption cross sections):

$$\frac{\sigma_{k,e}(E)}{\sigma_{k,t}(E) - \sigma_{k,a}(E)} \quad (3.8)$$

And again, MCNP(X) does this for every interaction in the cell.

If and only if the interaction was an inelastic one MCNP(X) will determine the type of inelastic reaction (block 3c). This is similar to the selection of the interaction type described for the general Monte Carlo case, except that only inelastic reactions will play a role. So if ξ is a random number between 0 and 1, then a particular inelastic reaction r is chosen out of $M_{k,i}$ possible inelastic reactions for nuclide k if:

$$\sum_{j=1}^{r-1} \sigma_{k,i}^j(E) < \xi \sum_{j=1}^{M_{k,i}} \sigma_{k,i}^j(E) \leq \sum_{j=1}^r \sigma_{k,i}^j(E) \quad (3.9)$$

where $\sigma_{k,i}^j$ is the cross section of the inelastic reaction of type j for nuclide k .

When the type of interaction is determined (either an elastic scattering or a particular inelastic interaction) the energy and direction of the outgoing tracks will be sampled according to the angular distributions and spectra available for that interaction (block 3d). Additional tracks created during this interaction will be banked for later use.

This approach to Monte Carlo transport is completely reflected in the structure of the MCNP(X) neutron library files (or ACE (A Compact ENDF) files). The first large data block contains the unionised energy grid (all cross sections use the same grid), the total cross section, the absorption cross section and the elastic scattering cross section. After this block of data all the different inelastic cross sections are listed.

3.3 Tally estimators

In the previous section, we've described the basic simulation process, which is what a Monte Carlo code will do even if the user asks for nothing else. The result of this basic Monte Carlo simulation is a set of interaction points with in between particle tracks with a track length l , energy E and their corresponding weight w . Expected values of parameters like particle flux, current, etc. can be derived or "tallied" (as it is known in Monte Carlo terminology) from this set of interaction points and tracks, either by demand of the user or for use by the code itself. In general, these parameters can be described using the following integral:

$$\int \int \int h(\mathbf{r}, E, \Omega) \varphi(\mathbf{r}, E, \Omega) dEd\Omega dV \quad (3.10)$$

where h is the response function needed to determine the quantity the user is interested in.

An important Monte Carlo tally estimator is the collision estimator which tallies a response function g at every collision in the cell or cells of interest:

$$\int \int \int g(\mathbf{r}, E, \Omega) \psi_c(\mathbf{r}, E, \Omega) dEd\Omega dV = \frac{1}{W} \sum_c w_c g(\mathbf{r}_c, E_c, \Omega_c) \quad (3.11)$$

where ψ_c is the collision density, W is the total initial weight of all simulated histories, w_c is the weight of the particle prior to the collision and $g(\mathbf{r}_c, E_c, \Omega_c)$ is the value of the response function at the collision site \mathbf{r}_c for the particle energy E_c and direction Ω_c before the collision. When the initial weight of every history is equal to unity the total initial weight W will be equal to the total number of histories H .

This collision estimator is normalised to the total initial particle weight (or to the number of source particles if their initial weight is equal to unity). As a result, the above estimator should always give us the average number of collisions per unit of particle weight when the response function $g = 1$. This is already obvious for analog Monte Carlo where the above estimator equals N_c / H where N_c is the total number of collisions in the cell if $g = 1$.

A variation on the collision estimator is the absorption estimator which tallies a response function g not at every collision but at every absorption:

$$\int \int \int g(\mathbf{r}, E, \Omega) \psi_a(\mathbf{r}, E, \Omega) dEd\Omega dV = \frac{1}{W} \sum_a w_a g(\mathbf{r}_a, E_a, \Omega_a) \quad (3.12)$$

where ψ_a is the absorption density, w_a is the weight of the particle prior to the collision and $g(\mathbf{r}_a, E_a, \Omega_a)$ is the value of the response function at the absorption site \mathbf{r}_a for the particle energy E_a and direction Ω_a before the absorption.

The collision density ψ_c and the absorption density ψ_a are related to the angular flux φ respectively through the total macroscopic cross section σ_t^* and

the macroscopic absorption cross section σ_a^* in the cell:

$$\varphi(\mathbf{r}, E, \Omega) = \frac{\psi_c(\mathbf{r}, E, \Omega)}{\sigma_t^*(\mathbf{r}, E)} = \frac{\psi_a(\mathbf{r}, E, \Omega)}{\sigma_a^*(\mathbf{r}, E)} \quad (3.13)$$

so that the expected value given by equation 3.10 is estimated as:

$$\int \int \int h(\mathbf{r}, E, \Omega) \varphi(\mathbf{r}, E, \Omega) dEd\Omega dV = \frac{1}{W} \sum_c \frac{w_c}{\sigma_t^*(\mathbf{r}_c, E_c)} h(\mathbf{r}_c, E_c, \Omega_c) \quad (3.14)$$

with the collision estimator and with:

$$\int \int \int h(\mathbf{r}, E, \Omega) \varphi(\mathbf{r}, E, \Omega) dEd\Omega dV = \frac{1}{W} \sum_a \frac{w_a}{\sigma_a^*(\mathbf{r}_a, E_a)} h(\mathbf{r}_a, E_a, \Omega_a) \quad (3.15)$$

for the absorption estimator.

The collision and absorption estimators have unfortunately a large disadvantage in that they require interactions to take place in the cell where the estimator is used. In the case of a cell where a lot of particles pass through without interacting (such as a thin interface between two other cells) these estimators are not very interesting.

The track length estimator is another type of Monte Carlo estimator that does not have the previous problem. It actually uses the particle's track length l_t to tally the flux averaged value of the response function h and is therefore capable of giving results when the particles pass through the cell:

$$\int \int \int h(\mathbf{r}, E, \Omega) \varphi(\mathbf{r}, E, \Omega) dEd\Omega dV = \frac{1}{W} \sum_t l_t w_t h(\mathbf{r}_t, E_t, \Omega_t) \quad (3.16)$$

For Monte Carlo burn-up applications, we are mostly interested in estimating the integrals in equation 2.14. The numerator in this equation is the volume averaged reaction rate associated with a reaction r on the nuclide of type i through the microscopic cross section $\sigma_{i,r}$ and the denominator is the volume averaged total scalar flux. The response function needed for these integrals will therefore be:

$$h(\mathbf{r}, E, \Omega) = \sigma_{i,r}(E) \quad (3.17)$$

$$h(\mathbf{r}, E, \Omega) = 1 \quad (3.18)$$

A Monte Carlo code such as MCNP(X) uses the track length estimator so that the reaction rate and the total flux will be given by:

$$\int \int \sigma_{i,r}(E) \phi(\mathbf{r}, E) dEdV = \frac{1}{W} \sum_t l_t w_t \sigma_{i,r}(E_t) \quad (3.19)$$

$$\int \int \phi(\mathbf{r}, E) dEdV = \frac{1}{W} \sum_t l_t w_t \quad (3.20)$$

3.4 Criticality and fixed source calculations

Within Monte Carlo calculations we can make a distinction between two different types of calculations: fixed source calculations and iterative source calculations. In the case of a fixed source calculation the Monte Carlo code will simulate a pre-set number of particles starting from a source given by the user. Fixed source calculations follow the previously described Monte Carlo simulation process to the letter. Iterative source calculations on the other hand are used to solve eigenvalue problems. In particular, nuclear criticality problems solve for an eigenvalue and an eigenvector, namely the effective multiplication factor k_{eff} and the critical fission distribution. Such calculations are often referred to as criticality calculations.

The effective multiplication factor k_{eff} gives us information about the stability (or criticality) of nuclear systems. It gives us the average number of neutrons created per fission that will in turn lead to another fission event. For the nuclear chain reaction to be stable, k_{eff} must equal 1. In all other cases, the nuclear chain reaction is inherently unstable. We talk about supercriticality or supercritical systems when k_{eff} is larger than 1: more neutrons will be created every generation. The reverse (k_{eff} is smaller than 1) is subcriticality: the nuclear chain reaction will extinguish in time because there are too few neutrons available to sustain it.

Within the Monte Carlo method, calculating k_{eff} consists of estimating the average number of fission neutrons created in a fission generation. Such a fission generation is also known as a cycle in Monte Carlo methods. It consists of all neutrons born from fission up to their removal from the system through fission, escape or parasitic absorption.

In a criticality calculation a number of successive cycles is simulated using a varying number N_s of source particles per cycle. For the initial cycle, these are source points provided by the user. For the following cycles, these points will be the fission sites of the previous cycles. The repetitive use of the fission sites in one cycle as the source for the next cycle is known as the power iteration method.

The number N_s of source points will vary from cycle to cycle but the total source weight W_s will be the same for every cycle. Convergence of the fission source is very important for any criticality calculation because the estimate of k_{eff} (and all other user requested tallies) are very sensitive to this fission source distribution. The first few cycles of a criticality calculation (known as the inactive cycles) are therefore used to converge the fission source without accumulating any results. In some cases like systems with loose neutronic coupling, fission source convergence can be a large problem which often leads to erroneous results. Currently, a new and very effective method for fission source convergence is being developed at LANL [33].

Particle transport during a fission cycle in MCNP(X) is performed using the standard simulation flow for MCNP(X) except for the fact that fission is

treated as pure absorption. In addition, the following three steps are performed for every interaction during the cycle:

- accumulate the prompt fission lifetime;
- accumulate the estimates for the effective multiplication factor k_{eff} if the interaction occurred within a cell containing fissionable material;
- store the fission sites for use in the next cycle.

The value of the effective multiplication factor k_{eff} is estimated through the use of a collision, absorption and track length estimator. At the end of the criticality calculation, these three estimators are combined to give a final value for k_{eff} .

For the collision and track length estimator, the Monte Carlo code will use the following response function:

$$h(\mathbf{r}, E, \Omega) = \sum_i n_i \bar{v}_{i,t}(E) \sigma_{i,f}(E) \quad (3.21)$$

where n_i is the atomic density for fissionable nuclide i , $\bar{v}_{i,t}$ is the total average number of neutrons per fission of this nuclide and $\sigma_{i,f}$ is the microscopic fission cross section for fissionable nuclide i . Because the microscopic fission cross section is used, these estimators are only accumulated for cells that contain materials with fissionable nuclides.

The collision and track length estimator for k_{eff} will therefore be given by:

$$k_{\text{eff}}^c = \frac{1}{W} \sum_c \frac{w_c}{\sigma_t^*(\mathbf{r}_c, E_c)} \sum_i n_i \bar{v}_{i,t}(E_c) \sigma_{i,f}(E_c) \quad (3.22)$$

$$k_{\text{eff}}^t = \frac{1}{W} \sum_t l_t w_t \sum_i n_i \bar{v}_{i,t}(E_t) \sigma_{i,f}(E_t) \quad (3.23)$$

A third estimator for the value of k_{eff} is the absorption estimator. This estimator works a bit differently from the general absorption estimator given above in that it uses absorption by fissionable nuclides only and that it also differs slightly for analog and implicit capture. For a Monte Carlo criticality calculation with analog absorption, the estimator is given by:

$$k_{\text{eff}}^a = \frac{1}{W} \sum_a w_a \bar{v}_{i,t}(E_a) \frac{\sigma_{i,f}(E_a)}{\sigma_{i,a}(E_a)} \quad (3.24)$$

where summation a is done for all absorptions on a fissionable nuclide and where $\sigma_{i,f}$ and $\sigma_{i,a}$ are respectively the fission and absorption cross section of the fissionable nuclide i for which the absorption was sampled. The particle weight w_a is the particle weight (which doesn't change after the collision

although it can differ from unity when using other variance reduction techniques).

In the case of implicit capture, the absorption estimator is given by:

$$k_{\text{eff}}^a = \frac{1}{W} \sum_a (w_a - w'_a) \bar{v}_{i,t}(E_a) \frac{\sigma_{i,f}(E_a)}{\sigma_{i,a}(E_a)} \quad (3.25)$$

where the weight w'_a is the reduced weight of the particle after the implicit capture event (see equation 3.7). $w_a - w'_a$ is therefore the weight absorbed in the capture event:

$$w_a - w'_a = w_a \frac{\sigma_{i,a}(E_a)}{\sigma_{i,t}(E_a)} \quad (3.26)$$

Nothing is particularly hard if you divide it into small steps.

Henry Ford (1863 - 1947)

4

Analysis of Monte Carlo with burn-up

4.1 Nuclear data tables and code performance

During the basic Monte Carlo simulation, every particle is tracked separately from its point of creation to that of its destruction. The transport of these particles is completely ruled by interaction probabilities, which are determined by the various microscopic cross sections, angular distributions and energy spectra that are involved.

The microscopic cross sections form the bulk of the data required for the basic Monte Carlo simulation. Depending on the type of Monte Carlo (either continuous energy or multi-group) and on the implementation of the Monte Carlo code, these cross section tables can have several formats which will have an important impact on the code's performance.

In a multi-group Monte Carlo code, the cross section table consists of the group structure and associated group cross sections either with or without an associated scattering matrix. The size of the group structure also differs from code to code. The MCNP(X) family of continuous energy Monte Carlo codes has the capability for multi-group Monte Carlo for which infinite dilute (i.e. non self-shielded) data is provided in about 30 groups [34]. Codes like TRIPOLI [35] and MCBEND [36] on the other hand have multi-group data using a group structure that is sufficiently large to alleviate the self shielding effects of the resonances in the cross sections.

For completeness we also mention here the Monte Carlo code TART [37] which uses a special type of multi-group cross sections (multi-band cross sections) in about 600 groups. These multi-band cross sections are similar to the unresolved resonance probability tables of MCNP(X), but they cover all reactions over the entire energy range instead of only unresolved resonances in the unresolved resonance energy range. With its 600 groups, these multi-band cross sections are equivalent with normal multi-group cross sections of a few thousand groups.

For a continuous energy Monte Carlo code the cross sections are piecewise continuous functions of energy, being a grid of energy points with associated cross section values. For MCNP(X), these cross section tables are prepared by the NJOY data preprocessing code [38]. NJOY reads an ENDF file, reconstructs the cross sections and linearises them on a unionised energy grid so that all reactions of the same nuclide will have the same energy grid (see chapter 6 for more information). We will refer to these tables as unionised cross section tables.

A special case of these unionised cross section tables is the table where the energy grid for every material and reaction is the same. This is already the case for multi-group Monte Carlo but this is also true for continuous energy Monte Carlo if all nuclides would use the same unionised energy grid. We will refer to this case as universal unionised cross sections.

A third possible format is the case where every cross section (even for the same nuclide) is linearised on a different energy grid (which would be true for cross sections linearised by PREPRO [39]). We will refer to these as non-unionised cross sections. To our knowledge, no continuous energy Monte Carlo code exists that uses either of these two last cross section formats.

These three types of cross section table formatting have all their own advantages and disadvantages. Universal unionised tables will definitely take a lot more memory than unionised tables because the universal unionised energy grid must be capable of representing any reaction of any nuclide within a certain accuracy. Non-unionised cross section tables have tailor made grids for each reaction. A smooth cross section will therefore have a small grid while a reaction with resonances will have a much larger grid. As a result, these cross section tables will require much less memory space than universal unionised tables. Unionised cross section tables have a bit of both worlds: nuclides with simple cross sections and few resonances will have a smaller grid than more complicated nuclides. As a result, the memory needs for unionised cross section tables will be somewhere in between non-unionised and universal unionised. Either way, the actual size of the resulting energy grid or grids will ultimately depend upon the accuracy of the reconstruction, linearisation and Doppler broadening of the cross sections.

To retrieve a cross section value σ_i for any energy E in cross section interval i between E_i and E_{i+1} from such a table, a continuous energy code needs to perform an energy grid search and a linear interpolation (see figure 4.1):

$$\sigma_i(E) = \sigma_i + \frac{\sigma_{i+1} - \sigma_i}{E_{i+1} - E_i} (E - E_i) \quad (4.1)$$

$$\sigma_i(E) = \frac{\sigma_i E_{i+1} - \sigma_{i+1} E_i}{E_{i+1} - E_i} + \frac{\sigma_{i+1} - \sigma_i}{E_{i+1} - E_i} E = a_i + b_i E \quad (4.2)$$

A multi-group code also has to perform such an energy grid search to identify the proper group cross section value to return. So basically, a Monte Carlo code will only calculate a cross section value when it needs one.

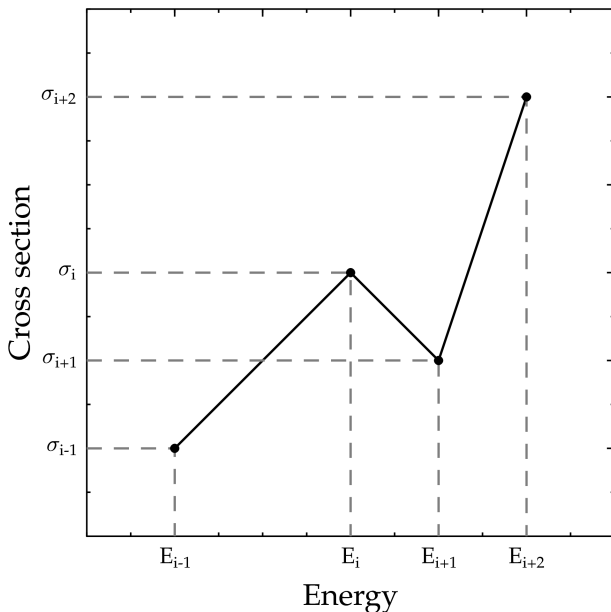


Figure 4.1: Piecewise continuous cross sections and linear interpolation.

To perform the grid search, the bisection method (also known as interval halving or binary search) is the most stable and efficient approach. The number of operations required to find the proper cross section interval is of the order of $\log_2(n)$ where n is the number of points in the grid [40]. For MCNP(X) cross section tables, looking up a cross section value of a light nuclide such as ^1H (which has a unionised energy grid of about 500 points) will roughly take about half the time of looking up a cross section of an actinide like ^{238}U (which has an energy grid of the order of 10^5 points).

For the linear interpolation, only a few more operations are required. The total number of operations (and therefore also the time) required to retrieve a cross section value will thus be of the order of $a + \log_2(n)$ with a the number of operations required for the linear interpolation. As such, the cross section retrieval time will vary with the energy grid size in a logarithmic way.

The remainder of the nuclear data used by the Monte Carlo code consists of angular distributions and energy spectra for emitted particles. The energy grids involved are generally smaller than the cross section grids. Although this type of data can be quite complex (especially in the latest nuclear data evaluations), the time required to retrieve these values will be small compared to the time required to retrieve a cross section value.

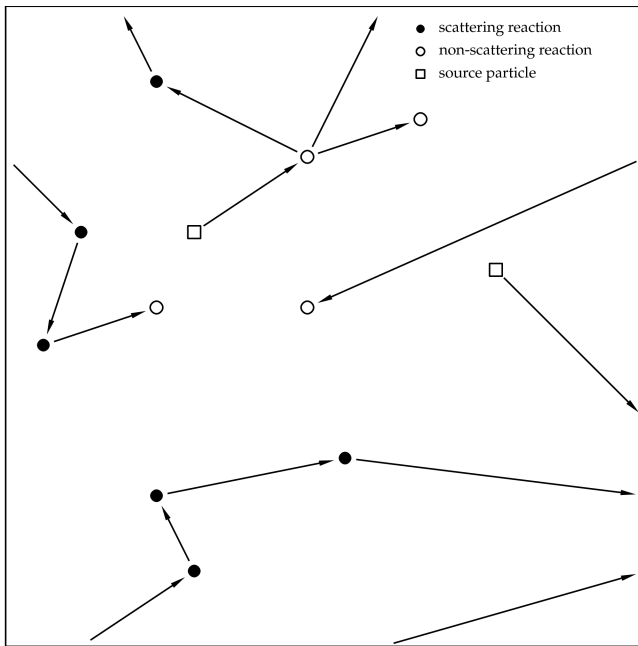


Figure 4.2: Examples of particle tracks in a cell: there are 9 particle tracks entering the cell, there are 10 interactions in the cell and 4 tracks are killed during the simulation.

4.2 Monte Carlo simulation time

For any Monte Carlo code, the overall time t_s needed for the Monte Carlo simulation in a cell will depend on the total number of cross section values to be retrieved, and particularly on the number of times that the grid search needs to be performed. In what follows, we will assume that the time required to obtain any cross section value is independent of the nuclide. As we indicated earlier, the time required for the grid search will be of the order of $\log_2(n)$ where n is the number of points in the grid. As such, the cross section retrieval time will depend on the energy grid size but assuming a mean time will simplify the reasoning without affecting the ultimate result.

To determine this simulation time, we now need to know how many cross section values the code needs to retrieve. To do this, let us consider a simple cell filled with a material consisting of N different nuclides. When there are N_e particle tracks that enter our particular cell (including those created through variance reduction techniques like geometry splitting), N_i interactions that take place in this cell and N_k tracks that are killed in the cell, then the total

number of tracks N_{tr} in the cell will be given by:

$$N_{tr} = N_e + N_i - N_k \quad (4.3)$$

In figure 4.2 we illustrate the various tracks in a typical cell. Four particle tracks enter the cell from neighbouring cells, two particle tracks enter through source points in the cell and three particle tracks are created after an interaction so that the number of entering tracks $N_e = 9$. There are a total of ten interactions in the cell ($N_i = 10$) and four tracks are killed ($N_k = 4$). Therefore, the total number of particle tracks in the cell must be equal to 15 ($9 + 10 - 4 = 15$).

As there are N nuclides in our particular cell, $N_{tr}N$ total cross section values have to be determined to perform block 1 and 2 in the simulation process (to see whether or not the particle interacts in the cell and if so with which nuclide). If M is the mean number of possible reactions per nuclide in the cell, then the number of cross section values required to determine the interaction type (block 3 in the simulation process) will be N_iM . The total number of cross section values needed in the simulation is thus given by:

$$N_{tr}N + N_iM \quad (4.4)$$

The implementation and formatting of the cross section table can play an important role in this. A Monte Carlo code using non-unionised cross sections will have to carry out the cross section interval search for every cross section value that it needs. On the other hand, MCNP(X) and any other code using unionised cross section tables will only require a single grid search to retrieve any reaction cross section at the same energy of a single nuclide. A universal unionised cross section table is even better: only one grid search is needed to retrieve any cross section value of any nuclide at a given energy. For the remaining cross section values only the linear interpolation is required. This linear interpolation requires only a fraction of the time needed to retrieve a cross section value. From now on, we will call this time fraction for the linear interpolation f_x ($0 \leq f_x \leq 1$). This leads us to the simulation time estimates for Monte Carlo codes using non-unionised, unionised and universal unionised cross section tables given in table 4.1.

Table 4.1: Simulation time estimates.

Cross section table	t_s
non-unionised	$\propto N_{tr}N + N_iM$
unionised	$\propto N_{tr}N + f_x N_iM$
MCNP(X)	$\propto N_{tr}N + f_x [(2 - f_k) N_i + (1 - f_e) (1 - f_k) N_i M_i]$
universal unionised	$\propto N_{tr} + f_x (N_{tr} (N - 1) + N_i M)$

Because of optimisations in the Monte Carlo simulation process, the estimate for the simulation time for unionised cross section tables given in table 4.1 does not apply entirely to MCNP(X). As was the case for general Monte Carlo, a total of $N_{tr}N$ values of the total cross section $\sigma_{i,t}$ have to be evaluated to determine the target nuclide in MCNP(X). It is at this point that things start to differ.

After the selection of the particular isotope j , a total of N_i absorption cross sections $\sigma_{j,a}$ are needed for every interaction in the cell to determine the neutron's absorption probability. When analog capture is used, the particle will then be killed if it is absorbed and the simulation will continue with a new source track or with a previously banked track. In the case of implicit capture, the particle's weight is simply lowered and the simulation process continues. The track can still be killed if its weight drops below the weight cut-off and if it doesn't survive the game of Russian roulette (see section 3.1 and 3.2.2).

When the track is not killed, MCNP(X) will then test to see if the interaction is elastic scattering or another type of inelastic reaction. If f_k is the fraction of all interactions where a track is killed (for analog capture this is the fraction of all interactions that are absorptions), then a total of $(1 - f_k) N_i$ elastic cross section values are calculated (the total and absorption cross sections that were calculated earlier were retained). After this, MCNP(X) will only determine the inelastic cross section values if it was not an elastic scattering. So if we define f_e as the fraction of all remaining interactions that are elastic and if M_i is the mean number of possible inelastic reactions per nuclide, then MCNP(X) needs to calculate $(1 - f_e)(1 - f_k) N_i M_i$ different cross section values to do this.

The simulation time t_s for the case of MCNP(X) can therefore be given by the following equation:

$$t_s \propto N_{tr}N + f_x [(2 - f_k) N_i + (1 - f_e)(1 - f_k) N_i M_i] \quad (4.5)$$

The second term in this equation is always lower than the corresponding term for the general case of Monte Carlo with unionised cross section tables. In the general case, all reactions are treated equally while MCNP(X) distinguishes between elastic and inelastic reactions. And because elastic scattering is (most of the time) more probable than an inelastic reaction the number of cross section values that have to be determined in the MCNP(X) case will always be lower than in the general case, leading to a better performance.

The linear interpolation takes little extra time above the grid search, so that the value of f_x will in most cases be close to zero. The case $f_x = 0$ can be set as the lower limit on the simulation time. In this case, we assume that when the position in the energy grid is known, the calculation of additional cross section values at the same energy won't take any time at all. Under these assumptions, the performance of MCNP(X) and the general case of Monte Carlo with unionised cross section tables will be the same. In the same way we can use the estimate for the simulation time of non-unionised cross section tables ($f_x = 1$) as an upper limit because it is the worst case scenario.

Table 4.1 also illustrates the power of universal unionised cross section tables. The ratio of the simulation time for continuous energy Monte Carlo codes with unionised cross section tables (t_s^{MC}) to multi-group Monte Carlo or continuous energy Monte Carlo with universal unionised cross section tables (t_s^{MG}) is given by:

$$\frac{t_s^{MC}}{t_s^{MG}} \approx \frac{N_{tr}N + f_x N_i M}{N_{tr} + f_x (N_{tr} (N - 1) + N_i M)} \quad (4.6)$$

This is of course only valid if the grid size of the unionised tables and universal unionised tables are comparable. Because the linear interpolation takes little to no extra time above the energy grid search (f_x close to 0) this would mean that the simulation time in a cell for codes like MCNP(X) increases linearly with the number of nuclides N in the cell when compared to universal unionised cross section tables:

$$\frac{t_s^{MC}}{t_s^{MG}} \approx N \quad (4.7)$$

This notion is of importance for Monte Carlo with burn-up. During a burn-up calculation, the number of nuclides in the different burn-up zones will increase due to the accumulation of activation products or fission products. Because of this effect, the Monte Carlo simulation will gradually slow down if it uses unionised cross section tables. However, if the code would use universal unionised cross section tables the CPU time required for the Monte Carlo simulation would not increase very much.

4.3 Criticality calculation correction

The simulation times given above apply to a fixed source calculation. For a criticality calculation it is however a bit different. Additional cross section values are required to estimate, for every cycle in the criticality calculation, the value of the effective multiplication factor k_{eff} (using the collision, absorption or track length estimators) as well as the prompt neutron generation time. The code also needs to determine the fission source to be used in the following cycle. To take this into account, the simulation time needs to be corrected.

Consider for instance the calculation of the effective multiplication factor k_{eff} using the track length estimator (see equation 3.23):

$$k_{\text{eff}}^t = \frac{1}{W} \sum_t l_t w_t \sum_i n_i \bar{v}_{i,t} (E_t) \sigma_{i,f} (E_t) \quad (4.8)$$

where w_t and E_t are the weight and energy of a track with distance l_t to the previous interaction in a cell with fissionable nuclides (with atomic densities n_i , neutrons per fission $\bar{v}_{i,t}$ and fission cross sections $\sigma_{i,f}$).

To determine this value in a cell containing N fissionable nuclides, the values of $\bar{v}_{i,t}$ and $\sigma_{i,f}$ need to be retrieved for each nuclide and every track in the cell. For the fission cross section this will be a total of $N_{tr}N$ values, once per nuclide and per particle track in the cell. Using the fraction f_x to account for the use of a unionised grid, this operation will take a time t_k proportional to:

$$t_k \propto f_x N_{tr} N \quad (4.9)$$

Just for this single estimator, the increase in the number of cross sections to be calculated is of the same order as for the simulation. The time increase due to the calculation of all those extra cross section values can however be smaller than the simulation time (due to the possibility of unionised grids). We therefore need to introduce a criticality calculation correction t_k to the simulation time t_s . It is however quite difficult to quantify this due to the various implementation possibilities and due to the fact that many cross sections values are used in different estimators, etc. In any case, this correction will be of the following form:

$$t_k \propto M_1 + f_x M_2 \quad (4.10)$$

where M_1 is the number of cross sections for which the grid search must be performed and M_2 the number of cross section values for which this search is not required.

The criticality correction also applies to Monte Carlo codes using universal unionised cross section tables, but here it will be $f_x(M_1 + M_2)$ because only one grid search is necessary for every particle track. For Monte Carlo with non-unionised cross section tables, this correction is $M_1 + M_2$ because all reactions have different grids.

4.4 Reaction rate calculation time

Now that we have looked at the different components in the Monte Carlo simulation time, it is time to turn our attention to the reaction rates themselves. Consider the situation where an additional number R_j of reaction rates for nuclide j have to be determined in our cell for a total of N_r nuclides above the basic Monte Carlo simulation. The total number of reaction rates R to be calculated will thus be given by:

$$R = \sum_{j=1}^{N_r} R_j \quad (4.11)$$

When a track length estimator is used, an additional amount of $N_{tr}R$ cross section values must be calculated, one for every reaction rate and every track in the cell. Similar to what we have done for the simulation time, we can now estimate the reaction rate calculation time for all our different cases. The resulting equations can be found in table 4.2.

Because the MCNP(X) multiplier bins used for reaction rate calculation do not appear to take advantage of the unionised cross section table used by the code, every reaction rate (even the ones of the same nuclide) must be counted separately (this is illustrated in the examples in section 4.5.2 and 4.5.3). As a result, the performance of MCNP(X) in the calculation of reaction rates will be comparable to that of a Monte Carlo code with non-unionised cross section tables. It is the worst case possible.

When the Monte Carlo code uses the full potential of unionised cross section tables, only one grid search would be required for every track and every nuclide. So if the multiplier bins of MCNP(X) would be optimized to use this advantage of unionised cross section tables, it could already alleviate some of the CPU time problems (provided that multiple reaction rates of the same nuclide were requested).

As was the case with the simulation time, universal unionised cross section tables offer the best performance: no additional grid searches are required. This means that calculating the reaction rates will actually take little or no extra time compared to the basic Monte Carlo simulation.

4.5 CPU time increase

4.5.1 Time increase in MCNP and MCNPX

Now that we have quantified the various contributors to the CPU time usage in Monte Carlo burn-up calculations, we can now determine the fractional increase in computation time (relative to the simulation time t_s and the criticality correction t_k) in a cell due to the calculation of R reaction rates (both zero and non-zero). These are given in table 4.3.

The equations in table 4.3 are only valid for single cells. In a multiple cell problem, the calculation time for simulating particle transport in every cell j is given by $t_{s,j}$ with a criticality correction $t_{k,i}$ only for every cell i with fissionable material. An additional amount of calculation time $t_{r,l}$ must be taken into account for every cell l where we wish to tally an additional R_l reaction rates. So, the time increase for Monte Carlo with unionised cross section tables in a

Table 4.2: Reaction rate calculation time estimates.

Cross section table	t_r
non-unionised	$\propto N_{tr}R$
unionised	$\propto N_{tr} [N_r + f_x (R - N_r)]$
MCNP(X)	$\propto N_{tr}R$
universal unionised	$\propto f_x N_{tr}R$

Table 4.3: CPU time increase when calculating reaction rates in a single cell.

Cross section table	$\frac{t_s + t_r + t_k}{t_s}$
non-unionised	$1 + \frac{N_{tr}R}{N_{tr}N + N_iM + M_1 + M_2}$
unionised	$1 + \frac{N_{tr}R}{N_{tr}N + f_xN_iM + M_1 + f_xM_2}$
MCNP(X)	$1 + \frac{N_{tr}R}{N_{tr}N + f_x[(2-f_k)N_i + (1-f_e)(1-f_a)N_iM_i] + M_1 + f_xM_2}$
universal unionised	$1 + \frac{f_xN_{tr}R}{N_{tr} + f_x(N_{tr}(N-1) + N_iM) + f_x(M_1 + M_2)}$

multiple cell problem will be given by:

$$1 + \frac{\sum_l t_{r,l}}{\sum_j t_{s,j} + \sum_i t_{k,i}} = 1 + \frac{\sum_l N_{tr,l}R_l}{\sum_j [N_{tr,j}N_j + f_xN_{i,j}M_j] + \sum_i [M_{1,i} + f_xM_{2,i}]} \quad (4.12)$$

If $R_l = R$ for every cell l , then the only variable in equation 4.12 will be the amount R of reaction rates. In other words, the total CPU time t_{MC} required for a single step in the Monte Carlo burn-up calculation compared to the basic simulation time (including the criticality correction) has a linear dependence on the number of reaction rates R :

$$\frac{t_{MC}}{t_s + t_k} = 1 + \alpha R \quad (4.13)$$

Due to the previous analysis of Monte Carlo burn-up we are also capable of formulating an upper and lower limit on that time increase. As was explained in section 4.2, the cases of $f_x = 0$ and $f_x = 1$ correspond to a lower and upper limit on the simulation time (and the criticality correction if it is present). Because we have to divide the reaction rate calculation time by the simulation time and because the reaction rate calculation time doesn't depend on f_x we can therefore say that these cases also correspond to an upper limit ($f_x = 0$) and a lower limit ($f_x = 1$) of the relative time increase. As a result, the value of α observed for MCNP(X) should lie in between the following values (neglecting the criticality correction):

$$\frac{\sum_l N_{tr,l}}{\sum_j [N_{tr,j}N_j + N_{i,j}M_j]} \leq \alpha \leq \frac{\sum_l N_{tr,l}}{\sum_j N_{tr,j}N_j} \quad (4.14)$$

4.5.2 Example: a cell of ^{238}U

A fixed source and criticality calculation in a simple cell containing ^{238}U can be used as a simple example to show the validity of the theoretical discussion

given above. We take ^{238}U in this analysis because its energy grid is the largest in the data that we used, namely 82037 points for JEF 2.2 data and 122528 points for JEFF 3.1.

In the previous sections, we have assumed that the time required to obtain any cross section value is independent of the nuclide although the cross section interval search depends on the energy grid size (through the logarithmic behaviour of the bisection method). In this case, there is only one isotope used in the problem ($N = 1$) so that the assumption is exact.

Using MCNPX 2.5.0 we first performed only the particle simulation and afterwards we calculated several instances (1, 5, 10, etc. up to 30) of the same reaction rate. We considered different reactions to do this with, namely the (n,γ) , $(n,2n)$ and (n,p) reactions. The measured time increases along with the upper ($f_x = 0$) and lower bound ($f_x = 1$) of the time increase as calculated by equation 4.14 for both the fixed source and criticality calculation can be found in figures 4.3 and 4.4. Because we cannot accurately estimate the criticality correction, the values of M_1 and M_2 are set to zero for this example. The value of M for this example is 32 for JEF 2.2 and 52 for JEFF 3.1 (^{238}U has 32 possible reactions in JEF 2.2 data versus 52 reactions in JEFF 3.1).

The number of tracks in both types of calculations (criticality and fixed source) is different so that we cannot compare the individual calculation times. We can however compare the ratio of reaction rate calculation time t_r to the simulation time t_s (and the criticality correction t_k for the criticality calculation) because those are independent of the absolute number of tracks. For the criticality calculations, the simulation time used is the time of the active cycles because MCNP(X) only tallies results during the active cycles.

In all cases, we can see that the calculation time increases linearly with the number of times that we calculated a given reaction rate, as predicted by equation 4.13. Because we calculated multiple instances of the same reaction rate, this clearly indicates that MCNP(X) calculates the reaction rates independently of one another. So for every reaction rate, MCNP(X) needs to determine the energy interval of the cross section even if it was done already for a previous reaction rate for that particular nuclide.

We also observe that the time increase depends upon the reaction type. For the JEF 2.2 fixed source case (at the top of figure 4.3) the required CPU time increases respectively by a factor 26.14, 7.03 and 24.32 when calculating the (n,γ) , $(n,2n)$ and (n,p) reaction rate 30 times.

In JEF 2.2 data, the (n,γ) reaction of ^{238}U is defined over the entire energy range (10^{-5} eV to 20 MeV) while the (n,p) reaction is not defined at all. This is also true for the JEFF 3.1 case, although the (n,γ) reaction of ^{238}U is defined up to 30 MeV. Still, the time increase for the (n,p) reaction rate is very close to the time increase of the (n,γ) reaction rate. It appears that MCNP(X) performs the energy grid search for the reaction rate calculation before it checks if the reaction is defined. And because the cross section doesn't exist, the linear interpolation to determine the exact cross section value is not performed which

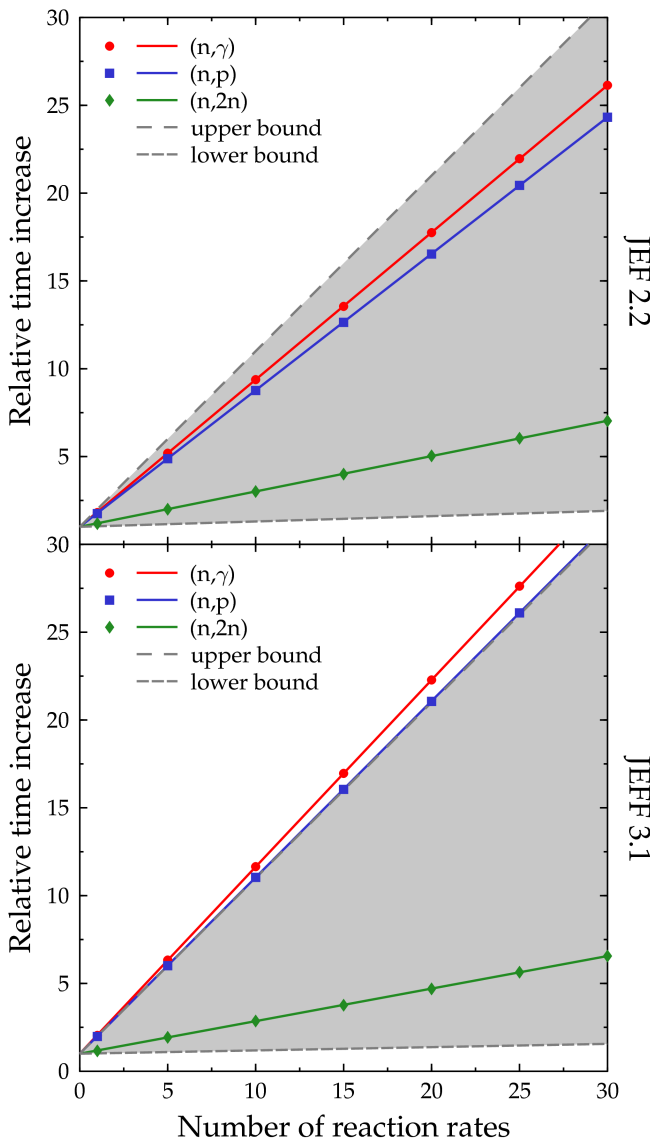


Figure 4.3: Estimated and observed relative time increase when calculating multiple instances of the (n,γ) , (n,p) and $(n,2n)$ reaction rates in a ^{238}U cell for a fixed source calculation using JEF 2.2 and JEFF 3.1 evaluated nuclear data files.

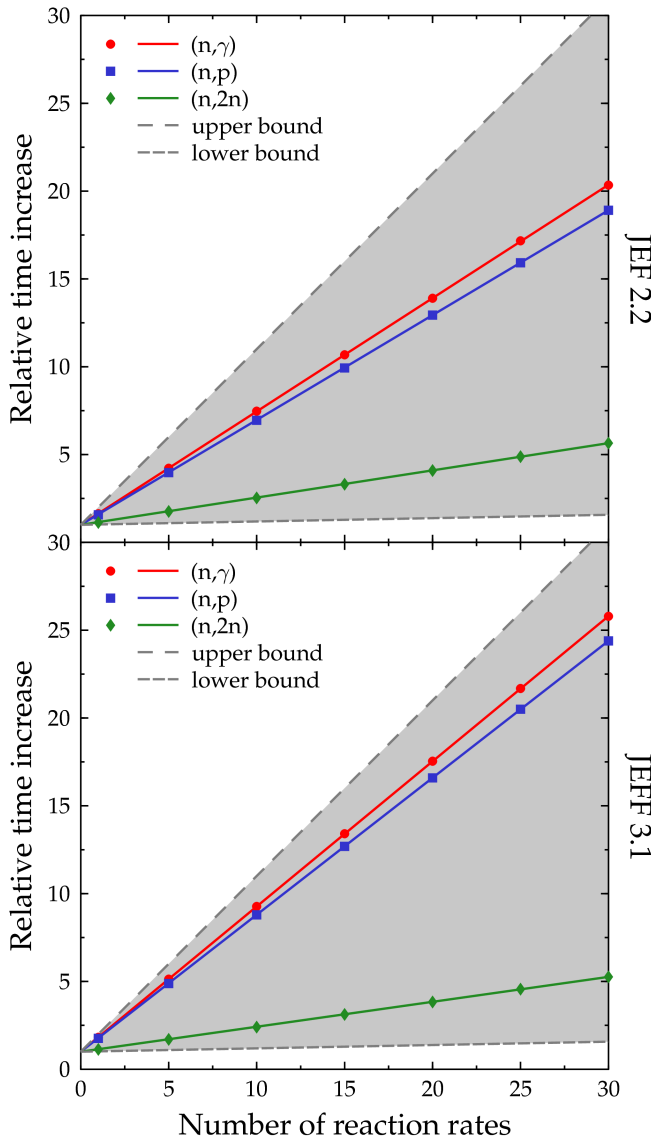


Figure 4.4: Estimated and observed relative time increase when calculating multiple instances of the (n,γ) , (n,p) and $(n,2n)$ reaction rates in a ^{238}U cell for a criticality calculation using JEFF 2.2 and JEFF 3.1 evaluated nuclear data files.

explains why the time increase is slightly lower than with the (n,γ) reaction rates. The difference between both can give us an indication of the amount of time required to perform the linear interpolation which is small but still not negligible.

For a threshold reaction like $(n,2n)$, MCNP(X) performs the grid search only if the track energy is above the threshold value. And this takes less time compared to a normal reaction, which explains why the time increase for the $(n,2n)$ reaction rate is a lot lower than the one for the other reactions. In the case of the JEF 2.2 ^{238}U data, the $(n,2n)$ reaction is only defined on the last 38 points of an 82037 point unionised grid. In the JEFF 3.1 case this is the last 129 points of a 122528 point grid. Taking into account the logarithmic behaviour of the bisection method, this would mean that the grid search for the $(n,2n)$ reaction would be about 3.1 times faster than the one required for the entire unionised grid for JEF 2.2 data and 2.4 times faster for JEFF 3.1 data.

When we look at the different curves for the criticality calculation and the fixed source calculation, we see that the curves for the criticality calculations are always below the ones of the fixed source calculation. This is as we expected due to the extra cross section values that are needed for the criticality calculation to estimate k_{eff} , etc. This illustrates nicely that the criticality correction to the estimate of the simulation time introduced by equation 4.10 cannot be neglected.

As a final observation, we can also see that all curves lie nicely in between the upper and lower bound that we derived in this chapter except for the the (n,γ) and (n,p) curves for the fixed source calculation with JEFF 3.1 data. We also observe that the observed time increase for the JEFF 3.1 case is larger than the corresponding JEF 2.2 curve.

When we derived the upper and lower limit for the time increase, we focused on the cross section interval search as the main cause of the time increase. As a result, we didn't take into account the time required for instance for generating a random number, for sampling an angular distribution or the outgoing particle's energy distribution, for sampling the unresolved resonance probability tables, etc. Either way, even with our assumptions we obtained estimates of the same order of magnitude as the observed time increase which shows that the grid search is indeed a large contributor to the problem.

4.5.3 An infinite lattice of fuel pins

Although the previous example demonstrates our case perfectly, it is not a very realistic example for the problem of Monte Carlo burn-up. The infinite lattice of fuel pins is on the other hand a quite common exercise in burn-up applications. In this case, we have used a more realistic model being an infinite lattice of MOX fuel pins. This is also an example of a multiple cell problem.

The reaction rates to be calculated are the ones required by ORIGEN to

perform depletion calculations, being the (n,γ) , $(n,2n)$, $(n,3n)$ and the fission reaction for actinides and the (n,γ) , $(n,2n)$, (n,α) and (n,p) reaction for fission and activation products for both the JEF 2.2 and JEFF 3.1 nuclear data library. We have considered 5 sets of nuclides: ^{238}U , all actinides from the WIMS inventory model, all actinides from the nuclear data library, all actinides from the nuclear data library plus the fission products from the WIMS inventory model and all nuclides from the nuclear data library. For JEF 2.2 this resulted in a total of 4, 84, 166, 578 and 1154 reaction rates. For JEFF 3.1 these are 4, 88, 294, 709 and 1498 reaction rates.

The measured time increase can be found in figure 4.5. The observed time increase again lies nicely in between the two estimated curves for both nuclear data libraries. It also is closest to the upper boundary defined by equation 4.12 with $f_x = 0$, which is logical since for MCNP(X) f_x is quite close to zero. The α value for this example is a lot lower than for the ^{238}U cell ($\alpha = 0.024$ versus lower and upper estimates of 0.015 and 0.029 for JEF 2.2 and $\alpha = 0.026$ versus lower and upper estimates of 0.019 and 0.029 for JEFF 3.1). Calculating the reaction rates of the entire JEF 2.2 and JEFF 3.1 library resulted respectively in a time increase of a factor 29.3 and 41.3.

All points do not lie perfectly on the straight line. Processes that run in the background can slow down a calculation. When performing the previous ^{238}U cell calculations, we noticed drifts in the calculation time of 5 to 10 %. If such a drift occurs for this example, differences in calculation time of the order of hours would be possible. We also assumed that an $(n,2n)$ reaction rate takes as much time to calculate as an (n,γ) reaction rate, which is not correct (see the previous example). Because of this, the time increase could indeed be a bit lower than the estimates.

The assumption that the total time to calculate a cross section value is the same for every isotope is also no longer valid in this case. However, this example still shows a “linear” time increase as predicted. And the measured time increase still lies nicely in between our upper and lower boundaries.

4.6 Accumulation of fission products

We now have treated the problem of calculating reaction rates and its impact on the calculation time. For depletion calculations there is also another effect that will have an influence on the calculation time, namely the accumulation of fission and activation products. Contrary to the reaction rates, this effect is physical in nature. In order to properly model the neutron absorption and the resulting neutron spectrum we must take into account the absorption by these fission and activation products. Doing this will however increase the number of nuclides in the problem.

Furthermore, the number of fission and activation products created is also quite large. For a typical depletion calculation, ORIGEN 2.2 will give non-

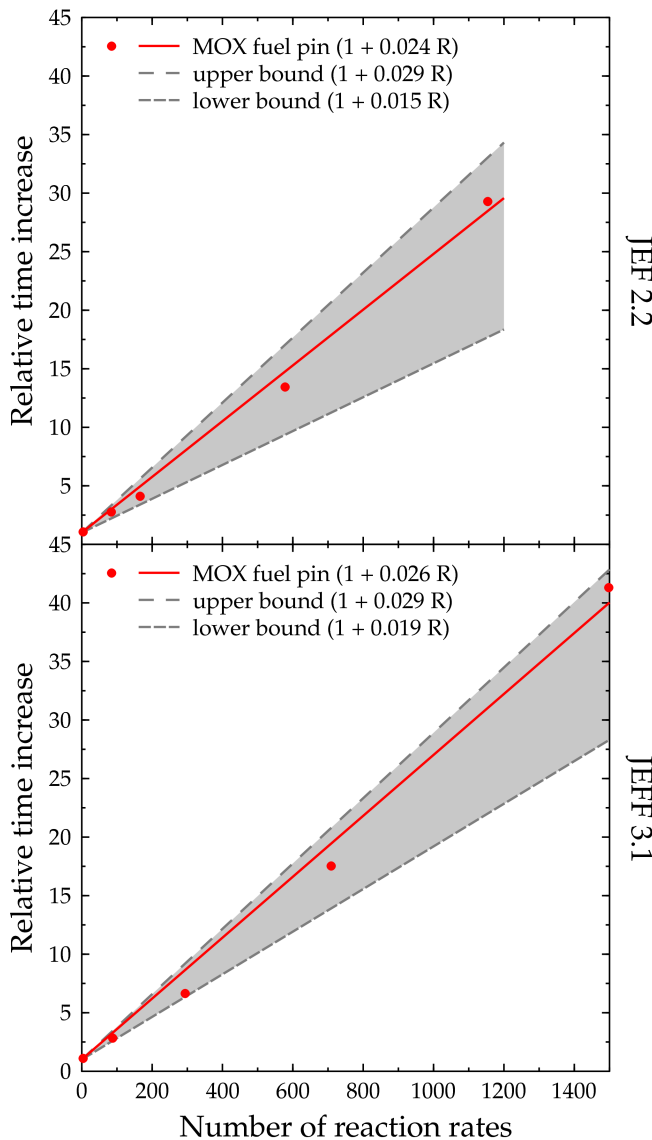


Figure 4.5: Estimated and observed relative time increase when calculating reaction rates for use in ORIGEN 2.2 for an infinite lattice of MOX fuel pins using the JEF 2.2 and JEFF 3.1 nuclear data libraries.

zero compositions of around 600 or more nuclides. Most of these don't even have a continuous energy library for use in a Monte Carlo code. And in most cases, the importance of absorption by the fission products is limited (in a thermal system the fission products are responsible of around 1 % of the total absorption in the fuel).

As we saw in section 4.2, the simulation time for a code like MCNP(X) which uses unionised cross section tables is roughly proportional to the number of nuclides in the cell (see table 4.1). The simulation time will therefore increase as more and more fission products are accumulated. The reaction rate calculation time will however remain the same provided that the number of tracks remains the same and that the number R of reaction rates to be calculated is not changed. For a Monte Carlo code with multi-group or universal unionised cross section tables this should not be a problem because the simulation time is roughly proportional to the number of tracks, regardless of the number of nuclides in the cell.

4.7 The optimum for Monte Carlo burn-up

Thus far, we have shown that the enormous CPU time consumption of Monte Carlo burn-up codes is mainly due to the calculation of all the cross section values during the Monte Carlo simulation for the purpose of reaction rate calculation. A simple way of mitigating the problem is to limit the number of reaction rates to be calculated every step. This can be done either by setting a fixed number of reaction rates from the start or to use a method in which reaction rates for nuclides are only calculated when these nuclides become "important".

This last case is rather subjective because the question is *when* a nuclide becomes important. Is a nuclide important when a certain mass of it is produced or when its total neutron absorption reaches a certain limit? Such an absorption based criterion should be preferred over a mass based criterion because this one takes into account the influence that a nuclide has on the neutron population of the system, while the first one only uses the number of atoms or simply the total mass. However, for the absorption criterion to work properly one needs to know the reaction rates of the nuclide in advance.

In addition, for which nuclides do you need reaction rates for the initial step? Only for those nuclides already present or for a list which must be set in advance? Such a method is definitely prone to misjudgement by the users unless the code determines a list in advance (like the isotope generation algorithm used in MCNPX 2.6.a and above [16]).

Furthermore, when the material becomes important a significant amount will have been produced already. So when one starts calculating the reaction rates for this nuclide, one will start with an incorrect initial composition because one didn't use correct data to model the chains around this nuclide in

the first place until it became important enough. Obviously, to be as accurate as possible one should have to calculate reaction rates for all possible nuclides by default, which brings us back to our initial problem.

In every calculation there should be a balance between accuracy and what is (reasonably) achievable. So when the simulation time is as low as possible and if calculating the reaction rates takes little or no extra time compared to this simulation time, then we can actually be as accurate as we want. And that is the optimum situation for Monte Carlo burn-up calculations.

From our previous analysis (see tables 4.1, 4.2 and 4.3) we can conclude that *the* solution for the problem is to adopt some form of universal unionised cross section tables (either multi-group or continuous energy). The effect of adopting this format is twofold:

- the time increase when calculating reaction rates compared to simulation time will be negligible ($f_x \approx 0$):

$$1 + \frac{f_x N_{tr} R}{N_{tr} + f_x (N_{tr} (N - 1) + N_i M) + f_x (M_1 + M_2)} \approx 1 \quad (4.15)$$

- it will actually minimise the Monte Carlo simulation itself and it gives us a significant acceleration when compared to unionised cross section tables (see equation 4.7):

$$\frac{t_s^{MC}}{t_s^{MG}} = N \quad (4.16)$$

With this cross section format it might even be possible to compete with deterministic codes on the level of calculation speed in addition to accuracy, especially for the more exotic applications. Unfortunately, up to this point no Monte Carlo code exists that uses universal unionised cross section tables (except of course for the obvious multi-group Monte Carlo codes).

Our best option in solving the CPU time problem is thus to optimize the process of reaction rate calculation so that it becomes negligible to the simulation time for existing Monte Carlo codes like MCNP(X). This obviously requires radical changes in the way that reaction rates are calculated.

*Citius, altius, fortius.
Swifter, higher, stronger.*

Olympic Games motto



Accelerating Monte Carlo with burn-up

5.1 An alternate approach to calculating reaction rates

In the previous chapter, we have shown that the grid search is the main cause of the slowness of the Monte Carlo burn-up calculation. Parallel processing (that is, simply apply brute calculation power) is one of the easiest solutions to the problem. It could indeed be a possibility for small scale problems but for large and complex burn-up calculations it would require vast amounts of processors, a luxury that not everybody has.

By reducing the number of grid searches for the reaction rate calculation, we will effectively reduce the calculation time. In the case of MCNP(X), we can already do this by performing some optimisation in the multiplier bin calculation used for reaction rates. As was pointed out before, microscopic cross sections of a single nuclide used by MCNP(X) are linearised on the same energy grid. Because of this, the cross section energy interval is determined only once during the simulation process so that calculating one or more cross section values of the same nuclide will take about the same amount of time. This does not appear to be the case in the multiplier bins where the interval is determined even if it was done already for a previous bin. If this could be changed, then the calculation time could be reduced significantly provided that multiple reaction rates of the same nuclide were requested. Another optimisation would be to test every reaction to see if it is defined in the cross section table before performing the cross section interval search.

These optimisations are already quite capable of alleviating the calculation time increase, but it is still possible to do even better. A way to do this is to let the simulation run its course and to calculate the reaction rates after the Monte Carlo simulation is finished. And that is what we do with the multi-group binning approach.

The estimators for the reaction rate and the total flux given by equations 3.19 and 3.20 are not the only way we can calculate these integrals. By definition, these integrals can also be given as a sum over infinitely small energy intervals:

$$\int \int \sigma_{i,r}(E) \phi(\mathbf{r}, E) dEdV = \lim_{g \rightarrow \infty} \sum_g \sigma_g \phi_g \quad (5.1)$$

$$\int \int \phi(\mathbf{r}, E) dEdV = \lim_{g \rightarrow \infty} \sum_g \phi_g \quad (5.2)$$

so that the spectral averaged single group microscopic cross sections σ are calculated as:

$$\sigma = \frac{\lim_{g \rightarrow \infty} \sum_g \sigma_g \phi_g}{\lim_{g \rightarrow \infty} \sum_g \phi_g} \quad (5.3)$$

in which σ_g and ϕ_g are the average cross section and the spectrum of the energy interval g with boundaries E_{g-1} and E_g :

$$\sigma_g = \frac{\int_{E_{g-1}}^{E_g} \sigma(E) dE}{E_g - E_{g-1}} \quad (5.4)$$

$$\phi_g = \frac{\int_{E_{g-1}}^{E_g} \phi(E) dE}{E_g - E_{g-1}} \quad (5.5)$$

with $\sigma(E)$ the energy dependent microscopic cross section of the material for which we calculate the reaction rate and $\phi(E)$ the energy dependent spectrum within the burn-up zone. Because the energy intervals are infinitely small, there is also no need to use a weighting spectrum for the multi-group cross section (as would be the case for a low number of groups) since the fine group structure is perfectly capable of representing the individual resonances.

For this approach to be an acceptable alternative, it must satisfy a number of conditions:

- *Nuclear data consistency*

The microscopic cross sections used in the Monte Carlo simulation must be the same as the ones used for the reaction rate calculation. In the case of traditional Monte Carlo burn-up this data consistency is insured by default as the reaction rates are calculated during the simulation. So for the multi-group binning approach we must also use the same data for calculating the multi-group cross section given by equation 5.4. This can be achieved easily if proper care is taken in the preparation of the cross section libraries for MCNP(X) and the multi-group binning approach.

- *Accuracy*

This approach of calculating the integrals is exact but to make this approach work numerically we will need a finite number of intervals. Fortunately, it is always possible to select an energy structure for these intervals so that the estimate of the single group cross section given by equation 5.3 differs only by an amount ϵ from the exact value. As a result, the size of the energy grid chosen simply depends on the required accuracy:

$$\left| \sigma - \frac{\lim_{g \rightarrow \infty} \sum_g \sigma_g \phi_g}{\lim_{g \rightarrow \infty} \sum_g \phi_g} \right| \leq \epsilon \quad (5.6)$$

We must therefore find an appropriate accuracy criterion and an energy structure that goes with it.

- *Stability*

The actual difference between the new and traditional method must be relatively independent of the convergence of the Monte Carlo simulation. When using fine energy intervals, the statistical errors of individual intervals can be relatively high. On the other hand, the weight of every interval compared to the whole will be quite small.

We should note that this method is neither an approximation nor is it a true hybrid method (which is a combination of Monte Carlo and deterministic methods) as it does not interfere in any way with the Monte Carlo simulation itself. At its core, it is just another way to calculate an integral. The name of the multi-group binning approach might be a bit misleading as it refers specifically to a well known technique in deterministic codes although the sheer scale on which we will apply it is entirely different.

The multi-group binning approach is only one solution. An alternative to the multi-group binning approach would be to gather the required data for the track length estimator (being the energy E_t , the track length l_t and weight w_t) and store them separately. After the Monte Carlo code finishes the simulation, the data should be sorted in increasing values of energy so that it is possible to go over these values energy by energy while going through the linearised cross sections interval by interval. By working in this way, it would only be necessary to go through an entire cross section only once without having to use a cross section interval search at all. Furthermore, the traditional tally estimators can still be used. Some care should be taken to correctly take the probability tables in the unresolved resonance range into account when using this strategy.

This solution is similar to the multi-group binning approach (both calculate the reaction rates when the Monte Carlo simulation has finished) but this

alternate solution would require major changes to the Monte Carlo code involved, which is why we preferred the multi-group binning approach.

5.2 An efficient and optimal approach

In the multi-group binning approach only a multi-group spectrum has now to be calculated by the Monte Carlo code. For this spectrum calculation, the Monte Carlo code has to determine in which energy bin to accumulate the flux and to perform the operations required for the track length estimator of the flux: calculating the product $l_t w_t$ and adding it to the previous result. And this has to be done for every track in the cell.

So the Monte Carlo code still has to perform an energy grid search, but only once for every particle track, regardless of the number of reaction rates. The time required to perform this grid search will be (approximately) the same as the cross section interval search (if the size of both grids are comparable). On the other hand, the number of operations that is needed after the grid search is smaller than those for the linear interpolation. The time required per track to accumulate the flux will therefore be a bit lower than the time to retrieve a cross section value.

If we now define f_t as the fraction of the cross section value retrieval time required for the flux accumulation, then the time t_m required to calculate the multi-group spectrum will be proportional to the number of tracks N_{tr} :

$$t_m \propto f_t N_{tr} \quad (5.7)$$

In most cases, the value of f_t will be close to 1. This estimate is quite similar to the reaction rate calculation time in MCNP(X) or a code taking advantage of unionised cross section tables ($t_r \propto N_{tr}R$ and $t_r \propto N_{tr}N_r$), but with $R = N_r = f_t$. It is almost equivalent to the situation where we only have to calculate one reaction rate to know all of them, which is definitely an improvement over the normal situation.

In the multi-group binning approach using MCNP(X) for the Monte Carlo simulation, the relative time increase in a single cell will thus be given by:

$$1 + \frac{t_m}{t_s + t_k} = 1 + \frac{f_t N_{tr}}{N_{tr}N + f_x N_i M + M_1 + f_x M_2} \quad (5.8)$$

In this equation, we do not use the simulation time estimate derived specifically for MCNP(X) (see equation 4.5). Instead we use the simulation time estimate of a general Monte Carlo code with unionised cross section tables because the cases of $f_x = 0$ and $f_x = 1$ are respectively a lower and upper boundary for the simulation time that also apply to MCNP(X).

For a multiple cell problem (see equation 4.12) this time increase will be given by:

$$1 + \frac{\sum_l t_{m,l}}{\sum_j t_{s,j} + \sum_i t_{k,i}} = 1 + \frac{f_t \sum_l N_{tr}}{\sum_j [N_{tr}N_j + f_x N_{i,j}M_j] + \sum_i [M_{1,i} + f_x M_{2,i}]} \quad (5.9)$$

In other words, the time increase due to reaction rate calculation with the multi-group binning approach behaves as (even for multiple cell problems):

$$1 + \frac{t_m}{t_s} = 1 + f_t \alpha \quad (5.10)$$

where the α value given here is the same as the one in equations 4.13 and 4.14.

The gain in CPU time of the multi-group binning approach (t_{MGB}) to that of traditional Monte Carlo (t_{MC}) becomes even greater when the number of reaction rates increases:

$$\frac{t_{MC}}{t_{MGB}} = \frac{1 + \alpha R}{1 + f_t \alpha} \quad (5.11)$$

So when using the multi-group binning approach, the dependence upon the number of reaction rates actually disappears. And the time increase is therefore constant, regardless of the number of reaction rates!

There is of course the calculation of the multi-group cross sections but with the proper method the CPU time required to calculate the multi-group cross sections will be negligible compared to the Monte Carlo simulation time. Furthermore, if a fixed energy grid is chosen then the calculation of the multi-group cross sections can be performed during the preparation of the nuclear data libraries.

The calculation time of every burn-up step is almost reduced to that of the basic Monte Carlo simulation, i.e. without any reaction rate to calculate. This is the optimal situation for Monte Carlo codes using unionised cross section tables like MCNP(X). This places the multi-group binning performance in between Monte Carlo with unionised and universal unionised cross section tables, as can be seen in table 5.1.

Table 5.1: Overview of Monte Carlo burn-up CPU time performance (assuming $f_x = 0$).

Type	t_s	t_r	$(t_s + t_r) / t_s$
non-unionised	$\propto N_{tr}N + N_iM$	$\propto N_{tr}R$	$\propto 1 + N_{tr}R / (N_{tr}N + N_iM)$
MCNP(X)	$\propto N_{tr}N$	$\propto N_{tr}R$	$\propto 1 + R/N$
unionised	$\propto N_{tr}N$	$\propto N_{tr}N_r$	$\propto 1 + N_r/N$
multi-group binning	$\propto N_{tr}N$	$\propto f_t N_{tr}$	$\propto 1 + f_t/N$
universal	$\propto N_{tr}$	≈ 0	≈ 1

5.3 Accuracy

5.3.1 The concept of accuracy

Choosing the appropriate energy intervals is very important in the multi-group binning approach. It is always possible to select an energy structure for these intervals so that the estimate of the single group cross section given by equation 5.3 differs only by an amount ϵ from the exact value:

$$\left| \sigma - \frac{\lim_{g \rightarrow \infty} \sum_g \sigma_g \phi_g}{\lim_{g \rightarrow \infty} \sum_g \phi_g} \right| \leq \epsilon \quad (5.12)$$

An appropriate accuracy criterion would be that the values calculated by the multi-group binning approach must be within one standard deviation of the values obtained by the traditional method. This way, we can ensure that reaction rates calculated with the multi-group binning approach cannot be distinguished from Monte Carlo values due to the statistical uncertainty of the latter. From a statistical point of view, both methods will give the same answer.

Less strict accuracy criteria of two or three standard deviations could also be acceptable under specific circumstances, for example when the statistical error is already quite small (there is little difference between an accuracy of for instance 0.02 % and three times this value). The choice of the accuracy criterion (or ϵ itself) will ultimately determine the size of the energy grid.

5.3.2 Optimising the energy structure

To create and optimise an energy structure that adheres to the one standard deviation criterion, we again used the single MOX fuel pin (see section 4.5.3). As ^{238}U is known to have the most resonances of all nuclides, ^{238}U (and the (n,γ) reaction in particular) is a perfect match to optimise the group structure. To demonstrate that this group structure is universally applicable, we performed these calculations using both data from the JEF 2.2 and JEFF 3.1 nuclear data library. The results from this optimisation process can be found in figure 5.1. This figure plots the ratio of the relative difference between the multi-group binning approach and Monte Carlo (δ_{MG}) to the Monte Carlo standard deviation (δ_{MC} , as given by MCNPX 2.5.0) for several ^{238}U cross sections.

The simplest energy structure that we can use consists of a large number of groups that are equally distributed (using lethargy) between the upper and lower cross section limit, which we did for a structure of 100000 groups. As we can see in figure 5.1, the cross section for $(n,2n)$, $(n,3n)$ and fission are well within one standard deviation (the relative difference δ_{MG} is at least less

than 1 % of the standard deviation δ_{MC}). The (n,γ) reaction is just within one standard deviation, but this one is already extremely low compared to the other reaction rates (0.08 % for the JEF 2.2 case and 0.09 % for the JEFF 3.1 case). This example already shows that the multi-group binning approach is a viable alternative to the traditional Monte Carlo method for calculating reaction rates.

Although the 100000 group structure does the trick just nicely, we can cut the required number of groups in two by using proper optimisation. For instance, by using very fine energy intervals in the resonance region of a cross section (between 1 eV and 1 MeV) and by using a more coarse structure over the rest of the energy range, we can account correctly for the resonance self shielding effect of the cross section. The best way to optimise the energy structure is to start with a small number of groups and to monitor the evolution of δ_{MG}/δ_{MC} when gradually adding more groups, as can be seen in figure 5.1.

Even for the smallest group structure that we considered (3250 groups with 1000 groups for every 4 orders of magnitude between 10^{-5} eV and 10 MeV and 250 groups between 10 and 20 MeV) the value of the single group cross sections (except for the (n,γ) reaction) are already well within one standard deviation of the Monte Carlo value. The (n,γ) reaction is unfortunately a tougher nut to crack due to the numerous resonances in this reaction. For this reaction, the relative difference is at least 400 times larger than the standard deviation.

When increasing the number of groups, the difference between the multi-group binning approach and Monte Carlo for the (n,γ) reaction drops rapidly. After increasing the number of groups by four (from 3250 to 13000 groups), the difference between ALEPH and MCNPX has already dropped by a factor 10. Instead of gradually adding more and more groups to the entire energy range, we can start adding more groups to problem areas. By thus increasing the number of groups in the resonance region between 1 eV and 1 MeV by 30000 to obtain a group structure of 43000 groups in total (4000 groups for every order of magnitude between 1 eV and 1 MeV except between 100 eV and 100 keV where we use 10000 groups), the value given by the multi-group binning approach falls nicely within one standard deviation of the Monte Carlo value for the JEF 2.2 case. For the JEFF 3.1 case, the relative difference with the Monte Carlo value is just outside the range (0.10 % difference versus a standard deviation of 0.09 %). Considering the extremely low value of the standard deviation, this is more than close enough. This will be the standard group structure that we will continue to use from now on.

At this point, it is possible to continue the optimisation to reduce the differences even further. Figure 5.1 contains for instance the results for three additional group structures above 43000 for which the difference between the multi-group binning approach and traditional Monte Carlo continues to decrease. The usefulness of this is however debatable. As stated in our conclusion to chapter 4, there should always be a balance between accuracy and what is (reasonably) achievable in every calculation. Using an optimised structure

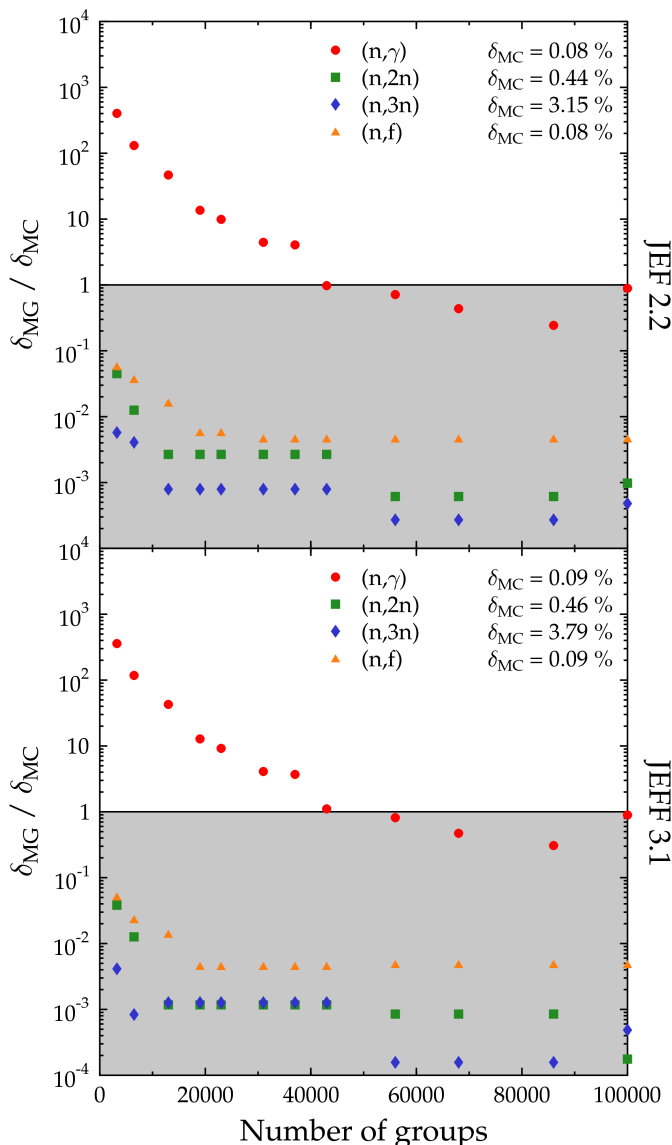


Figure 5.1: Ratio of the relative difference between the multi-group binning approach and MCNPX 2.5.0 (δ_{MG}) to the Monte Carlo standard deviation (δ_{MC}) for ^{238}U single group cross sections as a function of the group structure size for JEF 2.2 and JEFF 3.1 nuclear data in a single MOX fuel pin.

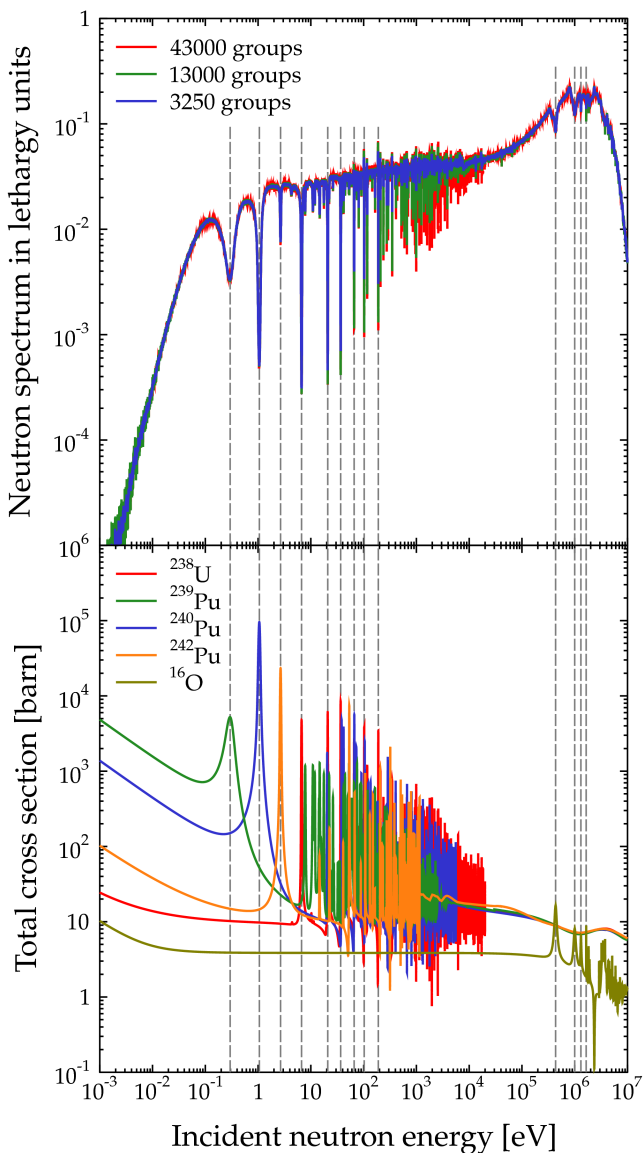


Figure 5.2: Neutron spectra in 3250, 13000 and 43000 groups for use by the multi-group binning approach (as calculated by MCNPX 2.5.0 in a single MOX fuel pin) compared to the total microscopic cross sections from the JEFF 3.1 nuclear data library of ^{238}U , ^{239}Pu , ^{240}Pu , ^{242}Pu and ^{16}O and the positions of some of their individual resonances.

twice the size of our standard structure might minimize the difference in the cross section values but it will also consume twice as much memory. And that can be quite important, especially when using parallel Monte Carlo where multiple processes have to share a limited amount of memory.

We now have a second group structure that adheres to our accuracy criterion, but with half the size of the first one. Figure 5.2 gives the spectrum for the single MOX fuel pin as calculated in the 3250, 13000 and 43000 group structures compared with the total microscopic cross sections of ^{238}U , ^{239}Pu , ^{240}Pu , ^{242}Pu and ^{16}O .

The spectrum in 43000 groups is quite detailed and actually shows the influence of individual resonances of various nuclides on the neutron spectrum in the MOX fuel pin. As ^{16}O and ^{238}U are the most abundant nuclides in the MOX fuel, their resonances will dominate the spectrum although large resonances of other nuclides can still have a significant influence. The large flux dips at 0.296 eV, 1.056 eV and 2.670 eV are for instance a result of the ^{239}Pu resonance at 0.296 eV, the ^{240}Pu resonance at 1.056 eV and the ^{242}Pu resonance at 2.670 eV. Figure 5.2 also shows the positions of 6 of the major resonances of ^{238}U (at 6.674, 20.871, 36.682, 66.030, 102.557 and 189.681 eV) which can all be easily identified in the MOX spectrum. In between some of these large dips we can also see the impact of some of the smaller resonances. The small dips in between the ^{238}U resonances between 6.674 and 20.871 eV can for instance be attributed to ^{239}Pu . The higher we go in energy, the more resonances start to appear. Between 100 eV and 100 keV there are so many that we can no longer visually distinguish the different resonances. ^{16}O itself has only resonances above 400 keV (the first ^{16}O resonances appear at 435 keV and at 1, 1.31 and 1.651 MeV) so their influence is limited to that energy region.

5.3.3 Global agreement

Now that we have found an appropriate energy structure that works well for ^{238}U , we must verify if this structure also works for all the other nuclides. For this purpose, we have calculated all possible one group cross sections that can be used by ORIGEN 2.2 from the JEF 2.2 and JEFF 3.1 nuclear data libraries for our MOX fuel pin. The results of this exercise can be found in table 5.2.

The table gives the number of cross section values computed by the multi-group binning approach that are within one standard deviation as compared to the values that were obtained directly with MCNPX 2.5.0. This table only lists the non-zero cross section values (the JEF 2.2 and JEFF 3.1 nuclear data libraries can provide respectively 958 and 1317 non-zero cross sections for use in ORIGEN 2.2).

Again, we observe that agreement between the multi-group binning approach and MCNPX is reached very quickly for all reactions except the (n,γ) reaction. For most threshold reactions, namely the $(n,2n)$, $(n,3n)$, (n,α) and (n,p) reactions, this is logical as these have very smooth cross sections that can

Table 5.2: Agreement between the multi-group binning approach and traditional Monte Carlo: the number of single group cross sections within one standard deviation (as given by MCNPX 2.5.0) for the entire JEF 2.2 and JEFF 3.1 nuclear data library in a single MOX fuel pin. The rows labelled MCNPX give the total number of non-zero reaction rates calculated by MCNPX 2.5.0 for the corresponding data library.

Groups	JEF 2.2					
	(n, γ)	(n,2n)	(n,3n)	(n,f)	(n, α)	(n,p)
MCNPX	284	155	36	39	222	222
3250	181	155	36	35	221	222
6500	221	155	36	37	221	222
13000	262	155	36	39	222	222
19000	276	155	36	39	222	222
23000	280	155	36	39	222	222
31000	283	155	36	39	222	222
37000	283	155	36	39	222	222
43000	284	155	36	39	222	222
56000	284	155	36	39	222	222
68000	284	155	36	39	222	222
86000	284	155	36	39	222	222
100000	284	155	36	39	222	222
Groups	JEFF 3.1					
	(n, γ)	(n,2n)	(n,3n)	(n,f)	(n, α)	(n,p)
MCNPX	362	273	62	57	282	281
3250	245	273	62	53	280	280
6500	297	273	62	56	280	280
13000	331	273	62	57	282	281
19000	349	273	62	57	282	281
23000	358	273	62	57	282	281
31000	361	273	62	57	282	281
37000	361	273	62	57	282	281
43000	361	273	62	57	282	281
56000	362	273	62	57	282	281
68000	362	273	62	57	282	281
860000	362	273	62	57	282	281
100000	362	273	62	57	282	281

be described with very few points and as such by few groups (in the case of 3250 groups, there are already 500 groups between 1 and 20 MeV). The only exception in the JEF 2.2 library is the (n,α) reaction of ^{16}O and for JEFF 3.1 these are the (n,α) reactions of ^{16}O and ^{60}Ni and the (n,p) reaction of ^{37}Cl . These nuclides all have over 1000 points in their linearised cross sections above 1 MeV so they need at least as many groups to properly calculate the reaction rate. In all these cases, 13000 groups (with 2000 groups above 1 MeV) appears to suffice.

For fission rates, a group structure of at least 13000 groups was needed to get all values within a single standard deviation. We can also see that at 31000 groups all values are within one standard deviation, except one: the (n,γ) reaction of ^{238}U for which 43000 groups. At 31000 groups, the difference between traditional Monte Carlo and the multi-group binning approach for this reaction is 0.35 % with JEF 2.2 and 0.37 % with JEFF 3.1 (see figure 5.1), which is in both cases just outside the range of three standard deviations. For a system with little or no ^{238}U , this group structure would most likely suffice.

We can now conclude that the multi-group binning approach and MCNPX are in excellent agreement (all values are within one standard deviation) by using the standard group structure of 43000 groups. Furthermore, the energy structure optimisation technique using ^{238}U presented here is very flexible and can be applied to any other problem or data set, should the need arise.

5.4 Convergence and stability

The third condition that the multi-group binning approach must adhere to is stability of the method. This means that the actual difference between the new and traditional method must be independent of the convergence of the Monte Carlo simulation. Otherwise it wouldn't make much sense to use a new method that accelerates one part the calculation and on the other hand looses what was gained because we need more precision for it to work. Using a fine group structure will indeed result in very poor statistics in many of those groups which will result in the presence of "noise" in the spectrum. This noise on the spectrum is already visible in figure 5.2.

Compared with the 3250 group spectrum, our spectrum in 43000 groups appears to exhibit quite a lot of noise. This is clearly visible below 10 eV and above 100 keV where we see a lot of spikes around the smooth 3250 groups spectrum. However, we also see that many of the resonances visible between 1 eV and 1 MeV do not appear at all in the 3250 group spectrum because this energy structure is just too coarse in that energy range. The same applies to the 13000 group spectrum, although there are already a lot more resonances visible. Quite a large amount of noise is also visible below 10^{-2} eV and above 10 MeV but the importance of the spectrum at those energies is so low (less than 10^{-4}) that it has almost no bearing on the final result.

Table 5.3: The relative errors δ_{MC} and δ_{MG} for ^{238}U cross sections calculated using MCNPX 2.5.0 and the multi-group binning approach in a single MOX fuel pin for different levels of convergence.

n/cycle	JEF 2.2							
	(n, γ)		(n,2n)		(n,3n)		(n,f)	
	δ_{MC}	δ_{MG}	δ_{MC}	δ_{MG}	δ_{MC}	δ_{MG}	δ_{MC}	δ_{MG}
20	2.650	0.064	14.520	0.021	51.280	0.148	2.870	0.002
200	0.810	0.045	4.340	0.002	37.700	0.053	0.830	0.000
2000	0.260	0.080	1.370	0.003	8.730	0.011	0.260	0.000
20000	0.080	0.078	0.440	0.001	3.150	0.002	0.080	0.000
n/cycle	JEFF 3.1							
	(n, γ)		(n,2n)		(n,3n)		(n,f)	
	δ_{MC}	δ_{MG}	δ_{MC}	δ_{MG}	δ_{MC}	δ_{MG}	δ_{MC}	δ_{MG}
20	2.620	0.106	18.360	0.014	82.550	0.022	2.750	0.004
200	0.810	0.097	4.490	0.001	29.880	0.001	0.820	0.001
2000	0.260	0.088	1.420	0.001	11.360	0.016	0.260	0.000
20000	0.080	0.100	0.450	0.001	3.780	0.005	0.080	0.000

The error in an individual group can indeed be large, but the contribution of a particular group to the one group reaction rate and its error will still be small. If this were not the case, we would not get 100 % agreement with normal Monte Carlo unless we used a very large number of particles to reduce the influence of the noise. Fortunately, this does not appear to be the case. This is illustrated in table 5.3 which gives the relative error δ_{MC} on ^{238}U cross sections calculated by MCNPX 2.5.0 and the difference δ_{MG} with the multi-group binning approach for different levels of Monte Carlo convergence and for the JEF 2.2 and JEFF 3.1 nuclear data libraries.

For the Monte Carlo standard deviation values, we observe the normal Monte Carlo convergence behaviour: the error is inversely proportional to the square root of the number of particles. For instance, the relative error on the (n, γ) reaction decreases by a factor 33.125 when increasing the number of particles by 1000 ($\sqrt{1000} = 31.623$). The relative difference with the multi-group binning approach however remains roughly the same, which is in all cases well within one standard deviation and less than 0.2 % even when the standard deviation is over 50 %.

We can thus conclude that the multi-group binning approach will always give numerical results very close to the value given by Monte Carlo, even if the statistical error on those values is large.



Knowledge is power.

Sir Francis Bacon (1561 - 1626)

Get the facts, or the facts will get you. And when you get them, get them right, or they will get you wrong.

Dr. Thomas Fuller (1654 - 1734)

Nuclear data for burn-up applications

6.1 Nuclear data requirements

In the previous chapters we discussed the calculation of the most important part of the nuclear data needed for a depletion calculation, being the cross sections themselves. Although these cross sections form the bulk of the data needed, the importance of the rest of the data needed by the depletion code cannot be ignored either:

- isomer branching ratios;
- direct fission product yields;
- total average neutron yield per fission;
- total recoverable energy per fission;
- decay data.

All of these data can be found in Evaluated Nuclear Data Files (or ENDF files) [23], in one form or another. By using data from these ENDF files, we would have no need of other third party data or models. The use of these ENDF files will therefore provide us with a consistent set of data, for both the depletion and transport module. This approach will also allow us to quickly change our data when newer (and better) evaluations become available, making the burn-up code very flexible in its use of nuclear data (which is exactly what the ENDF format was designed for). Furthermore, using ENDF files will automatically insure nuclear data consistency because the Monte Carlo code will use the same ENDF files and the same data preprocessing code.

6.2 ENDF - Evaluated Nuclear Data File

6.2.1 The ENDF format and nuclear data libraries

The ENDF format and its associated evaluated ENDF/B library is being developed and maintained by the National Nuclear Data Center (NNDC) of Brookhaven National Laboratory (BNL) and a group of various national laboratories, industry and universities in the US and Canada represented in the Cross Section Evaluation Working Group (CSEWG). The format is designed for the storage and retrieval of evaluated nuclear data required for various applications in the nuclear field. As a consequence the data included in the ENDF file must be *complete* for the intended application and it must be the best and most reliable data available.

Completeness means that reaction data has to be represented over the entire energy range of interest for the application (even if the available experimental data doesn't cover it entirely) because otherwise transport calculations using the ENDF file as basic data would simply be worthless.

In some cases there will be no experimental data available to the evaluator so that he will have to rely solely on model calculations. Because an evaluation has to contain the best and most reliable data, the work of an evaluator is never finished and it probably never will be. Unfortunately the importance of nuclear data is often overlooked or outright ignored by many.

A basic characteristic of the ENDF format is that it is application and code independent. In order to use the data in an ENDF file for a specific application using a specific code the data needs to be processed by a data pre-processing code like NJOY [38] or PREPRO [39].

Earlier versions of the ENDF format allowed for representation of neutron cross sections and distributions, photo-atomic interaction data, thermal neutron scattering data, fission yield and radio-active decay and radio-active nuclide production data. The first version of the ENDF format dates back to the early 60s. The format was originally only used for the ENDF/B nuclear data library. As a result, all these previous versions of the ENDF format and the associated ENDF/B library are referred to with the same name (for instance ENDF/B-V refers to both the format and the ENDF/B-V nuclear data library).

ENDF is now de facto the international standard for storage and exchange of evaluated nuclear data, although the CSEWG and NNDC still maintain control over the ENDF format. The current version of the ENDF format (denoted as ENDF-6) was created in 1990 for use with the ENDF/B-VI nuclear data library. Its last revision dates back to 2005 (see the ENDF manual report ENDF102 [23]) to update the format for use with the ENDF/B-VII evaluations.

ENDF-6 has the capabilities of the previous versions, with the addition of higher incident energies (an increase from the original 15 MeV to 20 MeV), more complete descriptions of emitted particles, new resonance parameter formats, etc. With the creation of sub-libraries it also became possible to use

the ENDF format for other particles like protons, deuterons, α particles, etc. in addition to the original neutrons and photons.

Several evaluated nuclear data libraries are available in the ENDF-6 format: ENDF/B-VI.8 (and the forthcoming ENDF/B-VII) for the US, JEFF 3.1 (Joint Evaluated Fission and Fusion) for Europe, JENDL 3.3 (Japanese Evaluated Nuclear Data Library) for Japan, BROND for Russia and CENDL for China. All these nuclear data evaluations are freely available from different nuclear data centres in the world:

- National Nuclear Data Center: www.nndc.bnl.gov;
- Nuclear Energy Agency (NEA) Databank of the Organisation for Economic Cooperation and Development (OECD): www.nea.fr;
- Nuclear Data Section of the International Atomic Energy Agency (IAEA-NDL): www-nds.iaea.org.

The previously mentioned nuclear data libraries contain all the required information to perform detailed neutron transport calculations. In the case of ENDF/B-VI.8 and JEFF 3.1 the library also includes data for the transport of protons, deuterons, etc. Apart from these “particle transport capable” nuclear data libraries, there are also what we call the activation libraries. In general, these activation libraries (like for instance JEFF 3.0A and 3.1A) contain data for a lot more nuclides than their transport capable counterpart. They contain detailed data for activation and depletion calculations but they are not suited for transport calculations due to incomplete data (like for instance the elastic scattering cross section, angular distributions, etc.).

6.2.2 ENDF file and library structure

Before ENDF-6, all data pertaining to a specific material could be put into a single ENDF file. This included decay data, fission yields, etc. With ENDF-6 this was changed drastically with the introduction of sub-libraries. These sub-libraries include photo-nuclear data, photo-induced fission product yields, photo-atomic interaction data, radio-active decay data, spontaneous fission product yields, atomic relaxation data, incident neutron data, neutron induced fission product yields, thermal neutron scattering data, etc.

A complete library encompasses several of these sub-libraries. JEFF 3.1 for instance consists of the following sub-libraries:

- incident neutron data;
- incident proton data;
- thermal scattering data;
- neutron induced fission product yields;

- spontaneous fission product yields;
- radio-active decay data.

In practice these sub-libraries are “physically” separated from one another because they are stored in separate ASCII computer files, or “tapes” as they are called in ENDF terminology. The word “tape” is a remnant from the history of the ENDF format because the large ENDF files were stored on magnetic tapes. Back then, the master ENDF tapes were even stored in a vault at the NNDC as they were regarded as a strategic resource.

Every ENDF tape is in turn subdivided into materials, being parts of the tape dedicated to a single target material which can be either a single isotope, an element or a mixture of elements (like a compound, molecule, etc.). Isotopes in different isomeric states (like for instance ^{242}Am and $^{242\text{m}}\text{Am}$) are also considered as two different materials in the ENDF tape.

These materials are identified with a unique identifier, the four digit MAT number which ranges from 1 to 9999. The first two digits refer to the Z-number of the element. The last two digits are by definition 00 for the natural elements. For isotopes the last two digits are assigned in order of increasing mass in steps of three (allowing for the ground state and two isomeric states of the same isotope). The lightest stable isotope always starts at 25 so that the formulation can easily accommodate all the neutron excess nuclides. Following these rules, the MAT numbers of for instance ^{242}Am and $^{242\text{m}}\text{Am}$ are respectively 9546 and 9547. For ^{234}U , ^{235}U and ^{238}U these would be 9225, 9228 and 9237.

Every material is then subdivided into several “files”, designated with the MF number (a two digit number between 1 and 99). Every file contains specific data, as given in table 6.1. The MF-numbers are restricted to the values given in the table.

The files themselves are in turn subdivided into several sections identified with a three digit MT number between 1 and 999. These MT numbers can be subdivided into several categories: elastic scattering, simple single particle reactions, simple multi-particle reactions, complex reactions, radiative capture, fission, non-elastic reaction for photon production, special production cross section and auxiliary numbers. An overview of these MT numbers and their meaning can be found in appendix B of the ENDF102 report [23].

Some files and MT sections are restricted to particular sub-libraries. Certain MT numbers are even restricted to specific files. File 7 for instance is only found in the thermal neutron scattering data sub-library. On the other hand, every material of every sub-library must have an MF1 MT451 (descriptive data and directory) section but only file 1 may have an MT451 section.

The units of the data put into an ENDF file are also fixed. Cross section data must be given in barn (10^{-24} cm^2), temperatures must be given in Kelvin, time must be given in seconds, distributions must be given as probabilities (per unit cosine for angular distributions, per eV for energy distributions, etc.).

Table 6.1: Overview of ENDF MF numbers in ENDF-6.

MF-number	Description
1	General information
2	Resonance parameters
3	Reaction cross sections
4	Angular distributions for emitted particles
5	Energy distributions for emitted particles
6	Energy-angle distributions for emitted particles
7	Thermal neutron scattering law data
8	Radio-activity and fission product yield data
9	Multiplicities for radio-active nuclide production
10	Cross sections for radio-active nuclide production
12	Multiplicities for photon production
13	Cross sections for photon production
14	Angular distributions for photon production
15	Energy distributions for photon production
23	Photo- or electro-atomic interaction cross sections
26	Electro-atomic angle and energy distributions
27	Atomic form factors or scattering functions
28	Atomic relaxation data
30-35,39-40	Covariance data

The content of the various ENDF tapes, materials, files and sections is stored using basic ENDF building blocks, being TEXT, CONT (with special cases HEAD, END and DIR), LIST, TAB1, TAB2 and INTG. This last record was added in the last revision of the ENDF-6 format for use in ENDF/B-VII. These records consist of one or more lines of an 80 character FORTRAN record (the ENDF format was created with processing codes written in FORTRAN in mind). To read an ENDF section it is only necessary to implement functions capable of reading these basic ENDF building blocks.

6.3 Neutron cross section data

Reaction cross section data are given in file 3 as functions of the incident energy E (given in the LAB system). These consist of an energy grid with associated cross section values. The ENDF format allows for a number of possible interpolation schemes to describe the energy dependence of the cross section σ in between the different tabulated energy points:

- histogram: σ is constant between the two energy points;
- lin-lin: σ is linear in E ;

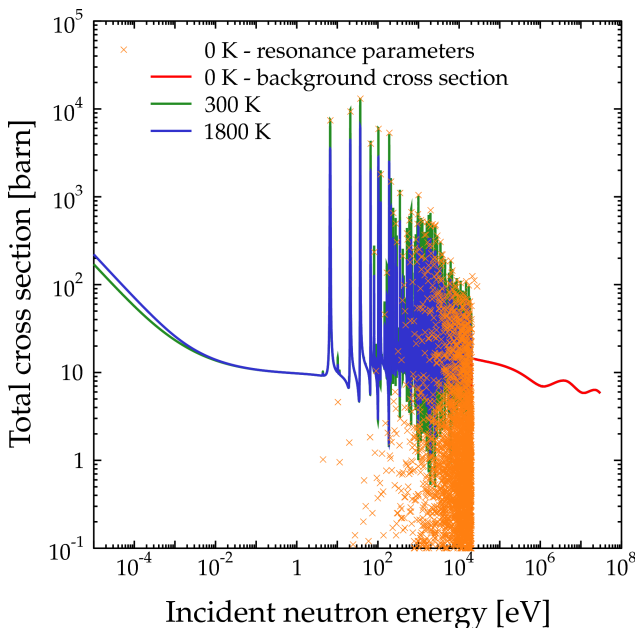


Figure 6.1: The total microscopic cross section of ^{238}U from the JEFF 3.1 nuclear data library: unreconstructed data at 0 K and reconstructed and Doppler broadened data at 300 and 1800 K.

- lin-log: σ is linear in $\ln(E)$;
- log-lin: $\ln(\sigma)$ is linear in E ;
- log-log: $\ln(\sigma)$ is linear in $\ln(E)$.

The lin-lin interpolation scheme is the most interesting one from an application point of view but it is not the most compact way. The other interpolation schemes are more compact and in some cases more suitable to represent the cross section. Take for instance the $1/v$ cross section behaviour in the thermal energy range. In a log-log scale, this is a simple straight line between two points so that the log-log interpolation scheme would only need two points to represent this behaviour.

For elastic scattering, fission and the (n,γ) reaction, the resolved and unresolved resonance parameters which are found in file 2 must be added to file 3 as well to obtain the complete cross section (the process of adding those resonance parameters to the cross section is called resonance reconstruction). If the resonances are not added to the cross section, file 3 will contain background cross sections (which can be negative in some cases).

Table 6.2: Cross sections required by ORIGEN 2.2 and their ENDF MT numbers.

MT number	Reaction	Material Types
16 or 875-891	(n,2n)	all materials
17	(n,3n)	actinides
18 or 19-21, 38	(n,fission)	actinides
102	(n, γ)	all materials
103 or 600-649	(n,p)	activation and fission products
107 or 800-849	(n, α)	activation and fission products

The cross sections are also given at a specific temperature (in practice this will be 0 K). To obtain the proper cross section at the proper temperature the ENDF file will have to be processed by a data pre-processing code to reconstruct and Doppler broaden the cross sections to the appropriate temperature. For ease of usage, the cross sections will also be linearised by the pre-processing code.

As a result from the Doppler broadening process, the resonances will decrease in height and increase in width. Contrary to popular knowledge, the area under the Doppler broadened resonances does not remain the same, unless $E \gg kT/A$ [38]. Furthermore, all resonances will develop an additional $1/v$ tail that has to be added to the existing $1/v$ cross section. A constant cross section (like the one found in elastic scattering) will also develop such a $1/v$ tail at lower energies while a $1/v$ cross section itself remains unchanged.

As an example, figure 6.1 gives the total microscopic cross section data as it can be found in the unreconstructed ENDF file of ^{238}U from the JEFF 3.1 nuclear data library: resonance parameters in file 2 and a background cross section above 20 keV in file 3. The figure also shows the reconstructed and Doppler broadened cross sections at 300 and 1800 K. We clearly see the effects of the Doppler broadening: the resonances at 1800 K are less pronounced than at 300 K and the cross section has developed an additional $1/v$ tail.

Table 6.2 gives an overview of the MT numbers for the various reactions required by ORIGEN 2.2. The (n, γ) and (n,3n) reaction are only associated with a single MT number (respectively 102 and 17). For the (n,2n), (n,p) and (n, α) reactions there are two possibilities as they can be represented using a summation cross section and by individual discrete levels and a continuum. This is similar to the way inelastic scattering is represented in the ENDF format. For the (n,2n) reaction these numbers are 16 for the summation and 875-891 for the discrete and continuum levels, for (n,p) this is 103 and 600-649 and for (n, α) this is 107 and 800-849. The fission reaction can also be defined as a summation cross section (MT-number 18) and with partials (MT-numbers 19-21 and 38 for first, second, third and fourth chance fission).

6.4 Isomeric branching ratio

The cross section data that we can read from the ENDF files will give us precise information on the disappearance of a particular material. The material created in the reaction is however another matter. First of all there is fission in which numerous different materials can be created. Even simple reactions can lead to the production of “different” materials in the form of isomeric states. These isomeric states are long-lived excited states of one and the same nuclide but their behaviour can be quite different.

The $^{241}\text{Am}(n,\gamma)^{242\text{g}}\text{Am}$ and $^{241}\text{Am}(n,\gamma)^{242\text{m}}\text{Am}$ reactions are a good example of why this distinction is important. Even though $^{242\text{g}}\text{Am}$ and $^{242\text{m}}\text{Am}$ are essentially the same nuclide, they will lead to very different transmutation paths. ^{242}Am in the ground state has a half-life of 16 hours and will therefore decay almost immediately to ^{242}Cm (with a half-life of 163 days) via β^- -decay and then to ^{238}Pu via α -decay whereas $^{242\text{m}}\text{Am}$ (the isomeric state with a half-life of 142 years) can be transmuted into higher Am and Cm isotopes like for instance in ^{243}Am (with a half-life of 7400 years).

In order to properly account for the production of isomeric states of the same nuclide (and the subsequent transmutation chains), we need to use the data from files 9 (multiplicities for radio-active nuclide production) and 10 (cross sections for radio-active nuclide production). The formatting in both files is exactly the same as for a normal cross section from file 3, but instead of containing only one set of tabulated cross section values these files can contain multiple sets corresponding to individual isomeric states.

The difference between both files is that file 9 actually gives the energy dependent branching ratio λ_s of the cross section σ_s towards a particular excited state s to that of the total reaction cross section:

$$\lambda_s(E) = \frac{\sigma_s(E)}{\sum_s \sigma_s(E)} \quad (6.1)$$

while file 10 gives the individual cross section σ_s towards the particular excited state s directly. The proper branching ratio can then be determined easily with the previous formula. A reaction that has resonance parameters (like the (n,γ) reaction) may not use file 10 to represent the different cross sections to the individual isomeric states. Only file 9 may be used for these reactions.

Unfortunately, isotopic branching ratio data is often not well known. This is nicely illustrated in figure 6.2 which shows the $^{241}\text{Am}(n,\gamma)$ branching ratio towards the ^{242}Am ground state from the ENDF/B-VI.8, JENDL 3.3 and JEFF 3.1 nuclear data libraries. Below 1 eV, about 90 % of all (n,γ) interactions with ^{241}Am go to the ^{242}Am ground state. From that point on, the libraries start to differ. The branching ratio from the JEFF 3.1 nuclear data library remains roughly the same and doesn't drop below 75 % while the JENDL 3.3 and ENDF/B-VI.8 nuclear data library continue to drop to a value of 50 %

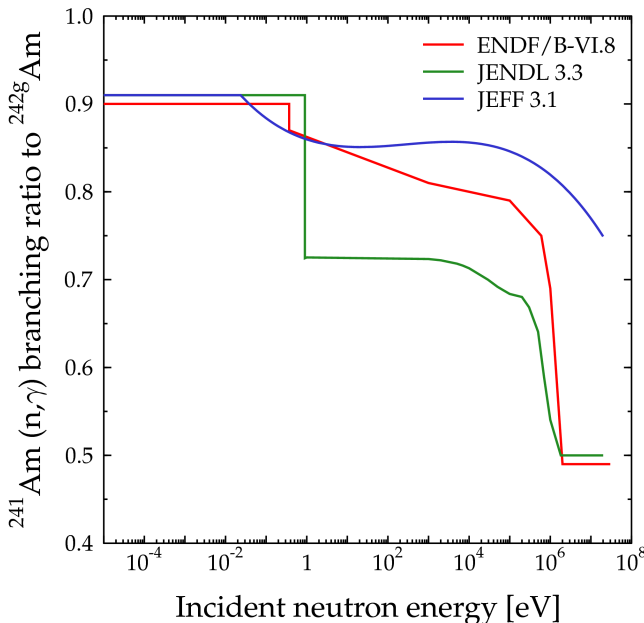


Figure 6.2: The ^{241}Am (n,γ) branching ratio towards the ^{242}Am ground state from the ENDF/B-VI.8, JENDL 3.3 and JEFF 3.1 nuclear data libraries.

above 1 MeV. In thermal systems this will have little influence but in fast spectrum systems like ADS this won't be the case.

ORIGEN 2.2 only needs branching ratio data for the ground state and first isomeric state for the nuclides produced in an (n,γ) and ($n,2n$) reaction. When the data are read from file 9, an average branching ratio λ_s must be calculated:

$$\lambda_s = \frac{\int \int \lambda_s(E) \sigma(E) \phi(\mathbf{r}, E) dE dV}{\int \int \sigma(E) \phi(\mathbf{r}, E) dE dV} \quad (6.2)$$

where σ is the total cross section for the reaction in question (which is found in file 3). Because this type of value cannot be calculated directly with Monte Carlo, we will need to calculate it ourselves using the same method as for the reaction rates:

$$\lambda_s = \frac{\lim_{g \rightarrow \infty} \sum_g \lambda_{s,g} \sigma_g \phi_g}{\lim_{g \rightarrow \infty} \sum_g \sigma_g \phi_g} \quad (6.3)$$

where σ_g is the cross section of group g calculated with equation 5.4 and $\lambda_{s,g}$

Table 6.3: Branching ratios towards the ground state calculated for a single MOX fuel pin with the JEFF 3.1 nuclear data library compared with the ORIGEN 2.2 values from PWRPUPU.LIB.

Nuclide	Reaction	File	JEFF 3.1	ORIGEN 2.2
^{45}Sc	(n, γ)	9	0.7719	0.6377
^{45}Sc	(n,2n)	10	0.6597	-
^{74}Ge	(n, γ)	9	0.7547	0.8827
^{76}Ge	(n, γ)	9	0.3305	0.6250
^{76}Ge	(n,2n)	10	0.3676	-
^{103}Rh	(n,2n)	10	0.3343	-
^{209}Bi	(n, γ)	9	0.7836	0.5758
^{237}Np	(n,2n)	9	0.2500	0.2585
^{241}Am	(n, γ)	9	0.8651	0.8900

is the branching ratio for group g calculated by:

$$\lambda_{s,g} = \frac{\int_{E_g}^{E_{g-1}} \lambda_s(E) \sigma(E) dE}{\int_{E_g}^{E_{g-1}} \sigma(E) dE} \quad (6.4)$$

When using file 10 data, the reaction rates σ_s for the ground state and the different isomeric states can be calculated directly with equation 5.3. The average branching ratio will then be given by:

$$\lambda_s = \frac{\sigma_s}{\sum_s \sigma_s} \quad (6.5)$$

As an illustration, we have calculated the values for the branching ratios towards the ground state for some nuclides from JEFF 3.1 for the single MOX fuel pin which we used to demonstrate the accuracy of the multi-group binning approach in chapter 5. The results can be found in table 6.3. For the (n,2n) reactions on ^{45}Sc , ^{76}Ge and ^{103}Rh we see that ORIGEN 2.2 didn't even make a distinction in the production of the reaction product in the ground state and a metastable state. In all other cases (except for the (n, γ) reaction on ^{76}Ge and ^{209}Bi) the calculated branching ratios are of the same order of magnitude as the ORIGEN 2.2 values. Recalculating the branching ratios instead of using a single fixed value will increase the precision in the modelling, especially for nuclides like ^{241}Am and its (n, γ) reaction product ^{242m}Am (see for instance chapter 10 for the influence of this branching ratio).

6.5 Direct fission product yields

In addition to the reaction data described above, direct fission yield data are required to correctly account for the fission products. Within the ENDF-6 format, fission yields all have their own sub-library. There is the sub-library for both neutron and proton induced fission yields, one for photo-induced fission product yields and one for spontaneous fission yields. In our case we are only interested in the neutron induced fission product yields, but they all use the same format.

The fission yields can be found in file 8 within the sections with MT numbers 454 (direct or independent fission yields) and 459 (cumulative fission yields). Direct fission yields are yields per fission prior to the emission of delayed neutrons, delayed beta radiation, etc. This is exactly what ORIGEN 2.2 needs to calculate the fission products. The sum of all direct yield values will equal 2.0 (in the ORIGEN 2.2 libraries the sum of these direct yields will be 200.0). Cumulative yields on the other hand account for all decay branches (including delayed neutrons).

Like any other nuclear data property, the fission product yields also have some energy dependence. The ENDF format has therefore foreseen the possibility of adding energy dependent fission product yields (as tabulated values, just like a cross section but with a fixed lin-lin interpolation scheme). The ENDF format states that the energy range over which the yields are given must be the same as the energy range of the fission cross section as it is defined in file 2 and/or 3.

Unfortunately this doesn't appear to be the case, even in the latest evaluated nuclear data libraries (like JEFF 3.1). In practice fission yield data are given for a maximum of 3 incident neutron energies: 0.0253 eV (thermal spectrum fission yields), 400 or 500 keV (fast spectrum fission yields) and 14 MeV (fusion spectrum fission yields). Furthermore, it is not advised to use these sets as energy dependent yields even though they use the official energy dependent format [41]. For the moment, a user should choose a specific set of fission product yields and stick with it. In some cases, only a single set of fission product yield data is given.

However, for advanced nuclear systems (like some GEN IV concepts, ADS systems, etc.) this energy dependence can become very important. In the case of an ADS, the spectrum at the centre of the core is a spallation spectrum (similar to a fission spectrum but with an additional high-energy tail) while this spectrum is more epithermal at the outside of the core [42]. Normal thermal and fast spectrum reactors do not have such drastic spectral shifts in their cores so this limitation in fission yield data is not likely to pose a big problem in those cases.

The CINDER capability within MCNPX 2.6.b [13, 16] already has an elegant solution to implement some form of energy dependence in the fission yields using the available thermal, fast and high energy fission product yields.

Every set has been associated with a specific energy range and for every material MCNPX determines the integral fission rate associated with those energy ranges. The fission yields of the set that has the majority of the fission events are then regarded as the most appropriate for the material in question. This is done separately for every burnable material so that it is possible that MCNPX will assign thermal yields for one material but high energy yields for another one. It should be noted that this approach only works properly if appropriate energy boundaries are chosen.

Another solution would be to use fission product yields determined by model calculations. This will however lead to a deviation of the nuclear data philosophy presented in section 6.1 which stated that all data should come from ENDF files and that no third party data and/or models would be accepted.

A lot of work has already been done in developing such energy and even temperature dependent fission yield models [43, 44]. This capability has already been implemented into the TALYS code [44].

TALYS is a nuclear reaction program created at NRG Petten (the Netherlands) and CEA Bruyères-le-Châtel (France), which simulates nuclear reactions involving neutrons, gamma-rays, protons, deuterons, tritons, helions and α -particles, in the 1 keV to 200 MeV energy range. A suite of nuclear reaction models has been implemented into TALYS which enables its user to evaluate basically all nuclear reactions beyond the unresolved resonance range. Some of the evaluations in the JEFF 3.1 evaluated nuclear data library have been produced with this code (like for instance the evaluations for Ti, Fe, Pb, ^{209}Bi , etc.).

The energy dependent fission yield capability of TALYS on the other hand was not used although it is now being investigated [41]. It is therefore possible that true energy dependent yields will be available in ENDF files within a few years.

Whenever true energy dependent yields become available, the spectral averaged value will be given by:

$$Y = \frac{\int \int Y(E) \sigma_f(E) \phi(\mathbf{r}, E) dEdV}{\int \int \sigma_f(E) \phi(\mathbf{r}, E) dEdV} \quad (6.6)$$

These integrals can be estimated in the same way as the branching ratio (see equation 6.3) and other integrals of this type:

$$Y = \frac{\lim_{g \rightarrow \infty} \sum_g Y_g \sigma_{f,g} \phi_g}{\lim_{g \rightarrow \infty} \sum_g \sigma_{f,g} \phi_g} \quad (6.7)$$

where $\sigma_{f,g}$ is the fission cross section of group g calculated with equation 5.4

and Y_g the direct fission yield of the isotope for group g calculated as follows:

$$Y_g = \frac{\int_{E_{g-1}}^{E_g} Y(E) \sigma_f(E) dE}{\int_{E_{g-1}}^{E_g} \sigma_f(E) dE} \quad (6.8)$$

6.6 Neutron yield per fission

The total average number of neutrons per fission \bar{v}_t (or total average neutron yield per fission) is not used in the Bateman equations themselves but it is still an important parameter for constant power calculations. ORIGEN 2.2 uses these values to calculate the infinite multiplication factor of the materials that it depleted.

The average neutron yield per fission is also important to transform normalised flux values calculated in an MCNP(X) criticality calculation to absolute flux values. The total flux ϕ is proportional to the normalized flux ϕ_{MC} (with a unit of neutrons $\text{cm}^{-2} \text{s}^{-1}$ source $^{-1}$) calculated by the Monte Carlo code. Due to the normalisation of the fission source, the effective multiplication factor k_{eff} of the system will be given by:

$$k_{\text{eff}} = \bar{v}_t \int \int \sigma_f^* \phi_{MC} dEdV \quad (6.9)$$

where σ_f^* is the macroscopic fission cross section. The power corresponding to the normalized flux ϕ_{MC} is thus given by:

$$P_{MC} = e Q_{s,f} \int \int \sigma_f^* \phi_{MC} dEdV = e Q_{s,f} \frac{k_{\text{eff}}}{\bar{v}_t} \quad (6.10)$$

with $Q_{s,f}$ the total recoverable energy per fission for the entire system. The value of the elementary electron charge e in this equation is used to renormalise eV to W.

Because the proportionality of the total flux ϕ to the normalized flux ϕ_{MC} is the same as the proportionality of the total system power P_t to the power level P_{MC} , the proportionality constant C will be given by:

$$C = \frac{\phi}{\phi_{MC}} = \frac{P_t}{e Q_{s,f} k_{\text{eff}}} \frac{\bar{v}_t}{\bar{v}_t} \quad (6.11)$$

The average number of neutrons per neutron induced fission (total, delayed and prompt) are given in file 1 in the sections with MT numbers 452 (total), 455 (delayed) and 456 (prompt) for every fissionable material in the

ENDF incident neutron data sub-library. According to the ENDF format procedures, the total number of neutrons per fission (MT number 452) must be given for every material that fissions. The average number of delayed and prompt fission neutrons are not required but if either of these is included in the ENDF file, the other must be given as well. In practice these last two are always included if the data are available because of their importance for reactor kinetics and dynamics (they define, among others, the value of the effective delayed neutron fraction β_{eff}).

The energy dependence of the total average neutron yield per fission can be represented as either a tabulated representation similar to that of the energy dependent cross sections in file 3 (see above) or by a polynomial representation:

$$\bar{v}(E) = \sum_{n=1}^{NC} C_n E^{n-1} \quad (6.12)$$

where $NC - 1$ is the order of the polynomial representation (the ENDF-6 format restricts NC to a maximum value of 4).

When delayed and prompt neutrons are given in file 1 as well, this polynomial representation is not allowed. In the most recent evaluations, this polynomial representation is only used to specify a constant value of the total number of neutrons per fission. These cases can be transformed easily to the tabulated format without loss of accuracy (it just requires two points equal to the value at the upper and lower boundary of the fission energy range).

Figure 6.3 illustrates the energy dependence of the total average number of neutrons per fission for ^{235}U , ^{238}U and ^{239}Pu (using data from the JEFF 3.1 nuclear data library). We can see that for ^{235}U and ^{238}U the total average number of neutrons per fission is almost constant (at a value of around 2.5 neutrons per fission) up to 100 keV. Above this energy, the value of \bar{v}_t increases quickly to a value of around 6.5. The data for ^{239}Pu shows the same behaviour, except for a resonance-like structure in between 10 and 650 eV. ^{239}Pu has this resonance-like structure because the data below 650 eV are based on experimental values while the value of \bar{v}_t above 650 eV is solely based on model calculations. ^{235}U and ^{238}U do not exhibit this feature because the total average number of neutrons per fission was determined by model calculations over the entire energy range.

This is a nice illustration of how the evaluation process works. For ^{239}Pu the evaluators decided that the experimental data were better than model calculations below 650 eV. ^{235}U also exhibits a resonance like structure in its \bar{v}_t data but this structure was probably not added to the evaluation because of conflicting experimental data obtained in the past. More recent experiments have solved this issue so this will probably be updated in future evaluations for ^{235}U [46]. ^{238}U on the other hand does not have such resonance like structure in its \bar{v}_t data so the model calculations were used for the entire energy range.

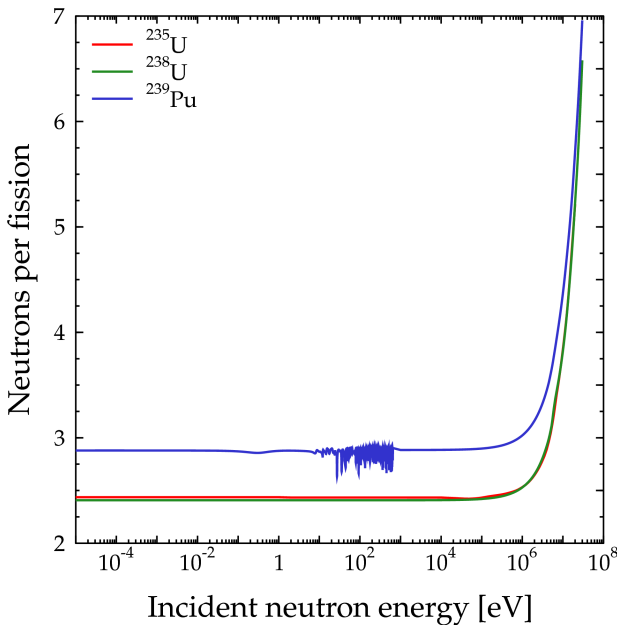


Figure 6.3: Total number of neutrons per fission for ^{235}U , ^{238}U and ^{239}Pu from the JEFF 3.1 evaluated nuclear data library.

As is the case with all the other data (cross sections, branching ratios, etc.) ORIGEN 2.2 only needs an average value for the total number of neutrons per fission. Taking into account the energy dependence discussed earlier, this average value will be given by:

$$\bar{\nu}_t = \frac{\int \int \bar{\nu}_t(E) \sigma_f(E) \phi(\mathbf{r}, E) dEdV}{\int \int \sigma_f(E) \phi(\mathbf{r}, E) dEdV} \quad (6.13)$$

These integrals can be estimated in the same way as the single group cross section (see equation 5.3):

$$\bar{\nu}_t = \frac{\lim_{g \rightarrow \infty} \sum_g \bar{\nu}_{t,g} \sigma_{f,g} \phi_g}{\lim_{g \rightarrow \infty} \sum_g \sigma_{f,g} \phi_g} \quad (6.14)$$

where $\sigma_{f,g}$ is the fission cross section of group g calculated with equation 5.4 and $\bar{\nu}_{t,g}$ the total number of neutrons per fission of group g calculated as fol-

lows:

$$\bar{v}_{t,g} = \frac{\int_{E_{g-1}}^{E_g} \bar{v}_t(E) \sigma_f(E) dE}{\int_{E_{g-1}}^{E_g} \sigma_f(E) dE} \quad (6.15)$$

As an illustration, we have calculated \bar{v}_t values from JEFF 3.1 for our single MOX fuel pin, like we did for the branching ratios. We have used the spectrum in 43000 groups, although a smaller energy structure would have sufficed for most nuclides. The results and comparison with the hard coded (thermal) \bar{v}_t data of ORIGEN 2.2 can be found in table 6.4.

The JEFF 3.1 nuclear data library contains \bar{v}_t data for a total of 63 fissionable nuclides. ORIGEN 2.2 on the other hand only has data for 31 of those nuclides along with a \bar{v}_t value for ^{253}Cf which is not included in JEFF 3.1. It is evident by inspection of the values in table 6.4 that the neutron yields calculated with JEFF 3.1 and those from ORIGEN 2.2 differ little for the nuclides of significance. ^{235}U and ^{238}U values vary respectively by 0.9 and 0.7 %. The ^{239}Pu and ^{241}Pu values are even better with respectively a difference of 0.02 % and 0.13 %. Even though the values might be similar, the completeness of the JEFF 3.1 data compared to the hard coded data from ORIGEN 2.2 does warrant the update of the \bar{v}_t data in ORIGEN 2.2. And for the sake of consistency, this should be done whenever the cross section data is updated as well.

6.7 The total recoverable energy per fission

6.7.1 Components of fission energy release

The total recoverable energy per fission $Q_{i,f}$ is an important parameter in any evolution calculation because it has to be used to calculate the equivalent flux in a constant power step (see equation 2.21) and because it determines the total burn-up of the fuel.

Due to the complexity of the fission phenomenon, energy is released in different ways. Whenever a nucleus is fissioned, excited fission fragments will be formed which will emit neutrons and γ -rays within a very short period of time (these are the so-called prompt neutrons and γ -rays). The deexcited fission fragments or primary fission products will then undergo radio-active decay, resulting in the emissions of even more γ -rays, β radiation (both electrons and positrons) and possibly even neutrons. These are the so-called delayed γ and β radiation and the delayed neutrons. Neutrinos and anti-neutrinos can also be emitted at this stage.

The energy released directly from fission is thus equal to the sum of the kinetic energy of the fission fragments and emitted neutrons (both prompt

Table 6.4: Total average neutron fission yield data calculated with equation 6.14 for a single MOX fuel pin using the JEFF 3.1 nuclear data library and comparison with the hard coded thermal ORIGEN 2.2 values.

Nuclide	JEFF 3.1	ORIGEN 2.2	Nuclide	JEFF 3.1	ORIGEN 2.2
²²³ Ra	1.570	-	²⁴³ Pu	3.022	-
²²⁶ Ac	1.977	-	²⁴⁴ Pu	3.301	-
²²⁷ Ac	2.136	-	²⁴⁶ Pu	3.578	-
²²⁷ Th	2.069	-	²⁴¹ Am	3.449	3.277
²²⁸ Th	2.203	-	²⁴² Am	3.276	3.360
²²⁹ Th	2.091	2.049	²⁴² Am	3.272	3.162
²³⁰ Th	2.288	-	²⁴³ Am	3.561	3.732
²³² Th	2.401	2.418	²⁴⁴ Am	3.156	-
²³³ Th	2.079	-	²⁴⁴ Am	3.157	-
²³⁴ Th	2.437	-	²⁴⁰ Cm	3.442	-
²³¹ Pa	2.527	-	²⁴¹ Cm	2.774	-
²³² Pa	2.288	-	²⁴² Cm	3.667	3.746
²³³ Pa	2.664	2.663	²⁴³ Cm	3.440	3.434
²³² U	3.146	-	²⁴⁴ Cm	3.539	3.725
²³³ U	2.495	2.499	²⁴⁵ Cm	3.600	3.832
²³⁴ U	2.641	2.631	²⁴⁶ Cm	3.864	3.858
²³⁵ U	2.443	2.421	²⁴⁷ Cm	3.827	3.592
²³⁶ U	2.598	2.734	²⁴⁸ Cm	3.431	3.796
²³⁷ U	2.559	-	²⁴⁹ Cm	3.397	-
²³⁸ U	2.827	2.807	²⁵⁰ Cm	3.959	-
²³⁵ Np	2.766	-	²⁴⁷ Bk	3.538	-
²³⁶ Np	2.411	-	²⁴⁹ Bk	3.692	3.760
²³⁷ Np	2.912	3.005	²⁵⁰ Bk	3.589	-
²³⁸ Np	2.794	-	²⁴⁹ Cf	4.068	4.062
²³⁹ Np	2.955	-	²⁵⁰ Cf	4.050	3.970
²³⁶ Pu	2.823	2.870	²⁵¹ Cf	4.142	4.140
²³⁷ Pu	2.831	-	²⁵² Cf	4.167	4.126
²³⁸ Pu	3.023	2.833	²⁵³ Cf	-	4.150
²³⁹ Pu	2.875	2.875	²⁵⁴ Cf	4.145	-
²⁴⁰ Pu	3.145	3.135	²⁵⁴ Es	4.092	-
²⁴¹ Pu	2.938	2.934	²⁵⁵ Es	4.022	-
²⁴² Pu	3.239	3.280	²⁵⁵ Fm	4.400	-

and delayed), the energy of both prompt and delayed γ and β radiation. The neutrinos and anti-neutrinos released during the fission process will also take energy with them but due to the extremely low interaction probability these neutrinos and anti-neutrinos are assumed to get out of the system without depositing any energy in the system. We can define the contributions of these individual components as:

- Q_k : the kinetic energy of the fission fragments
- $Q_{n,p}$ and $Q_{n,d}$: the kinetic energy of the prompt and delayed fission neutrons
- $Q_{\gamma,p}$ and $Q_{\gamma,d}$: the energy of the prompt and delayed γ -rays
- Q_β : the energy of the delayed β radiation
- Q_ν : the energy carried away by the neutrinos

so that the total energy release from fission $Q_{t,f}$ is given by:

$$Q_{t,f} = Q_k + Q_{n,p} + Q_{n,d} + Q_{\gamma,p} + Q_{\gamma,d} + Q_\beta + Q_\nu \quad (6.16)$$

or

$$Q_{t,f} = Q_k + Q_n + Q_\gamma + Q_\beta + Q_\nu \quad (6.17)$$

Neutrinos will not deposit their energy in the system so that the amount of recoverable energy $Q_{d,f}$ released into the system directly from fission will be equal to $Q_{t,f} - Q_\nu$:

$$Q_{d,f} = Q_{t,f} - Q_\nu = Q_k + Q_n + Q_\gamma + Q_\beta \quad (6.18)$$

Indirectly, the fission process will also result in an extra energy release in the system due to (n,γ) reactions in the fuel and structural materials of the system. If we now define Q_c as the average energy released by all (n,γ) reactions per fission, then the total recoverable energy per fission Q_f will be given by:

$$Q_f = Q_{d,f} + Q_c \quad (6.19)$$

or

$$Q_f = Q_k + Q_n + Q_\gamma + Q_\beta + Q_c \quad (6.20)$$

6.7.2 Energy and system dependence

The energy release from fission is dependent on the energy of the neutron that induced fission but it is also time dependent due to the delayed contributions (neutrons, γ -rays and β particles). We will disregard this time dependence because we are only interested in using the total recoverable energy from fission to calculate the burn-up of the fuel and to renormalise the power distribution

in the system during a time step in the depletion calculation. The energy dependence of the various components of the fission energy release is always of the following form [23, 45]:

$$Q_i(E) = Q_i(0) - \delta Q_i(E) \quad (6.21)$$

where $Q_i(0)$ is the energy of component i at an extrapolated incident energy of 0 eV. The value of $Q_i(0)$ for the different components are tabulated in the ENDF file of the nuclide in question (in file 1 MT458). The functions $\delta Q_i(E)$ on the other hand are purely analytical and are given by:

$$\delta Q_k(E) = 0 \quad (6.22)$$

$$\delta Q_{n,p}(E) = -1.307E + 8.07(\bar{v}_t(E) - \bar{v}_t(0)) \quad (6.23)$$

$$\delta Q_{n,d}(E) = 0.900E \quad (6.24)$$

$$\delta Q_{\gamma,p}(E) = 0 \quad (6.25)$$

$$\delta Q_{\gamma,d}(E) = 0.075E \quad (6.26)$$

$$\delta Q_{\beta}(E) = 0.075E \quad (6.27)$$

$$\delta Q_{\nu}(E) = 1.000E \quad (6.28)$$

$$\delta Q_{t,f}(E) = -1.057E + 8.07(\bar{v}_t(E) - \bar{v}_t(0)) \quad (6.29)$$

where $\bar{v}_t(E)$ is the total number of fission neutrons as a function of the incident neutron energy E (see section 6.6). The energy dependence of the total recoverable energy directly released by fission is thus given by:

$$Q_{d,f}(E) = Q_{t,f}(0) - Q_{\nu}(0) + 0.057E - 8.07(\bar{v}_t(E) - \bar{v}_t(0)) \quad (6.30)$$

The ENDF format assumes that there is no energy dependence on the kinetic energy of the fission fragments although experimental data seems to indicate that there is some form of dependence on the incident neutron's energy [46].

Figure 6.4 gives the total fission energy release $Q_{t,f}$ and the total recoverable energy $Q_{d,f}$ directly from fission for ^{235}U (using data from the JEFF 3.1 nuclear data library). As we can see, the energy dependence of the total fission energy release is quite important. $Q_{t,f}$ appears to be relatively constant between 10^{-5} eV up to 100 keV. At that point, the value of $Q_{t,f}$ increases quickly from about 202.5 MeV/fission at 100 keV to 223.5 MeV/fission at 20 MeV. The fission cross section is relatively low in this last energy area so for thermal spectrum reactors, total fission energy release will appear to be relatively independent of the incident neutron energy. For fast spectrum reactors this can have a profound influence. However, for depletion calculations we do not need this value. We need the total recoverable energy $Q_{d,f}$ directly from fission. And the energy dependence of that value is a lot less important than the total energy release from fission. It only changes by about 0.5 % over the

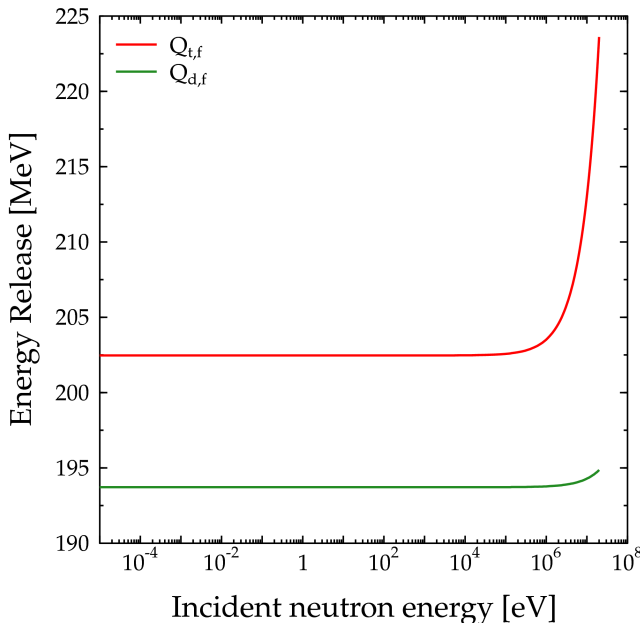


Figure 6.4: Total energy release from fission compared to total recoverable energy release directly from fission for ^{235}U from the JEFF 3.1 evaluated nuclear data library.

entire energy range (from 193.7 MeV/fission at 10^{-5} eV to 194.9 MeV/fission at 20 MeV).

The average energy Q_c released by all (n,γ) reactions per fission also has some energy dependence in it through the total average number of neutrons $\bar{v}_t(E)$ released by fission. There is also a link with the criticality of the system itself. The effective multiplication factor k_{eff} gives us the number of neutrons per fission that result in fission as well while the other released neutrons are either absorbed or removed from the system through leakage. By neglecting neutron leakage, a total of $\bar{v}_t(E) - k_{\text{eff}}$ neutrons will be absorbed in the system. For a critical system this will simply be $\bar{v}_t - 1$, which was used in deriving the original ORIGEN 2.2 formula for Q_f (see equation 2.23). With this minor change, the average energy Q_c will be given by:

$$Q_c(E) = (\bar{v}_t(E) - k_{\text{eff}}) Q_{c,\gamma} \quad (6.31)$$

so that the total recoverable energy release by fission will be given by:

$$Q_f(E) = Q_{d,f}(E) + (\bar{v}_t(E) - k_{\text{eff}}) Q_{c,\gamma} \quad (6.32)$$

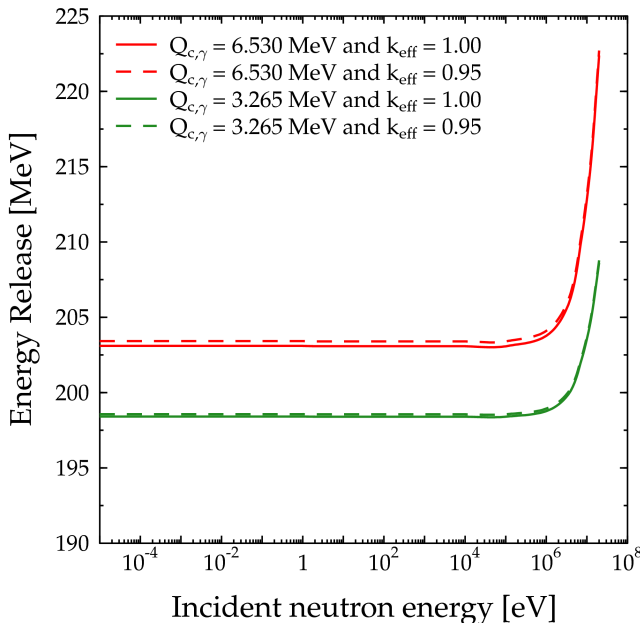


Figure 6.5: The dependence of the total recoverable fission energy for ^{235}U on the incident neutron energy, the average energy $Q_{c,\gamma}$ released by an (n,γ) reaction and the criticality of the system.

where $Q_{c,\gamma}$ is the average energy released per capture event.

By using the value of the effective multiplication factor k_{eff} we can effectively distinguish between critical and sub-critical systems. In a sub-critical system more neutrons will be absorbed when compared to a critical system. As a result, the contribution of neutron capture in the total recoverable energy from fission will be slightly higher in the sub-critical system.

The average energy $Q_{c,\gamma}$ per capture event is also a system dependent parameter as it depends on the composition of the materials in the system. In a system containing large amounts of ^{238}U most neutrons will be captured by this nuclide during slow down. However, the importance of, for instance, a light water moderator or a stainless steel reactor vessel cannot be ignored either.

Figure 6.5 now shows the final energy dependent form of the total recoverable fission energy for ^{235}U for two different values of average energy per capture event (the original value of 6.53 MeV/capture from Unik and Gindler and half of this value) and two values of the effective multiplication factor k_{eff} . The curve for $k_{\text{eff}} = 0.95$ always lies above the corresponding graph for

$k_{\text{eff}} = 1.00$ (as one would expect) although the impact is rather small. On the other hand, we also see that the energy dependence of Q_f for $Q_{c,\gamma} = 6.53 \text{ MeV}$ is a lot more profound than for the lower value.

6.7.3 Using the correct value

Taking into account the energy dependence discussed earlier, the total recoverable fission energy Q_f will be given by:

$$Q_f = \frac{\int \int Q_f(E) \sigma_f(E) \phi(\mathbf{r}, E) dEdV}{\int \int \sigma_f(E) \phi(\mathbf{r}, E) dEdV} \quad (6.33)$$

These integrals can be estimated in the same way as the single group cross section (see equation 5.3):

$$Q_f = \frac{\lim_{g \rightarrow \infty} \sum_g Q_{f,g} \sigma_{f,g} \phi_g}{\lim_{g \rightarrow \infty} \sum_g \sigma_{f,g} \phi_g} \quad (6.34)$$

where $\sigma_{f,g}$ is the fission cross section of group g calculated with equation 5.4 and $Q_{f,g}$ the total recoverable fission energy of group g calculated as follows:

$$Q_{f,g} = \frac{\int_{E_{g-1}}^{E_g} Q_f(E) \sigma_f(E) dE}{\int_{E_{g-1}}^{E_g} \sigma_f(E) dE} \quad (6.35)$$

Like for the branching ratios and the total average neutron yield per fission, we have calculated the total average recoverable energy Q_f for a single MOX fuel pin. These values are plotted in figure 6.6 next to the ORIGEN 2.2 curve given by equation 2.22 and the data from Unik and Gindler which was used to derive this empirical formula (see section 2.5.1). Because it is not possible to easily identify the various nuclides in this figure, the numerical values for Q_f can also be found in table 6.5. k_{eff} and $Q_{c,\gamma}$ were set to 1 and 6.53 MeV respectively to be consistent with the ORIGEN 2.2 formula.

We obtain values close to those predicted by the ORIGEN 2.2 formula, but they all lie above the ORIGEN 2.2 values. The maximum difference is about 5 %. This shows that the ORIGEN 2.2 equation is not that bad at predicting the value of the total average recoverable energy per fission.

Unfortunately, not every fissionable nuclide in the JEFF 3.1 nuclear data library has a file 1 MT458 entry with the components of fission energy release. We are only capable of calculating the value of Q_f for 25 nuclides while 63 nuclides have a fission cross section (see section 6.6) so we are missing data for

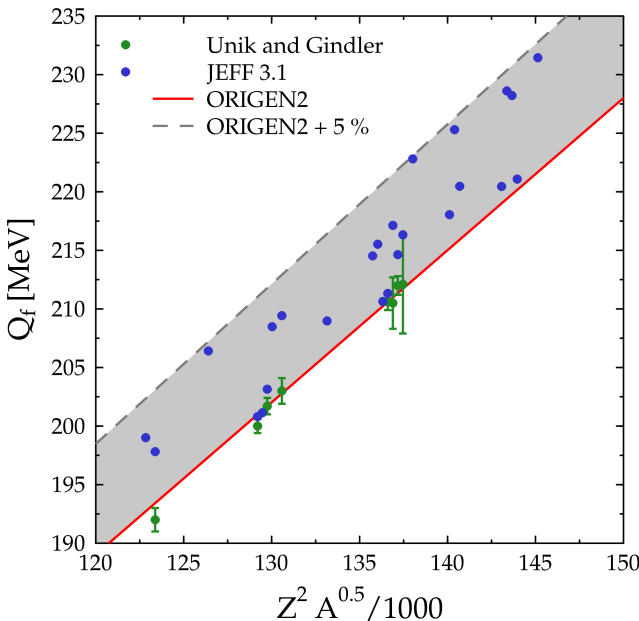


Figure 6.6: Total recoverable energy from fission Q_f : ORIGEN 2.2 semi-empirical formula versus Unik and Gindler data.

38 nuclides. However, the 25 nuclides for which we do have the data are the most important nuclides for our applications (see table 6.5). For the missing nuclides we can actually continue to use the ORIGEN 2.2 formula corrected by 2.5 % to be consistent with the trend from figure 6.6.

6.8 Decay data

Within the ENDF-6 format, radio-active decay data is always stored in a separate sub-library within a file 8 entry with MT number 457. The main purpose of this sub-library is to describe the energy spectra resulting from radioactive decay and give average parameters useful for applications like decay heat, waste disposal, depletion calculations, etc.

The information in an MF8 MT457 section can be subdivided into three distinct parts: general information (which contains the half-life, the isomeric state of the nuclide, the average decay energies, etc.), decay mode information and the resulting radiation spectra. For our applications, we are only interested in the data in the general information part and in the decay mode data.

Table 6.5: Total average recoverable energy per fission (in MeV) with equation 6.34 for a single MOX fuel pin using the JEFF 3.1 nuclear data library and comparison with the ORIGEN 2.2 empirical formula and Unik and Gindler data.

Nuclide	JEFF 3.1	ORIGEN 2.2	Unik and Gindler
^{230}Th	199.01	192.73	-
^{232}Th	197.81	193.42	192.0 ± 1
^{233}Pa	206.41	197.35	-
^{233}U	200.81	200.98	200.0 ± 0.6
^{234}U	201.14	201.34	-
^{235}U	203.15	201.70	201.7 ± 0.7
^{236}U	208.48	202.06	-
^{238}U	209.43	202.77	203.0 ± 1.1
^{237}Np	208.98	206.12	-
^{236}Pu	214.53	209.48	-
^{237}Pu	215.52	209.86	-
^{238}Pu	210.64	210.23	-
^{239}Pu	211.32	210.60	210.6 ± 0.7
^{240}Pu	217.13	210.97	210.5 ± 2.2
^{241}Pu	214.64	211.34	212.0 ± 0.8
^{242}Pu	216.33	211.71	212.1 ± 4.2
^{244}Pu	222.81	212.45	-
^{241}Am	218.05	215.16	-
^{242}Am	225.30	215.53	-
^{243}Am	220.47	215.91	-
^{241}Cm	220.46	219.01	-
^{242}Cm	228.61	219.39	-
^{243}Cm	228.22	219.78	-
^{244}Cm	221.08	220.16	-
^{248}Cm	231.45	221.69	-

Table 6.6: Fundamental decay modes in the ENDF format.

RTYP	Decay mode
1	β^- decay
2	β^+ decay and electron capture
3	isomeric transition
4	α decay
5	neutron emission
6	spontaneous fission
7	proton emission
10	unknown origin

The ENDF file gives the total half-life $T_{1/2}$ of the nuclide and the branching ratios L_j (which should sum to 1.0) for the various decay modes of the parent nuclide. The decay constant of a decay mode j is therefore given by:

$$\lambda_j = L_j \frac{\ln 2}{T_{1/2}} \quad (6.36)$$

The ENDF file will distinguish between the isomeric state of the daughter nuclide in the various decay modes. As a result, β^- decay to for instance the ground state and to the first isomeric state of the daughter nuclide are considered separate decay modes.

The decay modes themselves are represented by a decay type variable (RTYP) and an isomeric state flag (RFS) for the daughter nuclide. The ENDF format distinguishes between 8 fundamental types (given in table 6.6). These fundamental types can be used to define decay chains as well. The decay mode 1.5 is for instance used to specify β^- decay followed by neutron emission (this is often called delayed neutron decay). Other examples are 1.4 for β^- decay followed by α decay (like for instance in ^{16}N decay) and 2.4 for β^+ decay followed by α decay.

The ENDF format allows the use of complex decay chains into a single decay mode to the final daughter nuclide. Furthermore, it allows for daughter nuclides in the ground state and first and second isomeric state. ORIGEN 2.2 on the other hand needs specific decay modes and only uses nuclides in the ground state and first isomeric state. An overview of these decay modes can be found in table 6.7.

Decay modes in the ENDF file different from the ones given in table 6.7 for decay modes to the second isomeric state cannot be used by ORIGEN 2.2. Fortunately, this only occurs in some rare cases and if it does, the corresponding branching ratio is very small (so that the probability of this decay mode is very small). If this occurs, the branching ratios and the total half-life must be

Table 6.7: Decay modes for use in ORIGEN 2.2.

Decay mode	RTYP	RFS
β^- decay	1	0, 1
β^+ decay and electron capture	2	0, 1
α decay	4	
isomeric transition	3	0
spontaneous fission	6	
β^- decay & neutron emission	1.5	

renormalised to preserve the total number of disintegrations for every single decay mode.

If a nuclide has a total half-life $T_{1/2}$ and a number of decay branching ratios L_j (of which the total sum is 1.0) and if L_r is the fraction of all decay events with decay modes different from table 6.7, then the total half-life $T_{1/2,O}$ used by ORIGEN 2.2 will be given by:

$$T_{1/2,O} = \frac{T_{1/2}}{1 - L_r} \quad (6.37)$$

The remaining decay branching ratios will also have to be renormalised to 1.0 to be used by ORIGEN 2.2:

$$L_{j,O} = \frac{L_j}{1 - L_r} \quad (6.38)$$

The general information section of an MF8 MT457 section also contains the average decay energy for three different radiation types (light particles, electromagnetic radiation and heavy particles). The sum of these three general quantities is the total average recoverable energy per disintegration which is needed for decay heat calculations. This value excludes the neutrino contribution to the decay energy. These three quantities are always given but in some cases the individual components of these three quantities are also given. For the light particle decay energy this is for instance the average β^- and β^+ energy, the average Auger electron energy and the average conversion electron energy. For decay heat applications, ORIGEN 2.2 only needs the total average recoverable energy per disintegration so these individual components are not really necessary (although they can be useful to assess the importance of individual decay modes to the decay heat).

7

It is quality rather than quantity that matters.

Seneca (5 BC - 65 AD)

*Quality is never an accident. It is always the result
of intelligent effort.*

John Ruskin (1819 - 1900)

ALEPH-DLG: nuclear data preparation and validation

7.1 Validated application libraries

The importance of nuclear data is often overlooked or outright ignored by many although it encapsulates large parts of the physics behind the problem of particle transport. One can have the best codes in the world, but if the nuclear data fed into those codes are lacking, the results themselves will be worthless. Quality Assurance (QA) is therefore an important aspect in the preparation of a validated application library.

A set of library files can be considered to be a validated application library when the following requirements are met, regardless of the application or the data pre-processing codes involved in the preparation of the library [48]:

- *Verification*

The verification process ensures that no problems were found during processing (due to faulty data, bad formatting, etc.) and that corrective actions are taken or that a warning is issued if a problem was encountered. This verification process starts even before the first library file is produced with the selection of the processing path for the data pre-processing code and all relevant parameters.

- *Validation*

To ensure that the library is capable of providing accurate and reliable results, it must be validated. This can be done by testing the library against internationally accepted benchmarks. In order to validate nuclear data we also need to ensure that differences in benchmark results are really due to differences in data. Differences in library processing introduces “noise” and is therefore not acceptable when validating nuclear data. Examples of such influencing factors are for instance the version

of NJOY (99.00, 99.90, 99.112, etc.), different cross section reconstruction tolerances, etc.

- *Documentation*

Documenting every aspect in the creation of the library is important for future reference. A data pre-processing code (in our case NJOY) should never be used as a black box. With the documentation provided with the library, a user should be capable of producing exactly the same library and understand every aspect of its creation.

All this has resulted in the creation of ALEPH-DLG (Data Library Generator) and ALEPH-LIB (a multi-temperature neutron transport library for standard use by MCNP(X) and ALEPH). ALEPH-DLG is an auxiliary computer code to ALEPH [47], our own Monte Carlo burn-up code (see chapter 8). ALEPH-DLG automates the entire process of generating library files with NJOY and takes care of the first requirement of a validated application library: verify the processing. It produces tailor made NJOY input files using data from the original ENDF file (initial temperature, the fact if the nuclide is fissile or if it has unresolved resonances, etc.). When the library files have been generated, ALEPH-DLG will also process the output from NJOY by extracting all messages and warnings. If ALEPH-DLG finds anything out of the ordinary, it will either warn the user or perform corrective actions.

The temperatures included in the ALEPH-LIB library are 300, 600, 900, 1200, 1500 and 1800 K. Library files were produced for the JEF 2.2, JEFF 3.0, JEFF 3.1, JENDL 3.3 and ENDF/B-VI.8 nuclear data libraries. This will be extended with ENDF/B-VII when it becomes available.

7.2 Preparation of a nuclear data library

7.2.1 What was done in the past

NJOY is a modular program in which the different modules are called in sequence. Information is passed from module to module through the use of ENDF files. It is the NJOY module that regulates this data flow. It should be noted that data passed on in this way has all of the limitations of the ENDF format. An example being the use of only 6 significant digits which can cause NJOY warnings due to round-off when passing data from one module to another.

Before even starting with the production of a library, it is always good to examine what has been done in the past in the field of library preparation and verification. A good place to start is the documentation of older libraries like ENDF60, ENDF66, etc. [48, 49, 50, 51] to see what NJOY processing path they had chosen, what values they used for important parameters such as the

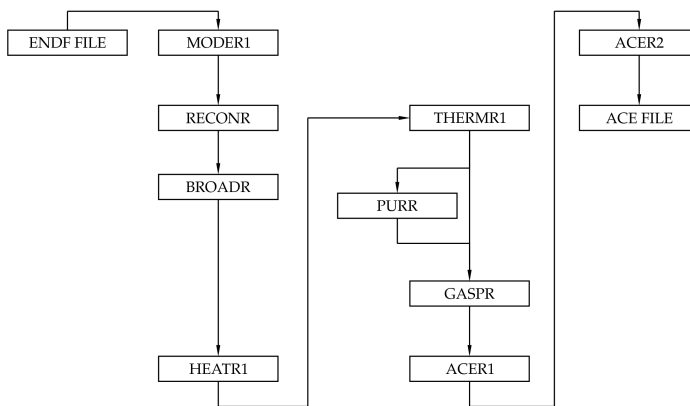


Figure 7.1: The standard NJOY processing path to prepare library files for use with MCNP(X).

reconstruction tolerance, etc. Other important information is the type of verification tests that were performed and what types of benchmarks were used to validate the library. And during this phase the most important question should be *why*. We should learn from all that experience and then decide upon our own approach. Figure 7.1 gives an overview of the typical processing path adopted for the preparation of library files for MCNP(X) (which are often referred to as ACE files or c-type libraries). It should be noted that NJOY can also process data for deterministic codes like WIMS, etc. Because of this, NJOY has a lot more modules than those depicted in figure 7.1 like the wimsr and groupr modules.

The moder module is used to convert ENDF, PENDF (Point-wise ENDF) and GENDF (Group ENDF) files from the NJOY binary mode to formatted (i.e. ASCII) mode and vice versa. In this case, the first moder run converts the raw ENDF file to binary mode. On older systems, the use of binary files allowed for a significant reduction in calculation time because binary files can be read faster than ASCII files. This is no longer an issue with current computer technology. The transformation of ASCII to binary is however still included because it is a good test for the formatting of an ENDF file. If there is something wrong with the formatting, this moder run will signal it.

The reconr module then reconstructs resonance cross sections using the resonance parameters (found in file 2 in the ENDF file) and linearises cross sections that use non-linear interpolation schemes (such as lin-log, log-lin, log-log, etc.). The result is a point-wise ENDF file where all cross sections have been set on a unionised energy grid. Cross sections that are the sum of

other cross sections, such as the total cross section and the total inelastic cross section, are recalculated as the sum of their constituent cross sections. All the cross sections are reconstructed to within a user specified accuracy. This module is always the first to be run because other modules, such as broadr, require linearised cross sections and/or an unionised grid.

After that, the broadr module is used to generate Doppler-broadened cross sections using a point-wise ENDF file. The basis for the reconr module is the SIGMA1 code (version 77-1, dated 1977), which is still part of the PREPRO codes [39] (under an evolved form).

The heatr module will add point-wise heating cross sections (also called kerma factors) and radiation damage energy production to the ENDF file that we are processing. The thermr module generates point wise neutron scattering cross sections in the thermal energy range and adds them to the library. As was the case for the unresr module, it is not required to run this module to create an MCNP(X) library [50]. For the creation of the ENDF66 libraries, thermr wasn't even used [48, 51].

The thermr module will also fail to process an ENDF file without elastic scattering. Because such an incomplete file cannot be used for transport calculations, the thermr module will thus provide us with a test on the completeness of the ENDF file in question.

The gaspr module adds charged particle production (also called gas production) to the library file. The module takes any cross sections of reactions in which secondary particles such as protons (MT103), deuterons (MT104), tritons (MT105), ^3He (MT106) and α -particles (MT107) are produced and adds the particle production from those cross sections to the library.

The purr module will prepare the probability tables for the treatment of the unresolved resonance self-shielding in MCNP(X). Unresolved resonance self-shielding is already treated by the unresr module using the Bondarenko method (also called the background cross section method). This method is however not very useful for continuous energy Monte Carlo codes. The probability table is a more natural approach to the effect of unresolved resonance self-shielding in Monte Carlo codes. When no unresolved resonances are present, it is not necessary to run this module as no probability tables will be produced.

The purr module will construct a series of resonance ladders that obey the statistical distributions given in file 2 of the ENDF file. Each of those ladders will be sampled randomly to produce contributions to a probability table. As a convergence test, a set of Bondarenko values is calculated at the same time and another set is calculated using the completed probability table.

The acer module prepares libraries in the ACE format (A Compact Endf) for use by MCNP(X). The ACE format contains all the details of the normal ENDF format but the representation of the data is different for the sake of efficiency. The first acer run will convert the previously calculated point-wise ENDF file along with other data from the original ENDF file into an ACE file.

All cross sections share a unionised energy grid. Detailed photon data will be generated directly from files 12, 13, 14, 15 and 16 if they were present in the ENDF file and delayed neutron data, angular distribution data, etc. will also be added to the ACE file by this module. The second acer run will perform a number of consistency tests on the produced ACE file and try to correct any problems that might surface.

NJOY is still evolving as more features are being added (some NJOY errors and warning messages are linked to this). Until a few years ago, post-processing of the libraries was still necessary to add essential features such as delayed neutron data (which is now handled by acer as of NJOY version 99.63, dated October 15, 2001), charged particle emission (handled by gaspr, an addition to NJOY 94.15, dated November 28, 1995), the addition of the probability tables for the unresolved resonances and the gamma production data (which is now handled by acer). To prepare the standard MCNP libraries LANL has had to use special post-processing codes to add some of the previous features to the final ACE tape. Post-processing is also required in the case of errors in the files. The following two problems for instance required post-processing for ENDF66:

- The heating numbers in the probability table for the unresolved energy range appeared to be inconsistent with what MCNP(X) expects. This problem has however been corrected with NJOY version 99.62 (dated September 28, 2001) so it is no longer necessary to deal with this problem.
- On some platforms, it is possible that MCNP compiled in 32 bit mode will fail when it tries to read numbers smaller than 10^{-37} . To correct this problem, numbers smaller than 10^{-37} were replaced by 10^{-35} .

During the preparation of the ENDF60 [49, 50] and ENDF66 [48, 51] standard libraries, the LANL nuclear data group also tested (and corrected) their library files using special purpose checking codes:

- CHECKTHRESH: this code performs reaction threshold processing to compare threshold energies with kinematic thresholds for negative Q-value reactions.
- CHECKND_NEUT: this checks the secondary neutron distributions. It verifies that the correct interpolation schemes are used (1 or 2), it identifies any negative probability density functions (or PDF) values and it checks if neutrons can be produced with an energy greater than the initial energy (including fission). In the case of negative PDF, the negative values are set to zero and the distribution is renormalized. It also corrects the secondary neutron distributions (except for fission) for energies greater than the incident neutron energy.
- CHECKND: this checks the secondary photon distributions.

- CHECK5: this checks data files using the MT5 reaction which is used to combine many reactions into one single reaction at high incident neutron energies (typically above 20 MeV).
- CHECK_URES: this checks the proper processing of the unresolved resonance probability tables.

None of these codes is available to us but most of these tests have been added to the internal NJOY testing. CHECKTHRESH's corrections and tests are now performed by the reconr module. The tasks of CHECKND_NEUT and CHECKND are now performed by acer itself or during the acer consistency check. Only the CHECK_URES and CHECK5 tests have not (yet) been added. Because the unresolved probability tables are a very important part of the library, we have provided testing of our own in ALEPH-DLG to ensure correct processing.

7.2.2 NJOY processing in ALEPH-DLG

The NJOY processing path used by ALEPH-DLG to process library files for MCNP(X) and ALEPH is depicted in figure 7.2. It is based on the standard processing path presented above with a few additions to extract data for use in ALEPH or to perform the necessary QA procedures.

A first addition is another moder run when the Doppler broadening has been performed on the original ENDF file to convert the NJOY binary file into a readable ASCII file for use in ALEPH. The ACE file produced at the end of the NJOY run and the ENDF file produced by this second moder run will contain the same cross section data. This will insure the required nuclear consistency in ALEPH. The approach of reading the cross section data from a separate ENDF file instead of the final ACE itself was chosen because certain data like branching ratios, fission yield data, etc. are not added to the ACE file. By using ENDF files all data required for the burn-up code can be restricted to a single file.

The additional heatr and unresr runs are used for QA purposes. The heatr run is there to check if everything is processed correctly. This type of run is also referred to as the kinematic check (see the NJOY manual page VI-18 [38]).

The unresr module produces self-shielded cross sections in the unresolved resonance range. For our purposes it is not necessary to run this module because the purr module will deal with the unresolved resonance range using probability tables. However, as part of the QA of the library, some results from unresr are compared to purr. This module will only be run if ALEPH-DLG detected unresolved resonances in file 2 of the initial ENDF file.

When performing ACE consistency runs, there is also the possibility to produce an instruction file for viewr to plot the data in the ACE file. The resulting postscript file can then be used to visually verify the proper processing of the ACE library.

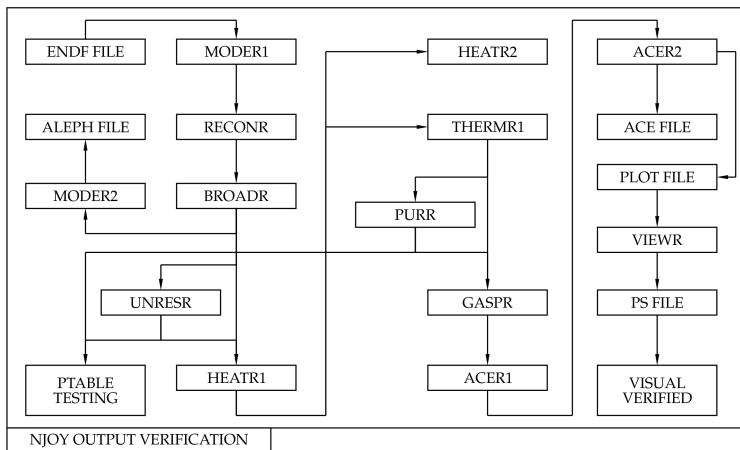


Figure 7.2: The standard NJOY processing path with the additions for ALEPH-DLG.

7.3 ALEPH-DLG and NJOY post-processing

7.3.1 Library QA

When NJOY has finished creating an ACE file, the data have to be verified to ensure proper processing as part of the QA process. Most of the time, we can rely upon NJOY itself to do this. NJOY verifies if the necessary data are available (and makes an approximation if necessary), the second acer run performs ACE consistency checks and corrects problems if any are found, etc. We can however not rely on NJOY alone. So in addition to the internal NJOY processing QA, we have to perform the following steps as well:

- Check the NJOY output to analyse warning messages and errors, to verify resonance reconstruction errors, to verify the correct processing of the unresolved resonance probability table, and to process the results from the acer consistency check.
- Check cross section plots to find anomalies.
- MCNP(X) testing to see if MCNP(X) accepts the ACE file.

ALEPH-DLG performs this first point automatically. It will extract all messages and warnings from NJOY and print out a short explanation of the message in question (see section 7.3.2 for some examples) in the output file. The same will be done with the consistency problems found by the second acer run. The summary table produced by the reconr module with estimates on

the resonance reconstruction is also extracted and reproduced in the output file from ALEPH-DLG (see section 7.3.3). And finally, ALEPH-DLG will read data from the unresr and purr module to test the probability tables on their correctness (see section 7.3.4).

7.3.2 Common NJOY warnings

Whenever NJOY encounters an abnormal situation or when the code has to make an approximation (due to missing or incomplete data, etc.) it will issue a warning message. In some cases, NJOY will take steps to correct the problem. All these messages have to be collected and understood before the produced library files can be approved.

The following is a list of some of the most common messages or messages that should not be ignored by the user (a complete overview of these messages can be found in [52, 53]):

- `changed threshold from ... to ... for mt...`

When reconr goes through the reactions given in the ENDF evaluation, it also checks the threshold energy E_{th} against the Q -value and the ratio AWR (the ratio between the atomic weight and the neutron mass) found in the ENDF file. If the condition

$$E_{th} \geq \frac{AWR + 1}{AWR} Q \quad (7.1)$$

is not satisfied, the threshold energy is changed and reconr will issue this warning.

Initially, NJOY only gave this warning if the change is greater than 0.1% but it appears that NJOY 99 will issue the warning regardless of the change so the majority of all warnings encountered will be this one. This warning can essentially be ignored if the change is low.

- `---message from hinit---mf4 and 6 missing, isotropy assumed for mt...`

This is an example of a message informing the user that NJOY had to make an approximation. In this case, NJOY assumes an isotropic angular distribution for a certain MT number because the ENDF file does not have corresponding entries in file 4 (angular distributions) or file 6 (energy-angle distributions).

- `---message from emerge---nonpositive elastic cross sections found`

The reconr module found a nonpositive elastic cross section and set it to a very small but positive value. This can occur due to a number of reasons (see the handbook on the ENDF format [23], p 2.26 to 2.28). This can

occur when Single Level Breit Wigner (SLBW) is used to represent the resonance parameters in file 2 of the ENDF file. In older evaluations, the negative cross section is most likely caused by this formalism. Although the use of SLBW is discouraged (and it is therefore no longer used in newer evaluations) in favour of formalisms such as Multi-Level Breit Wigner (MLBW), R-matrix, Reich-Moore and R-function formalisms it is still possible to have negative scattering cross sections. This message indicates that the ENDF file is fundamentally flawed and that it should be corrected.

- ---message from ptleg2---negative probs found

Secondary particle energy and/or angle distributions can be represented using a infinite serial decomposition in Legendre polynomials. Because an infinite series is not practical, it has to be cut off at a certain order (in the ENDF format, the upper limit is 64). Because the Legendre polynomials are not necessarily positive, this can introduce areas where the series leads to negative values - which is physically impossible. This message occurs when the acer module has found such a negative probability distribution function (or PDF) value. To "solve" the problem, acer has set the value to zero and has renormalized the distribution back to 1. An evaluation with this error should be corrected (for instance by using a higher order cut-off).

7.3.3 Resonance reconstruction

NJOY's reconr module reconstructs resonance cross sections using the resonance parameters and linearises cross sections that use non-linear interpolation schemes on a unionised energy grid. The reconstruction and linearisation of the cross section is controlled by a minimum and maximum reconstruction tolerance and the maximum resonance integral error.

First, the cross section is linearised until the cross section at the midpoint between two grid points is within the maximum reconstruction tolerance from the real cross section value. If the contribution of this interval to the error on the resonance integral:

$$\int \frac{\sigma(E)}{E} dE \quad (7.2)$$

is smaller than the maximum resonance integral error, then the cross section is declared converged. If the resonance integral criterion is not satisfied, the cross section will be linearised to within the minimum reconstruction tolerance. This is done to control the size of the file because a lot of cross section points are added during the resonance reconstruction.

After finishing the reconstruction, the reconr module will print a summary table with an estimate of the resonance integral error due reconstruction process. This table must be checked to see if the error is not too large. For ^{238}U

from JEFF 3.1 (using 0.1 %, 1 % and $5 \cdot 10^{-8}$ for the minimum and maximum reconstruction tolerance and the maximum resonance integral error), this summary looks like this (some lines were cut to save space):

estimated maximum error due to resonance integral check (errmax,errint)						
upper energy	elastic integral	percent error	capture integral	percent error	fission integral	percent error
1.00E-05						
1.00E-04	2.17E+01	0.000	1.84E+02	0.000	1.82E-03	0.000
1.00E-03	2.17E+01	0.000	5.81E+01	0.000	5.76E-04	0.000
1.00E-02	2.17E+01	0.000	1.84E+01	0.000	1.82E-04	0.000
...						
2.00E+03	1.48E+01	0.006	1.34E+00	0.129	2.91E-04	0.114
5.00E+03	1.78E+01	0.019	1.09E+00	0.362	9.05E-09	0.001
1.00E+04	1.03E+01	0.059	5.37E-01	0.912	6.96E-05	0.496

Just checking this table can already lead to some quite surprising results. This is for instance the resonance reconstruction summary for elemental sulfur from ENDF/B-VI.8:

estimated maximum error due to resonance integral check (errmax,errint)						
upper energy	elastic integral	percent error	capture integral	percent error	fission integral	percent error
1.00E-05						
1.00E-04	2.26E+00	0.000	3.58E+01	0.000	1.24E-01	0.000
1.00E-03	2.26E+00	0.000	1.13E+01	0.000	3.92E-02	0.000
1.00E-02	2.26E+00	0.000	3.58E+00	0.000	1.24E-02	0.000
...						
2.00E+05	5.86E+00	0.001	2.04E-03	0.247	1.30E-03	1.077
5.00E+05	2.48E+00	0.010	1.22E-03	0.866	6.59E-04	1.765
1.00E+06	1.52E+00	0.018	5.29E-04	1.057	2.69E-05	2.025

Apparently, this element has non-zero fission integrals! This is due to the fact that the fission widths in the resonance parameters are not zero so NJOY calculates the integral. This evaluation has been in use since 1979 and was included in the beta0 version of ENDF/B-VII (in the beta1 version released in October 2005 this element was removed).

7.3.4 Unresolved Probability Tables

A probability table can have a number of defects. First of all, there are the possible zero cross section values. They mostly occur in the first few bins where the cross section value can become very small. This is possibly due to round-off because ENDF files are used to transfer information (the number of significant digits is limited).

Negative cross section values on the other hand are physically impossible. When these occur, ALEPH-DLG will simply rerun the isotope with the unresolved probability table option switched off. For now, this is the only point where ALEPH-DLG takes corrective actions.

There is also the possibility to have cross section bins with zero probability. In this case, the bin will never be sampled so that negative or zero cross section values in this bin do not pose a problem. This problem also surfaced during the preparation of the URES library for MCNP (the first MCNP library to include probability tables) [50] but no corrective measures were taken at the time.

In some cases, all these problems can be found in a single example. This is for instance the case for the probability table of ^{22}Na from JEFF 3.1 at 300 K at an energy of 15 keV (in this example the column corresponding to the fission cross section and the probability bins 2 to 8 are omitted to save space):

bin	tot prob	cum prob	total	elastic ...	capture
1	0.000000E+00	0.000000E+00	0.000000E+00	0.000000E+00	...
...					
9	0.000000E+00	0.000000E+00	0.000000E+00	0.000000E+00	...
10	5.852375E-01	5.852375E-01	1.056769E-01	0.000000E+00	...
11	3.289687E-02	6.181344E-01	1.056798E-01	0.000000E+00	...
12	3.425000E-02	6.523844E-01	1.056858E-01	0.000000E+00	...
13	6.732500E-02	7.197094E-01	1.057690E-01	1.138332E-08	...
14	7.261250E-02	7.923219E-01	1.064582E-01	6.739630E-07	...
15	5.415938E-02	8.464812E-01	1.248099E-01	1.009233E-02	...
16	4.939687E-02	8.958781E-01	7.096786E-01	5.924746E-01	...
17	5.180000E-02	9.476781E-01	2.888497E+00	2.760378E+00	...
18	3.734063E-02	9.850187E-01	1.538414E+01	1.514680E+01	...
19	1.083750E-02	9.958562E-01	5.999406E+01	5.946302E+01	...
20	4.143750E-03	1.000000E-00	9.958044E+01	9.904143E+01	...
average probability table		1.912509E+00	1.793225E+00	...	-2.599318E-02
average ladder calculation		1.912509E+00	1.793225E+00	...	-2.599318E-02
diff [%]		0.0000	0.0000	...	0.0000
passed?		yes	yes	...	yes

Warning: did not pass 3 of 20 bin tests

Passed all average cross section tests - no problems found

Warning: did not pass negative test - 8 negative cross section were found

Warning: did not pass zero test - 30 abnormal zero cross section were found

Warning: 9 zero probability values found

7.3.5 Cross section plots and MCNP(X) testing

As mentioned before, the second acer run is capable of producing an input file for the viewr module to visualise the content of the ACE file. The human eye is a wonderfully complex tool, able to spot inconsistency and error with amazing precision. When looking over the various plots, a user should look for unexpected discontinuities in cross sections and examine outgoing energy and angular distributions, threshold regions and resonance regions.

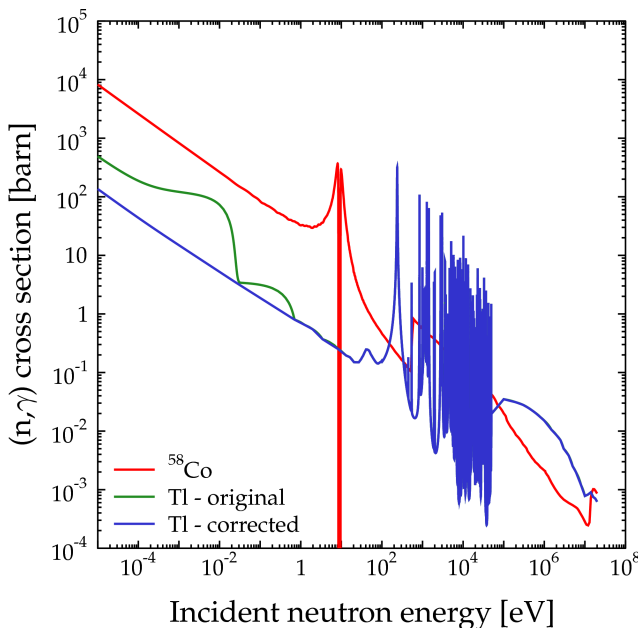


Figure 7.3: The ^{58}Co and Tl neutron capture cross section from the JEFF 3.1 library with cross section deficiencies.

This part of the verification process can help identify errors that were left undetected by NJOY. This is illustrated in figure 7.3. This figure shows the ^{58}Co and Tl neutron capture cross section from the JEFF 3.1 library. The first ^{58}Co neutron capture resonance at 9 eV is not properly reconstructed and has a zero cross section between 8.46 eV and 9.57 eV. The ^{58}Co background cross section in the original ENDF file appears to be cause of this problem. Unfortunately, this error is not detected by NJOY in any way (NJOY only detects this type of error in elastic scattering cross section data, see section 7.3.2).

The Tl neutron capture cross section is another example of how a cross section plot can help identify evaluation errors [54]. The original Tl neutron capture cross section does not have the typical $1/v$ behaviour one would normally expect. Instead, it looks like a stair type function. In this case, this error can be attributed to an erroneous interpolation scheme in the neutron capture background cross section below 1 eV in the original evaluation (lin-lin instead of a more logical log-log interpolation scheme as illustrated in figure 7.3) [55].

No amount of testing will be able to weed out all possible errors and deficiencies in the nuclear data files. When using nuclear data files, sooner or later some problems will surface that require changes to the original ENDF file to

prevent the error from occurring again. Some of these problems are so obscure and their occurrence so improbable that they can remain undetected for long times. This is for instance the case with the secondary photon distributions from JEFF 3.1 in the (n,γ) reaction of Ti (in MF6 MT102 of the original ENDF file) and in the continuum level of the (n,α) reaction on ^{209}Bi (in section MF6 MT849 of the original ENDF file). Under certain circumstances, MCNP(X) will fail to sample the outgoing photon energy from the secondary photon distributions, resulting in the abnormal termination of MCNP(X).

A secondary photon distribution usually consists of discrete photon lines along with a continuum distribution. The previously mentioned problem is caused by the continuum part of the energy spectrum. In both cases, for the first few points this continuum is set to zero so that there are only discrete photon lines. It is these zeros that cause the problems and they were therefore replaced by a very small but still non-zero number (similar to the problem mentioned in section 7.2.1).

7.4 Nuclear data validation

7.4.1 General remarks on library validation

Benchmarking the new libraries is a very important step in the development of a validated application library and must be as thorough and as complete as possible. The new libraries will be applied to a number of different fields: from thermal water moderated reactors, fast spectrum ADS systems to shielding applications, etc. Every application field has its specific demands on nuclear data (see for instance chapter 6 for the nuclear data requirements of burn-up applications). In thermal water moderated systems, the emphasis will lie on lower energy while ADS applications require high energy data. Certain nuclides can be of significant importance in one application while they are not for another application. Accurate high energy data for Pb and Bi are for instance required for ADS applications, structural material data for shielding applications, etc.

It is obvious that it is impossible to provide benchmarks for every possible material and application area so choices have to be made. We have therefore opted to perform a number of benchmarks that were previously used to validate the standard MCNP libraries, namely criticality benchmarks (which were already used for validating the standard MCNP(X) ENDF60 and ENDF66 libraries) and the Lawrence Livermore pulsed sphere experiments.

7.4.2 Criticality benchmarks

In April 1999, LANL released a suite of 86 criticality benchmarks [56] (along with the corresponding MCNP input files) for the specific purpose of validating nuclear data libraries for MCNP [57, 58]. The different benchmarks

in the suite were specifically chosen to obtain a set of problems that would test different energy regions, such as the high-energy region of fast critical assemblies and the thermal region of the solution experiments, and to test various reflector materials while maintaining an acceptable amount of benchmark problems.

This suite has been compiled using two compendiums of criticality experimental information: the Cross Section Evaluation Working Group (CSEWG) specifications and the International Criticality Safety Benchmark Evaluation Project (ICSBEP). The geometry and material specifications for the 86 benchmarks were taken primarily from the ICSBEP compendium.

There were 5 different categories of benchmarks in this suite: critical assemblies with ^{233}U , intermediate enriched ^{235}U , highly enriched ^{235}U , ^{239}Pu and mixed metal assemblies. Within every category there are bare, reflected (with Be, BeO, C, Al, Fe, Ni, W, Th, ^{233}U and natural uranium) and solution assemblies.

The detailed results of these benchmarks can be found in [52, 53]. To illustrate the use of these benchmarks for the validation of nuclear data, figure 7.4 gives the results (as the ratio of calculated over experimental values) for the 37 highly enriched ^{235}U assemblies in this suite. The JEF 2.2 nuclear data library appears to have the worst performance of all tested data libraries for this benchmark category. The JEFF 3.1 library on the other hand seems to give the best performance, only one of the 37 assemblies gives results with a difference of more than 1 % compared to the experimental result.

7.4.3 LLNL Pulsed Spheres

Starting from the late '60s, a series of pulsed sphere experiments have been performed at Lawrence Livermore National Laboratory (LLNL) [59] to investigate neutron cross sections (both at low and high neutron energy) and for the purpose of validating neutron transport codes that were being used at LLNL (such as SORS and TART) [60]. These experiments have also been used to benchmark MCNP [61] and to benchmark ENDF/B-VI data [62].

In these pulsed sphere experiments, an almost isotropic 14 MeV neutron source was placed at the centre of a spherical target assembly. This 14 MeV neutron source was produced by a $\text{T}(\text{d},\text{n})^4\text{He}$ reaction. A deuteron beam was accelerated by the Livermore Insulated Core Transformer (ICT) accelerator to an energy of 400 keV and directed toward a tritiated titanium disk of 1.2 cm in diameter at the centre of a cubical 40 ft. target pit. The target disk was held in place by a low mass structure made primarily of aluminium and stainless steel.

The neutron detectors (either the Pilot B or NE213 detector) that were used to measure the time of flight spectra were placed inside the target pit walls, behind collimators to protect them from the target pit background. Both the Pilot B and NE213 detector were operated at a 1.6 MeV neutron bias (neu-

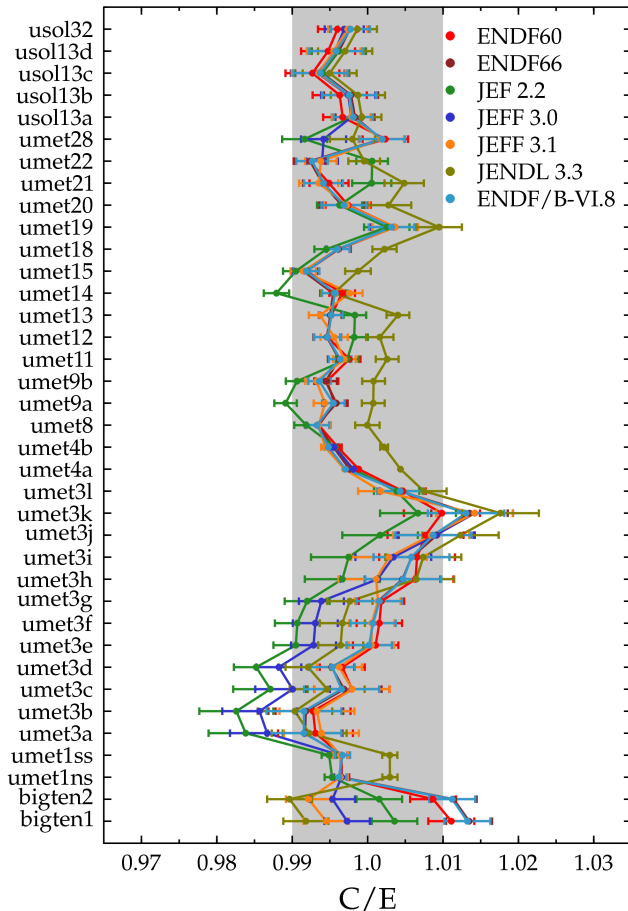


Figure 7.4: Criticality benchmark results with the standard MCNP(X) libraries ENDF60, ENDF66 and the JEF 2.2, JEFF 3.0, JEFF 3.1, JENDL 3.3 and ENDF/B-VI.8 nuclear data libraries for the highly enriched ^{235}U assemblies.

trons below this energy were not detected). The neutrons detected have energies ranging from about 16 MeV down to 2 MeV. As such, the pulsed sphere experiments described here are excellent benchmarks for the higher energy cross sections (above 2 MeV). The detectors were placed at 30 degrees and 120 degrees with respect to the beam line at distance between 750 and 925 cm (depending on the angle used and the experiment).

The resulting neutron emission spectra were then measured using time of flight techniques. Over the years, a large number of pulsed sphere experiments have been performed but the results are not available as part of a large database. Some of these pulsed sphere experiments can however be found in several LLNL reports.

The LLNL report [59] gives the results for a total of 51 experiments on 38 different target configurations using 16 different materials that have been performed for the high energy spectra. In an addendum to this report [63], an additional 10 experiments were reported on 5 different materials for low energy spectra. In 1976, LLNL released another set of pulsed sphere experiments [64, 65] (for both high and low energy spectra) in which some of the previous experiments were repeated with better equipment. These reports also contain data for ^{235}U , ^{238}U and ^{239}Pu . The pulsed sphere experiments continued after that (and these types of experiments are still being performed at LLNL) but no other publicly available data has been found up to this point.

From the validation point of view, this type of experiment is very interesting simply because the geometry is easy to model, because the neutron source is always the same and because very few materials are used. The pulsed sphere experiments are a lot more sensitive to cross section data and even angular distributions when compared to integral benchmarks. This aspect alone makes them prime candidates for validating nuclear data because even the smallest differences will be very clear.

A detailed overview of the results of the 51 spheres described in the LLNL report [59] can be found in [52, 53, 66]. The benchmark results of these spheres for ENDF/B-VII.0 can be found in [67].

In general, the following requirements must be met to obtain agreement between the experimental time of flight spectrum and those obtained through calculations:

- the correct total and total elastic cross section at around 15 MeV (the transmitted peak and the elastic region is sensitive to cross sections at that energy)
- the correct total cross section over the entire energy range
- the correct total and level inelastic scattering cross sections
- the correct angular distribution for elastic scattering and the levels of inelastic scattering

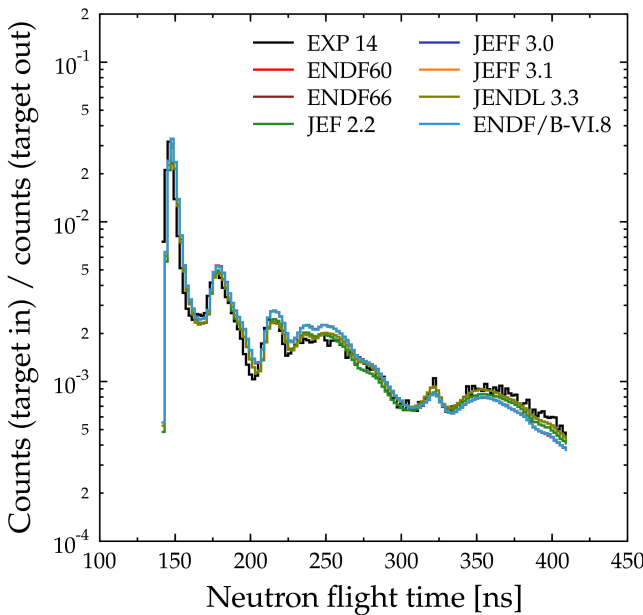


Figure 7.5: Time of flight spectra for a pulsed carbon sphere ($r = 20.96$ cm) at an angle of 30 degrees measured by the NE213 detector.

The neutron source itself (in particular the energy and angle distribution) must be well known because the position of the transmitted peak is determined by the neutron energy of the source under the measured angle.

The case of a solid carbon sphere is very interesting as an example because the transmitted peak, elastic, discrete inelastic and continuum inelastic regions are quite well separated. Figure 7.5 gives the calculated time of flight spectra using MCNPX 2.5.0 and different neutron libraries (the standard MCNP(X) libraries ENDF60 and ENDF66 and the JEF 2.2, JEFF 3.0, JEFF 3.1, JENDL 3.3 and ENDF/B-VI.8 libraries included in ALEPH-LIB).

The spectrum between roughly 160 and 225 ns is mainly determined by the first level of inelastic scattering (4.43 MeV). The second level (7.66 MeV) determines the spectrum between 200 and 325 ns, etc. This way, it can be quite easy to identify problems originating from those inelastic levels.

For the carbon sphere, we observe three families of curves: ENDF (consisting of ENDF60, ENDF66, ENDF/B-VI.8, JEFF 3.0 and JEFF 3.1), JEF 2.2 (based on ENDF/B-V) and JENDL 3.3. The global agreement between the different libraries is quite good (it should be said that all libraries except for JENDL 3.3 are based on ENDF/B data). The agreement with the measured spectrum is

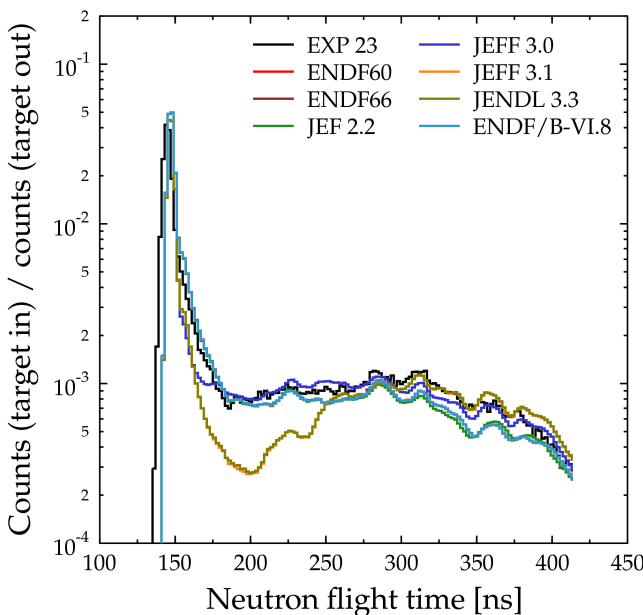


Figure 7.6: Time of flight spectra for a pulsed magnesium sphere ($r = 25.50$ cm) at an angle of 30 degrees measured by the Pilot B detector.

however the best for JENDL 3.3. This conclusion is supported by the other pulsed sphere experiments on solid carbon spheres.

A very good example that demonstrates the power of the pulsed sphere as a validation benchmark are the results for the solid Mg spheres (see figure 7.6). We can see that all the ENDF libraries and the JEFF 3.0 library are in relative good agreement with the measured spectrum. All these data libraries reproduce quite well the various features in the measured spectrum (like the transmitted peak and the various “bumps” at 225, 280, 310 and 355 ns).

The JENDL 3.3 and JEFF 3.1 data on the other hand show large differences between 150 and 250 ns (corresponding to neutron energies of 14 to 5 MeV). After a review of the data in question, we found that the JEFF 3.0 data (only elemental Mg) was based on JENDL 3.2 while the JENDL 3.3 data (the individual ^{24}Mg , ^{25}Mg and ^{26}Mg isotopes) were based on the same JENDL 3.2 data (with a few updates). The JEFF 3.1 data itself was simply taken over from JENDL 3.3.

As mentioned earlier, the first few levels of inelastic scattering determine the part of the time of flight spectrum just after the transmitted peak. In order to explain the differences between the spectra, we compared the data for the

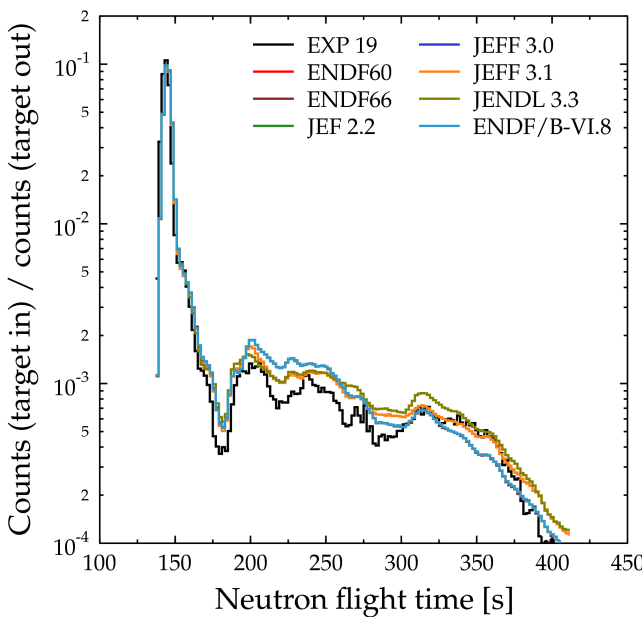


Figure 7.7: Time of flight spectra for a pulsed liquid oxygen sphere ($r = 10.48$ cm) at an angle of 30 degrees measured by the Pilot B detector.

first levels of inelastic scattering of ^{24}Mg , ^{25}Mg and ^{26}Mg from JEFF 3.1 with those of elemental magnesium from JEFF 3.0.

The individual levels of inelastic scattering associated with ^{24}Mg , ^{25}Mg and ^{26}Mg are all different from each other and can all be found in the elemental magnesium evaluation (an overview of the corresponding levels can be found in the comment section of the ENDF file). For example, the first level of ^{24}Mg (at 1.3686 MeV) is the third level of the elemental evaluation. The second level of ^{24}Mg (at 4.1200 MeV) is the 18th level in the elemental evaluation, etc. To transform the cross section of a level from an isotope to that of the element, we need to multiply the cross section by the isotopic abundance of the isotope (78.99 % for ^{24}Mg , 10.00 % for ^{25}Mg and 11.01 % for ^{26}Mg). The angular distributions of those inelastic levels do not need to be transformed. To transform the other cross sections (elastic, capture, etc.), we need to sum the cross sections of the individual isotopes multiplied by the isotopic abundances.

We found no differences in the cross sections, but we did find differences in the angular distributions of the first two levels of inelastic scattering in ^{24}Mg , (at 1.3686 and 4.1200 MeV) and ^{26}Mg (at 1.8087 and 2.9384 MeV). Apart from these differences, no other major differences were found in other cross sections

that can be important for the time of flight spectrum (such as elastic scattering, capture, ($n,2n$), etc.). The difference in the spectra is probably only caused by the difference of a few angular distributions.

Another example is the liquid oxygen sphere which can be found in figure 7.7. Contrary to the previous examples, this sphere wasn't a solid sphere made of a single material. The target configuration for this experiment consisted of an inner sphere filled with liquid nitrogen placed inside another sphere with vacuum in between.

As one can see, the agreement between the different libraries and the experimental results for the oxygen sphere is not very good (especially if we compare it with the previous carbon sphere where the agreement was almost perfect). This might (among other reasons) be caused by the temperature of the data used to calculate time of flight spectra (which is around 300 K while the liquid nitrogen is probably a lot colder).

We also observe some differences between the ENDF/B-VI.8 curve and the JEFF 3.1 curve while the oxygen data in JEFF 3.1 is taken from ENDF/B-VI.8. The differences in the curve are therefore related to differences in the data of the casing materials (68.6 % Fe, 20.0 % Cr, 8.4 % Ni, 2.0 % Si and 1.0 % Mn) of the liquid oxygen sphere. This example illustrates that special care must be taken when performing this type of benchmarks so that differences are not wrongfully attributed to a certain material.

8

No tool is so clever that it cannot be used by an idiot.

Confucius (551 BC - 479 BC)

Give us the tools and we will finish the job.

Sir Winston Churchill (1874 - 1965)

ALEPH: a Monte Carlo burn-up code

8.1 Efficient, flexible and easy to use

One of the goals of this work was to identify, develop and implement methods for Monte Carlo with burn-up to attain the highest accuracy for the smallest computing effort possible. In the previous chapters we have identified and developed such methods. Now the time has come to implement them into a functional code system which we have called ALEPH (the current version is 1.1.3) [47]. ALEPH is in essence an interface code using a modified version of ORIGEN 2.2 and any version of MCNP or MCNPX.

Our ultimate goal was to provide the Monte Carlo community with an efficient, flexible and easy to use alternative for Monte Carlo burn-up and activation calculations:

- *Efficiency*

The efficiency is achieved in ALEPH by using the multi-group binning approach which allows the code to perform burn-up calculations in a matter of days where other Monte Carlo codes would need weeks or even years to do exactly the same thing without loss of accuracy.

- *Flexibility*

ALEPH has been written in C++ using a highly modular design to allow for great flexibility. Replacing for instance MCNP or MCNPX by another Monte Carlo code would be quite easy because of this modular design. And the same applies to ORIGEN 2.2 as well. A great effort has also been made to optimize ALEPH for speed (the transition to fully object oriented code was essential for this).

ALEPH also offers flexibility in other areas. First of all there is the flexibility in nuclear data. We will only use data from ENDF files (see chapter 6) which will also allow us to quickly change our data when newer

(and better) evaluations become available. To facilitate this, the auxiliary module called ALEPH-DLG (Data Library Generator) has been developed (see chapter 7). The use of this auxiliary module will also insure the required nuclear data consistency between the Monte Carlo code and the depletion code. By providing the user with the capability of changing materials and geometry we also achieve flexibility in modelling the irradiation conditions in the system.

ALEPH is also very flexible in its application areas, contrary to its deterministic cousins. Due to its Monte Carlo nature, ALEPH can be used in application areas ranging from fuel cycle studies, waste characterisation, assessment of radioisotope production, fuel pin and fuel assembly calculations to complete full scale reactor calculations.

- *Easy to use*

Monte Carlo burn-up codes have often been stigmatized as not being very user friendly tools due to their complexity (since most codes use a script or link approach). A user would have to understand and manage a large number of input and output files while the conversion of data from one form into another would introduce approximate results due to successive round off.

ALEPH strives to solve this problem by wrapping itself around the various codes involved and by automating the entire process. The ORIGEN input files for instance are created by ALEPH itself without any intervention of the user. The use of ORIGEN is actually “hidden” from the user. The user doesn’t even have to provide a skeleton input file. By providing an easy to understand user interface, we also take away the burden from the user. For the user, it is as if he is running a simple MCNP(X) problem but with some “extra” options.

8.2 Calculation flow and features

A typical ALEPH calculation starts with the processing of the input file (the black arrow at the top of figure 8.1). The input consists of the ALEPH code options, along with an initial MCNP(X) input file. These ALEPH code options specify the irradiation history (including the points in time where the spectrum must be recalculated), the adopted energy group structure, the materials and ENDF libraries to be used, the ORIGEN and MCNP(X) executable names, volumes, etc. Other essential information (initial material composition, temperatures, etc.) is read from the initial MCNP(X) input file itself.

ALEPH contains a parser for MCNP(X) input files which is capable of extracting the necessary data. The parser is not a complete MCNP(X) parser so certain MCNP(X) input capabilities (such as the “like ... but ...” structure) cannot be used. But apart from these limitations, anything goes.

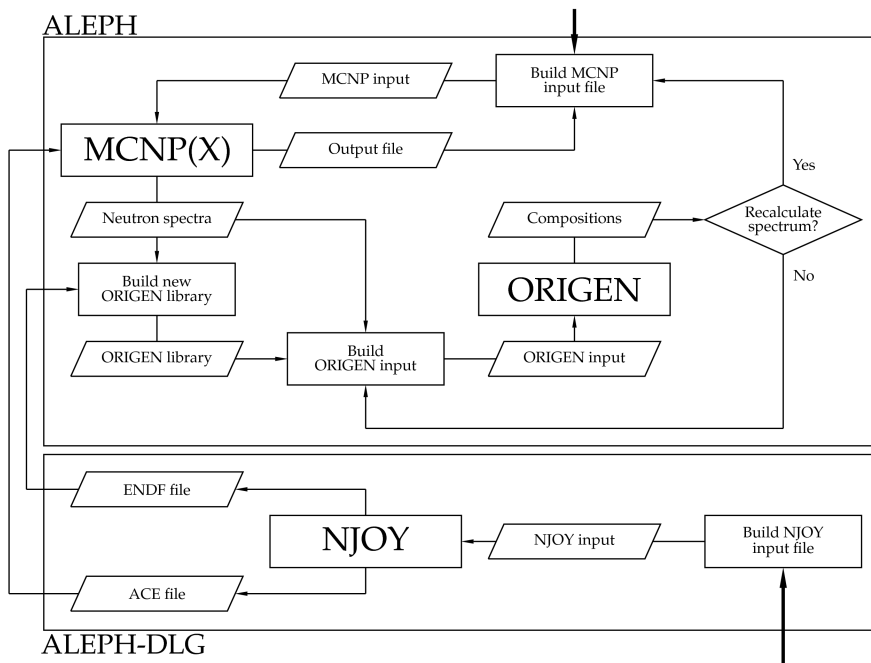


Figure 8.1: Calculation flow in ALEPH and ALEPH-DLG.

ALEPH can read both types of material specification possible in MCNP(X), being weight fractions and atomic fractions. The same goes for the densities specified on the cell entries: it may be specified in g/cm^3 or in $\text{atoms barn}^{-1} \text{cm}^{-1}$ as per normal MCNP(X). And it is also allowed for the input to be mixed (density in g/cm^3 and composition in atomic fractions and vice versa). By default, ALEPH will recalculate all materials to densities given in $\text{atoms barn}^{-1} \text{cm}^{-1}$ and compositions given in atom fractions, as MCNP(X) does internally.

To recalculate compositions (both from the MCNP(X) input file and the ORIGEN output files) to the standard $\text{atoms barn}^{-1} \text{cm}^{-1}$, the correct atomic mass of every possible nuclide is required. The atomic mass values used by ALEPH and by MCNP(X) itself must also be the same to ensure nuclear data consistency. MCNP(X) uses the values that are specified in the first part of the xsdir file, but until recently the standard xsdir files only contained atomic mass data from 300 to 400 nuclides while ALEPH requires atomic mass values for at least every nuclide possible in ORIGEN. We have therefore decided to update those atomic mass values by using the Atomic Mass Evaluation 2003 included into NUBASE [68] from the Atomic Mass Data Center.

Once the input file has been processed, ALEPH builds a new MCNP(X) input file based upon the input options of the user and starts an MCNP(X) calculation. The neutron spectra for the different burn-up zones (read from the MCNP(X) tally file) are passed on for building the new ORIGEN libraries and ORIGEN input files (one for every zone).

After the MCNP(X) run, the output file is also processed to determine if MCNP(X) has encountered any problems. Because the spectra are already stored in the tally file, ALEPH will also remove the tally results from the MCNP(X) output file to save disk space. In the case of criticality calculations, ALEPH also reads the value of the effective multiplication factor for use as an initial estimate for the next calculation. In that case, the fission source calculated in the previous calculation will also be used as the initial source in the next step.

The current version of ALEPH (version 1.1.3) only updates the cross section data in an ORIGEN library file. Updating branching ratio values, direct fission yields, decay data, average neutron yield from fission and energy release from fission data (as demonstrated in chapter 6.1) will be added in a future version. The linearized cross sections used to prepare the ORIGEN cross section library are read from individual ENDF files (one for every material considered in the evolution chains).

ALEPH is capable of using all irradiation features of ORIGEN: constant flux irradiation, constant power irradiation and simple decay. After the ORIGEN calculation, ALEPH reads the results and cleans up all the temporary files from ORIGEN. The number of significant digits used by ORIGEN in its output was increased from 3 to 5 to address the possibility of a round off problem, although tests showed little or no influence on the final result. The new compositions are then stored and passed on either to build a new MCNP(X) input file (for a new burn-up step) or new ORIGEN input files (to obtain compositions at intermediate points within the same burn-up step).

The material compositions of the different zones are updated at the beginning of every new burn-up step for which the cross section library must be recalculated. For the purpose of transport calculations we truncate the list of nuclides as calculated by ORIGEN using a fractional absorption criterion specified by the user (see section 8.4 for more information). This entire process continues until the end of the calculation.

ALEPH has also the capability of performing geometrical changes and material changes during irradiation. Geometry changes (by using surface transformations) allows for instance the simulation of control rod movement during the irradiation cycle, etc.

For the material changes, ALEPH distinguishes between 2 types of materials: variable materials and burnable materials. Variable materials are materials that can be changed by the user but that do not need to be burned. A user can therefore change the density and/or temperature of such a material (to for instance simulate heating effects of water) or even replace the material

by another one (to take into account changes in the boron concentration in the coolant of a PWR, etc.). A user can also change the temperature of a burnable material or even replace it with another burnable material (which can be a new material to simulate core reshuffling and reloading). For obvious reasons, a burnable material's density cannot be changed by the user. Burnable materials that are being taken out of the model will, by default, undergo decay so that these materials can be used again at a later point in the irradiation.

8.3 Irradiation capabilities

8.3.1 The specific normalisation power

The power in a system (and in the different materials that compose the system) is determined by the power distribution, which is in turn determined by the flux distribution. The power produced in a material j (consisting of N_j different nuclides i characterised by a proton number Z_i , mass number A_i with density ρ_i (and corresponding atomic density n_i) and fission cross section $\sigma_{i,f}$) is proportional to what we call the specific normalisation power $P_{0,j}$. This power $P_{0,j}$ represents the relative power distribution in all materials. In essence, $P_{0,j}$ is the total power produced through direct fission, delayed energy and neutron activation of the structural materials (expressed in MW):

$$P_{0,j} = e 10^{-24} \sum_{i=1}^{N_j} Q_{f,i} \frac{\rho_i V_j N_A}{A_i} (\sigma_{i,f} \phi_{0,j}) = e \sum_{i=1}^{N_j} Q_{f,i} n_i \sigma_{i,f} \phi_{0,j} \quad (8.1)$$

in which e is the elementary electron charge, N_A is the number of Avogadro, $\phi_{0,j}$ is a measure of the total flux in the material j (in fact, MCNP(X) will provide us with $\phi_{0,j} V_j$ per source particle for every material that we are burning) and where $Q_{f,i}$ is the total recoverable energy from fission of the nuclide i expressed in MeV (see section 6.7). For now, we still use the formula used inside ORIGEN:

$$Q_{f,i} = 1.29927 10^{-3} (Z_i^2 A_i^{0.5}) + 33.12 \quad (8.2)$$

ALEPH will use the specific normalisation power $P_{0,j}$ corresponding to the last spectrum calculated. In other words, the power is calculated by using the composition of the material when its spectrum was recalculated. So if the user has specified points without a spectral recalculation, the specific normalisation power $P_{0,j}$ will not be updated with the new composition.

It should be noted that - for now - the specific normalisation power $P_{0,j}$ will be zero for a material that doesn't contain actinides. It is therefore impossible to calculate the evolution of such materials by using constant power irradiation. Constant flux irradiation is the only possibility to do this. This will be fixed in a future version of ALEPH.

8.3.2 Constant power

The option of constant power irradiation is quite important because it is used in power reactor calculations. As we mentioned before in section 6.7, the Bateman equations use the absolute neutron flux so that it is necessary to calculate the equivalent flux in a constant power step. The power P produced in a reactor at every point in time is always proportional to the total neutron flux ϕ (see equation 2.21):

$$P = e \sum_i Q_{f,i} n_i \sigma_{f,i} \phi \quad (8.3)$$

where n_i is the atomic density (atoms barn⁻¹ cm⁻³), $\sigma_{f,i}$ the fission cross section (barn) and $Q_{f,i}$ the total recoverable energy from fission (MeV) for actinide i . Fortunately, ORIGEN 2.2 takes care of this for us so the user does not have to worry about this.

For ALEPH, we have foreseen four possibilities in specifying such a constant power step:

- The power for every material i is specified. In this case no further normalisation of the power will occur. This option should be avoided because it doesn't take into account the relative power distribution of the system.
- The total power P_t for all materials is given. The power of every material j is now determined by using the ratio of the relative power level $P_{0,j}$ of the material to that of all materials combined:

$$P_j = P_t \frac{P_{0,j}}{\sum_{l=1}^{N_b} P_{0,l}} \quad (8.4)$$

where N_b is the total number of materials being burned.

- The power P_i of a specific material i is given. The relative power level of every other material j to material i is now used to determine the power values of all burnable materials in the system:

$$P_j = P_i \frac{P_{0,j}}{P_{0,i}} \quad (8.5)$$

- The total power $P_{c,t}$ of a set of materials is given. This option is somewhat similar to the second and third option. For materials in the collection, the relative power level of the material to that of all materials in the set is used (see equation 8.4). For materials that are not in the set the relative power of that material to the power of any material from the collection is used (see equation 8.5).

When only a single material is being burned in the calculation, all four options will be equivalent.

The calculated power levels are then passed on to ORIGEN 2.2 to perform a step of constant power irradiation. These different options were foreseen in ALEPH to give the user a great deal of flexibility in specifying the power. If we take the example of the MALIBU experimental data (see chapter 10), only the power history of the fuel samples are known but in order to accurately model the depletion of the sample we must also burn the adjacent pins. ALEPH foresees this possibility so the user does not have to go through great lengths to calculate the total power which is often required by other Monte Carlo burn-up codes like MCNPX 2.6.a and above.

8.3.3 Constant flux

The second irradiation possibility provided by ORIGEN for use in ALEPH is the constant flux irradiation. Unlike the constant power irradiation it is the most basic way of performing a depletion calculation (the Bateman equations use the flux values directly).

We have foreseen two possibilities for the flux renormalisation:

- The absolute source strength S is specified. Because MCNP(X) provides us with flux values per source particle multiplied with the volume of the material, the flux for every material j is calculated as:

$$\phi_j = S \frac{\sum_{l=1}^{N_g} \phi_{0,j,l}}{V_j} \quad (8.6)$$

where $\phi_{0,j,l}$ is the flux per source particle of group l for material j (as calculated by MCNP(X)) and where V_j is the total volume of material j present.

- The absolute flux level ϕ_i of a specific material i is given. The flux ϕ_j of the other materials j is then calculated as:

$$\phi_j = \phi_i \frac{V_i}{V_j} \frac{\sum_{l=1}^{N_g} \phi_{0,j,l}}{\sum_{l=1}^{N_g} \phi_{0,i,l}} \quad (8.7)$$

As mentioned before (see section 6.6), it is also possible to determine the absolute flux levels in a system by using the total system power P , the value of the effective multiplication factor k_{eff} , the total average number of neutrons

per fission \bar{v}_t and the average recoverable energy per fission Q_f . The absolute number of source particles is then given by:

$$S = \frac{P}{e Q_{s,f} k_{\text{eff}}} \bar{v} \quad (8.8)$$

Although a user can use the first constant flux option to give the number of source particles S determined with this equation, this option has not been automated into ALEPH due to its limitations. First of all, the total system power P must be known (which is not always the case). Furthermore, its use is limited to criticality calculations. All the constant power and constant flux options implemented into ALEPH on the other hand can be used in both fixed source and criticality calculations.

8.3.4 Calculating burn-up

An important quantity in depletion calculations is the burn-up accumulated by a material during the irradiation. Burn-up is usually expressed as GWd per ton initial heavy metal (GWd/tHM) or MWd per kg initial heavy metal (MWd/kgHM). So, in the case of an irradiation step with constant power the burn-up BU_j accumulated by material j which produced a power P_j (MW) will be given by:

$$BU_j = 10^6 \frac{P_j t}{\rho_{a,j} V_j} \quad (8.9)$$

where $\rho_{a,j}$ is the density (g cm^{-3}) of the actinides initially present in the material and t is the irradiation period in days. V_j is the volume of the cells containing the material j .

For a step with constant flux irradiation of material j with flux ϕ_j , this becomes:

$$BU_j = 10^6 \frac{P_{0,j} t}{\rho_{a,j} V_j} \frac{\phi_j}{\phi_{0,j}} \quad (8.10)$$

where $P_{0,j}$ is the specific normalisation power of material j and $\phi_{0,j}$ is a measure of the total flux in the material j (as mentioned earlier, MCNP(X) will provide us with $\phi_{0,j} V_j$ per source particle for every material that we are burning), see equation 8.1.

8.4 Updating material compositions

In every calculation there should be a balance between accuracy and what is (reasonably) achievable. With the multi-group binning method we have reduced the reaction rate calculation time to a minimum compared to the Monte Carlo simulation time. As a result, we can actually be as accurate as we want

in modelling the transmutation chains by using as many nuclides as we possibly can from the beginning. By combining an entire evaluated nuclear data library like JEFF 3.1 with an activation library like JEFF 3.0A we will have data for around 800 nuclides (for a total of more than 3000 reaction rates). And that list will not change during the entire calculation. We therefore have no need for importance criteria to see when a nuclide becomes important enough to calculate its reaction rates (see section 4.7).

This however only applies to the calculation of reaction rates. During the depletion new nuclides will be created and others will disappear. This can have significant effects on the system's spectrum (take for instance the creation of Pu in a UO₂ fueled reactor) and must therefore be taken into account. This is done by updating the material compositions at every burn-up step. Unfortunately the addition of nuclides to the system will have an adverse effect on the simulation time because MCNP(X) uses unionised cross section tables. We have shown that the MCNP(X) simulation time in a single cell will be roughly proportional to the number of nuclides used in the material (see table 5.1):

$$t_s \propto N_{tr}N \quad (8.11)$$

It is therefore necessary to make a selection of the most important nuclides for inclusion in the Monte Carlo simulation to minimise the impact on the simulation time. As we have already mentioned (see section 4.7) a fractional absorption criterion is the best way of doing this. For this purpose, the ratio of the absorptions by a nuclide to the total number of absorptions in the material is computed and sorted in decreasing importance. Only those nuclides responsible for a cumulative total of e.g. 99.9 or 99.99 % of all absorptions are included (nuclides that were originally present are added by default and do not necessarily contribute to the fractional absorption). The material composition for transport calculations is re-evaluated for every point where the user wishes to recalculate the ORIGEN libraries. As such, it is possible that this list is changed significantly after long periods of decay.

The density used in the transport calculation is renormalized to this list of transport nuclides to conserve the absolute number of atoms. The full list of nuclides created during the irradiation is saved until the end of the calculation so nuclides left of the transport list are not expunged from the calculation. This entire process continues until the end of the calculation.





A million experiments can't prove me right, but one experiment can prove me wrong.

Albert Einstein (1879 - 1955)

High burn-up fuel

9.1 Self-shielding and the high burn-up structure

The self-shielding effect in a nuclear reactor is both energetic and spatial in nature. The energy self-shielding results from the resonances in the various cross sections of the different nuclides present in the fuel. The spatial self-shielding effect results from the heterogeneity of a reactor. Neutron absorption in the outside of a fuel pellet will effectively shield the inside of the pellet, resulting in a neutron flux dip in the centre of the fuel pin. This is strongly influenced by the neutron spectrum of the reactor in question. As a result of this effect, the burn-up at the edge of the fuel pellet will be larger than the burn-up in the centre. The distribution of fission products and other nuclides like Pu will also be dependent upon the radial position in the fuel pellet. At higher burn-up levels, this will have a significant effect on the pellet thermal properties, fission gas retention, etc. and therefore on the fuel performance itself [69, 70].

When the local burn-up in a fuel pellet reaches about 60 MWd/kgHM, the UO₂ grains in the outer region of the fuel pellet will start to recrystallise. This is a direct result of accumulated fission products and irradiation damage sustained by the fuel at temperatures below 1400 K. This transformed fuel microstructure is often referred to as the high burn-up structure (HBS). This structure consists of sub-micron grains and a large concentration of pores with a typical diameter of 1 to 2 μm . The high burn-up structure is characterised by the loss of Xe from the fuel matrix. As such, a measured radial profile of Xe content in a fuel pellet can indicate to which extent the high burn-up structure has already developed.

The consequences on the thermo-mechanical behaviour of UO₂ fuels of this recrystallisation process has been and continues to be the subject of intense research. Such research is important to the electrical utilities who continuously strive to increase the burn-up at which a fuel assembly is discharged from a reactor. This is motivated by a decrease of fuel cycle cost and a reduction of the amount of spent fuel that has to be reprocessed or stored. Since

1980 the average burn-up of spent fuel assemblies has increased from 30 to over 50 MWd/kgHM and it is projected to increase above 70 MWd/kgHM over the next decade [70].

In this chapter, we will present the validation of ALEPH for simulating the rim-effect and in particular for high burn-up PWR UO₂ fuel in collaboration with the Institute for Transuranium Elements (ITU, Germany) of the European Union's Joint Research Centre (JRC) [71]. We will compare calculations of both absolute values and radial profiles of Pu and Nd by ALEPH and the TUBRNP module [72, 73] of the TRANSURANUS fuel performance code [74] with experimental data obtained by means of Electron Probe MicroAnalysis (EPMA) or Inductively Coupled Plasma Mass Spectrometry (ICP-MS).

9.2 TRANSURANUS and TUBRNP

In order to predict the behaviour and life-time of fuel rods in nuclear reactors, complex computer codes are required that perform a consistent analysis of the thermal, mechanical, and neutron-physical processes, such as the TRANSURANUS code developed at ITU [74]. In present LWR conditions the large radial gradient of the concentrations of fissile isotopes in the periphery of the fuel (due to spatial self-shielding) leads to a strong radial dependence of the power generation. An adequate evaluation of the local concentrations of actinides and fission products inside the fuel pin is therefore essential. Within TRANSURANUS, this evaluation is covered by the TUBRNP model and can be performed for up to 500 radial zones in the fuel pellet.

Because in fuel performance codes the absolute value of the generated power is given on input, the primary objective of TUBRNP is to provide a correct normalized radial power distribution that is closely related to the normalized shape of the Pu and burn-up distributions. The TUBRNP model limits its computations to the most abundant isotopes that are either fissile or fertile. In each time step and in each radial node, the local concentrations of the isotopes ²³⁵U, ²³⁸U, ²³⁹Pu, ²⁴⁰Pu, ²⁴¹Pu, ²⁴²Pu are calculated by applying one-group effective cross-sections for fission and neutron capture [72].

A radial form factor is used to account for the absorption of resonance neutrons in ²³⁸U and ²⁴⁰Pu. The calculated increment of the U and Pu isotope concentrations are proportional to the burn-up increment. The values calculated by TUBRNP hence do not depend on details of the irradiation history. In addition, the local concentrations of the elements Nd, Xe, Kr and Cs are evaluated as products of the fission reaction. They are used in TRANSURANUS as source term for the fission gas behaviour [75].

The prediction of the radial power profile by the TUBRNP module is of primary importance, as it constitutes the source term of the temperature calculations as well as the radioactive fission products. The validation of this module requires experimental data, like those obtained through EPMA or ICP-MS.

Apart from experimental data, the application of a simplified neutronic module like TUBRNP also relies on the definition of the proper one-group cross sections which can only be obtained by means of a neutron transport code calculation. To this end ALEPH has been selected, since it provides a fast and reliable Monte Carlo transport calculation combined with a depletion calculation for the various isotopes. However, prior to using ALEPH to define the improved cross sections at very high burn-up, the experimental validation of ALEPH itself at those burn-up levels is required.

9.3 Modelling high burn-up fuel pins with ALEPH

Two 3.5 % enriched ^{235}U fuel rods (labelled 12C3 and 12H3) were subjected to an extended irradiation in a 15×15 assembly of a pressurized light water reactor (PWR). The irradiation lasted for 2631 effective full power days (EFPD) over 8 reactor cycles for rod 12H3 and 2913 effective full power days spread over 9 reactor cycles for rod 12C3 in a commercial Siemens PWR at Gösgen (Switzerland). After the fourth irradiation cycle, the original fuel assemblies had reached their nominal discharge burn-up around 60 MWd/kgHM. For the following cycles, the 12H3 and 12C3 fuel rods were taken out of their original assembly and placed inside new carrier assemblies containing partially burned fuel. This step was repeated for every subsequent reactor cycle, leading to an accumulated fuel rod average burn-up of 89.5 MWd/kgHM for rod 12H3, and 97.8 MWd/kgHM for rod 12C3.

Two high power (HP) and two low power (LP) samples were taken from these rods. The high power samples were taken as slices between 312.0 cm to 312.7 cm from the rod bottom and the low power samples between 31.6 and 32.3 cm from the rod bottom, implying a slice average burn-up of 95 MWd/kgHM for 12H3-HP, 102 MWd/kgHM for 12C3-HP, 65 MWd/kgHM for 12H3-LP and 69 MWd/kgHM for 12C3-LP.

A significant source of uncertainty in any depletion calculation is the axial distribution of the power along the fuel rod. In this case, only the maximum average linear power along a pin is given as a time-average for each irradiation cycle (see table 9.1 [70]).

According to basic reactor theory, the initial axial power distribution of a fuel rod can be described by a cosine function which will flatten during burn-up. In the middle of the fuel rod (where the HP samples are located) this distribution will thus change weakly as a function of the axial position. We therefore scaled the maximum average linear power values from 98 MWd/kgHM to the target of 102 MWd/kgHM.

Because the exact positions of the 12H3 and 12C3 pins within these fuel assemblies have not been published, we were unable to account for the influence of the neighbouring fuel pins and/or guide tubes. Furthermore, the precise compositions or burn-up levels of the partially depleted fuel within the

Table 9.1: Power history and burn-up evolution in the high burn-up fuel pin [69, 70].

Reactor cycle	Linear power W cm ⁻¹	Average burn-up MWd/kgHM
1	340	19
2	290	18
3	230	11
4	200	11
5	180	8
6	170	5
7	160	10
8	140	8
9	140	8

carrier assemblies were also unknown. We have therefore used a 2D model of a fuel pin representing a 15×15 assembly in a standard infinite lattice. In order to maintain the fuel to moderator ratio of the original 15×15 fuel assembly, the pitch of the rod model was increased from the original value of 1.43 cm to 1.496 cm. This approach takes into account the fact that only 204 out of 225 positions in the 15×15 fuel assembly are occupied by fuel pins. The remaining positions are taken by guide tubes and instrumentation tubes.

In order to be able to perform a detailed simulation of the strong neutron absorption at the surface of the fuel pellet, the pellet was subdivided into 10 radial zones with a dichotomic procedure. This procedure starts by dividing the pellet radius into two and the outer part is then continuously divided into two until the proper resolution at the edge of the fuel pin has been reached. An overview of the fuel pellet and pin dimensions, materials, temperatures, etc. used in the ALEPH calculations are given in table 9.2.

The entire irradiation history was divided into steps corresponding to an average burn-up of 1 MWd/kgHM with an additional decay step after every reactor cycle. For every one of those burn-up steps, a criticality calculation (10000 particles/cycles, 50 inactive cycles for a total of 500 cycles) was used to determine the neutron spectrum in every burn-up zone. The error on the total flux of every burn-up zone is of the order of 0.02 %, which is very low for this type of applications.

We performed these calculations with the JEFF 3.1 evaluated nuclear data library for both the criticality and depletion calculations. For the depletion calculations in every step, the JEFF 3.1 data were supplemented with data from the JEFF 3.0A activation data library so that ALEPH effectively calculates cross sections for 793 different nuclides for use in ORIGEN 2.2 for every radial zone and every time step in the burn-up calculation.

Table 9.2: Fuel pellet and pin design characteristics used in ALEPH calculations [69, 70].

Initial ^{235}U enrichment [%]	3.5
Fuel density [g cm^{-3}]	10.45
Fuel pins	204
Guide & instrumentation tubes	21
Fuel pin pitch [cm]	1.43
Equivalent pin cell model pitch [cm]	1.496
Fuel pellet radius [cm]	0.465
Inner cladding radius [cm]	0.484
Outer cladding radius [cm]	0.5375
Guide tube inner radius [cm]	0.6502
Guide tube outer radius [cm]	0.6934
Moderator temperature [K]	600
Cladding Temperature [K]	600
Fuel Temperature [K]	900
Moderator boron concentration [ppm]	420
Cladding material	Generic Zircaloy

9.4 Experimental measurements

A detailed description of the EPMA technique and equipment that is in operation at ITU is given in [76]. The instrument is specially shielded with lead and tungsten to permit the analysis of irradiated nuclear fuel.

An advantage of EPMA is that it is capable of quantifying both the absolute concentrations as well as their relative radial profile with the same experimental technique. It should be noted that the measurement of absolute concentrations only makes sense for major components of the sample. Measuring absolute concentrations of minor constituents (below a few weight % of the mass of the entire sample) can be problematic and therefore result in large errors [77].

The EPMA data analysed in this work were obtained from the batch of measurements described in [69]. The measurement procedure for Nd is given therein whereas specifics of the Pu measurement can be found in [72] as well as in [70]. The data points used to construct the radial profiles of Nd and Pu were spaced at $50 \mu\text{m}$ in the outer region of the nuclear fuel ($r/r_0 > 0.9$), at $100 \mu\text{m}$ in the intermediate part and at $150 \mu\text{m}$ in the central region of the fuel pellet ($r/r_0 < 0.5$). A number of such EPMA measurements for different levels of burn-up and initial ^{235}U enrichment had been considered earlier [78, 79].

In addition to all these EPMA data, measurements with ICP-MS of the absolute Pu and Nd concentration are available as well [80].

9.5 Evolution of the neutron spectra

Fission neutrons in a PWR do not generally interact with nuclides in the fuel pin where they were created. These fission neutrons have a mean energy at around 2 MeV which is above the resonance energy region and they can therefore get out of the fuel pin with relatively few interactions. When they enter the water moderator, they are slowed down considerably before entering another fuel pin.

At this point, the neutrons entering a fuel pin are more susceptible to the self-shielding effect compared to the fission neutrons created in the fuel pin. A neutron with an energy corresponding to a resonance of a nuclide in the fuel has a much higher probability of being absorbed compared to neutrons with an energy further away from the resonance. The outer regions of the fuel pin will therefore act as a filter on the neutron spectrum for the inner regions because neutron energies corresponding to resonances will be gradually filtered out. This is clearly visible in figure 9.1. This figure plots the neutron spectra in three radial zones of the fuel pin at the beginning of the irradiation and at the end for a burn-up of 102 MWd/kgHM.

In both cases we can see that the influence of the resonances is more pronounced in the inside region than at the outside. At the beginning of the irradiation, the ^{238}U resonance at 6.674 eV causes for instance a spectrum dip that is 300 times deeper in the centre of the pellet ($r < 2.30\text{ mm}$) than in the outer shell of the pellet ($r > 4.64\text{ mm}$). Even at a penetration depth of about 0.5 mm from the outside of the pellet, this ^{238}U resonance results already in a spectrum dip that is 3 times deeper than the one we observe in the outer shell.

In figure 9.1 we can also observe the effect of burn-up on the neutron spectrum. The thermal part decreases slightly and new resonance dips appear due to the creation of several Pu isotopes. We can for instance observe the creation of spectrum dips due to the ^{239}Pu resonance at 0.296 eV, the ^{240}Pu resonance at 1.056 eV and the ^{242}Pu resonance at 2.670 eV. Furthermore, the filtering effect of these resonances in the fuel pellet is clearly visible (although it is less pronounced than the filtering effect of the ^{238}U resonance at 6.674 eV).

9.6 Absolute plutonium and neodymium content

Figure 9.2 shows the absolute Pu content as a function of slice averaged burn-up and includes all available EPMA data, as well as the value obtained by means of ICP-MS. The ALEPH and TUBRNP calculation is given for sample 12C3 (the red curves) along with the results for different levels of initial enrichment in ^{235}U (2.9 % and 3.8 %). The power history used in the ALEPH calculations for the other enrichments is the same as the one used for 3.5 %.

The concentration of Pu in the analysed fuel is particularly low compared to the total mass of the fuel (the initial heavy metal density is 9.2 g cm^{-3}). At

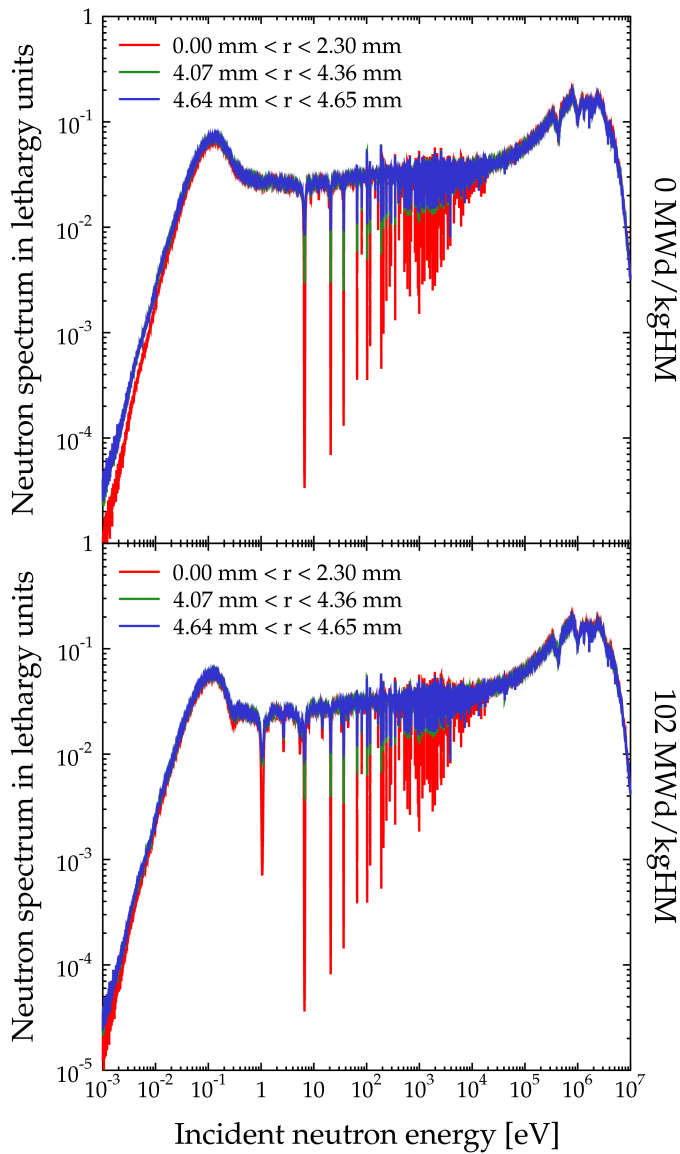


Figure 9.1: Neutron spectra for the 12C3 UO₂ fuel sample at the beginning of the irradiation and after a burn-up of 102 MWd/kgHM for different radial zones in the fuel.

102 MWd/kgHM ALEPH predicts for instance a value of around 0.015 g of Pu per gram of initial U. The various experimental values provided by EPMA have a good overlap with the calculations even though the EPMA measured concentration values are quite dispersed.

For the 12C3 sample (which has the highest burn-up), an ICP-MS value is also included for completeness, and underlines the scatter of the experimental data. This single ICP-MS value confirms the validity of the ALEPH calculation. It should be noted that the ICP-MS value provides a lower value for the Pu content, which might be due to Pu still contained in the residue after the dissolution process.

It appears that the sensitivity of the ALEPH and TUBRNP calculations to the initial enrichment in ^{235}U is low. The TUBRNP curves predict a fast build-up of Pu up to a burn-up of 50 MWd/kgHM. After that, the curves evolve slowly towards a maximum at around 80-90 MWd/kg after which the Pu concentration starts to drop. Such a behaviour is not confirmed by the experimental results, which show an increasing trend. This is probably due to limitations of TUBRNP, mainly the use of only the most abundant Pu isotopes and only two types of reactions, being fission and neutron capture.

In contrast, ALEPH is based on ORIGEN 2.2 which includes over 1000 isotopes (of which ALEPH recalculates 793 nuclides for every burn-up step and zone) with 8 basic nuclear reactions, being fission, neutron capture, ($n,2n$), ($n,3n$), (n,p), (n,α) and production of isomeric states by capture and ($n,2n$). ALEPH therefore predicts the observed increasing trend of Pu production at 100 MWd/kHM quite well.

This also indicates that refinements will be required when applying the TUBRNP model to burn-up above 100 MWd/kgHM. Such refinements may consist of including more isotopes (e.g. ^{238}Pu , ^{235}U and ^{236}U) and/or modifying the one-group effective cross sections with the aid of ALEPH.

As one would expect, Pu builds up faster for a lower enrichment in ^{235}U for low burn-up levels because there is initially more ^{238}U available and because the flux has to be higher to obtain the same burn-up under the same irradiation conditions as the other calculations. When the burn-up increases, the Pu consumption kicks in sooner because there is less fissile ^{235}U available from the start when using a lower enrichment in ^{235}U . This behaviour is also visible with the TUBRNP curves although this effect is more pronounced when compared to the results of ALEPH.

On one hand, all this indicates that ALEPH is adequate for predictions at even higher burn-up, whereas an extension will be required when applying the TUBRNP model to burn-up above 80 MWd/kgHM. It is planned to include more isotopes (e.g. ^{235}U , ^{236}U , ^{238}Pu , etc.) and/or modifying the one-group effective cross sections. On the other hand, in view of the primary objective of TUBRNP to predict only the relative radial profile of the isotopes and in view of the spread of the experimental data, the agreement between measured and calculated values is satisfactory. In fact, the agreement is similar to

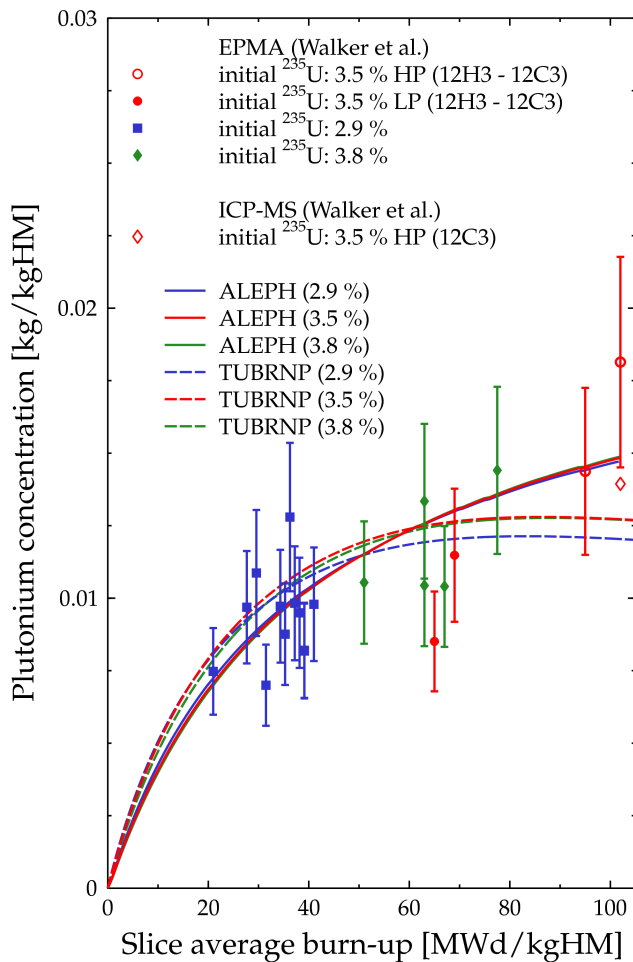


Figure 9.2: The absolute Pu concentration in a PWR UO₂ fuel pin as a function of burn-up as calculated by ALEPH and TUBRNP for different ²³⁵U enrichments (2.9 %, 3.5 % and 3.8 %) compared to EPMA and ICP-MS measurements.

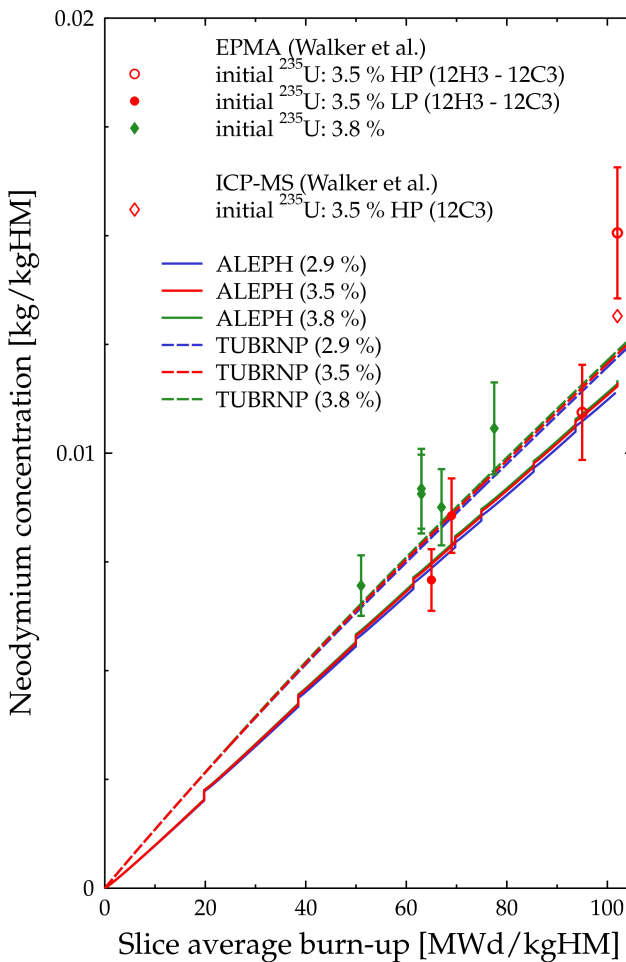


Figure 9.3: The absolute Nd concentration in a PWR UO_2 fuel pin as a function of burn-up as calculated by ALEPH and TUBRNP for different ^{235}U enrichments (2.9 %, 3.5 % and 3.8 %) compared to EPMA and ICP-MS measurements.

that observed previously for burn-ups up to 80 MWd/kgHM [72, 73].

Because burn-up cannot be measured directly, certain fission products that are known to be characterized by a linear behaviour with respect to burn-up are used as “burn-up indicators” (whatever the spectrum conditions may be nearby the sample during the irradiation). Nd isotopes are broadly recognized as accurate burn-up indicators, experimentally determined by radiochemistry.

The correctness of the burn-up predictions is confirmed in figure 9.3, where the Nd content obtained by means of EPMA is compared with the TUBRNP and ALEPH predictions as a function of slice average burn-up. The small “steps” in the ALEPH curve are caused by fission product decay resulting in Nd production during the shut-down period in between the various reactor cycles. Such small steps are also present in the ALEPH Pu curves of figure 9.2 but they are barely visible due to the long half-life of the Pu isotopes.

As was the case with the experimental data for Pu, there appears to be some dispersion of the experimental points (although this is less pronounced as there are fewer points available). Both the EPMA and ICP-MS value at 102 MWd/kgHM appear to be too high compared to the ALEPH prediction although the other Nd points for an initial ^{235}U enrichment of 3.5 % support the slope of the corresponding ALEPH curve.

The Nd points for an initial ^{235}U enrichment of 3.8 % all lie above the corresponding ALEPH curve. To calculate this curve we have used the irradiation history of the 12C3 sample because we had no other data available. Longer shutdown periods could for instance result in a higher Nd content. The deviation of the experimental results can be attributed to this fact and the relative uncertainty on the EPMA measurements.

9.7 Radial plutonium and burn-up profiles

The radial Pu and burn-up profiles are plotted in figures 9.4 to 9.7, showing very similar results calculated by ALEPH and TRANSURANUS. Although we only calculated the 12C3 sample for a burn-up of 102 MWd/kg, we also included a comparison with the radial profiles of the 12H3 samples. There is good agreement of the calculated profiles with the EPMA measurements, except for the Pu profiles of the 12H3 sample which exhibit large fluctuations. These fluctuations do not appear in the Pu profiles of the 12C3 sample, although some minor fluctuations can still be discerned. Furthermore, no experimental errors are available for these radial profiles.

Despite assumptions on the irradiation history and irradiation conditions that had to be made for the ALEPH computations, the radial profiles are well predicted even with the simple geometrical model used. A sensitivity study of the irradiation history has been carried out with ALEPH and revealed no significant differences in our results. This sensitivity study included the absolute Pu and Nd content. Slight variations in the irradiation history or even sim-

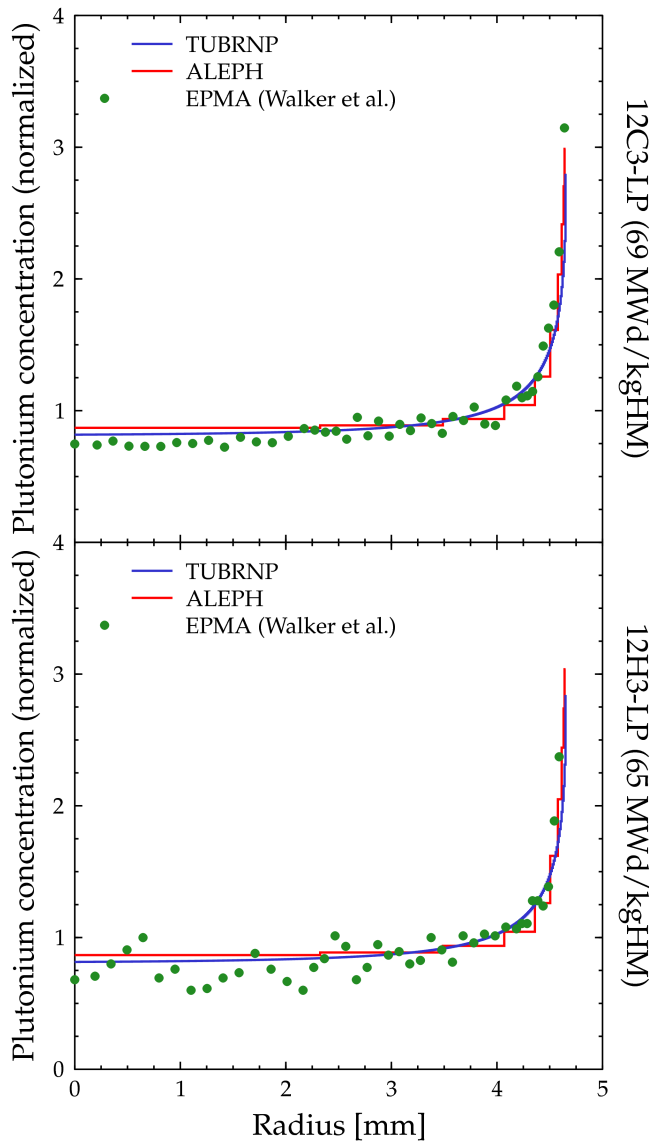


Figure 9.4: The radial Pu profiles for the low power samples of the 12C3 and 12H3 fuel pin for burn-up levels of 69 MWd/kgHM and 65 MWd/kgHM.

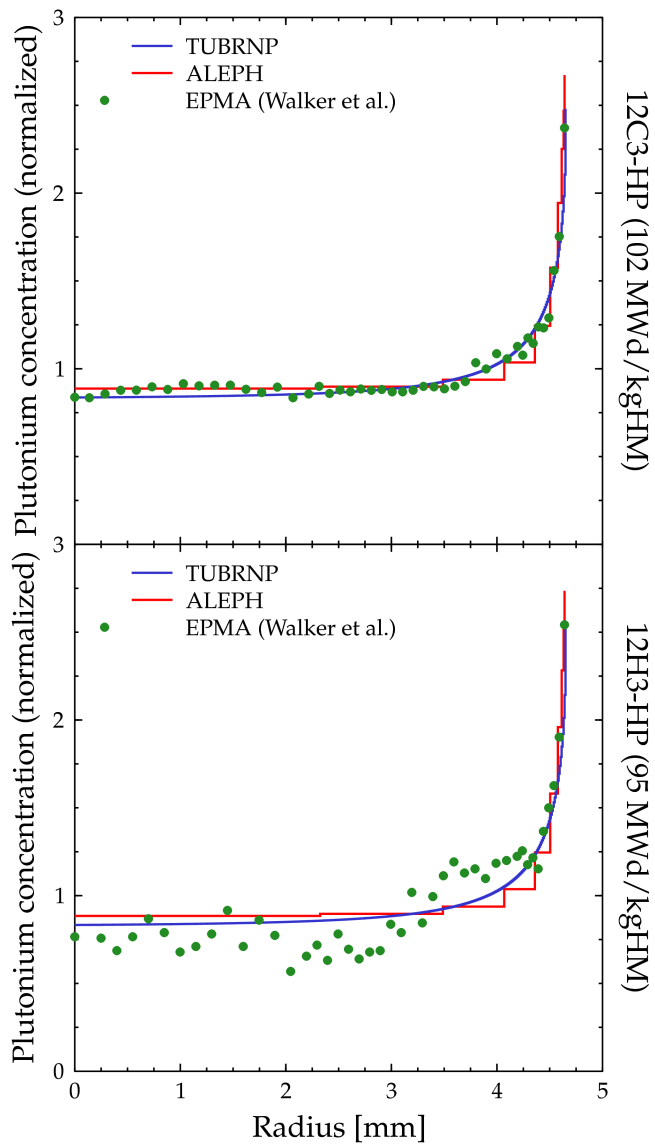


Figure 9.5: The radial Pu profiles for the high power samples of the 12C3 and 12H3 fuel pin for burn-up levels of 102 MWd/kgHM and 65 MWd/kgHM.

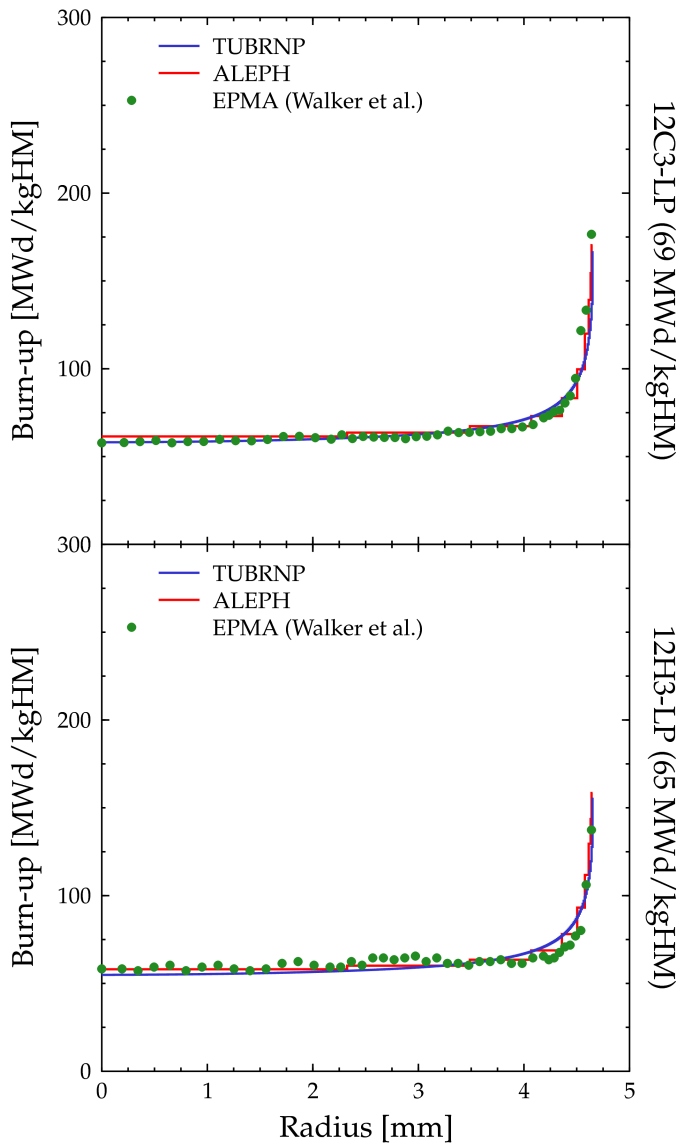


Figure 9.6: The radial Nd profiles for the low power samples of the $^{12}\text{C}_3$ and $^{12}\text{H}_3$ fuel pin for burn-up levels of 69 MWd/kgHM and 65 MWd/kgHM .

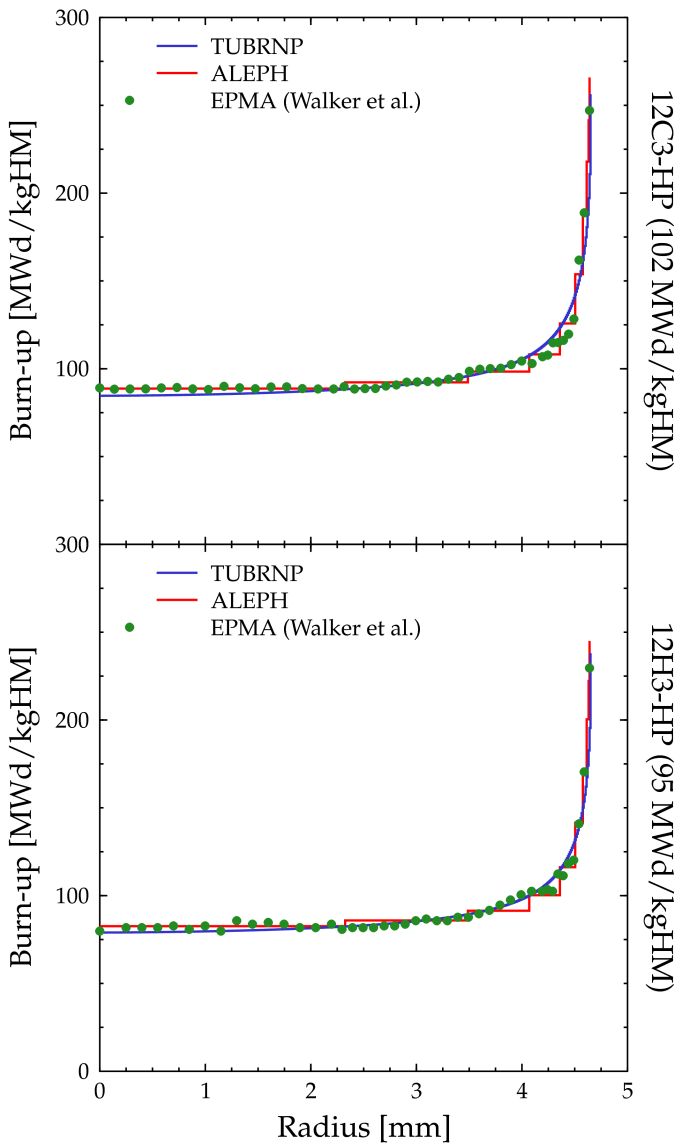


Figure 9.7: The radial Nd profiles for the high power samples of the 12C3 and 12H3 fuel pin for burn-up levels of 102 MWd/kgHM and 65 MWd/kgHM.

plifications (by using an overall average power level for the entire irradiation history) resulted in very similar radial profiles.

We can therefore conclude that the normalised radial distributions of both Pu and Nd are dependent on the final burn-up, but that they are rather independent on how the burn-up was accumulated. This observation is consistent with previous analyses of radial Pu profiles at lower burn-up [72, 73] which also show a good agreement between calculation and experiment despite the independence of TUBRNP on the path of burn-up accumulation.

The test of all knowledge is experiment.

Richard P. Feynman (1918 - 1988)

10

The MALIBU experimental data

10.1 The MALIBU program

The MALIBU International Program was launched in June 2003 as a collaboration between nuclear research centres, nuclear industry, nuclear regulatory bodies and electrical utilities from 6 different countries (Belgium, France, Germany, Japan, Switzerland and the United States). The program was supposed to run from 2003 through 2006 but in 2006 it was decided to extend the program and to add an additional partner from Sweden.

The major objective of the MALIBU program is to provide an experimental determination of the isotopic inventory of spent fuel, which is of major importance for numerous applications such as:

- the definition of basic licensing data for UO₂ and MOX fuels (for both PWR and BWR reactors) which necessitates the prediction of the fuel isotopic composition at various steps of the irradiation cycles and at the end of life
- the criticality licensing for transportation, storage and reprocessing of spent fuel based on burn-up credit because the current increase of fuel enrichment for power reactors may require re-evaluation of licenses
- the calibration and benchmarking of source term codes
- safeguards issues
- fundamental research programs on actinides

The project focuses on two aspects. First of all, it provides a large set of experimental data on irradiated fuel. There is a large number of samples and a large selection of measured isotopes (including major and minor actinides, burn-up indicators, long-lived fission products, etc.). Some of these are even measured in very low concentration. The second aspect of this program is

to confer on these data a minimized and reliable uncertainty level by cross-checking the results obtained on selected samples between different laboratories using similar or different high performance techniques.

To fulfil these objectives, the project is centred around four axes:

- the selection of suitable UO₂ and MOX fuel samples irradiated in commercial light water reactors (LWR)
- the selection of laboratories performing routine radiochemical measurements after fuel dissolution, each according to its own procedures of fuel analysis. Radiochemistry departments of SCK•CEN (Belgium), PSI (Switzerland), CEA (France) and Studsvik (Sweden) were selected for the MALIBU program. This selection is based on the past experience of these laboratories in radiochemistry, on the on-site availability of fuel and on the wish of these laboratories to be involved in the MALIBU cross-check exercise
- the exchange between laboratories of solid samples submitted to a common program of measurements
- to provide neutronic characterization of the selected fuel samples, including a detailed power history and macro-cell description allowing to generate accurate cross-sections for source term and burn-up codes

The fuel samples selected for the MALIBU program include four PWR and six BWR samples, most of them either duplicated or triplicated in order to allow radiochemical analysis (and thus cross-check) by different laboratories.

The axial positioning of the samples in the selected mother fuel rods are performed on the basis of ¹³⁷Cs gamma spectrometry measurements over the rod length. The BWR fuel samples are cut from different axial zones in order to analyse the local void effects on radionuclide productions. Each individual sample includes three pellets, cut from mid-to-mid pellet in order to avoid measurement bias resulting from volatile fission product migration.

10.2 Calculating the GGU2 fuel sample

10.2.1 Modelling a PWR fuel assembly

The sample chosen for this work is the PWR UO₂ sample designated GGU2 with a burn-up of around 47 MWd/kgHM. This sample comes from the lower part of a fuel pin from a 15×15 fuel assembly that was irradiated in a commercial PWR at Gösgen (Switzerland) between 1997 and 2001 during 4 cycles.

In order to properly simulate the evolution of the fuel, it is imperative to have complete and detailed data on both geometry, irradiation conditions and measurements. The fuel assembly dimensions and characteristics (guide tube

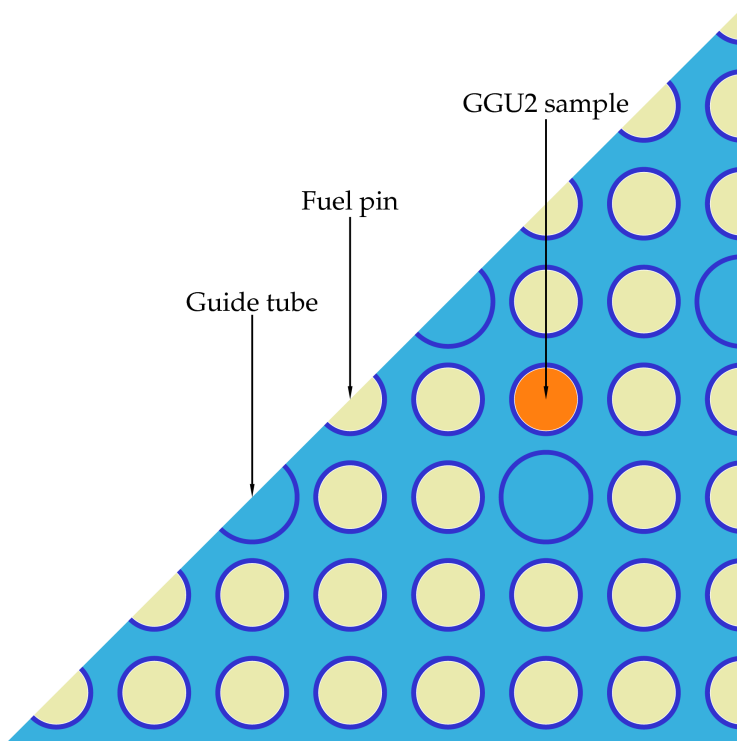


Figure 10.1: The 1/8 PWR 15×15 fuel assembly with reflective boundary conditions (taking into account the assembly pitch) used by ALEPH to model the irradiation of the GGU2 fuel sample.

and fuel pin dimensions, material compositions and densities, etc.) must for instance be well known and accessible in an easy format. On the other hand, the irradiation history and conditions must be as detailed as possible (shutdown periods, neighbouring assemblies, etc.). All of this data is provided in the MALIBU irradiation data reports [81].

For this work, we modelled 1/8 of the fuel assembly containing the GGU2 sample in 2D (see figure 10.1), which is a common way of modelling PWR assemblies in deterministic codes. Every pin is modelled separately so we will use 32 burn-up zones.

The water moderator in this model contains an average boron concentration (although a time dependent boron concentration is specified in the irradiation report). The moderator and fuel pin cladding temperatures are set to 600 K and the fuel temperature at 900 K.

The irradiation history for the GGU2 fuel sample was subdivided into steps of 1 MWd/kgHM for a total of 50 steps (including the shut-down periods in between the different cycles). For comparison with the experimental results, we performed decay steps to the measurement day, taking into account separation of certain elements from others (like for instance the separation of Pu, Am and Cm).

As we did for the high burn-up calculations in chapter 9 we have calculated the GGU2 sample using a combination of the JEFF 3.1 evaluated nuclear data library supplemented with the JEFF 3.0A activation data library. ALEPH effectively calculates cross sections for 793 different nuclides for use in ORIGEN 2.2 for every burn-up zone and every time step in the burn-up calculation. A separate calculation with the older JEF 2.2 nuclear data library was performed as well to assess the improvements made over the years in the European nuclear data libraries. The relative difference with the experimental values (as measured at SCK•CEN) can be found in figure 10.2. The grey area in this figure represents the experimental uncertainty.

10.2.2 Burn-up indicators

Before looking to any other nuclide, it is always interesting to look at the prediction of a burn-up indicator like Nd. In the case of the GGU2 sample, the compositions of seven Nd isotopes were analysed. For our JEFF 3.1 calculation, five of these are predicted within 1 % of the experimental value. Only for ^{142}Nd do we observe a large underestimation of around 15 %. It should be noted that the cumulative fission yield for ^{142}Nd is actually 9 orders of magnitude lower than for instance ^{148}Nd (which is the most important burn-up indicator) and that the error on this value is of the order of 25 % (as given in JEFF 3.1). The observed deviation of ^{142}Nd might therefore be attributed to the fission yields in the ORIGEN libraries.

Some of these Nd isotopes are underestimated while the others are overestimated by approximately the same amount. This error spread for the entire set of Nd isotopes (excluding ^{142}Nd due to its large error) seems to indicate that there is no systematic error on the irradiation history. If the errors had all been positive or negative, we would have to adjust the irradiation history in order to minimise the error on these burn-up indicators. This is a common practice in depletion calculations but it does not appear to be necessary in this case.

This is also the case for the results using the JEF 2.2 nuclear data library, although the individual relative errors on the Nd isotopes are larger (about 2 to 3 %) than with the JEFF 3.1 library. These differences are however caused by differences in the actinide cross sections data (which cause different fission rates). The Nd cross section data included in JEFF 3.1 is exactly the same as those in JEF 2.2, with the exception of ^{143}Nd . This difference in ^{143}Nd is limited to an increase of 4 % of the $1/v$ part of the neutron capture cross section.

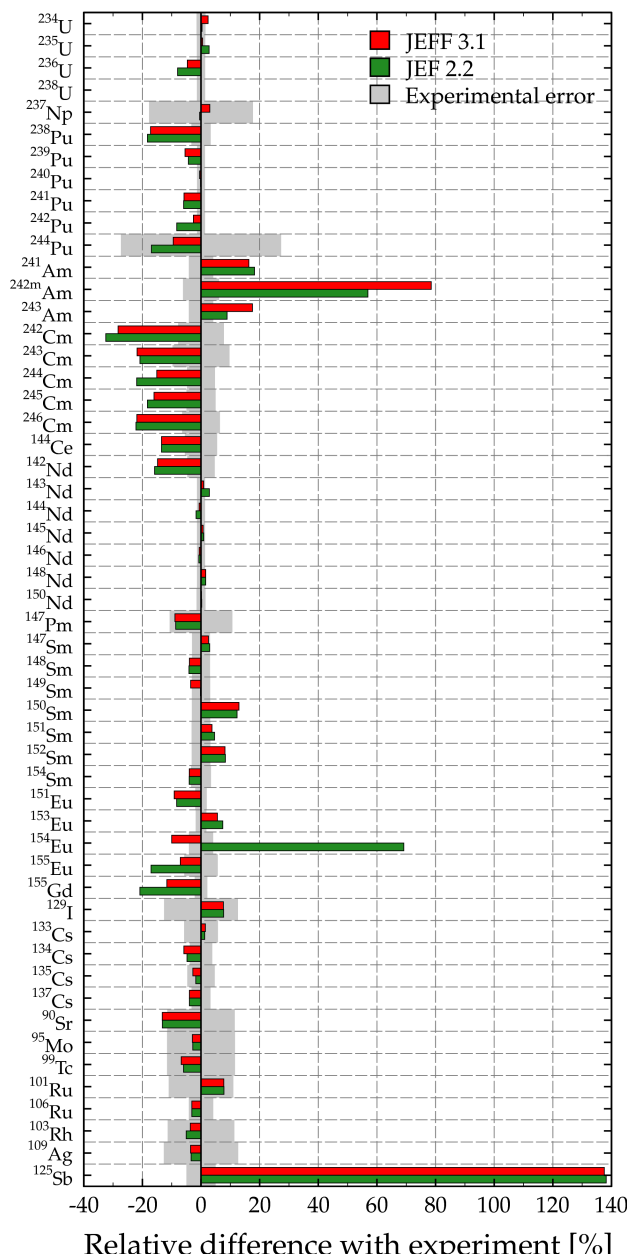


Figure 10.2: The relative difference with the experimental values for JEFF 3.1 and JEF 2.2 calculations on the GGU2 PWR UO_2 fuel sample.

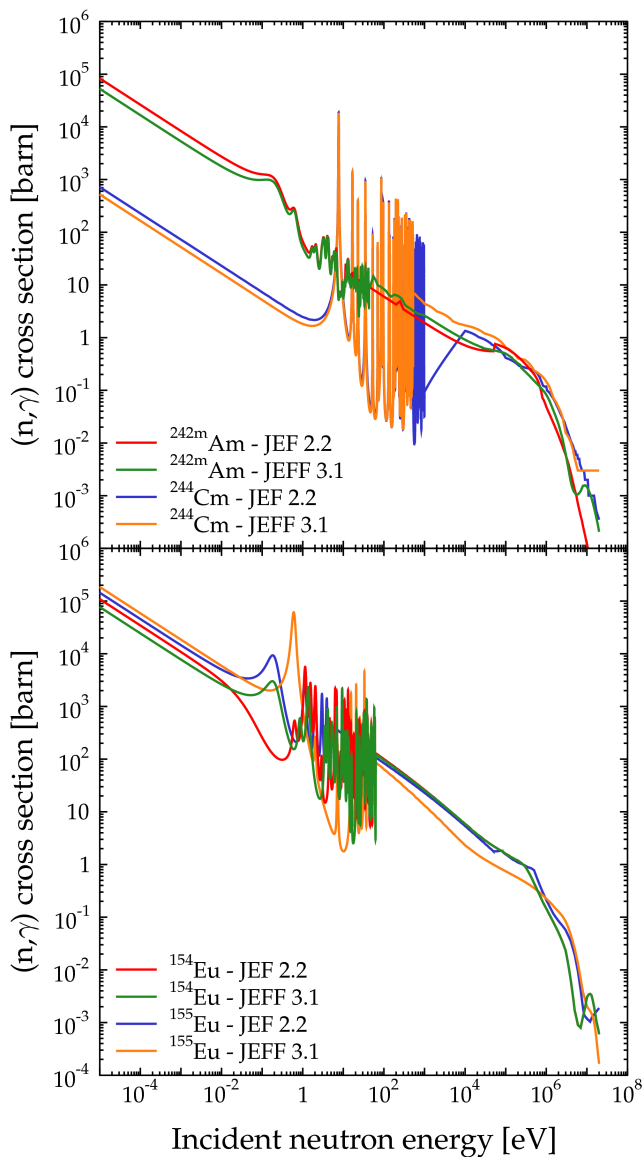


Figure 10.3: Microscopic (n,γ) cross sections for ^{242m}Am , ^{244}Cm , ^{154}Eu and ^{155}Eu from JEFF 3.1 and JEF 2.2 as used for the GGU2 PWR UO₂ fuel sample calculations.

10.2.3 Actinides

The compositions for 18 different actinides were analysed for the GGU2 sample. The U isotopes (except ^{236}U) and ^{237}Np are estimated within 3 % (using both JEFF 3.1 and JEF 2.2 nuclear data). The ^{235}U content is particularly well estimated with JEFF 3.1 (the difference is only 0.5 %). The only issue for these nuclides is ^{236}U which is underestimated by respectively by 5 and 8 % in the JEFF 3.1 and JEF 2.2 calculations.

The JEFF 3.1 and JEF 2.2 calculations also seem to give similar results on the Pu isotopes, although the ^{242}Pu and ^{244}Pu estimate with JEFF 3.1 appears to be a lot better than the one obtained with JEF 2.2. Except for ^{238}Pu and ^{244}Pu , all Pu isotopes are estimated within 6 % from the experimental value by JEFF 3.1. The ^{244}Pu content in the sample is actually very small (about 20000 times smaller than ^{242}Pu) but it is still predicted within 10 %. Furthermore, all Pu isotopes are all underestimated, contrary to the U isotopes.

The largest deviations in the actinide results can be found in the Am isotopes. With JEFF 3.1 data, ^{241}Am and ^{243}Am are overestimated by maximum 17.5 % while this is 78.5 % for $^{242\text{m}}\text{Am}$. The Cm isotopes on the other hand are all underestimated by 15 to 22 %.

Compared with JEFF 3.1, JEF 2.2 performs better on the Am isotopes but not on the Cm isotopes. This is due to the Am and Cm cross sections in these two nuclear data libraries. The $^{242\text{m}}\text{Am}$ and ^{244}Cm neutron capture cross sections are shown in figure 10.3. The $1/v$ part of the cross section for both isotopes is about 10 % higher in JEF 2.2 than in JEFF 3.1. This results in an increased production of ^{243}Am with JEF 2.2 (as we can see in the GGU2 results) so that ultimately a larger quantity of the higher Cm isotopes will be produced. Because the ^{244}Cm neutron capture cross section is also higher it would seem that more ^{244}Cm is lost by neutron capture than what is actually gained due to increased neutron capture in $^{242\text{m}}\text{Am}$ and ^{243}Am .

Finding the cause of some of the large deviations or systematic deviations in these results (like the overestimation of Am and underestimation of Cm) is not an easy task. Figure 10.4 represents the actinide evolution chains that are dominant in thermal reactions. Although other neutron induced reactions like $(n,3n)$, (n,p) , etc. will also occur in a thermal reactor, only neutron capture and the $(n,2n)$ reaction are included in this figure.

Decay events with a half-life longer than 500 years are also not included because we are only interested in the short term sensitivity (the nuclides are measured only a few years after the end of the irradiation). This simplified overview of the evolution chains already exhibits a lot of cyclic chains so that a variation in the content of one nuclide will ultimately influence all the others.

Take for instance the ^{238}Pu content which is underestimated by ALEPH by 17.2 %, which is rather bad compared to the other U and Pu isotopes. Furthermore, the other Pu isotopes (except ^{240}Pu) are underestimated by 2-6 %, which can be due to an underestimation of the Pu neutron capture chain that starts

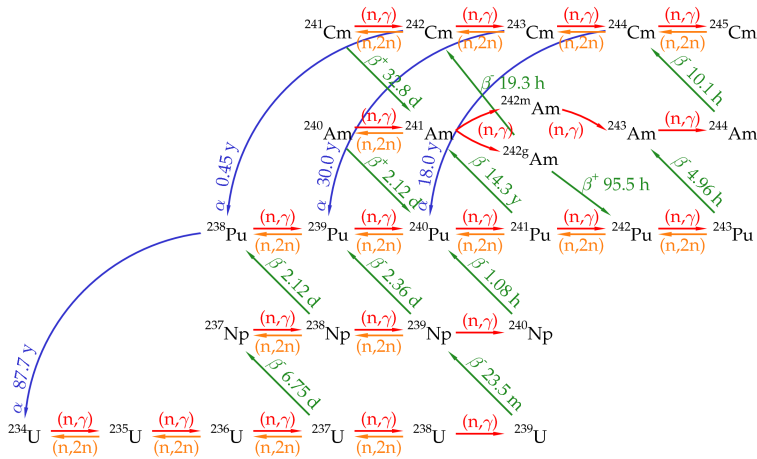


Figure 10.4: The short term dominant actinide evolution chains in a thermal reactor.

with ^{238}Pu (although the chain starting with ^{239}Pu produced from ^{238}U will be more important). An improvement of the result for ^{238}Pu will therefore also yield slightly better results for the other Pu isotopes.

As we can see in figure 10.4, ^{238}Pu is created primarily through successive neutron capture on U isotopes (like ^{234}U and ^{235}U) up to ^{237}U which decays to ^{237}Np . With neutron capture, this is transformed into ^{238}Np which in turn decays to ^{238}Pu . In this production path, it will ultimately be the cross sections of ^{235}U , ^{236}U and ^{237}Np that determine the accuracy of the ^{238}Pu production.

It has already been shown [82] that the thermal ^{237}Np (n, γ) cross section is most likely 10 % too low. An increase of this cross section will result in a decrease in ^{237}Np , an increased production of ^{238}Np and therefore in an increase of ^{238}Pu .

This is supported by our calculations where we observe an overestimation of ^{237}Np by about 3 % which could be caused by a low ^{237}Np (n, γ) cross section. This could also be due to an overproduction of ^{237}U , which is supported by the underestimation of ^{236}U that we observe in the GGU2 sample. As we will show in section 10.3.1, the ^{236}U data (or at least the fission data of this nuclide) is definitely in need of a major revision.

Another important path of ^{238}Pu production is the the α -decay of ^{242}Cm . The primary source of ^{242}Cm is β^- -decay of ^{242}gAm which is created through neutron capture on ^{241}Am . This brings us to another issue in our GGU2 results, being the large overestimation of ^{242}mAm which is most likely due to the ^{241}Am (n, γ) branching ratio to the ground state of ^{242}Am . In section 10.3.2 we will determine the sensitivity of our results due to this branching ratio.

10.2.4 Fission products

A total of 34 fission products (including the Nd isotopes from section 10.2.2) were analysed for the GGU2 sample. We should note here that the direct fission yields are extremely important to get the fission products right. In the case of ALEPH, we use the yields as given in the original ORIGEN library. As a result, the differences between JEFF 3.1 and JEF 2.2 are only caused by differences in the cross sections of the actinides and fission products. In general, we can say that with JEFF 3.1 all fission products (except ^{125}Sb) are predicted within 15 % of the experimental value.

All Sm fission products (except ^{150}Sm and ^{152}Sm) are predicted within 5 %. Because the Sm cross section data in JEFF 3.1 (except for ^{149}Sm) was taken over from JEF 2.2 we observe little difference between both data sets (as was the case with the Nd burn-up indicators). Compared with JEF 2.2, the $1/v$ part of the neutron capture cross section of ^{149}Sm in JEFF 3.1 was increased by about 3 % which results in a 3 % improvement in the prediction of the ^{149}Sm content.

Another set of important fission products are Eu and Gd. Contrary to the results for Sm, we observe large differences between JEFF 3.1 and JEF 2.2, especially for ^{154}Eu , ^{155}Eu and ^{155}Gd . This is only due to changes in the Eu cross sections because no changes were made to the Gd cross sections in JEFF 3.1 compared to JEF 2.2 (except for the addition of ^{152}Gd from JENDL 3.2).

The changes in the Eu cross sections came from two sources: JENDL 3.2 (with some minor revisions) for ^{152}Eu and ^{153}Eu and ENDF/B-VI.7 for ^{154}Eu and ^{155}Eu . The neutron capture cross sections of these last two nuclides can be found in figure 10.3.

We see that they are very different from each other, even the resonances are different. These radical changes in the cross section data has significantly improved the Eu predictions, and especially for ^{154}Eu for which JEF 2.2 gives us an overestimation of 70 %. With JEFF 3.1 this is reduced to an underestimation of 10 %. With these in the Eu compositons, the underestimation of 21 % by JEFF 2.2 for ^{155}Gd is reduced to 12 % in JEFF 3.1.

The only remaining issue in these results is the ^{125}Sb content which is overestimated by 138 %. Calculations using the older ARIANE data (the predecessor of the MALIBU program) which dates back to the early '90s lead to large overestimations for most metallic fission products [83, 84].

At the time, this was attributed to possible problems with the dissolution of those metallic fission products. During the 10 years that passed since the end of the ARIANE program and the start of the measurements for the MALIBU program, a lot of progress in measurement techniques in radiochemistry was made. And this is entirely reflected in our results for the GGU2 fuel sample. All metallic fission products are predicted within 15 % except for ^{125}Sb .

The severe overestimation of ^{125}Sb by 138 % is most likely a cross section problem, and not the result of other experimental issues. A review of relevant

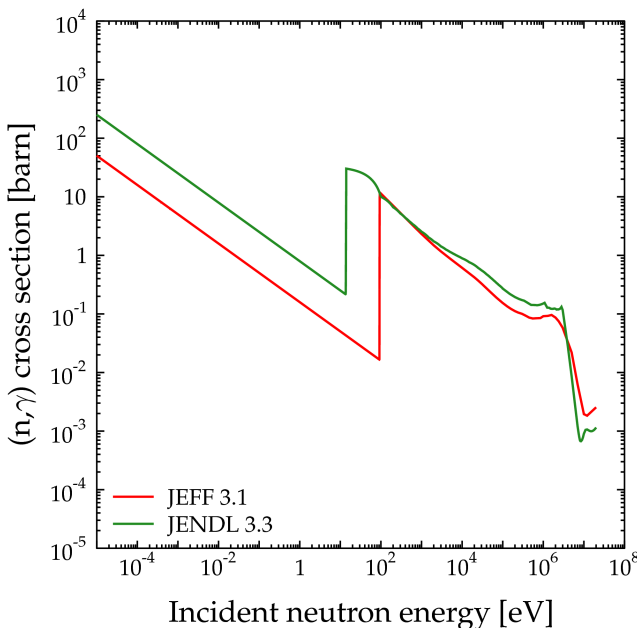


Figure 10.5: The ^{125}Sb neutron capture cross section from the JEFF 3.1 and JENDL 3.3 nuclear data libraries.

cross section data showed that there exist two different evaluations in the case of ^{125}Sb . The first being an old ENDF/B-V evaluation which is used in JEF 2.2, JEFF 3.0, JEFF 3.1 and ENDF/B-VI.8 and a second more recent evaluation prepared for JENDL 3 which will be adopted in ENDF/B-VII. The neutron capture cross sections for these two different evaluations are shown in figure 10.5. The difference between both evaluations in the $1/v$ component of this cross section is a factor 5 while the cross section values above 100 eV are rather similar for both evaluations. The cross section jump at 10 eV for the JENDL evaluation and 100 eV for the JEFF 3.1 evaluation also indicates a more fundamental problem, namely the lack of experimental cross section and resonance data with which a proper cross section can be constructed. There is also no experimental data for ^{125}Sb available in EXFOR, which is the database used to collect experimental data and their associated bibliographical references [85].

No other major differences between JEFF 3.1 and JEF 2.2 can be discerned for the remaining fission products. This is mainly due to the fact that the cross section data of most of these fission products in JEFF 3.1 and JEF 2.2 is the same. Only the data for ^{133}Cs , ^{129}I , ^{95}Mo , ^{99}Tc and ^{103}Rh are different but they do not significantly change the results.

10.3 Sensitivity to nuclear data

10.3.1 The ^{236}U fission cross section

We have come a long way since the discovery of the neutron in 1932 by James Chadwick and one might therefore think that the cross sections of “basic” nuclides like ^{234}U , ^{235}U , ^{236}U and ^{238}U are already quite well known. Unfortunately, this is not always the case. Experimental data on the ^{236}U fission cross section is for instance very scarce. For thermal neutrons, only one recent measurement by Wagemans et al. for this value is available (0.3 ± 1 mbarn) [86] and for the fission resonances there are conflicting measurements by Theobald et al. [87] and Parker et al. [88]. This has lead to large discrepancies in ^{236}U evaluated fission data. For instance, the JEF 2.2 thermal fission cross section is 46.8 mbarn while this is 61.3 mbarn for JEFF 3.1 and 47.3 mbarn for the latest ENDF/B-VII b3 ^{236}U evaluation. These values are at least two orders of magnitude larger than the reported experimental value.

Recent measurements of the resonance region in the ^{236}U fission cross section at the GELINA facility of IRMM (Belgium) and the nTOF facility of CERN (Switzerland) [89] have resolved this issue. The dominant ^{236}U fission resonance lies at 5.45 eV and the next resonance only occurs at around 1.3 keV. The resonances in between these two energies reported by Theobald et al. [87] (which are adopted by all nuclear data evaluations up to this day) are not due to fission but correspond to (n,γ) resonances erroneously identified as fission resonances.

The thermal fission cross section measurement of 0.3 ± 1 mbarn and the new resonance measurements by Wagemans et al. [89] are now a coherent set of data and should be adopted in future nuclear data evaluations. Figure 10.6 shows this data set compared to the ^{236}U fission cross section from the JEF 2.2 and JEFF 3.1 nuclear data libraries.

Adopting this new data set will decrease the importance of fission in ^{236}U significantly. With the JEFF 3.1 ^{236}U evaluation, fission accounts for about 5 % of all absorptions in ^{236}U at the beginning of the irradiation for the GGU2 sample. With the new data, this will be reduced to a fraction of that value which will in turn reduce the underestimation of ^{236}U that we observed for the GGU2 sample because less ^{236}U will be fissioned.

To assess the influence ^{236}U fission data on depletion calculations, we performed a calculation on the GGU2 sample using the JEFF 3.1 evaluation from which all references to fission were removed (this includes resonance widths, background cross sections and angular and energy distributions). The impact on the heavy metal isotopes can be found in figure 10.7.

We observe that the actual influence on the ^{236}U content itself is quite small. The initial underestimation of 4.7 % is reduced by only 0.4 %. The change in ^{237}Np and ^{238}Pu is however more significant. The ^{237}Np overestimation increases by 1.4 % to almost 4.4 %. This increased overestimation of

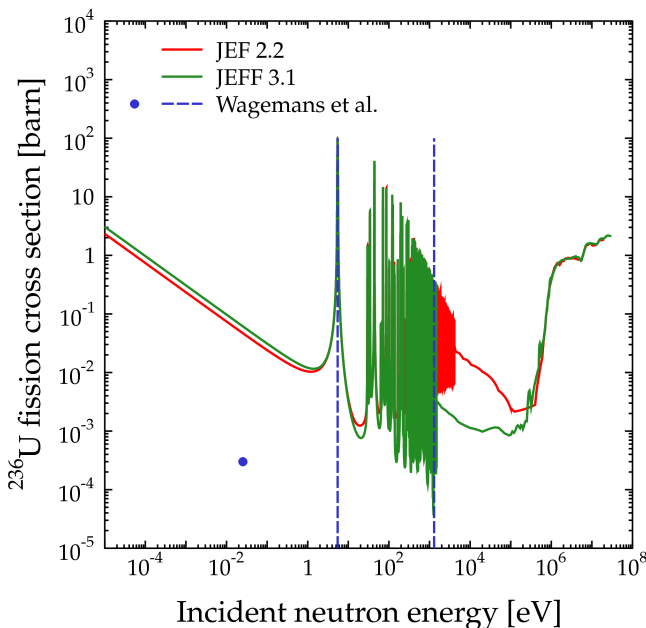


Figure 10.6: The ^{236}U fission cross section from the JEF 2.2 and JEFF 3.1 nuclear data libraries compared to the experimental thermal fission cross section and the positions of the first two fission resonance at 5.45 eV and 1.3 keV [86, 89].

^{237}Np supports the conclusion of a low $^{237}\text{Np}(\text{n},\gamma)$ cross section. The under-prediction of the ^{238}Pu content is improved by 0.8 % from 17.2 % to 16.4 %. The relative difference with the experimental values for the other Pu isotopes also changes favorably due to the neutron capture chain that starts with ^{238}Pu , although the impact is small (about 0.2 % improvement for all Pu isotopes except ^{244}Pu).

We can thus conclude that major revisions in the ^{236}U evaluation and some minor revisions in the ^{237}Np evaluation will significantly improve the predictions of actinide build-up in thermal reactors.

10.3.2 The $^{241}\text{Am}(\text{n},\gamma)$ branching ratio to ^{242g}Am

^{242}Am in the ground state has a half-life of 16 hours and will therefore decay almost immediately to ^{242}Cm (with a half-life of 163 days) via β^- -decay and then to ^{238}Pu via α -decay whereas ^{242m}Am can be transmuted into higher americium isotopes like, for instance, ^{243}Am (with a half-life of 7400 years)

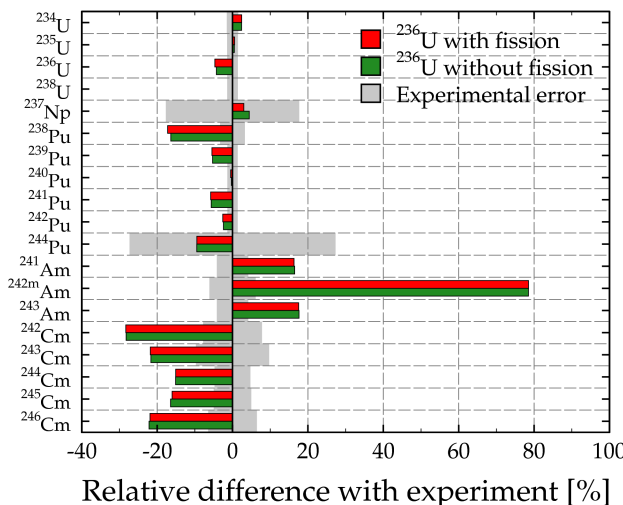


Figure 10.7: The relative difference with the experimental values for the heavy metal isotopes when using ^{236}U data with and without fission.

and to ^{244}Cm . The branching ratio of the ^{241}Am (n,γ) reaction to ^{242}gAm is therefore of great importance for the prediction of Am and Cm in spent fuel.

The ORIGEN library used as a basis for the ALEPH calculations in our JEFF 3.1 reference calculation has set this branching ratio to 0.80. 20 % of all neutron capture on ^{241}Am will thus result in the creation of ^{242}mAm . Due to the overestimation by 78.5 % of the ^{242}mAm content in the sample, we must conclude that the value of 0.80 is too low for this branching ratio.

By using the spectrum in the GGU2 fuel pin and data from file 9 of the JEFF 3.1 ^{241}Am evaluation as described in section 6.4, we found that the initial value should be 0.845 instead of 0.80. The direct production of ^{242}mAm from ^{241}Am is reduced by 25 %. Furthermore, we already saw that the branching ratio toward the ground state for a Pu dominated spectrum was approximately 0.865 (see table 6.3). We can therefore expect an increase of the branching ratio as a function of burn-up. Because ALEPH is as yet not capable of simulating burn-up dependent isomeric production ratios we have performed two calculations in which we set the branching ratio value to 0.845 and 0.865. The influence on the heavy metal isotopes due to a change of the ^{241}Am branching ratio to ^{242}mAm can be found in figure 10.8.

We observe that the influence is significant for ^{242}mAm and the lower Cm isotopes (^{242}Cm and ^{243}Cm). The initial ^{242}mAm overestimation is respectively reduced to 38.3 and 20.6 % for a value of 0.845 and 0.865. When a burn-up dependent branching ratio treatment is implemented into ALEPH the overes-

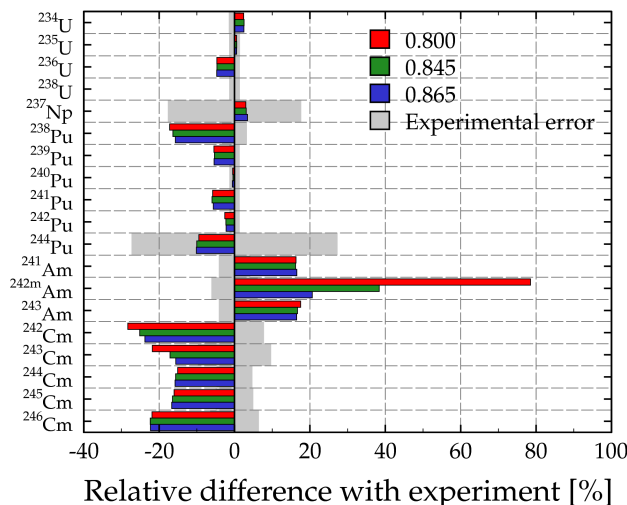


Figure 10.8: The relative difference with the experimental values for the heavy metal isotopes for different values of the ^{241}Am (n,γ) branching ratio to $^{242}\text{g Am}$.

timation will most likely be found in between these two values.

The underestimation of ^{242}Cm and ^{243}Cm is reduced by at least 3 to 5 % because more $^{242}\text{g Am}$ is produced. This also effects the ^{238}Pu in where we observe an improvement of 1 to 1.5 %. Because α -decay from ^{238}Pu to ^{234}U creates a cyclic chain, the increase in ^{238}Pu ultimately effects the ^{237}Np overestimation which increases by a maximum of 0.5 %. On the other hand, the underestimation of the higher Cm content increases slightly simply because less $^{242\text{m}}\text{Am}$ is transmuted to those isotopes.

The example of the sensitivity to ^{236}U fission data and the influence of the ^{241}Am branching ratio illustrates the complexity of depletion calculations and that a problem in predictions cannot be attributed to a single issue. In many cases like the ^{238}Pu content, there is no easy fix so it will be a combination of small effects that will resolve the problem. And as always, the importance of nuclear data cannot be ignored even for “well known” nuclides like U, Np and Pu.

10.4 Sensitivity to modelling effects

In our previous calculations, we have chosen to model every pin separately without any radial zones thus neglecting spectral effects due to spatial self-

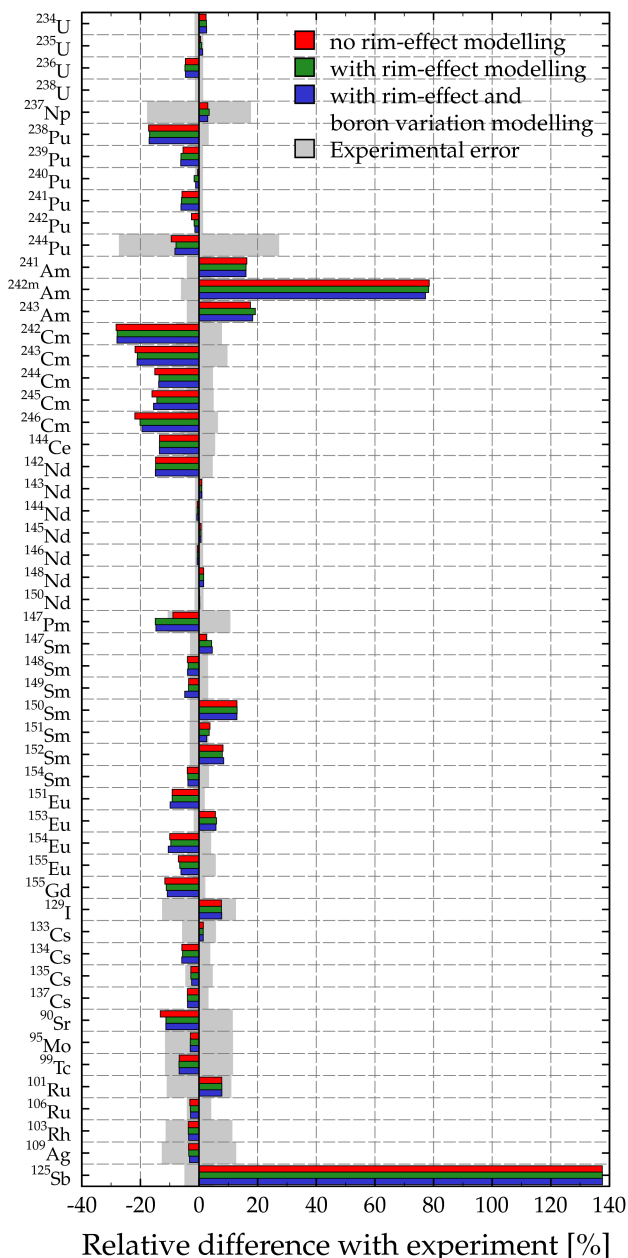


Figure 10.9: The influence of spatial self-shielding and the variation of the boron concentration for the GGU2 PWR UO_2 fuel sample.

shielding in the fuel pins. Furthermore, we assumed an average boron concentration for every cycle.

To assess the influence of spectral changes due to spatial self-shielding, we have divided every pin into 5 radial zones (bringing the total number of burn-up zones and materials to 160) using the same dichotomic procedure as described in section 9.3. In a second calculation, we combined this with the evolution of the boron concentration in the coolant. This boron variation was modelled in discrete steps by adjusting the boron concentration at the beginning of every burn-up step.

Figure 10.9 gives the influence of these modelling effects on our GGU2 sample calculations. In general, this influence is quite small and definitely not as severe as for instance the ^{241}Am (n,γ) branching ratio to ^{242g}Am . In most cases, the influence is less than 1 % with some exceptions like for instance ^{147}Pm (the underestimation increases by 7 %) and ^{146}Cm (the underestimation decreases by 2.5 %).

These modelling effects do not seem to add a global improvement on our results. In some cases the difference with the experimental results are reduced while it increases in other cases. We can therefore conclude that spatial self-shielding and the variation of the boron concentration are of secondary importance next to the sensitivity due to nuclear data. Major improvements in the prediction of spent fuel compositions will therefore be achieved by improving the quality of nuclear data in general and the treatment of this data in depletion codes. Validation experiments like spent fuel characterisation in the MALIBU program are imperative to this effort because they help in identifying potential problem areas, as we have demonstrated in this chapter with the GGU2 fuel sample.

*The only way to discover the limits of the possible
is to try the impossible.*

Arthur C. Clark (1917 - ...)



Control plate movement in the High Flux Isotope Reactor

11.1 Description of the HFIR

As indicated earlier, ALEPH has the capability of using surface transformations to simulate changes in geometry during the irradiation which would allow a user to simulate the movement of control rods or control plates. This capability has been tested on evolution calculations for cycle 400 of the High Flux Isotope Reactor (HFIR) of ORNL in collaboration with Dr. Ned Xoubi and Mr. Trent Primm of ORNL [90].

We performed a number of ALEPH calculations using different sets of nuclear data and with different levels of precision for a single cycle of the HFIR reactor. The main purpose was to evaluate the evolution of the effective multiplication factor k_{eff} and some critical nuclides from day to day during the cycle. As part of the collaboration, an equivalent MONTEBURNS calculation was performed on the same core.

The HFIR is a multi-purpose isotope production and test reactor with a rated power of 100 MW and is currently operated at 85 MW. The average operating cycle at a power level of 85 MW varies between 22 and 24 days, depending on the quantity and type of material that is being irradiated. The HFIR has the world's highest thermal flux ($2.6 \cdot 10^{15} \text{ n cm}^{-2} \text{ s}^{-1}$), making it a one-of-a-kind facility.

The HFIR is a pressurized light-water cooled and moderated flux-trap type reactor using highly enriched ^{235}U fuel. The reactor core consists of two concentric annular regions, each approximately 61 cm high. The centre of the core is the flux trap, which is a 12.7 cm cylindrical hole containing 37 experimental target positions. The flux trap is surrounded by two concentric fuel elements (consisting of involute shaped fuel plates) separated by a water region.

The flux trap has a total of 37 experimental positions (31 sites located in the interior of the basket and 6 sites on the periphery of the basket). The target region was specifically designed for rods containing ^{242}Pu as target material

for producing Cf. Later, sufficient quantities of Cm became available for use as target material. One location contains a rabbit system (a hydraulic tube allowing for the insertion of specimens while the reactor is operating). When Cf production targets are not present in the central target region, these locations are occupied by aluminium dummy targets. These can be either solid aluminium rods filling the region intended to be occupied by the Cf production targets or shrouded aluminium rods. The shrouded rods contain a small diameter core and are vented to allow water ingress to the region between the core and shroud.

The inner fuel element contains 171 fuel plates and the outer element contains 369 plates. The fuel itself is an aluminium-clad highly enriched uranium oxide distributed along the arc of the involute aluminium plate (U_3O_8 -Al cermet). The inner fuel element also contains an amount of ^{10}B as a burnable poison, primarily to help shift the power distribution from the inner element to the outer element. Generally, the core will be loaded with 9.4 kg of ^{235}U and 2.8 g of ^{10}B .

The fuel region is surrounded by a concentric ring of beryllium with a thickness of 30 cm that serves as a reflector. This reflector is subdivided into three regions: the removable reflector, the semi-permanent reflector (which contains the control element access plugs), and the permanent reflector. The beryllium is in turn surrounded by a water reflector of effectively infinite thickness. In the axial direction, the reactor is reflected by water.

Due to embrittlement caused by radiation, the inner beryllium reflector must be replaced after 40 cycles of operation of the reactor. At the start of cycle 400, a new removable beryllium reflector was therefore placed in the reactor. The semi-permanent reflector is replaced every 80 cycles. The beryllium reflector contains 20 experimental positions, being 8 large positions designated in pairs located in the removable beryllium zone, 4 small positions located in the semi-permanent beryllium reflector and 8 control plate access plug facilities located in the semi-permanent beryllium reflector.

The permanent beryllium reflector extends approximately 20 cm beyond the outside radius of the semi-permanent reflector. It is surrounded by approximately 50 cm of water and then by the steel pressure vessel. This permanent beryllium reflector is replaced every 135 cycles.

The reactor also has two thin, poison-bearing concentric cylindrical plates in an annular region between the outer fuel element and the beryllium reflector. These plates are driven in opposite directions. Reactivity is increased by downward motion of the inner cylinder, which is used only for shimming and regulation (it has no fast safety function). The outer control cylinder consists of four separate quadrants, each having an independent drive and safety release mechanism. Reactivity is increased as the outer plates are raised. All control plates have three axial regions of different poison content (a black region containing Eu_2O_3 , a grey region containing Ta and a white region containing aluminium) designed to minimize the axial peak-to-average power-density ratio

throughout the core lifetime. Any single rod or cylinder is capable of shutting down the reactor.

The reactor core assembly is contained in a 244 cm diameter steel pressure vessel located in a pool of water. The top of the pressure vessel is 518 cm below the pool surface, and the reactor mid plane is 838 cm below the pool surface.

11.2 Modelling burn-up in the HFIR with MONTEBURNS and ALEPH

The HFIR depletion calculations performed at ORNL were carried out with MONTEBURNS, which is an interface code between MCNP (MCNP5 was used in this case) and ORIGEN 2.2 just like ALEPH. Due to the limitations in MONTEBURNS on the number of materials (99 materials) and the maximum number of materials that can be depleted (49 materials), a simplified HFIR model had to be constructed in which the entire core was divided into only 17 radial burn-up zones without any axial segmentation (the inner and outer fuel element have respectively 9 and 8 radial burn-up zones).

As a result, the burn-up will be averaged in the axial direction. Further simplifications included the replacement of actual experiments in the flux trap from cycle 400 by dummy aluminium targets and the replacement of the experiments in the periphery target positions by a single generic experiment.

ALEPH on the other hand is capable of using any MCNP model regardless of its detail. Furthermore, the number of burn-up zones in ALEPH is essentially limitless although in practice it is limited by the available physical memory. As a result, none of the simplifications mentioned above were used. Furthermore, every one of the 17 radial burn-up zones were each subdivided into 10 axial zones for a total of 170 burn-up zones.

In addition, ALEPH also allows for the modelling of the control plate movement with relative ease by using simple surface transformation cards (which was already used in the original HFIR model to easily adjust the control plate position). The continuous movement of the control plates was modelled by moving the plates in discrete steps to their actual positions at the end of the day. MONTEBURNS didn't have this capability so the movement of the control plates was modelled manually in a multi-step process.

Control element burn-up was not taken into account as this should have only a minimal effect because the control elements' reactivity worth does not generally change over the lifetime of the elements. In fact, it even increases slightly with use due to the transmutation of Eu to Gd (which has a higher neutron absorption) and ^{181}Ta to ^{182}Ta by neutron capture.

For the MONTEBURNS calculations, the standard MCNP library ENDF66 (based on ENDF/B-VI.6) at 293.16 K has been used. Due to the limited number of nuclides in ENDF66 (173 nuclides and elements) a total of 46 nuclides that

MONTEBURNS deemed important did not have MCNP(X) cross section files. For the ALEPH calculations, we have used a ENDF/B-VI.8 library containing 311 nuclides and elements prepared by ALEPH-DLG. Only at the highest fractional absorption value (99.999 %, see section 11.6) did ALEPH issue warnings for 4 nuclides without libraries.

MONTEBURNS uses tallies to determine reaction rates so that this code suffers from the standard Monte Carlo burn-up problem of excessive computer time. Because of this, the total number of neutrons simulated in the criticality calculations in MONTEBURNS was reduced by a factor 4 from what is normally used. Because ALEPH does not suffer from this problem, no reduction in the number of particles was made. The ALEPH calculations ran on 3 Xeon 3 GHz CPUs for a total of 350 hours (wall time). More details on the MCNP model of the HFIR and the burn-up modelling itself for cycle 400 can be found in [90].

11.3 Control plate movement

Due to fuel burn-up it is impossible to maintain the criticality of a reactor without external effort. At every point in time during the operation of the reactor, the amount of positive reactivity invested into the fuel must be compensated through various sources of anti-reactivity. Some of these sources are inherent to the reactor design like the Doppler feedback effect. The rest of the anti-reactivity is introduced through means of active control mechanisms (control rods or control plates) and/or the application of burnable absorbers.

In the HFIR these sources of anti-reactivity are ^{10}B burnable absorber included in the inner fuel element and control plates located at the outside of the core. These control plates have a significant influence on the neutron flux and spectra in the reactor because they locally introduce very strong absorbers. The axial flux in the core will be depressed parallel to the black region and to a lesser extent parallel to the grey region of the fuel plates.

This ultimately has an effect on the local burn-up in the reactor and the movement of the plates must thus be taken into account to reflect the actual flux in the reactor at every point in the cycle. Figure 11.1 illustrates the importance of modelling this movement. The figure shows the evolution of the effective multiplication factor k_{eff} of the HFIR when the control plates are simply left at their outer most position during a burn-up calculation and when their movement is properly modelled in ALEPH.

When leaving the control plates in their outer most position, we see that k_{eff} drops quickly in the first couple of days which is due to the accumulation of fission products like ^{135}Xe and ^{149}Sm . After that, the value of k_{eff} remains roughly constant for a couple of days until it starts decreasing rapidly again. On the other hand, the k_{eff} curve for which the control plate movement was properly modelled is practically constant for the entire cycle.

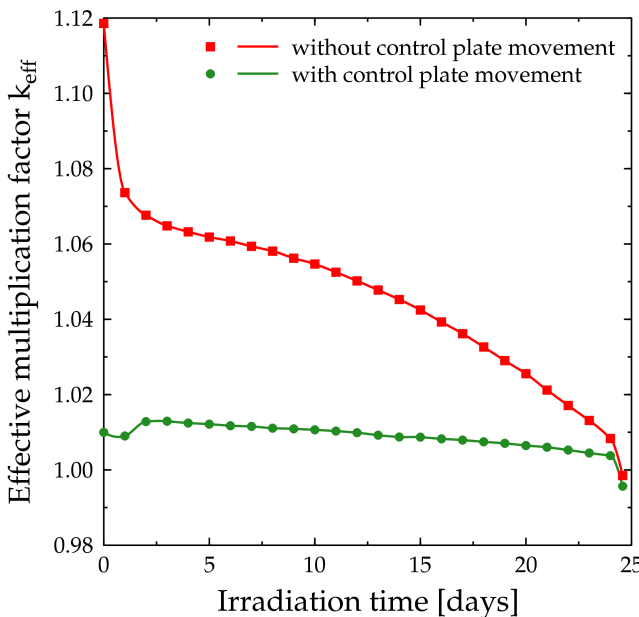


Figure 11.1: The evolution of the effective multiplication factor of the HFIR with and without control plate movement.

A comparison of the evolution of the k_{eff} multiplication factor (with control plate movement) as calculated by ALEPH and MONTEBURNS can be found in figure 11.2. Generally speaking, one would expect that the value of k_{eff} doesn't change as time progresses when modelling the control plate movement. This is however not entirely the case due to reactivity effects of individual nuclides which are either too large or too small than in reality due to nuclear data, resulting in a net deviation from the original k_{eff} value. The fact that we modelled the movement as discrete steps instead of continuous movement also contributes to this effect.

We observe a different k_{eff} behaviour for the ALEPH and MONTEBURNS calculations. During the irradiation, the k_{eff} values calculated by MONTEBURNS continues to increase. The maximum deviation Δk from the initial k_{eff} is around 0.010. The ALEPH curve first drops a bit at day 1, increases to a maximum at day 2 and decreases gradually from that point on. The large decrease at the end corresponds to the shut-down position of the control plates. The largest deviation Δk from the initial k_{eff} is only 0.006.

The fission product treatment by MONTEBURNS appears to be inadequate and is the principal cause of the difference between the two code sys-

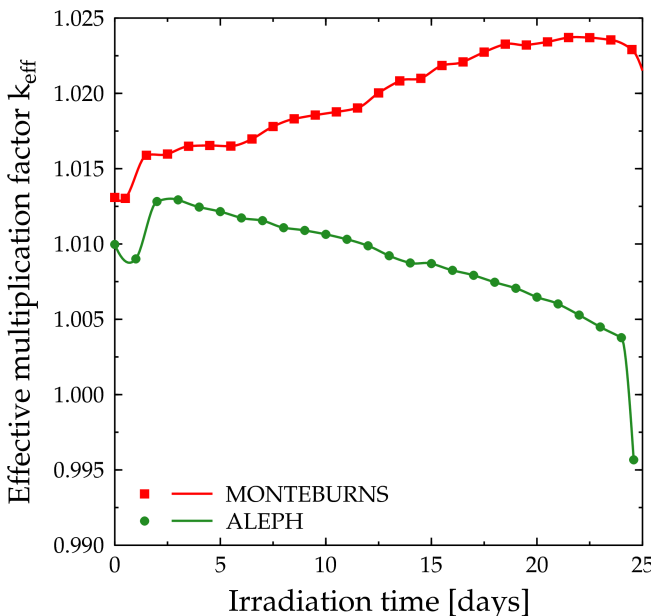


Figure 11.2: The evolution of the effective multiplication factor of the HFIR calculated with ALEPH and MONTEBURNS with control plate movement.

tems [90]. A large number of fission products could not be modelled in the transport calculations and were therefore omitted. Unfortunately, some of these nuclides appear to be very important fission products from an absorption point of view.

The seven most important fission products for the HFIR are (in decreasing order of importance) ^{135}Xe , ^{149}Sm , ^{105}Rh , ^{147}Nd , ^{151}Sm , ^{133}Xe and ^{149}Pm . The last five nuclides of this small list do not even have a cross section file in the ENDF66 library. The omission of these and other nuclides in the transport calculations results in a more transparent core which leads to increased absorption by fissile nuclides, an increased neutron production and finally to an overestimation of k_{eff} .

ALEPH on the other hand uses the fractional absorption criterion to determine which nuclides to use for the next transport calculation (see section 8.4) in combination with a more complete nuclear data library. The ENDF/B-VI data used by ALEPH has around 300 “transport-ready” nuclides, which includes (among others) ^{105}Rh , ^{147}Nd , ^{151}Sm , ^{133}Xe and ^{149}Pm which were missing from ENDF66.

11.4 Neutron spectra and flux values

One of the perks of using ALEPH is that a user obtains very detailed neutron spectra for the different burn-up zones he has considered *by default* (see for instance figure 9.1 for an example of these spectra in different radial zones of a single PWR fuel pin). Due to the large number of burn-up zones used in the HFIR calculations, plotting the different fractions of the total flux as a function of the radial position in the core is a better way of assessing the spectral changes due to burn-up in the HFIR core. We did this in figure 11.3 and 11.4. The grey shaded areas in these figures corresponds to the position of the fuel elements.

Even though the reactor core is quite small, the spectral differences in the core can be significant. About 39.2 % of the total flux in the centre of the flux trap ($r = 0$ cm) appears to be thermal at the beginning of the cycle and this increases respectively to 40.9 % and 42.5 % after 12 days and 24 days of operation.

In the fuel elements, this thermal component only accounts for 3.9 to 15.1 % of the total flux. After 24 days, this has increased to 5.5 % and 23.8 %. The minimum in the thermal component can also be found in the outer fuel element, as one would expect. The thermalisation of the fuel spectrum is the most obvious in the inner fuel element. There the thermal fraction of the flux has increased by 4.2 to 8.6 % while this increase is only 1.7 to 6.2 in the outer fuel element. The largest increase in the thermal component can be found in the inner fuel element (due to its high burn-up) and at the outside of the core ($r = 25$ cm).

The epithermal component of the flux also increases slightly towards the end of the cycle, although it is less pronounced than the increase of the thermal component. The maximum increase is only of the order of 1 %. Furthermore, this component practically doesn't change in the central flux trap.

With the increase of the thermal and epithermal component, the importance of the fast flux (with an energy above 1 eV) is reduced. For the fast flux between 1 and 100 eV, the decrease is quite small (less than 1 %). In the region between both fuel elements we even observe a very small increase. For the fast flux above 1 MeV, the importance drops by at least 1 %.

11.5 Evolution of individual nuclides

11.5.1 Fuel depletion

For a typical HFIR operating cycle, the reactor is loaded with around 9.4 kg of ^{235}U . The evolution of this ^{235}U content in the reactor on a day-to-day basis can be found in figure 11.5. For the case of HFIR cycle 400 ALEPH and MONTE-BURNS gave very similar values on the remaining fissile ^{235}U content (being

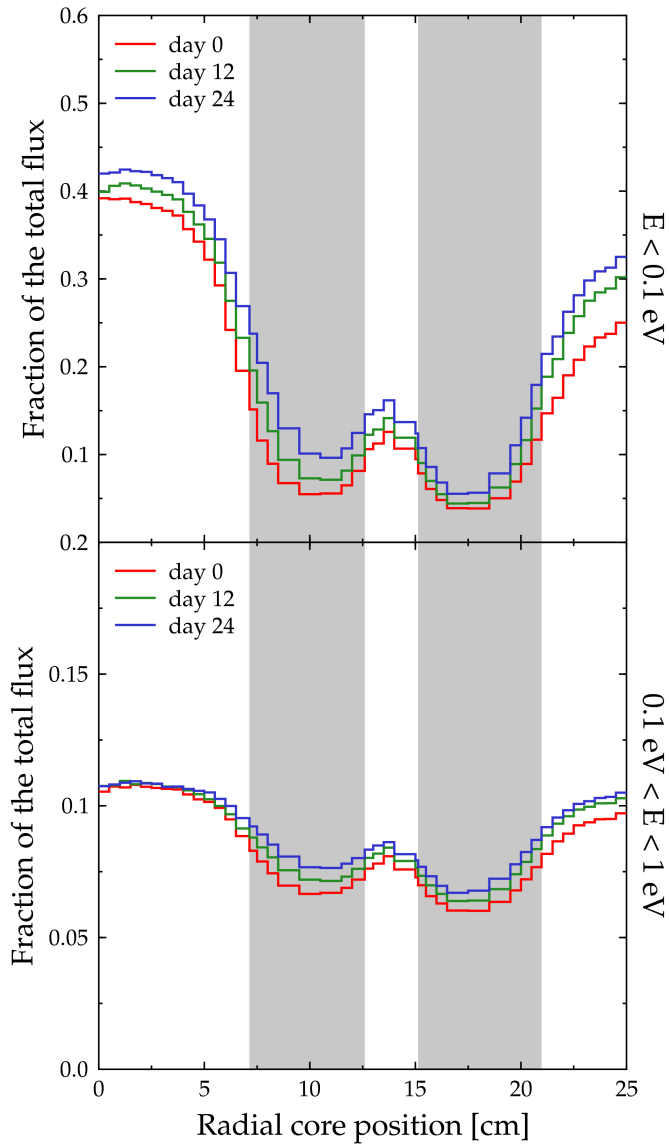


Figure 11.3: The fractions of the thermal and epithermal neutron flux in the core midplane of the HFIR as a function of time.

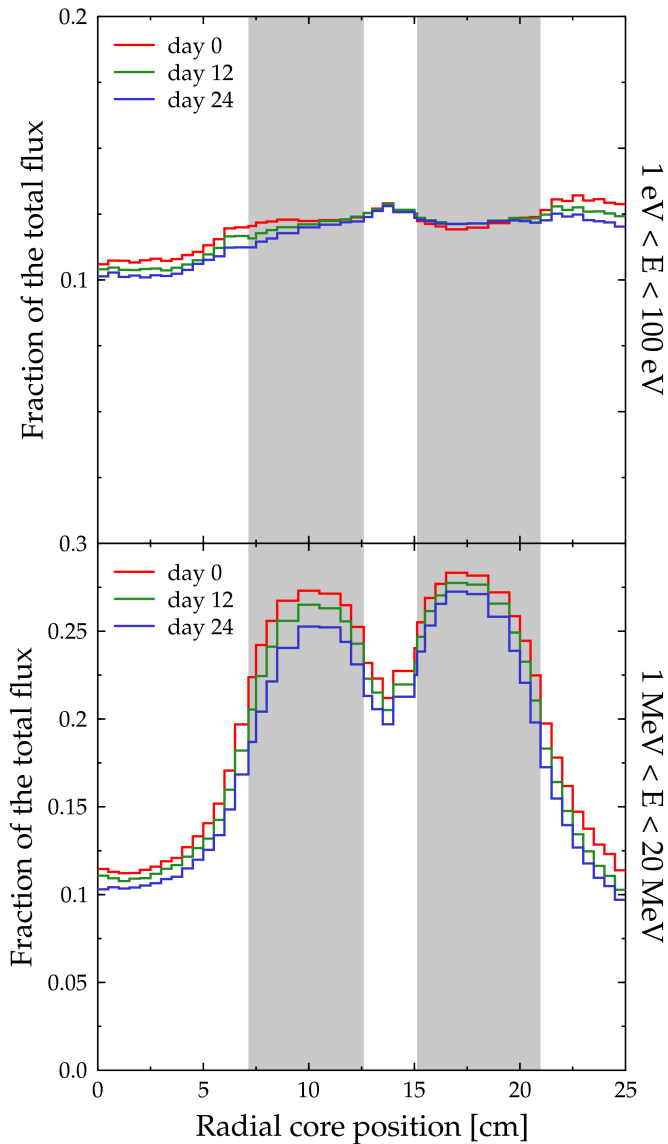


Figure 11.4: The fractions of the fast neutron flux in the core midplane of the HFIR as a function of time.

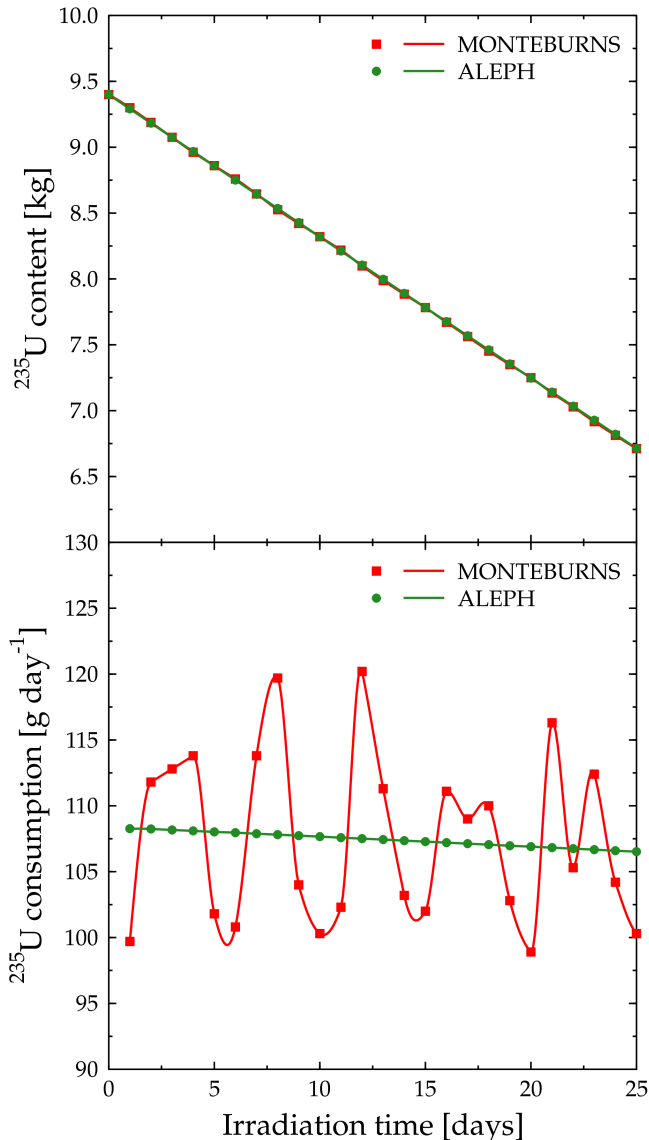


Figure 11.5: The evolution of the global ^{235}U content in the HFIR core and the consumption of ^{235}U per day as a function of time.

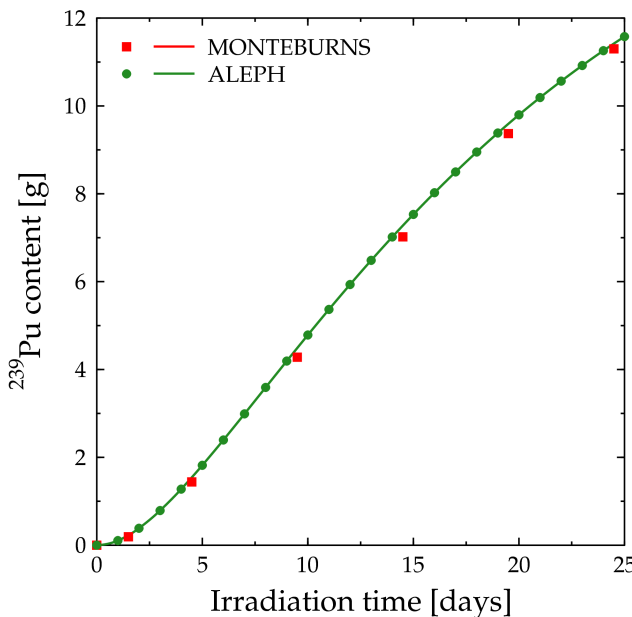


Figure 11.6: The net production of ^{239}Pu in the HFIR core as a function of time.

6.785 kg for ALEPH versus 6.779 kg for MONTEBURNS) after a total power production of 2068 MWd. These values correspond very well with what is observed in reality (the end of cycle ^{235}U content is approximately 6.8 kg).

In the global ^{235}U content in figure 11.5 we can already see a slightly oscillating behaviour of the MONTEBURNS result around the result given by ALEPH. This oscillating behaviour is very visible when we look at the ^{235}U consumption per unit of power. MONTEBURNS predicts an oscillating consumption of ^{235}U and fluctuates with up to 15 g of ^{235}U per day. This swing in the ^{235}U mass is quite small and does obviously not affect the final outcome of the cycle. This is most likely a result of burn-up oscillations in the MONTEBURNS calculation (see also section 11.7).

ALEPH on the other hand gives an almost constant depletion of ^{235}U that decreases slightly near the end of the cycle (even though the power remained constant). The ^{235}U fission rate therefore appears to be rather constant during the entire cycle. The slight decrease near the end of the cycle is compensated by the creation and fissioning of other fissile nuclides like ^{239}Pu from ^{238}U (see figure 11.5). Within the HFIR, fission of ^{239}Pu accounts for only 0.52 % of the total fission rate in the second day of operation while it accounts for 5.92 % of

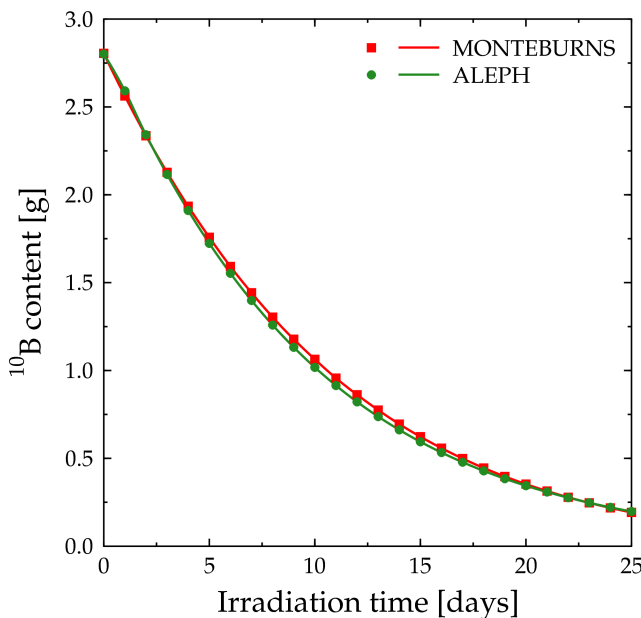


Figure 11.7: The depletion of the boron burnable poison in the inner HFIR fuel element as a function of time.

the total fission rate at the end of cycle. Near the end of the cycle, a net amount of almost 12 g of ^{239}Pu will have been produced.

11.5.2 Depletion of burnable poison

The inner fuel element contains ^{10}B as a burnable poison in the form of B_4C . In the present HFIR inner fuel element, 2.80 g of ^{10}B is distributed in the aluminium filler of the plates. The distribution of the burnable poison is chosen as to minimise the ^{235}U burn-up at the plate edges and to flatten the fission rate density in the plates to help shift the power distribution from the inner element to the outer element.

Figure 11.7 shows the depletion of this burnable absorber as calculated by ALEPH and MONTEBURNS. We can see that the ^{10}B inventory is almost completely depleted towards the end of the cycle. ALEPH apparently predicts a faster depletion than MONTEBURNS in the middle of the cycle between days 3 and 14 (the ALEPH curve lies below the curve of MONTEBURNS) but in the end both codes predict almost the same final value at the end of the cycle (0.198 g for ALEPH and 0.192 for MONTEBURNS).

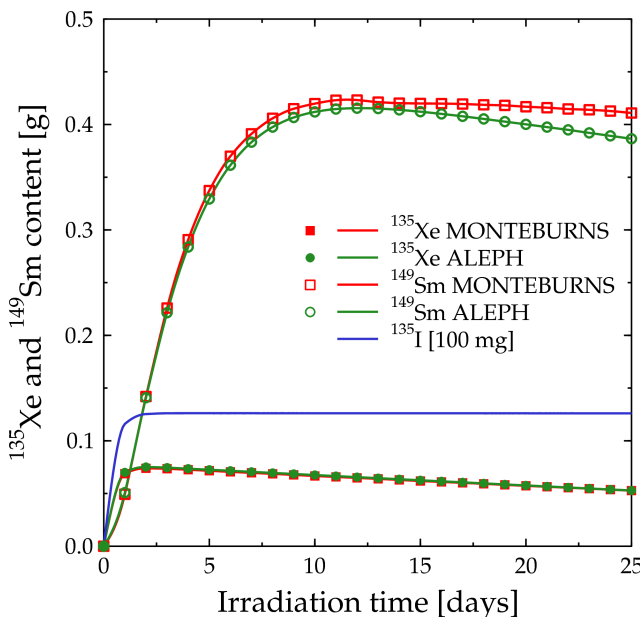


Figure 11.8: The evolution of the fission products ^{135}Xe , ^{149}Sm and ^{135}I as a function of time.

11.5.3 Fission product accumulation

The most important fission products produced in the HFIR are ^{135}Xe and ^{149}Sm , the classic fission products encountered in any thermal reactor. Together they are responsible for about 90 % of all absorptions by fission products in the HFIR [90].

The absorption cross section (used in the first depletion step in the ALEPH calculation) for these nuclides in the different burn-up zones ranges from 10^5 to 10^6 barn for ^{135}Xe and between 3000 and 20000 barn for ^{149}Sm . Other important fission products are ^{105}Rh (between 700 to 3500 barn), ^{151}Sm (between 500 to 3000 barn) and ^{149}Pm (between 80 to 400 barn).

The ^{135}Xe and ^{149}Sm content as calculated by ALEPH and MONTEBURNS can be found in figure 11.8. As with the previous nuclides, both codes show consistent results throughout the entire cycle. In the case of ^{135}Xe , both codes show the same exact mass build-up of this nuclide during the whole cycle. As can be seen in figure 11.8 the mass build-up of ^{135}Xe at any point during the cycle as calculated by either code lies on top of the other.

The ^{135}Xe content builds up very rapidly with burn-up until it reaches a maximum value of 0.074 g after about 2 days of operation. From that point

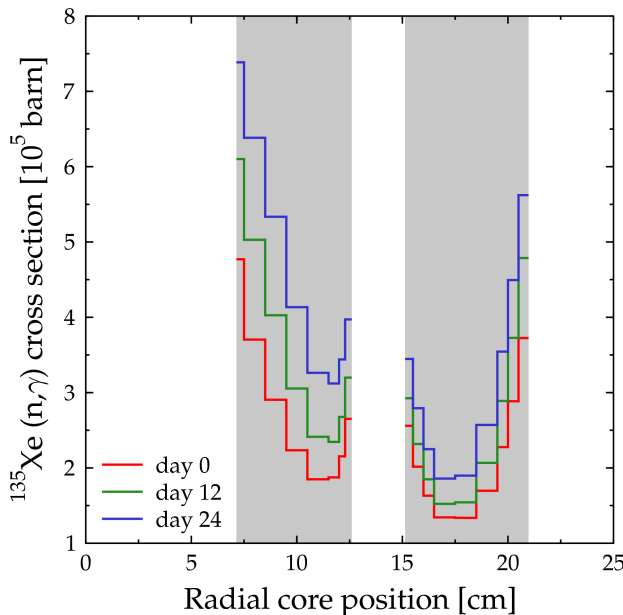


Figure 11.9: Evolution of the effective ^{135}Xe (n,γ) cross section for the depletion calculations for the burn-up zones at the fuel centreline.

on, the ^{135}Xe content starts to decrease to about 0.055 g at the end of the cycle. Theoretically speaking [91], the ^{135}Xe content should reach an equilibrium value and stay there until the reactor is shut down or when the power level is changed, but this does not appear to be the case. This is due to the spectral changes in the HFIR core during burn-up and due to the way ^{135}Xe is produced and consumed.

Basically, ^{135}Xe is created through fission and by β^- decay of ^{135}I (with a half-life of 30 s). ^{135}I is in turn produced by fission and β^- decay of ^{135}Te (with a half-life of 6.7 h). Production of any of these nuclides through neutron activation is highly unlikely. The production of ^{135}Xe directly through fission is quite low as well (the direct ^{235}U fission yield of ^{135}Xe used by ALEPH is only 0.05 % per fission) so that almost all ^{135}Xe is created by β^- decay from ^{135}I and ^{135}Te .

^{135}Xe itself is removed from the material inventory through neutron capture to ^{136}Xe and by β^- decay to ^{135}Cs with a half-life of 9.2 hours. Due to the extremely high (n,γ) cross section of ^{135}Xe it will be this mechanism that is mainly responsible for the removal of ^{135}Xe from the core during reactor operation.

As we have already seen, the fission rate in the HFIR remains almost constant during the entire cycle so that the amount of ^{135}I and ^{135}Te produced through fission remains roughly the same for the entire cycle. As a result, a global (but not localised) equilibrium build-up of ^{135}Xe for the entire cycle will be established. This is evidenced by the ^{135}I content in the core which reaches an equilibrium composition of 1.261 g at around day 3 (the blue line in figure 11.8 is the ^{135}I content in units of 100 mg).

During burn-up, the spectra in the HFIR core change radically (see figures 11.3 and 11.4) which results in an ever increasing ^{135}Xe (n,γ) cross section, as can be seen in figure 11.9. This increase is different for every burn-up zone considered because it is directly linked to the burn-up of the fuel. We know that the areas of highest burn-up can be found at the edges of the fuel elements. In those areas, less fission neutrons will be created so that the spectrum will be more and more dominated by slowing down neutrons, resulting in a burn-up dependent spectral thermalisation effect which in turn results in higher ^{135}Xe (n,γ) cross sections. Due to this effect, the removal of ^{135}Xe will gradually increase with time. Combined with the equilibrium production of ^{135}Xe this results in a gradually decreasing ^{135}Xe content.

The ^{149}Sm content exhibits a similar behaviour. We can see that ^{149}Sm build-up increases until it reaches a maximum value of around 0.42 g. We also observe a decrease of the ^{149}Sm content towards the end of the cycle. This decrease is a bit more pronounced in the results provided by ALEPH than in the MONTEBURNS results. This decrease toward the end of cycle can also be attributed to the spectral changes in the HFIR due to burn-up and to an increase in thermal flux in the core at the end of the cycle, just like we observed for ^{135}Xe .

11.6 Fractional absorption criterion

The fractional absorption criterion is used by ALEPH to update the material compositions in the MCNP(X) runs. The procedure consists of evaluating for every nuclide the ratio of absorption by this nuclide to all absorption in the material. Afterwards, this list is sorted in decreasing importance and nuclides are selected for inclusion in the MCNP(X) runs if they contribute to for e.g. 99.9 or 99.99 % of all absorptions. Nuclides that were present from the start are added by default and do not necessarily contribute to this fractional absorption criterion.

Figure 11.10 shows the influence of this parameter on the evolution of the effective multiplication factor for cycle 400 in the HFIR. We see that for a value of 99.9, 99.99 or even 99.999 % for the fractional absorption the different k_{eff} curves are very similar. In the case of 99.99 and 99.999 % it is even difficult to distinguish the different curves from each other. The curve corresponding with a fractional absorption of 99 % however gives an evolution of k_{eff} that is

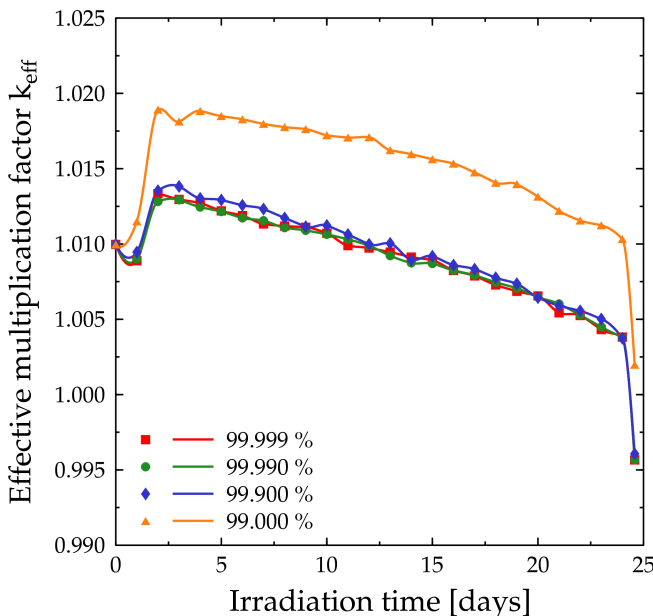


Figure 11.10: The evolution of the effective multiplication factor of the HFIR for different values of the fractional absorption criterion used by ALEPH.

quite different from the other three. This is simply related to the accumulation of fission products.

In the HFIR, the most important fission products are (in decreasing order of absorption) ^{135}Xe , ^{149}Sm , ^{105}Rh , ^{147}Nd , ^{151}Sm , ^{133}Xe and ^{149}Pm . Only the first fission product from this list (^{135}Xe) is deemed important enough to be included in the transport calculation at day 1 when using 99 % for the fractional absorption. On day 2 ^{149}Sm and ^{105}Rh are included followed by ^{147}Nd and ^{151}Sm on day 4, ^{133}Xe on day 5 and ^{149}Pm on day 6. When using 99.9 % all 7 nuclides are added on day 1. For 99.999 % a total of 51 fission products is added to the different burn-up zones at day 1.

At day 25, respectively 32, 66, 103 and 129 new nuclides were added to the existing list when using fractional absorption criteria of 99, 99.9, 99.99 and 99.999 %. In the case of 99.999 % the list of additional nuclides even included ^2H (deuterium created through activation of ^1H) and ^7Li (created through the (n,α) reaction on the ^{10}B burnable absorber found in the inner fuel element). It is therefore clear that a fractional absorption criterion of 99.9 or 99.99 % (or something in between) will be sufficient for most applications.

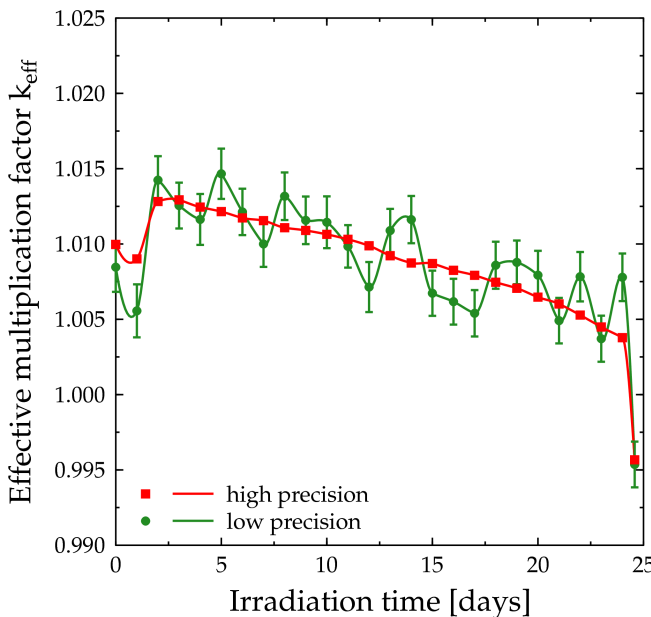


Figure 11.11: The effect of calculation precision and burn-up oscillations on the evolution of the effective multiplication factor of the HFIR.

11.7 Burn-up oscillations

Due to large statistical errors on cross sections, particle flux, etc. it is possible that the fissile material within a burn-up zone is depleted either too fast or too slow compared to reality during a time step. This results respectively in a lower and higher flux during the next step which compensates the error in the previous step. This effect is commonly referred to as burn-up oscillations. We have already encountered this effect with the daily consumption of ^{235}U calculated by MONTEBURNS (see figure 11.5).

This effect can also be simulated by significantly decreasing the number of simulated particles. Figure 11.11 gives the evolution of the effective multiplication factor for two ALEPH calculations with different levels of precision. In this case, the low precision curve uses 100 times less particles than the high precision curve (resulting in a difference in accuracy of a factor 10) which is reflected in the large error bars (corresponding with a single standard deviation) of the low precision curve. The error bars for the high precision curve are not shown because they would not be visible.

We observe that the low precision curve oscillates around the other curve

due to the effect of burn-up oscillations and that the difference is within at least two standard deviations. This shows that this type of low precision calculations can be used for initial assessments of the effect of burn-up on the system before starting a high precision calculation.

The difference in calculation time is also significant. For the high precision calculation, 3 Xeon 3 GHz CPUs required a total of 350 hours (wall time) to complete the calculation while a single Xeon 3 GHz CPU only needed about half a day to complete the low precision calculation.

When faced without a challenge, make one.

Dr. Peter Safar (1942 - 2003)

12

Fuel management in hybrid systems

12.1 The physics of sub-critical multiplying systems

The basis for the study of every neutron multiplication and transport problem is the Boltzmann equation (see equation 2.1). It describes the detailed neutron balance in a system, i.e. the production and loss at every point in the phase space (energy E , position \mathbf{r} , direction Ω and time t). In reactor physics, it is customary to rewrite the Boltzmann equation using a fission operator F , a neutron loss operator L and an external source operator s_e so that:

$$\frac{1}{v} \frac{\partial}{\partial t} \varphi(\mathbf{r}, E, \Omega, t) = F\varphi(\mathbf{r}, E, \Omega, t) - L\varphi(\mathbf{r}, E, \Omega, t) + s_e \quad (12.1)$$

or

$$\frac{1}{v} \frac{\partial}{\partial t} \varphi(\mathbf{r}, E, \Omega, t) = T\varphi(\mathbf{r}, E, \Omega, t) + s_e \quad (12.2)$$

with T the neutron transport operator (which is the sum of the operators L and F). All these operators are dependent on the position \mathbf{r} , the energy E and the direction Ω in the phase space. The operators L , F and s_e now uniquely characterise any system in which neutrons are transported and multiplied.

A fundamental parameter of any multiplying system (either critical, sub-critical or supercritical) is the effective multiplication factor k_{eff} . As we mentioned in section 3.4, this multiplication value gives us information about the stability (or criticality) of nuclear systems. In reactor physics, the effective multiplication factor is also known as the fundamental eigenvalue of a system with the associated fundamental mode φ_0 so that:

$$\frac{1}{k_{\text{eff}}} F\varphi_0(\mathbf{r}, E, \Omega) - L\varphi_0(\mathbf{r}, E, \Omega) = 0 \quad (12.3)$$

The previous equation is the associated reactor equation of the system. In this equation, φ_0 is the flux (or fundamental mode) of the associated critical system characterized by the operators L and F/k_{eff} . The effective multiplication factor is used to modify the neutron production by fission in the fission operator F to make the system stationary without the use of an external source.

Another important function for any system is the adjoint flux φ_0^+ . The adjoint flux is a direct measurement of a neutron's importance in the multiplication process. This adjoint flux satisfies the adjoint associated reactor equation:

$$\frac{1}{k_{\text{eff}}} F^+ \varphi_0^+ (\mathbf{r}, E, \Omega) - L^+ \varphi_0^+ (\mathbf{r}, E, \Omega) = 0 \quad (12.4)$$

By multiplying the associated reactor equation (equation 12.3) with the adjoint flux and then integrating the result over the entire phase space, we obtain the following expression for the value of k_{eff} :

$$k_{\text{eff}} = \frac{\langle \varphi_0^+, F\varphi_0 \rangle}{\langle \varphi_0^+, L\varphi_0 \rangle} \quad (12.5)$$

where the brackets represent the integration over the entire phase space. For this equation, we say that the integration is weighed with the adjoint flux.

It is clear that the definition of k_{eff} , the fundamental mode φ_0 and the adjoint flux φ_0^+ is independent of the external source operator s_e . This means that two sub-critical systems with a different external source operator s_e (different from 0) but with the same operators L and F will have the same value of k_{eff} . Because of the difference in the external source operator, the neutron flux distribution in both systems will be different. This implies that the effective multiplication factor k_{eff} cannot fully characterise the multiplication process in a sub-critical system with an external source. This does not mean that k_{eff} is not an important parameter of these systems. However, we have to take into account the external source in the multiplication process so we will have to introduce the concept of the source multiplication factor k_s .

For a sub-critical system (defined by the operators L , F and s_e and with a flux distribution given by φ_s) in stationary conditions, we have:

$$F\varphi_s (\mathbf{r}, E, \Omega) - L\varphi_s (\mathbf{r}, E, \Omega) + s_e = 0 \quad (12.6)$$

To obtain the neutron balance over the entire system, we need to integrate this equation over the entire phase space:

$$\langle F\varphi_s \rangle - \langle L\varphi_s \rangle + \langle s_e \rangle = 0 \quad (12.7)$$

The first term is the neutron production rate (by fission only), the second term is the neutron loss rate and the third term is the external neutron source rate. In this case, the integration over the phase space is unweighted.

The source multiplication factor k_s is now defined as the ratio of the total number of neutrons produced through fission to the total number of neutrons produced through all possible means (being fission and the external source):

$$k_s = \frac{\langle F\varphi_s \rangle}{\langle L\varphi_s \rangle} = \frac{\langle F\varphi_s \rangle}{\langle F\varphi_s \rangle + \langle s_e \rangle} \quad (12.8)$$

The definition of this multiplication factor is quite similar to the definition of the effective multiplication factor, except that the quantities are unweighted and that the true flux distribution of the sub-critical system with the external source is used.

The effective multiplication factor k_{eff} can therefore be associated with the ADS system where the proton beam is switched off while the source multiplication factor k_s is associated with the same system with the beam switched on. The source efficiency φ^* is used to describe the relation between k_s and k_{eff} for such a sub-critical system:

$$\varphi^* = \frac{\frac{1-k_{\text{eff}}}{k_{\text{eff}}}}{\frac{1-k_s}{k_s}} \quad (12.9)$$

For a sub-critical system close to criticality, it can be shown that the neutron source efficiency represents the relative efficiency of the source neutrons compared to the fission neutrons and that it is defined as the ratio of the average importance of the external source neutrons to the average importance of the fission neutrons produced in the sub-critical core [92]:

$$\varphi^* \approx \frac{\frac{\langle \varphi_0^+ s_e \rangle}{\langle s_e \rangle}}{\frac{\langle \varphi_0^+ F \varphi_s \rangle}{\langle F \varphi_s \rangle}} \quad (12.10)$$

The neutron source efficiency relates to the total power P generated by fission in a sub-critical system through the following equations:

$$P = \langle F \varphi_s \rangle \frac{Q_{s,f}}{\nu} = \langle s_e \rangle \frac{k_s}{1-k_s} \frac{Q_{s,f}}{\nu} = \langle s_e \rangle \varphi^* \frac{k_{\text{eff}}}{1-k_{\text{eff}}} \frac{Q_{s,f}}{\nu} \quad (12.11)$$

where $Q_{s,f}$ is the total energy release per fission averaged for the entire system and ν is the total average number of fission neutrons. For an ADS, the neutron source rate $\langle s_e \rangle$ can be written as the beam current I_p multiplied by the average neutron yield Y_s of the spallation target so that:

$$P = I_p Y_s \frac{k_s}{1-k_s} \frac{Q_{s,f}}{\nu} \quad (12.12)$$

The neutron yield Y_s is defined as the average number of neutrons produced per proton in the beam through any means different from fission. There are a number of reactions or reaction mechanisms that contribute to this neutron yield. This includes intra-nuclear cascade interactions (initiated by high energy neutrons or protons) in the spallation target, (p,xn) interactions initiated by protons in the spallation target and (n,xn) interactions (mostly $(n,2n)$ and $(n,3n)$) interactions in the fuel initiated by either spallation-born neutrons or fission neutrons). It will be this last component that will vary as a function of burn-up (due to the burn-up of the fuel) and therefore result in an

additional time dependence in the total system power in addition to the time dependence induced by the multiplication factors themselves.

It is also clear that increasing the importance of the source neutrons (i.e. increasing the neutron source efficiency φ^*) can therefore reduce the required beam current for a given level of sub-criticality and power. For large systems, it will therefore be beneficial to maximize the neutron source efficiency.

12.2 The MYRRHA Accelerator Driven System

The Multi-purpose hYbrid Research Reactor for High-tech Applications or MYRRHA [1] is an Accelerator Driven System (ADS) under development at the Belgian Nuclear Research Center SCK•CEN in Mol, Belgium and aims to serve as a basis for a European experimental ADS to provide protons and neutrons for various R&D applications including materials testing, transmutation experiments, etc. It consists of a linear proton accelerator delivering a proton beam to a windowless liquid Lead Bismuth Eutectic (LBE) spallation target which is placed inside a sub-critical core. The spallation target produces a primary neutron source that is subsequently multiplied in the sub-critical core.

In June 2006, the pre-design studies of MYRRHA has been endorsed as the starting point towards the design of the eXperimental facility demonstrating the technical feasibility of Transmutation in an Accelerator Driven System (XT-ADS), in the framework of the European Sixth Framework IP-EUROTRANS project. The main objective of this project is to carry out a first advanced design of a 50 to 100 MW XT-ADS and to achieve a generic conceptual design (for several 100 MW) of the European Facility for Industrial Transmutation (EFIT). The XT-ADS with initial loading of standard MOX fuel, is intended to operate as a test-bench for the main components and for the operation scheme for the EFIT.

In the framework of the present IAEA Coordinated Research Project (CRP) on "Studies of Innovative Reactor Technology Options for Effective Incineration of Radioactive Waste", MYRRHA has been taken as the prototype for the benchmark on LBE liquid-cooled sub-critical facilities loaded with solid fuel containing ^{238}U fertile isotope. The CRP benchmarking exercise is focused on the analysis of the behaviour the MYRRHA conceptual design in various accidental conditions. The leading design parameters of the MYRRHA facility used in this benchmark exercise are listed in table 12.1.

For the benchmark exercise a 600 MeV proton beam was adopted, as for the XT-ADS instead of 350 MeV leaving the beam intensity as a free parameter to be adjusted in such a way as to achieve a fission power release of 50 MW within the sub-critical core. Besides SCK•CEN (Belgium), NRG and JRC-Petten (The Nederlands), have been involved in the benchmark either for calculating safety-related neutronics parameters or carrying out transient and thermal-hydraulic studies.

Table 12.1: MYRRHA main characteristics.

Parameter	Value
Proton beam energy	600 MeV
Nominal power	50 MW
Initial sub-criticality	-5000 pcm
Fuel active length	60 cm
Core diameter	100 cm
Core height	180 cm
Vessel inner diameter	440 cm
Vessel total height	700 cm
Vessel internal volume	100 m ³
LBE volume	65 m ³
Gas plenum height above coolant	50 cm
Primary coolant	LBE
Secondary coolant	water or steam
Coolant pressure	atmospheric + hydrostatic
Core inlet temperature	473 K
Core average outlet temperature	610 K
Coolant average velocity	2 m s ⁻¹
Primary coolant flow rate	2500 kg s ⁻¹

Design details on the MYRRHA ADS can be found in [1, 93]. A pool-type design has been chosen for MYRRHA, not only from a safety point of view (in acknowledgement of the inertia of many hundreds of tons of LBE), but also to provide an extremely flexible core management for the fuel sub-assemblies and the experimental irradiation devices. Also, the design has been made in such a way that all in-vessel components can be removed and replaced during the lifetime of the installation for maintenance and investment protection.

The spallation loop is characterized by an off-centre layout (the confinement vessel of the spallation loop is located beside the sub-critical core). Several reasons justify such a configuration, the main one is the need of a high neutron flux in the sub-critical core. The LBE contained in the feed tank flows by gravity in an annular tube surrounding the proton beam tube. The flow rate is determined by the tube geometry and by the height difference between the LBE free surfaces in the feed tank and in the spallation target.

The LBE recirculation in the loop is insured by a mechanical pump. In addition, a magneto hydraulic pump is foreseen to provide the fine tuning of the feed flow. A Light Detection And Ranging (LIDAR) system measures the vertical position of the target free surface and adjusts the flow of the magneto hydraulic pump in order to keep the position of the free surface constant.

The sub-critical core consists of 99 channels, enabling one to accommodate various loading configurations including fuel assemblies or experimental de-

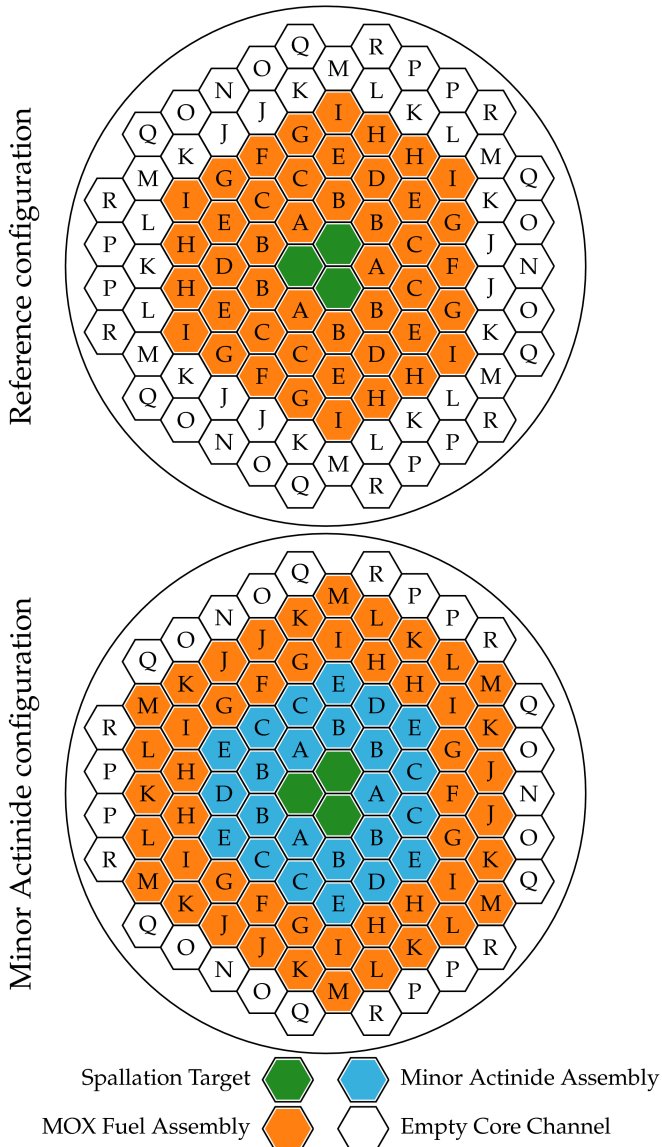


Figure 12.1: The MYRRHA reference configuration (45 MOX assemblies) and the minor actinide configuration (24 minor actinide assemblies and 48 MOX assemblies).

vices. To keep the fuel assemblies in place, the sub-critical core is enclosed in a core barrel. The availability of numerous spare channels grants a higher flexibility as to the facility exploitation as an experimental machine. The core can be adapted to fit various experimental rigs. For the IAEA CRP benchmark exercise, two core configurations were adopted.

The core is designed to operate with standard MOX driver fuel but can manage a few minor actinide (MA) oxide fuel assemblies. The reference sub-critical core of MYRRHA is displayed in figure 12.1. It consists of a single batch of 45 fuel assemblies containing 30 wt% Pu-enriched $(U\text{-Pu})O_2$ MOX fuel pins.

Figure 12.1 shows a second core configuration in which MYRRHA is operated as an experimental small scale minor actinide “transmuter”. It consists of a two batch U-free MA (Pu and Am in a MgO matrix) and MOX core containing 48 MOX fuel assemblies at the outside of the core configuration. The minor actinide load consists of 24 assemblies similar in geometry to the MOX driver assemblies, but housing the fuel rods containing inert matrix fuel pellets consisting of 45 vol. % $(Pu_{0.5}Am_{0.5})O_{1.88}$ fuel and 55 vol. % MgO matrix.

12.3 Modelling burn-up in an ADS

The difference of ADS systems with our previous examples is that the flux distribution is determined by the external proton source. As a result, not criticality calculations but fixed source calculations have to be used to properly calculate the depletion of an ADS system.

For both configurations, we have calculated the evolution of the core during two cycles of 90 days with a shut-down period of 30 days in between. For the reference configuration, the 90 day cycles were subdivided into 11 steps (4 initial steps of 5 days and 7 steps of 10 days). For the minor actinide configuration, the cycles were divided into 18 steps of 5 days. In every one of those steps, the proton current was assumed to be constant.

The fuel assemblies in the core are divided into radial burn-up zones corresponding to the different core channels. The active fuel length of 60 cm of every pin in every assembly has been subdivided into three equal axial zones to take the axial burn-up effect into account because the fuel will reach a higher burn-up in the centre of the assembly due to higher flux. The fuel pins of such a radial zone are considered to be a single burn-up zone. The reference configuration therefore consists of 27 burn-up zones and the minor actinide configuration has 42 zones (15 zones for the MA assemblies and 27 for the outer MOX assemblies).

Like with the previous examples, the combination of the JEFF 3.1 data library supplemented with the JEFF 3.0A activation data library was used for these calculations. The fuel temperature has been set to 1200 K for the entire core. The LBE coolant and structural materials have a temperature of 600 K.

12.4 Fuel management calculations

12.4.1 Requirements for fuel management

As mentioned in chapter 1, fuel management ensures that a reactor core load meets the demanded operational requirements within adequate safety margins. Fuel management calculations analyse the depletion characteristics from the beginning to the end of the operational cycle. In fuel management calculations, three principle characteristics of the reactor core have to be determined:

- the evolution of the core reactivity (and therefore the multiplication factors) and other integral system parameters
- the power and flux distributions
- the isotopic inventory at the end of the cycle

but also the evolution of other reactor physics parameters such as the control rod worth, the effective delayed neutron fraction β_{eff} and the effective neutron lifetime Λ_{eff} have to be determined for the purpose of safety analysis over the course of the operational cycle.

As we will show in the following paragraphs, ALEPH can provide these three characteristics in a single calculation just like a normal fuel management code. Reactor physics parameters like the effective delayed neutron fraction β_{eff} and the effective neutron lifetime Λ_{eff} have to be determined with separate calculations. The evolution of the material compositions calculated by ALEPH will also serve as basic input for this purpose [94].

By calculating these parameters with Monte Carlo as well [95, 96], a coherent system for fuel management fully based on Monte Carlo can be created. If the same Monte Carlo code (e.g. MCNPX 2.5.0 or MCNP5) and if the same nuclear data (e.g. JEFF 3.1 with the addition of JEFF 3.0A) is used for all aspects of the fuel management calculations, then such a fuel management system will be fully consistent in both method and nuclear data.

12.4.2 Integral system parameters

The values for the multiplication factors k_{eff} and k_s , source efficiency φ^* , total system power P and average neutron yield Y_s for both configurations at the beginning and end of every irradiation cycle can be found in table 12.2. The indicated errors correspond with one standard deviation (68 % confidence interval). The evolution of these parameters over the two entire cycles can also be found in figures 12.2 and 12.3.

Both configurations start out with the same source multiplication factor k_s , being 0.9583 which corresponds with an initial power level of 50 MWth (with a beam current of 1.9 mA for the reference configuration and 2.0 mA for the minor actinide configuration). The value of the effective multiplication factor

Table 12.2: The effective multiplication factor k_{eff} , source multiplication factor k_s , source efficiency φ^* , total system power P and average neutron yield Y_s for the reference and minor actinide configuration.

Reference configuration					
Time [days]	k_{eff}	k_s	φ^*	P [MW]	Y_s [n/p]
0 (BOC1)	0.95476 (12)	0.95827 (31)	1.08810 (896)	50.0	16.0
90 (EOC1)	0.94007 (12)	0.94499 (40)	1.09514 (874)	37.8	15.8
120 (BOC2)	0.94006 (12)	0.94475 (40)	1.09030 (867)	37.7	15.8
210 (EOC2)	0.92832 (12)	0.93446 (46)	1.10092 (850)	31.2	15.6
Minor actinide configuration					
Time [days]	k_{eff}	k_s	φ^*	P [MW]	Y_s [n/p]
0 (BOC1)	0.95533 (12)	0.95828 (31)	1.07402 (886)	50.1	15.5
90 (EOC1)	0.94569 (12)	0.95020 (36)	1.09569 (872)	41.2	15.4
120 (BOC2)	0.94542 (12)	0.94994 (37)	1.09554 (868)	41.0	15.4
210 (EOC2)	0.93744 (16)	0.94282 (41)	1.10037 (879)	35.4	15.3

differs a bit more ($\Delta k = 0.00057$) but this difference is of the same magnitude as the 99 % confidence interval (three standard deviations).

Over the first cycle, the decrease Δk of the source multiplication factor k_s amounts to 1328 pcm (i.e., about 15 pcm day $^{-1}$) while loss in k_{eff} is 1469 pcm (i.e., 16 pcm day $^{-1}$) for the reference configuration. These multiplication factor losses are a lot lower in the minor actinide configuration, respectively 809 pcm (or about 9 pcm day $^{-1}$) and 964 (or about 11 pcm day $^{-1}$).

The multiplication factor losses in the second cycle are a bit lower compared to the first cycle because less material will be fissioned due to the lower power levels (and thus flux levels). For the reference configuration, the loss in k_s and k_{eff} is respectively 1030 pcm (or about 11 pcm day $^{-1}$) and 1174 pcm (or about 13 pcm day $^{-1}$), which is 300 pcm lower than the first cycle. For the minor actinide configuration this is respectively 712 and 798 pcm, which is 100 pcm less than the first cycle.

After 65 days in the second cycle, the minor actinide configuration reaches the level of sub-criticality that the reference configuration reached at the end of the first cycle. The burn-up swing in the minor actinide configuration is definitely smaller than in the reference configuration. In the first cycle, k_s decreases steadily in the reference configuration while this multiplication factor in the minor actinide configuration remains almost constant for the first 5 days after which it starts to decrease although more slowly than with the reference configuration.

For both configurations, the value of k_{eff} also drops faster than k_s . At the beginning of the first cycle, the difference between both multiplication factors

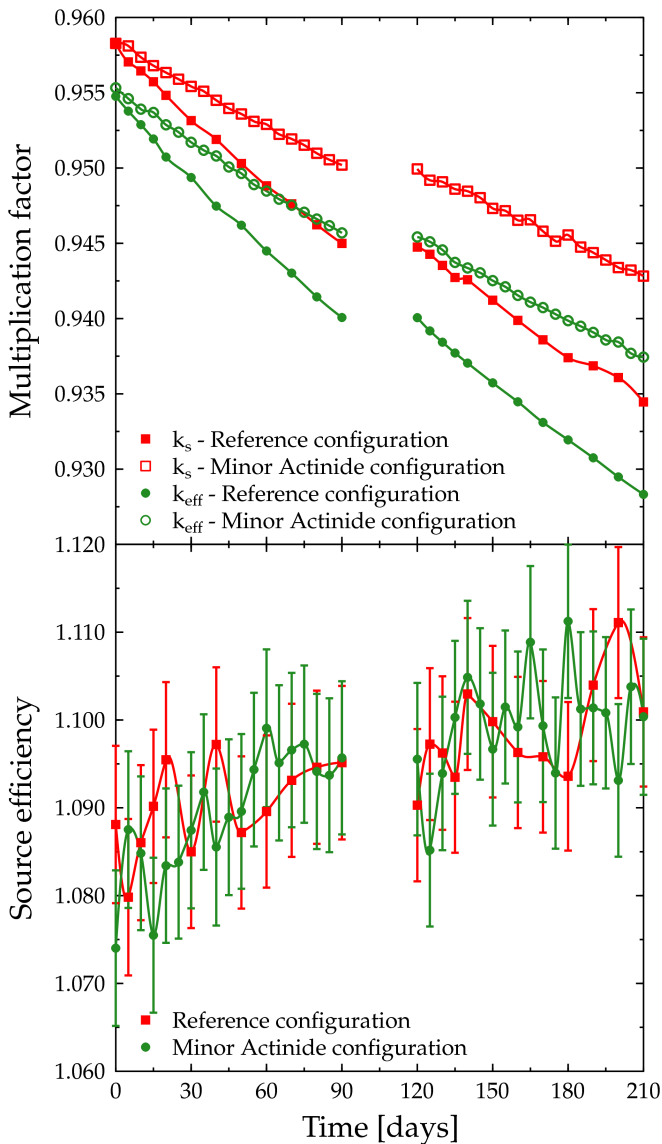


Figure 12.2: Evolution of the effective and source multiplication factor and the source efficiency of the reference configuration and the minor actinide configuration for two 90 day cycles.

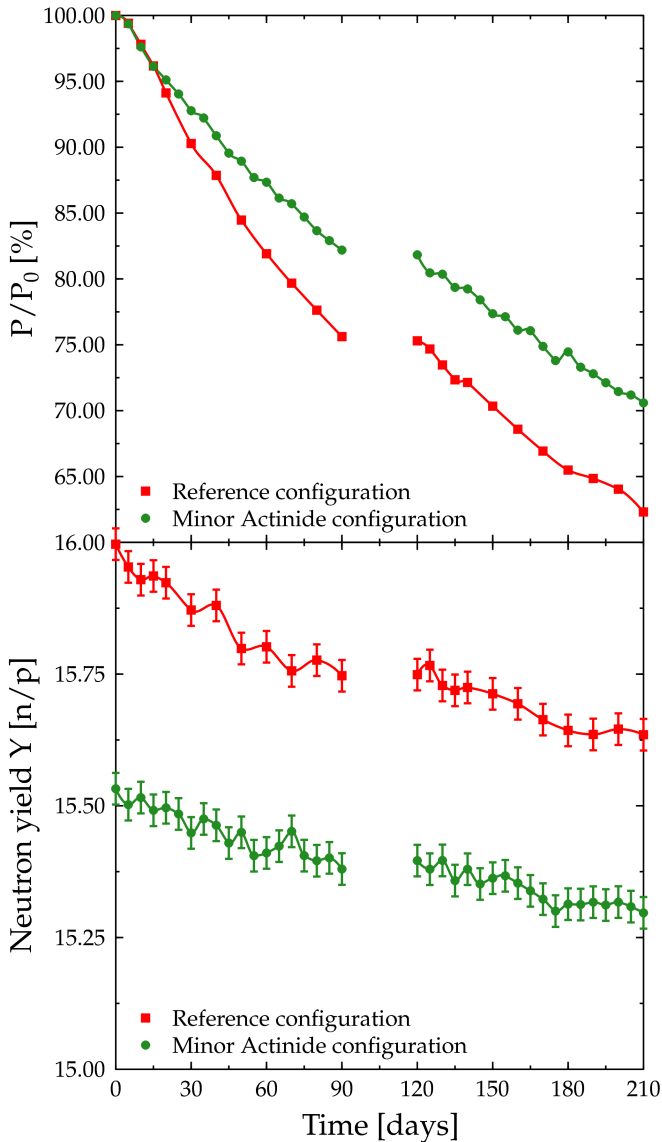


Figure 12.3: Evolution of the total system power and neutron yield of the reference configuration and the minor actinide configuration for two 90 day cycles.

is respectively 351 and 295 pcm for the reference and minor actinide configuration. After 90 days of irradiation, this difference has increased to 492 and 451 pcm.

Because of the higher initial value of k_{eff} , fission multiplication will be slightly more important in the minor actinide configuration at the beginning of the first cycle. On the other hand, the importance of the primary source is roughly the same because the value of k_s is the same for both configurations. As a result, the initial source efficiency will be smaller in the minor actinide configuration. Figure 12.2 shows an increasing source efficiency as a function of time. The error on the source efficiency is quite large, but the trend cannot be denied. This increase is a result of the evolution of the multiplication factors. Both the neutron yield of the spallation source (see figure 12.3) and the fission multiplication decrease with burn-up. The decrease in fission multiplication is however more important which results in an increase of the source efficiency.

Due to the burn-up of the core, the reference configuration has lost about 25 % of its nominal power level (50 MW) in the first cycle while the minor actinide configuration has lost only 17.5 %. Because the decrease in the multiplication factor is lower in the second cycle, the drop in the system's power is also lower: the reference configuration has lost an additional 13.2 % and the minor actinide configuration an additional 11.3 %.

12.4.3 Flux, power and burn-up distributions

Figure 12.4 gives the total flux maps for both configurations at the beginning and at the end of the first cycle. Figure 12.5 gives the same for the assembly power and burn-up distributions. The burn-up accumulated in every assembly for the two cycles can be found in figure 12.6.

The absolute flux levels are higher in the reference configuration because of the compactness of this configuration compared to the minor actinide configuration (45 MOX assemblies are used in the reference configuration versus 72 MA and MOX assemblies in the minor actinide configuration). The initial flux levels of the minor actinide configuration is about the same as the flux distribution of the reference configuration at the end the cycle.

One of the major effects of burn-up is that it tries to equalize flux and power in the entire core. In regions with high flux, the fuel is burned faster resulting in a rapidly dropping neutron production. In regions with low flux, the fuel is burned slowly resulting in a slowly decreasing neutron flux. Because the assembly power is proportional to the flux, the power distribution will show the same effect.

This effect is clearly visible in figures 12.4 and 12.5. The total flux in assembly A drops by about 24 % with respect to the initial value while in assembly I, it drops by about 25 % in the reference configuration. The absolute difference in flux between both channels therefore decreases. In the beginning of the cy-

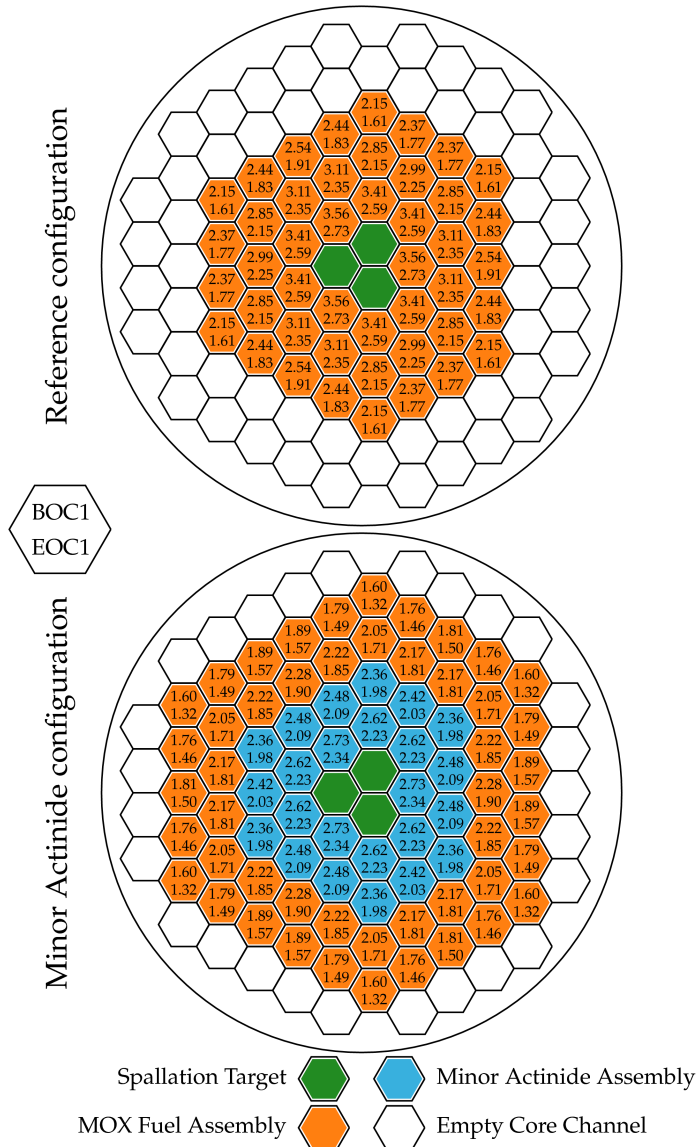


Figure 12.4: The distribution of the total neutron flux ($10^{15} \text{ n cm}^{-2}\text{s}^{-1}$) for the reference configuration and the minor actinide configuration at the beginning and end of the first cycle.

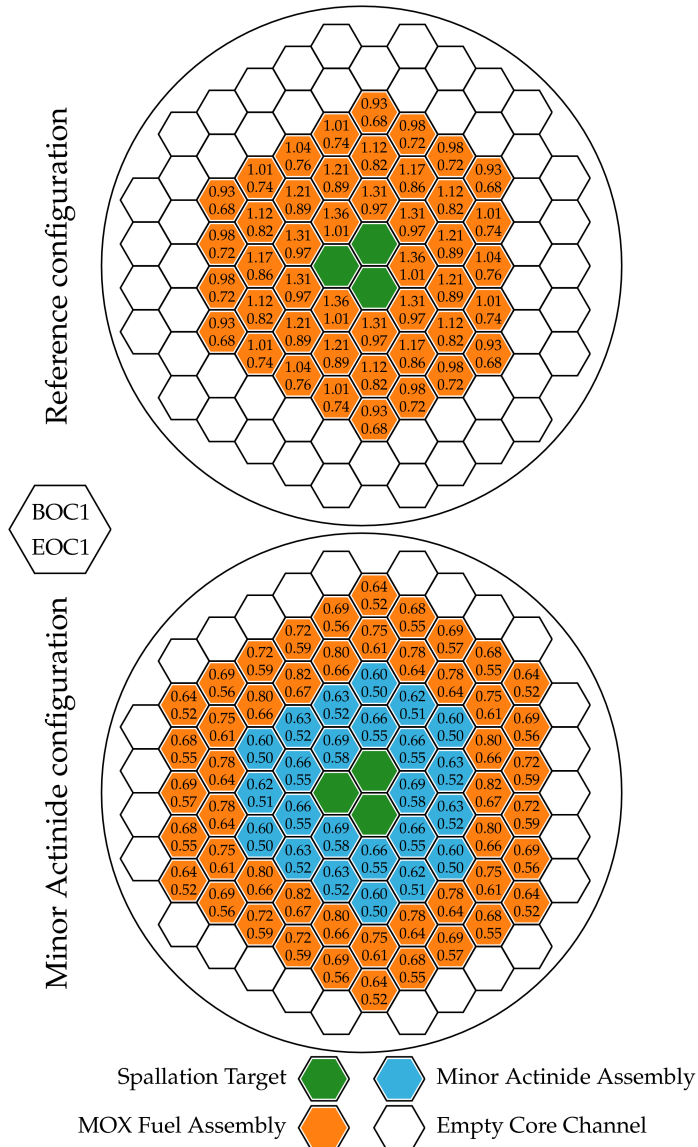


Figure 12.5: The power distribution (in MW) for the reference configuration and the minor actinide configuration at the beginning and end of the first cycle.

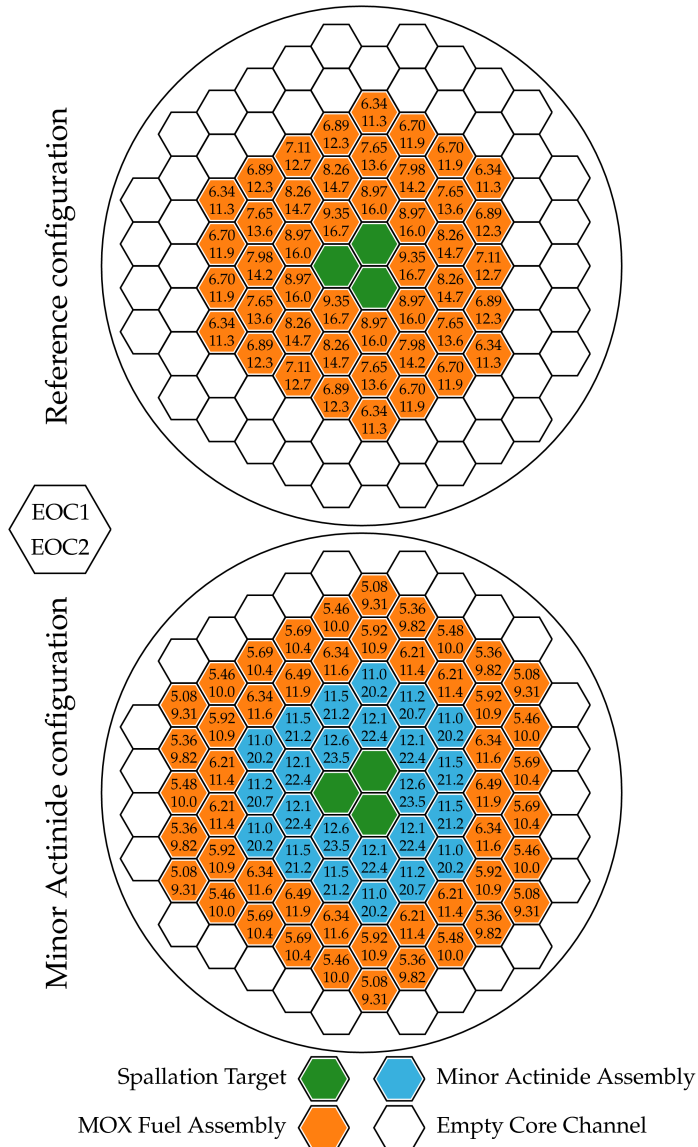


Figure 12.6: The distribution of burn-up (in MWd/kgHM) for the reference configuration and the minor actinide configuration at the end of the first and second cycle.

cle, the difference in flux between assembly A and I is $1.41 \cdot 10^{15}$. After 90 days this difference has dropped to $1.12 \cdot 10^{15}$.

In case of the power distribution we can clearly see in figure 12.5 that for the reference configuration at the end of the first cycle, the assemblies in position A produce 0.34 MW less power while the assemblies in position I only produce 0.25 MW less power compared to the beginning of the irradiation. The difference between the powers of the outer assemblies to the power of the inner assemblies has also decreased. For instance, in the beginning there is a difference of 0.43 MW between assemblies A and I. After 90 days that difference has already been reduced to 0.33 MW.

The total average burn-up of this entire reference core is 7.60 MWd/kgHM. This means that the fuel can remain in the core for 5 to 10 cycles for a total of about 40 to 80 MWd/kgHM respectively (so the total residence time will be around 450 to 900 days), provided that proper the power levels remain the same in the following cycles.

The equalising effect of burn-up is also visible to a lesser extent in the flux distribution of the minor actinide configuration. The difference in flux between an MA assembly in channel A and the MOX assembly placed in channel M decreases from $1.13 \cdot 10^{15}$ to $1.02 \cdot 10^{15}$ after 90 days of irradiation. The flux in channel A drops by about 14.2 % in the first cycle while the flux in channel M drops by 17.5 %.

The power produced in the MA assemblies in channels A to E is lower than the power produced by the MOX assemblies in this configuration. An MA assembly in channel A produces for instance 0.66 MW at the beginning of the cycle and 0.55 MW at the end while this is 0.75 and 0.61 MW for a MOX assembly in channel I. This is because the heavy metal density in the MA assemblies is about half of that in the MOX assemblies (the initial heavy metal density is 4.07 g cm^{-3} in an MA assembly and 9.31 g cm^{-3} in an MOX assembly).

This difference in heavy metal density also has a large effect on the burn-up distribution in the minor actinide configuration. Even though the power levels in the MA assemblies are lower than in the MOX assemblies, the burn-up are a lot higher in the MA assemblies. On average, the MA assemblies reach a burn-up of 11.6 MWd/kgHM at the end of the first cycle which increases to 21.5 at the end of the second cycle. For the MOX assemblies, this is respectively 5.8 and 10.6 MWd/kgHM. The core average burn-up (combining the MA and MOX assemblies) is 6.8 MWd/kgHM at the end of the first cycle which increases to 12.5 MWd/kgHM at the end of the second cycle.

12.4.4 Mass balance and transmutation performance

Table 12.3 gives the mass balance of the reference configuration at the beginning and end of both irradiation cycles. The initial amount of heavy metal loaded is 508.4 kg consisting of 355.9 kg of U (1.437 kg of fissile ^{235}U , the rest

Table 12.3: The mass balance of the reference configuration.

Nuclide	m_0 [g] 0 days	Δm [g] 90 days	Δm [g] 120 days	Δm [g] 210 days
U	355926.18	-1784.36	-1784.06	-3199.70
^{234}U	10.95	3.48	4.68	8.04
^{235}U	1437.90	-51.76	-51.55	-91.34
^{236}U	35.73	12.34	12.65	22.41
^{238}U	354441.60	-1749.89	-1749.89	-3140.07
Pu	152539.35	-2412.63	-2417.56	-4311.17
^{238}Pu	1936.98	-58.23	-59.31	-104.13
^{239}Pu	94391.39	-1958.34	-1909.90	-3426.92
^{240}Pu	35847.09	116.98	116.65	201.89
^{241}Pu	13652.21	-521.91	-573.72	-995.52
^{242}Pu	6711.69	8.71	8.71	13.36
Np		58.64	11.44	60.25
^{237}Np		10.32	11.44	19.75
^{239}Np		48.32	0.01	40.49
Am		206.23	258.14	443.25
^{241}Am		156.26	208.05	353.36
^{242m}Am		0.39	0.39	1.54
^{243}Am		49.55	49.70	88.29
Cm		1.76	1.64	5.89
^{242}Cm		1.15	1.03	3.93
^{243}Cm				0.02
^{244}Cm		0.61	0.60	1.93
^{245}Cm				0.01

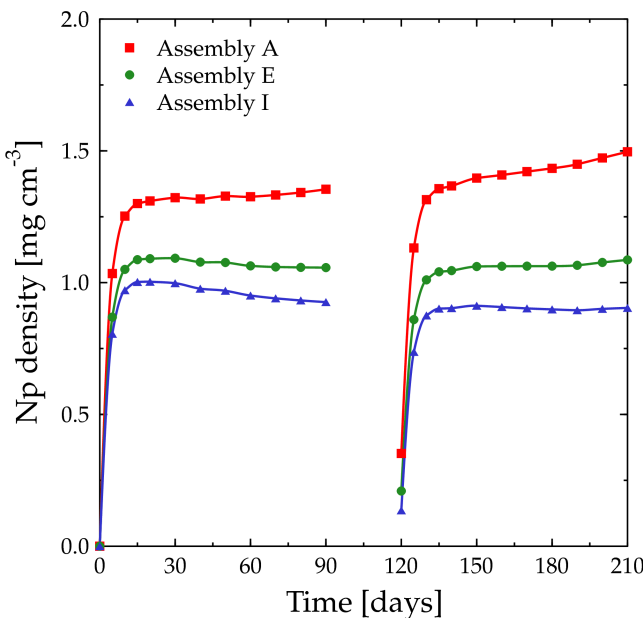


Figure 12.7: The build-up of the Np density in MOX assemblies placed in channels A, E and I of the reference configuration.

is fertile ^{234}U , ^{236}U and ^{238}U) and 152.5 kg of Pu (108.1 kg of fissile ^{239}Pu and ^{241}Pu , the rest is fertile ^{238}Pu , ^{240}Pu and ^{242}Pu).

After 90 days of irradiation, 1.78 kg of U (0.35 % of the initial amount) has been burned. 51.8 g of ^{235}U (3.6 % of the initial amount) has been consumed. 2.41 kg (1.6 % of the initial amount) of Pu has been used of which 1.96 kg of ^{239}Pu and 0.52 kg of ^{241}Pu . In the second cycle, the total U and Pu consumption is lower than in the first cycle due to the lower power levels. In this cycle 1.42 kg of U and 1.89 kg of Pu has been consumed.

The Np content in the fuel builds up fast during the irradiation after which it remains roughly constant until the end of the cycle. This is shown in figure 12.7. At the beginning of the second cycle, 48.3 g ^{239}Np (with a half-life of 2.36 days) has decayed to ^{239}Pu so that only a small amount of ^{237}Np remains.

After 90 days of irradiation, the fuel also contains a total amount of 206.2 g of Am (mainly ^{241}Am and ^{243}Am) and 1.8 g of Cm (mainly ^{242}Cm and ^{244}Cm). At the end of the second cycle, this increases to 443.3 g of Am and 5.9 g of Cm.

The main purpose of the minor actinide configuration is to transmute the minor actinides in the MA assemblies. In this case, this is limited to Am alone although Cm can be added to the mix as well [42]. The mass balance tables

Table 12.4: The mass balance of the MA assemblies in the minor actinide configuration.

Nuclide	m_0 [g] 0 days	Δm [g] 90 days	Δm [g] 120 days	Δm [g] 210 days
U		6.26	8.39	14.88
^{234}U		5.63	7.55	13.39
^{235}U		0.17	0.22	0.43
^{236}U		0.45	0.61	1.06
^{238}U				0.01
Pu	58666.99	-1006.52	-975.20	-1689.50
^{238}Pu	2968.48	18.91	77.29	226.62
^{239}Pu	22240.78	-712.15	-712.06	-1304.67
^{240}Pu	17781.95	-96.20	-95.08	-176.43
^{241}Pu	7749.92	-302.50	-331.89	-589.86
^{242}Pu	7925.86	85.09	86.37	154.38
Np		14.93	19.90	34.04
^{237}Np		14.91	19.88	34.00
^{239}Np		0.02	0.02	0.02
Am	59065.98	-1322.75	-1306.03	-2414.09
^{241}Am	39377.43	-1071.37	-1047.00	-1937.51
$^{242\text{m}}\text{Am}$		183.54	183.47	329.97
^{243}Am	19688.54	-442.51	-442.50	-813.09
Cm		923.36	867.12	1492.04
^{242}Cm		506.62	451.45	730.00
^{243}Cm		1.64	1.64	4.70
^{244}Cm		412.71	411.64	749.30
^{245}Cm		2.38	2.38	7.99

Table 12.5: The mass balance of the MOX assemblies in the minor actinide configuration.

Nuclide	m_0 [g] 0 days	Δm [g] 90 days	Δm [g] 120 days	Δm [g] 210 days
U	379654.59	-1485.51	-1484.74	-2740.30
^{234}U	11.68	3.76	5.05	8.69
^{235}U	1533.76	-43.15	-42.91	-78.47
^{236}U	38.11	10.56	10.89	19.78
^{238}U	378071.04	-1457.80	-1457.80	-2691.26
Pu	162708.64	-1951.63	-1966.58	-3600.24
^{238}Pu	2066.11	-48.76	-49.95	-90.09
^{239}Pu	100684.15	-1581.60	-1539.24	-2849.92
^{240}Pu	38236.89	132.88	132.53	240.76
^{241}Pu	14562.36	-463.71	-519.34	-916.90
^{242}Pu	7159.14	9.41	9.41	15.78
Np		49.65	8.17	51.04
^{237}Np		7.35	8.17	14.36
^{239}Np		42.30	0.01	36.67
Am		211.76	267.47	462.52
^{241}Am		167.79	223.40	380.97
^{242m}Am		0.34	0.34	1.40
^{243}Am		43.59	43.73	80.09
Cm		1.43	1.33	5.07
^{242}Cm		1.00	0.90	3.59
^{243}Cm				0.01
^{244}Cm		0.43	0.43	1.46
^{245}Cm				0.01

Table 12.6: Spectral averaged microscopic cross sections (barn) for MA assemblies in channel A and E of the minor actinide configuration calculated by ALEPH ($t = 0$ days).

Nuclide	Channel A		Channel E	
	Fission	Capture	Fission	Capture
^{238}Pu	0.41371	1.29048	0.40795	1.26715
^{239}Pu	0.37095	1.71138	0.36211	1.69777
^{240}Pu	0.37731	0.48852	0.37224	0.47124
^{241}Pu	0.38998	2.25785	0.38474	2.23902
^{242}Pu	0.37959	0.37361	0.37389	0.35678
^{237}Np	1.19367	0.45621	1.17854	0.43808
^{239}Np	1.49423	0.59603	1.47479	0.57847
^{241}Am	1.43672	0.37654	1.42815	0.35711
$^{242\text{m}}\text{Am}$	0.39395	2.75128	0.39262	2.73640
^{243}Am	1.26764	0.27840	1.25742	0.26283
^{242}Cm	0.35292	0.75038	0.34719	0.72948
^{243}Cm	0.21492	2.92022	0.21024	2.90143
^{244}Cm	0.67416	0.56076	0.66880	0.53952
^{245}Cm	0.42617	2.42410	0.42365	2.40403

of the MOX assemblies and the MA assemblies of this configuration can be found in tables 12.5 and 12.4.

The mass balance of the MOX assemblies in this configuration is about the same as the one from the reference configuration. Although there are more assemblies, the flux levels are lower so that the mass balance is actually a bit lower than the reference configuration.

At the end of the first cycle a net amount of 1 kg of Pu and 1.3 kg of Am has been consumed in the MA assemblies. Most of the loss in Pu can be attributed to fission of the fissile ^{239}Pu and ^{241}Pu isotopes (respectively 82 % and 85 % of all interactions with these nuclides are fission). However, fission is also the main interaction mechanism for ^{238}Pu as can be seen in table 12.6 (76 % of all interactions with ^{238}Pu will be fission). For the other Pu isotopes, fission and neutron capture are roughly equally important.

The loss in Am is mainly due to neutron capture. Roughly 400 g of Am is actually destroyed through fission. The rest is just transformed Cm (see figure 12.6). Respectively 20 % and 18 % of all interactions with ^{241}Am and ^{243}Am is fission. The rest of the interactions is mainly neutron capture to $^{242\text{g}}\text{Am}$, $^{242\text{m}}\text{Am}$ and ^{244}Am . These Am isotopes (except $^{242\text{m}}\text{Am}$) decay quickly to Cm, which explains the quick build-up of Cm (at the end of the first cycle 923.4 g of Cm has been created).

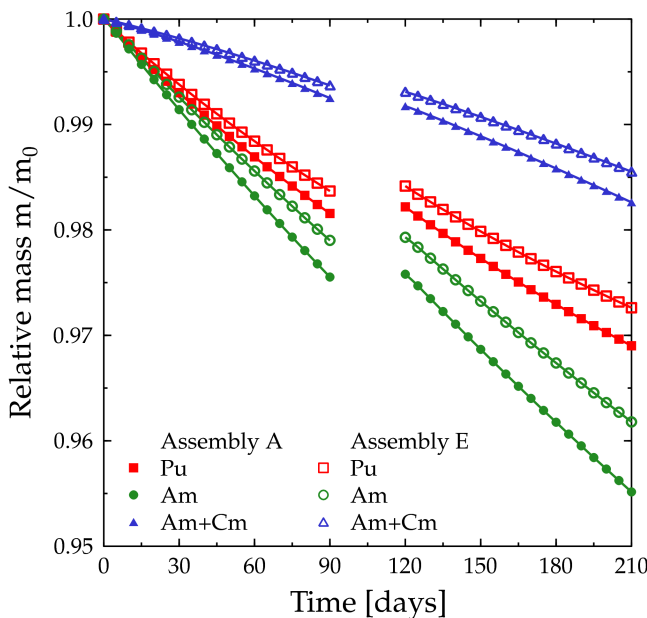


Figure 12.8: Evolution of the relative content ($m\ m_0^{-1}$) of Pu, Am and Cm with time in the MA assemblies.

As long as there is Am in the fuel, Cm will be created. ^{242}Cm (mostly created through decay from ^{242}Am) decays back to ^{238}Pu after a relatively short amount of time (the half-life is 0.45 years), effectively closing the loop. All the other Cm isotopes have “relatively” long half-lives (of the order of years to thousands of years). Fortunately, fission is quite important for most Cm isotopes.

This continues in the second cycle where an additional 714 g and 1.1 kg of Pu and Am are consumed and 625 g of Cm is created in the MA assemblies. Averaged over the entire core, about 1.5 kg of U, 3 kg of Pu and 1.1 kg of Am are consumed in this configuration and 925 g of Cm has been produced at the end of the first cycle. At the end of the second cycle, this has respectively increased to 2.7 kg, 5.3 kg, 1.95 kg and 1.5 kg.

It is no good to try to stop knowledge from going forward. Ignorance is never better than knowledge.

Enrico Fermi (1901 - 1954)

Never discourage anyone who continually makes progress, no matter how slow.

Plato (427 BC - 347 BC)

13

Final conclusions and future developments

13.1 An optimal approach to Monte Carlo burn-up

The first objective of this work was to identify, develop and implement methods for Monte Carlo with burn-up to attain the highest accuracy for the smallest computing effort possible. In every calculation there should be a balance between accuracy and what is (reasonably) achievable. So when the simulation time is as low as possible and if calculating the reaction rates takes little or no extra time compared to this simulation time, then we can actually be as accurate as we want. That is the optimum situation for Monte Carlo burn-up calculations.

We have categorised Monte Carlo codes using the cross section data format that they use. First there are the non-unionised tables where every cross section (even for the same nuclide) is linearised on a different energy grid. For a unionised cross section table, every cross section of the same nuclide has the same energy grid. The universal unionised table is a special case of this last table as every cross section is linearised on the same energy grid.

Universal unionised tables will take a lot more memory than unionised tables because the universal unionised energy grid must be capable of representing any reaction of any nuclide within a certain accuracy. Non-unionised cross section tables have tailor made grids for each reaction so that they will require much less memory space than universal unionised tables. The memory needs for unionised cross section tables will be somewhere in between non-unionised and universal unionised. The actual size of the resulting energy grid or grids will however depend upon the accuracy of the reconstruction, linearisation and Doppler broadening of the cross sections.

We have analysed and estimated the efficiency of these types of data tables for both the basic Monte Carlo simulation and the calculation of reaction rates required for a depletion calculation (see tables 4.1, 4.2 and 4.3). We have shown that it is the retrieval of cross section values (and in particular the en-

ergy grid search) that determines the calculation time in a Monte Carlo code. For a Monte Carlo burn-up code this has proved to be the main bottleneck because a large number of reaction rates have to be calculated.

This analysis has also shown that there are possibilities for optimisation in the multiplier bin calculation of MCNP(X) that can alleviate the calculation time problem of Monte Carlo burn-up. MCNP(X) uses unionised cross section tables but the code does not take advantage of it in its multiplier bins (the cross section interval is determined even if it were done already for a previous bin). If this could be changed, then the calculation time could be reduced significantly provided that multiple reaction rates of the same nuclide were requested. Another optimisation would be to test every reaction to see if it exists before performing the cross section interval search.

The conclusion of this analysis is that *the* solution for the problem would be to adopt some form of universal unionised cross section tables (either multi-group or continuous energy). With this cross section format, the time increase when calculating reaction rates compared to simulation time will become negligible and it will also give us a significant acceleration in the basic Monte Carlo simulation compared to unionised cross section tables.

By using these universal unionised data tables, it might even be possible to compete with deterministic codes on the level of calculation speed in addition to accuracy, especially for the more exotic applications. Unfortunately, up to this point no Monte Carlo code exists that uses universal unionised cross section tables (except of course for the obvious multi-group Monte Carlo codes).

Our best option in solving the CPU time problem was thus to optimise the process of reaction rate calculation so that it becomes negligible to the simulation time for existing Monte Carlo codes like MCNP(X). By reducing the number of grid searches for the reaction rate calculation, we will effectively reduce the calculation time. We achieved this by adopting the multi-group binning approach instead of using the track length estimator to calculate the reaction rates:

$$\int \int \sigma_{i,r} (E) \phi (\mathbf{r}, E) dEdV = \lim_{g \rightarrow \infty} \sum_g \sigma_g \phi_g \quad (13.1)$$

This method is neither an approximation nor is it a true hybrid method as it does not interfere in any way with the Monte Carlo simulation itself. At its core, it is just another way to calculate an integral.

With proper optimisation of the group structure used for the integration, this new method and traditional Monte Carlo are in excellent agreement (all values are within one standard deviation). Furthermore, we have shown that the multi-group binning approach will always give numerical results very close to the value given by Monte Carlo, even if the statistical error on those values is large.

By adopting the multi-group binning approach, it is as if we only have to calculate *one* reaction rate to know all of them. The dependence upon the

number of reaction rates in the calculation time disappears. The time increase due to reaction rate calculation is therefore constant, regardless of the number of reaction rates. This allows us to achieve maximum accuracy for a minimum of CPU time because we can actually calculate as much reaction rates as we want *by default*.

An alternative to the multi-group binning approach would be to gather the required data for the track length estimator (being the energy E_t , the track length l_t and weight w_t) and store them separately. After the Monte Carlo code finishes the simulation, the data should be sorted in increasing values of energy so that it is possible to go over these values energy by energy while going through the linearised cross sections interval by interval. By working in this way, it would only be necessary to go through an entire cross section only once without having to use a cross section interval search at all. Furthermore, the traditional tally estimators can still be used. Some care should be taken to correctly take the probability tables in the unresolved resonance range into account when using this strategy.

This solution is similar to the multi-group binning approach (both calculate the reaction rates when the Monte Carlo simulation has finished) but this alternate solution would require major changes to the Monte Carlo code involved, which is why we preferred the multi-group binning approach.

13.2 Nuclear data and ALEPH-DLG

The second objective of this work was to provide consistent sets of nuclear data that encompass all aspects of the burn-up calculation. Apart from the obvious cross section data, a depletion code also needs other data like branching ratios for isomer production, direct fission yield data, neutron yield per fission data, total recoverable energy per fission data and decay data. All these data can be found in one form or another in the various ENDF files that make up evaluated nuclear data libraries like JEFF 3.1 and ENDF/B-VII.

By using data from these ENDF files, we would have no need of other third party data or models. The use of these ENDF files will therefore provide us with a consistent set of data, for both the depletion and transport module in the depletion code. This approach will also allow us to quickly change our data when newer (and better) evaluations become available, making the burn-up code very flexible in its use of nuclear data (which is exactly what the ENDF format was designed for). Furthermore, using ENDF files will automatically insure nuclear data consistency because the Monte Carlo code will use the same ENDF files and the same data preprocessing code.

In this work, we have shown how these data should be processed to obtain the values and quantities required by the depletion code. In the case of branching ratios, neutron yield per fission, etc. a variation of the multi-group binning approach can be used.

We also gave special attention to the total recoverable energy per fission. The total recoverable energy from fission has basically three distinct components: the prompt energy release (the kinetic energy of the fission fragments, prompt β and γ radiation, etc.), the delayed energy release (delayed β and γ radiation, etc.) and the γ radiation resulting from structural material activation. This last component is often overlooked because it would require a coupled neutron and γ calculation.

ORIGEN 2.2 uses a semi-empirical formula to quantify the recoverable energy per fission. This includes an estimate for the energy release due to (n,γ) reactions in the system. It was assumed that the total recoverable energy per fission was independent of the energy of the neutron that induced the fission event and the estimate for the average energy released by all (n,γ) reactions per fission assumed a single type of critical reactor. By using recent fission energy release data from the ENDF files, we obtained values close to those predicted by the ORIGEN 2.2 formula, but they all lie above the ORIGEN 2.2 values. The maximum difference is about 5 %. This shows that the ORIGEN 2.2 equation is not that bad at predicting the value of the total average recoverable energy per fission. In the future, we can therefore use the ORIGEN 2.2 equation (corrected by 2.5 %) as an estimate of the total recoverable energy per fission for nuclides that do not have fission energy release data in their ENDF files.

The importance of nuclear data is often overlooked or outright ignored by many although it encapsulates large parts of the physics behind the problem of particle transport. One can have the best codes in the world, but if the nuclear data fed into those codes are lacking, the results themselves will be worthless. Quality Assurance (QA) is therefore an important aspect in the preparation of a validated application library. A set of library files can be considered to be such a validated application library if the processing has been verified, if the files are validated and if everything has been well documented.

All this has resulted in the creation of ALEPH-DLG (Data Library Generator) and ALEPH-LIB (a multi-temperature neutron transport library for standard use by MCNP(X) and ALEPH). ALEPH-DLG automates the entire process of generating library files with NJOY and takes care of the first requirement of a validated application library: verify the processing. It produces tailor made NJOY input files using data from the original ENDF file (initial temperature, the fact if the nuclide is fissile or if it has unresolved resonances, etc.). When the library files have been generated, ALEPH-DLG will also process the output from NJOY by extracting all messages and warnings. If ALEPH-DLG finds anything out of the ordinary (like for instance errors in the unresolved resonance probability tables), it will either warn the user or perform corrective actions.

To ensure that the library is capable of providing accurate and reliable results, it must also be validated. As we have shown, this can be done by testing the library against internationally accepted benchmarks (such as criticality

benchmarks and experiments like the LLNL pulsed spheres). In order to validate nuclear data we also need to ensure that differences in benchmark results are really due to differences in data. Differences in library processing introduces “noise” and is therefore not acceptable when validating nuclear data. Examples of such influencing factors are for instance the version of NJOY (99.00, 99.90, 99.112, etc.), different cross section reconstruction tolerances, etc.

The validation of nuclear data is an ongoing and probably never ending process. The LLNL pulsed sphere experiments are a lot more sensitive to cross section data and even angular distributions when compared to integral benchmarks. This aspect alone makes them prime candidates for validating nuclear data because even the smallest differences will be very clear. This fact has been made particularly clear with the example of the magnesium spheres where differences in angular distribution data lead to large deviations.

13.3 ALEPH

The ultimate goal of this work was to provide the Monte Carlo community with an efficient, flexible and easy to use alternative for classical Monte Carlo burn-up and activation calculations, which is what we did with ALEPH.

ALEPH is a Monte Carlo burn-up code that uses ORIGEN 2.2 as a depletion module and any version of MCNP or MCNPX as the transport module. For now, ALEPH has been limited to updating microscopic cross section data only.

The efficiency is achieved in ALEPH by using the multi-group binning approach which allows the code to perform burn-up calculations in a matter of days or weeks where other Monte Carlo codes would need weeks or even years to do exactly the same thing without loss of accuracy.

ALEPH achieves flexibility in many ways. The code has for instance been written in C++ using a highly modular design so that replacing MCNP or MCNPX by another Monte Carlo code would be quite easy. And the same applies to ORIGEN 2.2 as well. By providing the user with the capability of changing materials and geometry we also achieve flexibility in modelling the irradiation conditions in the system. ALEPH is also very flexible in its application areas, contrary to its deterministic cousins. Due to its Monte Carlo nature, ALEPH can be used in application areas ranging from fuel cycle studies, waste characterisation, assessment of radio-isotope production, fuel pin and fuel assembly calculations to even complete full scale reactor calculations. ALEPH also offers flexibility in its use of nuclear data. The code only uses data from ENDF files which will allow us to quickly change our data when newer (and better) evaluations become available.

Monte Carlo burn-up codes have often been stigmatized as not being very user friendly tools due to their complexity (since most codes use a script or link approach). A user would have to understand and manage a large num-

ber of input and output files while the conversion of data from one form into another would introduce approximate results due to successive round off. ALEPH strives to solve this problem by wrapping itself around the various codes involved and by automating the entire process. The ORIGEN input files for instance are created by ALEPH itself without any intervention of the user. The use of ORIGEN is actually "hidden" from the user. The user doesn't even have to provide a skeleton input file. By providing an easy to understand user interface, we also take away the burden from the user. For the user, it is as if he is running a simple MCNP(X) problem but with some "extra" options.

ALEPH has been used to study four different applications which were chosen to illustrate the power of the code. The first application illustrates how ALEPH can be used to improve fuel performance codes like TRANSURANUS by providing burn-up dependent cross sections for specific reactor types and configurations (in this case a single PWR UO₂ fuel pin). Comparisons with experimental data have shown that ALEPH predicts the build-up of Pu very well, even at an extremely high burn-up of 100 MWd/kgHM. For this application, a radial subdivision of the fuel pin was made to properly calculate the radial Pu and burn-up distribution. These radial profiles are also in good agreement with experimental data. All this indicates that ALEPH is adequate for predictions of the Pu concentration at even higher burn-up, whereas an extension will be required when applying the TUBRNP model from TRANSURANUS to burn-up above 80 MWd/kgHM.

The second application consisted of calculating an entire PWR UO₂ fuel assembly to determine the composition of a fuel sample from one of the pins in the assembly and compare them with experimental results. In this application, the power history of the sample itself was used to renormalise the power distribution in the assembly, without the intervention of the user. This illustrates the flexibility of ALEPH in modelling the irradiation conditions.

The Nd burn-up indicators were predicted within 1 % of their experimental value except for ¹⁴²Nd but this can be attributed to a possible fission yield problem. The prediction of the compositions of the actinides was also very good. All U isotopes (except ²³⁶U) and ²³⁷Np were estimated within 3 % and the Pu isotopes (except ²³⁸Pu and ²⁴⁴Pu) within 6 %. The Am and Cm compositions (except ^{242m}Am) were predicted within 20 to 25 %. ^{242m}Am exhibited a very large overestimation of almost 79 % but we have shown that this can mostly be attributed to the ²⁴¹Am (n,γ) branching ratio to the ground state of ²⁴²Am. And finally, all fission products (except ¹²⁵Sb) are predicted within 15 % of the experimental value.

The example of the sensitivity to ²³⁶U fission data and the influence of the ²⁴¹Am branching ratio illustrated the complexity of depletion calculations and showed that a problem in predictions cannot always be attributed to a single issue. In many cases like the ²³⁸Pu content, there is no easy fix so it will be a combination of small effects that will resolve the problem.

The third application was the High Flux Isotope Reactor of ORNL. In ad-

dition to a comparison with MONTEBURNS, this application featured the use of ALEPH's geometry modification during the calculation to simulate the control plate movement in the reactor. The material compositions predicted by ALEPH and MONTEBURNS showed little difference. The daily ^{235}U consumption calculated by MONTEBURNS did exhibit some oscillations while ALEPH showed an almost constant consumption (as one would expect when a reactor functions at full power) but other than that no major differences were observed.

The evolution of the effective multiplication factor k_{eff} did however differ significantly. The k_{eff} values calculated by MONTEBURNS continued to increase while the ALEPH curve showed a gradual decreases starting from day 2. The principal cause of this difference appeared to be the fission product treatment in both code systems. The seven most important fission products for the HFIR are (in decreasing order of importance) ^{135}Xe , ^{149}Sm , ^{105}Rh , ^{147}Nd , ^{151}Sm , ^{133}Xe and ^{149}Pm . The last five nuclides of this small list do not even have a cross section file in the ENDF66 library which was used by MONTEBURNS. The omission of these and other nuclides in the transport calculations results in a more transparent core which leads to increased absorption by fissile nuclides, an increased neutron production and finally to an overestimation of k_{eff} . ALEPH on the other hand uses the fractional absorption criterion to determine which nuclides to use for the next transport calculation in combination with a more complete nuclear data library, including (among others) ^{105}Rh , ^{147}Nd , ^{151}Sm , ^{133}Xe and ^{149}Pm which were missing from ENDF66.

The last application in which two configurations of MYRRHA were used demonstrates that ALEPH can provide the basic input data (the evolution of the core reactivity and other integral system parameters, the power and flux distributions and the isotopic inventory) for fuel management of advanced nuclear systems. ALEPH can provide these three characteristics in a single calculation just like a normal fuel management code. Reactor physics parameters like the effective delayed neutron fraction β_{eff} and the effective neutron lifetime Λ_{eff} have to be determined with separate calculations but the evolution of the material compositions calculated by ALEPH can also serve as basic input for these calculations.

13.4 Future developments

ALEPH is already quite capable of performing highly accurate depletion calculations in an acceptable amount of time, but there is still some room for improvement. For now, ALEPH has been limited to updating microscopic cross section data only. Other data like isomer production branching ratios, fission yields, etc. have been left unchanged in ORIGEN 2.2. The use of these data and on how they can be obtained from ENDF files was treated in chapter 6. This should be implemented into ALEPH as a first upgrade to obtain full nu-

clear data consistency. In the case of the isomer production branching ratios this will even increase the accuracy of the code (see for instance the influence of the ^{241}Am (n,γ) branching ratio to the ground state of ^{242}Am in chapter 10).

Another possible upgrade to ALEPH would be to replace ORIGEN 2.2 by a built-in depletion module to address some of the limitations of ORIGEN 2.2. This includes the use of more reaction channels (like (n,d), (n,t), etc.) to take advantage of all the reaction data available in an ENDF file, an extension of the number of actinides with direct fission yields (ORIGEN 2.2 has only 8 actinides with direct fission yields while the JEFF 3.1 fission yield sub-library contains data for at least 30 nuclides) and an extension of the decay channels to use all decay modes in the ENDF radio-active data sub-libraries. Such an upgrade of the depletion module would also allow the implementation of a better treatment for the total recoverable energy per fission.

ALEPH is currently limited to neutron activation alone. If a new depletion module is made for ALEPH, it could also allow for the extension to high energy activation and even other types of particles (like protons, deuterons, etc.).

The majority of the data required for fuel management can already be calculated directly with ALEPH. Reactor physics parameters like the effective delayed neutron fraction β_{eff} and the effective neutron lifetime Λ_{eff} have to be determined with separate calculations but the evolution of the material compositions calculated by ALEPH will also serve as basic input for this purpose. By automating this as well, ALEPH could become a very powerful fuel management tool. Furthermore, by calculating these parameters with Monte Carlo as well, a coherent system for fuel management fully based on Monte Carlo can be created. If the same Monte Carlo code (e.g. MCNPX 2.5.0 or MCNP5) and if the same nuclear data (e.g. JEFF 3.1 with the addition of JEFF 3.0A) is used for all aspects of the fuel management calculations, then such a fuel management system will be fully consistent in both method and nuclear data.

Bibliography

- [1] H. AIT ABDERRAHIM et al., "MYRRHA Pre-Design File - Draft 2", Report R-4234, Studiecentrum voor Kernenergie - Centre d'Etude de l'Energie Nucléaire, Belgium (2005)
- [2] J. F. BRIESMEISTER, "MCNP - A General Monte Carlo N-Particle Transport Code, Version 4C", LA-13709-M, Los Alamos National Laboratory, USA (2000)
- [3] J. S. HENDRICKS et al., "MCNPX, VERSION 2.6.a", LA-UR-05-8225, Los Alamos National Laboratory, USA (2005)
- [4] X-5 MONTE CARLO TEAM, "MCNP - A General Monte Carlo N-Particle Transport Code, Version 5 - Volume I:Overview and Theory", LA-UR-03-1987, Los Alamos National Laboratory, USA (2003)
- [5] S. LOUBIERE, R. SANCHEZ, M. COSTE, A. HEBERT, Z. STANKOVSKI, I. ZMIJAREVIC, "APOLLO2 - Twelve Years After", *Proc. Int. Conf. on Math. and Comp. M&C99*, Madrid, Spain, September 1999.
- [6] WIMS, "The ANSWERS Software Package - A General Purpose Neutronics Code", Serco Assurance, 1999
- [7] D. L. POSTON, H. R. TRUELLE, "User's Manual, Version 2.0 for MONTEBURNS Version 1.0", LA-UR-99-4999, Los Alamos National Laboratory, USA (1999)
- [8] R. L. MOORE, B. G. SCHNITZLER, C. A. WEMPLE, R. S. BABCOCK, D. E. WESSOL, "MOCUP: MCNP-ORIGEN2 Coupled Utility Program", INEL-95/0523, Idaho National Engineering Laboratory, Idaho Falls, USA (1995)
- [9] N. A. HANAN, A. P. OLSON, R. B. POND, J. E. MATOS, "A Monte Carlo Burnup Code Linking MCNP and REBUS", *1998 International Meeting on Reduced Enrichment for Research and Test Reactors*, Sao Paulo, Brazil, October 18-23 1998
- [10] J. CETNAR, W. GUDOWSKI, J. WALLENIUS, "User Manual for Monte-Carlo Continuous Energy Burnup (MCB) Code Version 1C", Royal Institute of Technology, Stockholm, Sweden (2002)
- [11] G. S. CHANG, J. M. RYSKAMP, "Depletion Analysis of Mixed-Oxide Fuel Pins in Light Water Reactors and the Advanced Test Reactor", *Nuclear Technology*, **129**, pp. 326-337 (2000)
- [12] Z. XU, "Design Strategies for Optimizing High Burnup Fuel in Pressurized Water Reactors", PhD thesis, Massachusetts Institute of Technology, 2003

- [13] J. S. HENDRICKS et al., "MCNPX, VERSION 2.6.b", LA-UR-06-3248, Los Alamos National Laboratory, USA (2006)
- [14] G. W. McKINNEY, "Transmutation Feature Within MCNPX", *10th UK Monte Carlo User Group Meeting*, Teddington, UK, March 15-16 2004
- [15] H. R. TRELLUE, "Use of MCNPX/CINDER90 for Residual Nuclide Production/Decay", LA-UR-04-8433, *SPIRAL 2 Workshop*, Caen, France, December 13-14 (2004)
- [16] M. L. FENSIN, J. S. HENDRICKS, H. R. TRELLUE, G. W. McKINNEY, "Advances in Monte Carlo Depletion Capabilities for MCNPX", LA-UR-06-3920, *American Nuclear Society Winter Meeting*, Albuquerque, USA, November 12-16 (2006)
- [17] M. L. FENSIN, J. S. HENDRICKS, H. R. TRELLUE, S. ANGHAIE, "Incorporation of a Predictor-Corrector Methodology and 1-group Reaction Rate Reporting Scheme for the MCNPX Depletion Capability", LA-UR-06-3925, *American Nuclear Society Winter Meeting*, Albuquerque, USA, November 12-16 (2006)
- [18] A. GLASER, "Neutronics Calculations Relevant to the Conversion of Research Reactors to Low-Enriched Fuel", PhD thesis, Technischen Universität Darmstadt, 2005
- [19] "The JEFF 2.2 Nuclear Data Library", JEF report 17, Nuclear Energy Agency - Organisation for Economic Cooperation and Development, France (2000)
- [20] "The JEFF 3.1 Nuclear Data Library", JEF report 21, Nuclear Energy Agency - Organisation for Economic Cooperation and Development, France (2006)
- [21] K. SHIBATA et al., "Japanese Evaluated Nuclear Data Library Version 3 Revision-3: JENDL-3.3", *J. Nucl. Sci. Technol.*, **39**, pp. 1125 (2002)
- [22] M. B. CHADWICK et al., "ENDF/B-VII.0: Next Generation Evaluated Nuclear Data Library for Nuclear Science and Technology", *Nuclear Data Sheets*, **107**, pp. 2931-3060 (2006)
- [23] M. HERMAN, "ENDF-102 - ENDF-6 Data Formats and Procedures for the Evaluated Nuclear Data File ENDF-VII", BNL-NCS-44945-01/04-Rev., Brookhaven National Laboratory, USA (2005)
- [24] S. GLASSTONE, G. I. BELL, "Nuclear Reactor Theory", Van Nostrand Reinhold Company, 1970

- [25] A. G. CROFF, "ORIGEN2 - A Revised and Updated Version of the Oak Ridge Isotope Generation and Depletion Code", ORNL-5621, Oak Ridge National Laboratory, USA (1980)
- [26] A. G. CROFF, "A User's Manual for the ORIGEN2 Computer Code", ORNL/TM-7175, Oak Ridge National Laboratory, USA (1980)
- [27] A. G. CROFF, "ORIGEN2: A Versatile Code for Calculating the Compositions and Characteristics of Nuclear Materials", *Nuclear Technology*, **62**, pp. 335-352 (1983)
- [28] S. M. BOWMAN, D. F. HOLLENBACH, M. D. DEHART, B. T. REARDEN, I. C. GAULD, S. GOLUOGLU, "SCALE 5: Powerful New Criticality Safety Analysis Tools", *The 7th International Conference on Nuclear Criticality Safety (ICNC2003)*, Tokai-Mura, Japan (2003)
- [29] B. DUCHEMIN, C. NORDBORG, "Decay Heat Calculation - An International Nuclear Code Comparison", NEACRP-319L, Nuclear Energy Agency - Organisation for Economic Cooperation and Development, France (1989)
- [30] J. P. UNIK, J. E. GINDLER, "A Critical Review of the Energy Released in Nuclear Fission", ANL-7748, Argonne National Laboratory, USA (1971)
- [31] R. J. J. STAMM'LER, M. J. ABBATE, "Methods of Steady State Reactor Physics in Nuclear Design", Academia Press, London, UK (1983)
- [32] I. LUX, L. KOBLINGER, "Monte Carlo Particle Transport Methods: Neutron and Photon Calculations", CRC Press, Boca Raton, USA (1991)
- [33] J. P. FINCH, J. S. HENDRICKS, C. K. CHOI, "Fission Source Convergence in Monte Carlo Criticality Calculations", *14th Biennial Topical Meeting of the Radiation Protection and Shielding Division*, Carlsbad, USA (2006)
- [34] R. C. LITTLE, "Neutron and Photon Multigroup Data Tables for MCNP 3B", X-6:RCL-87-225, Los Alamos National Laboratory, USA (1987)
- [35] J. P. BOTH, A. MAZZOLO, O. PETIT, Y. PENELIAU, B. ROESSLINGER, "User Manual for version 4.3 of the TRIPOLI-4 Monte Carlo method particle transport computer code", CEA-R-6044, Commissariat à l'Énergie Atomique - Saclay, France (2003)
- [36] G. A. WRIGHT, E. SHUTTLEWORTH, M. J. GRIMSTONE, A. J. BIRD, "The status of the general radiation transport code MCBEND", *Nucl. Instrum. Methods Phys. Res. B*, **213**, pp. 162-166 (2004)
- [37] D. E. CULLEN, "TART2005 - A Coupled Neutron-Photon 3-D, Combinatorial Geometry, Time Dependent Monte Carlo Transport Code", UCRL-SM-218009, Lawrence Livermore National Laboratory, USA (2005)

- [38] R. E. MacFARLANE, D. W. MUIR, "The NJOY Nuclear Data Processing System Version 91", LA-12470-M, Los Alamos National Laboratory, USA (1994)
- [39] D. E. CULLEN, "PREPRO 2004 - ENDF/B Pre-processing Codes", IAEA-NDS-39 Rev. 12, International Atomic Energy Agency, Austria (2004)
- [40] D. E. KNUTH, "The Art of Computer Programming - Volume 3: Sorting and Searching", Addison-Wesley, Reading, USA (1998)
- [41] R. MILLS (Nexia Solutions), Personal Communication
- [42] W. HAECK, E. MALAMBU, V. P. SOBOLEV, H. AIT ABDERRAHIM, "Assessment of americium and curium transmutation in magnesia based targets in different spectral zones of an experimental accelerator driven system", *J. Nucl. Mat.*, **352**, pp. 285-290 (2006)
- [43] M. DUIJVESTIJN, "Nucleon induced fission at intermediate energies", PhD thesis, Rijksuniversiteit Groningen, 2000
- [44] A. J. KONING, S. HILAIRE, M. C. DUIJVESTIJN, "TALYS: Comprehensive nuclear reaction modeling", *International Conference on Nuclear Data for Science and Technology - ND2004*, Santa Fe, USA (2004)
- [45] R. SHER, C. BECK, "Fission Energy Release for 16 Fissioning Nuclides", EPRI-NP-1771, Electrical Power Research Institute, USA (1981)
- [46] C. WAGEMANS (Ghent University), Personal Communication
- [47] W. HAECK, B. VERBOOMEN, "ALEPH - A Monte Carlo Burn-Up Code", Report BLG 1003, Studiecentrum voor Kernenergie - Centre d'Etude de l'Energie Nucléaire, Belgium (2005)
- [48] M. C. WHITE, J. M. CAMPBELL, S. C. FRANKLE, R. C. LITTLE, "Processing of Nuclear Data for Applications", LA-UR-02-1235, Los Alamos National Laboratory, USA (2002)
- [49] S. C. FRANKLE, "Experience with ENDF60 and QA of a Continuous-Energy Library", XTM:SCF-96-363, Los Alamos National Laboratory, USA (1996)
- [50] R. C. LITTLE, R. E. MacFARLANE, "ENDF/B-VI Neutron Library for MCNP with Probability Tables", LA-UR-98-5718, Los Alamos National Laboratory, USA (1998)
- [51] J. M. CAMPBELL, S. C. FRANKLE, R. C. LITTLE, "ENDF66: A Continuous-Energy Neutron Data Library Based on ENDF/B-VI Release 6", LA-UR-03-0954, Los Alamos National Laboratory, USA (2003)

- [52] W. HAECK, B. VERBOOMEN, "ALEPH-DLG (Data Library Generator) - Creating a General Purpose Validated Application Library for MCNP(X) and ALEPH", Report BLG 1002, Studiecentrum voor Kernenergie - Centre d'Etude de l'Energie Nucléaire, Belgium (2005)
- [53] W. HAECK, B. VERBOOMEN, "A Validated MCNP(X) Cross Section Library based on JEFF 3.1", Report BLG 1034 Rev. 0, Studiecentrum voor Kernenergie - Centre d'Etude de l'Energie Nucléaire, Belgium (2006)
- [54] O. CABELLOS, "Processing of the JEFF 3.1 Cross Section Library into a Continuous Energy Monte Carlo Radiation Transport and Criticality Data Library", NEA/NSC/DOC(2006)18, Nuclear Energy Agency - Organisation for Economic Cooperation and Development, France (2006)
- [55] E. DUPONT (Commissariat à l'Énergie Atomique), Personal Communication
- [56] S. C. FRANKLE, "A Suite of Criticality Benchmarks for Validating Nuclear Data", LA-13594, Los Alamos National Laboratory, USA (1999)
- [57] S. C. FRANKLE, "Criticality Benchmark Results Using Various MCNP Data Libraries", LA-13627, Los Alamos National Laboratory, USA (1999)
- [58] S. C. FRANKLE, J. M. CAMPBELL, R. C. LITTLE, "Comparison of Criticality Results for the ENDF60 and ENDF66 Libraries", LA-UR-03-0953, Los Alamos National Laboratory, USA (2003)
- [59] C. WONG, J. D. ANDERSON, P. BROWN, L. F. HANSEN, J. L. KAMMERDIENER, C. LOGAN, B. POHL, "Livermore Pulsed Sphere Program: Program Summary Through July 1971", UCRL-51144 Rev. I, Lawrence Livermore National Laboratory, USA (1971)
- [60] L. F. HANSEN, J. D. ANDERSON, E. GOLDBERG, E. F. PLECHATY, M. L. STELTS, C. WONG, "Time Spectra from Spheres Pulsed with 14 MeV Neutrons", *Nucl. Sci. Eng.*, **35**, 227-239 (1969)
- [61] D. J. WHALEN, D. A. CARDON, J. L. UHLE, J. S. HENDRICKS, "MCNP: Neutron Benchmark Problems", LA-12212, Los Alamos National Laboratory, USA (1991)
- [62] J. D. COURT, R. C. BROCKHOFF, J. S. HENDRICKS, "Lawrence Livermore Pulsed Sphere Benchmark Analysis of MCNP ENDF/B-VI", LA-12885, Los Alamos National Laboratory, USA (1994)
- [63] C. WONG, J. D. ANDERSON, P. BROWN, L. F. HANSEN, J. D. KAMMERDIENER, C. LOGAN, B. POHL, "Livermore Pulsed Sphere Program: Low Energy Measurements on Carbon, Iron and Concrete", UCRL-51144 Addendum, Lawrence Livermore National Laboratory, USA (1973)

- [64] W. WEBSTER, C. WONG, "Measurements of the Neutron Emission Spectra from Spheres of N, O, W, ^{235}U , ^{238}U and ^{239}Pu , Pulsed by 14 MeV Neutrons", UCID-17332, Lawrence Livermore National Laboratory, USA (1976)
- [65] W. WEBSTER, C. WONG, "Low Energy Time of Flight Spectra from Spheres Pulsed by 14 MeV Neutrons", UCID-17223, Lawrence Livermore National Laboratory, USA (1976)
- [66] W. HAECK, B. VERBOOMEN, "Validation of Nuclear Data using the Lawrence Livermore Pulsed Sphere Experiments", *14th Biennial Topical Meeting of the Radiation Protection and Shielding Division*, Carlsbad, USA (2006)
- [67] S. C. VAN DER MARCK, "Benchmarking ENDF/B-VII.0", *Nuclear Data Sheets*, **107**, pp. 3061-3118 (2006)
- [68] G. AUDI, O. BERSILLON, J. BLACHOT, A. H. WAPSTRA, "The NUBASE evaluation of nuclear and decay properties", *Nucl. Phys. A*, **729** 3-128 (2003)
- [69] R. MANZEL, C. T. WALKER, "EPMA and SEM of fuel samples from PWR rods with an average burn-up of around 100 MWd/kgHM", *J. of Nucl. Mat.*, **301**, 170-182 (2002)
- [70] C. T. WALKER, D. STAICU, M. SHEINDLIN, D. PAPAIOANNOU, W. GOLL, F. SONTHEIMER, "On the thermal conductivity of UO_2 nuclear fuel at a high burn-up of around 100 MWd/kgHM", *J. of Nucl. Mat.* **350**, 19-39 (2006)
- [71] W. HAECK, B. VERBOOMEN, A. SCHUBERT, P. VAN UFFELEN, "Application of EPMA Data for the Development of the Code Systems TRANSURANUS and ALEPH", accepted for publication in Microscopy and Microanalysis (2007)
- [72] K. LASSMANN, C. O'CARRROLL, J. VAN DE LAAR, C. T. WALKER, "The radial distribution of Plutonium in high burn-up UO_2 ", *J. of Nucl. Mat.* **208**, 223-231 (1994)
- [73] K. LASSMANN, C. T. WALKER, J. VAN DE LAAR, "Extension of the TRANSURANUS Burnup Model to Heavy Water Reactor Conditions", *J. of Nucl. Mat.* **255**, 222-233 (1998)
- [74] K. LASSMANN, "TRANSURANUS: A Fuel Rod Analysis Code Ready For Use", *J. of Nucl. Mat.* **188**, 295-302 (1992)
- [75] K. LASSMANN, H. BENK, "Numerical algorithms for intragranular fission gas release", *J. of Nucl. Mat.* **280**, 127-135 (2000)

- [76] C. T. WALKER, "Electron probe microanalysis of irradiated nuclear fuel: an overview", *J. of Analytical Atomic Spectrometry*, **14**, 447-454 (1999)
- [77] A. DOBNEY (SCK•CEN), Personal Communication
- [78] F. SONTHEIMER, H. LANDSKRON, "Puzzling features of EPMA radial fission gas release profiles: The key to realistic modeling of fission gas release up to ultra-high burn-up of 100 MWd/kgM with CARO-E", IAEA Technical Committee Meeting on Nuclear Fuel Behaviour Modelling at High Burnup, IAEA-TECDOC-1233, pp. 105-124, Lake Windermere, UK (2000)
- [79] R. MANZEL, C. T. WALKER, "High burn-up fuel microstructure and its effect on fuel rod performance", *Topical Meeting on LWR Fuel Performance*, Park City, USA (2000)
- [80] C. T. WALKER, V. V. RONDINELLA, D. PAPAIOANNOU, S. VAN WINCKEL, W. GOLL, R. MANZEL, "On the oxidation state of UO₂ nuclear fuel at a burn-up of around 100 MWd/kgHM", *J. of Nucl. Mat.* **345**, 192-205 (2005)
- [81] D. BOULANGER, P. VAN DEN HENDE, C. POTTE, "MALIBU Program - Irradiation Data Report", Report MA 2003/05, Belgonucleaire, Belgium (2006)
- [82] D. BERNARD, A. SANTAMARINA, "²³⁷Np Cross Section Experimental Validation - Proposal for JEFF 3 Modification", JEF/DOC-1044, Nuclear Energy Agency - Organisation for Economic Cooperation and Development, France (2006)
- [83] S. PILATE et al., "VALMOX: Validation of Nuclear Data for High Burn-Up MOX Fuels - Final Report", Contract nr FIKS-CT-00191 (2005)
- [84] R. W. MILLS, "Technical Note on Validation of JEFF 3.1 for decay heat and inventory calculations", JEF/DOC-1147, Nuclear Energy Agency - Organisation for Economic Cooperation and Development, France (2006)
- [85] V. MCLANE, "EXFOR Basics - A Short Guide to the Neutron Reaction Data Exchange Format", BNL-NCS-63380-00/05-Rev., Brookhaven National Laboratory, USA (2000)
- [86] C. WAGEMANS, O. SEROT, P. GELTENBORT, O. ZIMMER, "Experimental determination of the ²³⁶U (n_{th},f) cross section", *Nucl. Sci. Eng.*, **136**, 415-418 (2000)
- [87] J. P. THEOBALD, J. A. WARTENA, H. WEIGMANN, F. POORTMANS, "Fission components in ²³⁶U neutron resonances", *Nucl. Phys. A*, **181** 639-644 (1972)

- [88] W. E. PARKER, J. E. LYNN, G. L. MORGAN, P. W. LISOWSKI, "Intermediate structure in the neutron-induced fission cross section of ^{236}U ", *Phys. Rev. C*, **49** 672-677 (1994)
- [89] C. WAGEMANS, J. HEYSE, L. DE SMET, S. VERMOTE, O. SEROT, J. VAN GILS, "Measurement of the $^{236}\text{U}(\text{n},\text{f})$ cross section as a function of the neutron energy", *Nuclear Data 2007*, Nice, France, April 22-27 (2007)
- [90] N. XOUBI, "Characterization of Exposure-Dependent Eigenvalue Drift Using Monte Carlo Based Fuel Management", PhD thesis, University of Cincinnati, 2005
- [91] F. VANMASSENHOVE, "Reactortheorie: Deel 1", Ghent University (2001)
- [92] A. GANDINI, M. SALVATORES, "The Physics of Subcritical Multiplying Systems", *Nucl. Sci. Tech.*, **39** 673-686 (2002)
- [93] D. MAES, "Mechanical Design of the Small-Scale Experimental ADS: MYRRHA", *Energy Conversion and Management*, **47** 2710-2723 (2006)
- [94] E. MALAMBU, B. ARIEN, W. HAECK, S. HEUSDAINS, D. F. DA CRUZ, H. WIDER, "Hybrid Reactors with Solid Fertile Fuel: Lead-Bismuth-cooled MYRRHA ADS Benchmark", IAEA-TECDOC-xxxx, International Atomic Energy Agency, Austria (2007)
- [95] R. K. MEULEKAMP, S. C. VAN DER MARCK, "Calculating the effective delayed neutron fraction with Monte Carlo", *Nucl. Sci. Eng.*, **152**, 142-148 (2006)
- [96] B. VERBOOMEN, W. HAECK, P. BAETEN, "Monte Carlo calculation of the effective neutron generation time", *Ann. of Nucl. Energy*, **33**, 911-916 (2006)